Summer 2017

Durability behavior of fiber reinforced polymer and steel reinforced polymer for infrastructure applications

Wei Wang

Department: Civil, Architectural and Environmental Engineering

DURABILITY BEHAVIOR OF FIBER REINFORCED POLYMER AND STEEL REINFORCED POLYMER FOR INFRASTRUCTURE APPLICATIONS

by

WEI WANG

A DISSERTATION

Presented to the Faculty of the Graduate School of the

MISSOURI UNIVERSITY OF SCIENCE AND TECHNOLOGY

In Partial Fulfillment of the Requirements for the Degree

DOCTOR OF PHILOSOPHY

in

CIVIL ENGINEERING

2017

Approved by

John J. Myers, Advisor
Genda Chen
Lesley Sneed
K. Chandrashekhara
Matthew O'Keefe

ABSTRACT

Crack development in reinforced concrete (RC) structures is common in elements such as bridge decks. However, these cracks can impose significant problems over time, because they allow chlorides from deicing chemicals to infiltrate concrete which will then corrode steel bars as RC structures are exposed to harsh weather. In the last decade, composite reinforcement systems are internally or externally applied to concrete structures instead of traditional steel reinforcing bars, or to strengthen concrete elements in flexure and shear. However, studies regarding the long-term durability performance of composite reinforcement systems is limited. Therefore, in order to popularize the application of these systems, it is necessary to study the long-term properties and behaviors of concrete members reinforced with composite materials.

This study includes three topics: 1. Long-term durability of concrete panels reinforced with steel and glass reinforced polymer (GFRP). The main objective of this study is to investigate the mechanical properties of GFRP bars extracted from concrete panels after seven plus years of field exposure and examine any microscopic damage to the GFRP fiber and/or matrix resin; 2. Durability of concrete elements reinforced with Steel Reinforced Polymer (SRP). The key purpose of this study is to assess the bond behavior of SRP-to-concrete systems and provide durability study of SRP strengthening systems to supplement ACI 440; 3. Assessment of existing FRP bridge structures exposed to field conditioning. This study focuses on investigating the physical inspection for the existing FRP bridges in Rolla, MO and to characterize GFRP bars extracted from Southview Bridge (MO), Walker Bridge (MO), and Sierrita de la Cruz Bridge (TX) and surrounding concrete after several years of service.

ACKNOWLEDGMENTS

I would like to express my sincere thanks and appreciation to my advisor, Dr. John J. Myers. His guidance and support throughout my academic and scholarly studies was a great help.

I would also like to express my gratitude to my committee members, Dr. Genda Chen, Dr. Lesley Sneed, Dr. K. Chandrashekhara, and Dr. Matthew O'Keefe for their advice and assistance with this research.

Thank you to the Center for Infrastructure Engineering Studies (CIES) and the Department of Civil, Architectural, and Environmental Engineering at the Missouri University of Science and Technology, especially Brian Swift, Gary Abbott, John Bullock, Jason Cox, Mike Lusher, and Greg Leckrone for their technical support. I would like to express a great deal of gratitude to my friends and colleagues at Missouri S&T, who's help and advice was greatly appreciated throughout all aspects of the research project, particularly Eli Hernandez, Zuhair Al-Jaberi, Hayder Alghazali, Zena Riyadh, Michael Janke, and Saipavan Rallabhandhi.

I would like to thank Hardwire® LLC, Sika Corporation, and Hughes Brother, Inc. for their donations and materials used for my research. Thanks to Doug Gremmel of Hughes Brothers for his great interest and helpful feedback.

Last, but definitely not least, I would like to express my thanks to my parents for their loving support.

TABLE OF CONTENTS

LIST OF ILLUSTRATIONS

Page

LIST OF TABLES

Page

NOMENCLATURE

Symbol	Description
s_0	Stresses in concrete and reinforcing bars are no longer affected directly by the presence of this crack, in.
d_b	Bar diameter, in.
ρ	Reinforcement ratio
$N(\infty)$	Final tensile force, lb
σ_{av}	Estimate of the average concrete stress in the period after first cracking, ksi
ε_{sh}^*	Final shrinkage strain, in./in.
E_e^*	Final effective modulus for concrete, ksi
σ_{s2}^*	Final stress of steel bar at the crack, ksi
s	Crack spacing, in.
f_t	Tensile strength of concrete, ksi
s_0	Distance is stresses in concrete and reinforcing bars are no longer affected directly by the presence of this crack, in.
w	Final average crack width, in.
σ_{c1}^*	Final concrete stress away from the crack, ksi
α	Coefficient value for s_0
β	Coefficient value for s
σ	Pull-off bond strength, ksi
F_p	Pull-off force, lb
D	Diameter of the loading fixture, in.

1. INTRODUCTION

1.1. BACKGROUND

Cracks occur in concrete due to volume changes of a restrained concrete structure. The amount of restriction, which is generally the combined action of the deck and girders, depends on design characteristics of the bridge, for instance boundary conditions and/or superstructure relative stiffness. Construction techniques also influence the degree of restraint of concrete. Girders can confine the volume change of the bridge deck through some shear connectors when concrete shrinks, which will cause a downward displacement of deck-girder system. Thus, the tensile stress will develop in the deck with time. When the stress exceeds the tensile capacity of concrete, the concrete bridge deck will induce crack [1]. Accordingly, this will result in other damage like corrosion of reinforcement.

There are many bridge decks that develop transverse cracking, and most of these cracks occur at early ages. They generally develop after construction of a bridge or a bridge has been opened to traffic after a certain time. Transverse cracks usually appear when concrete is set [2-4] and widen gradually with time [5-7]. Early-age transverse cracking in concrete structures reinforced with steel with high ratios of surface area to volume has been a main serviceability problem [1]. These cracks can be observed in most geographical locations, and on many superstructure types. It is estimated that more than 100,000 bridges in the United States develop early transverse cracks [8]. These cracks are typically fully depth [8-10], located 3-10 feet (1-3 m) apart along the length of the span of concrete member [2, 3, 10]. They are observed over the transverse reinforcement [2, 4, 7, 8, 9]. These transverse cracks can decrease the service life of the reinforced concrete (RC) members, and increase the cost to maintain these structures. There are some factors that affect the transverse cracking such as construction techniques, material properties, design methods, environmental conditions, etc. [1].

In addition, when bridges reinforced with steel bars are exposed to a freezing environment, highway maintenance crews often use deicing salts or other chemicals to mitigate issues of ice formation on bridge decks because freezing temperature can make the reinforced concrete decks form a layer ice. These deicing salts and similar agents

contain chlorides which are extremely harmful for concrete decks reinforced with steel bars. Transverse cracks that allow chloride to penetrate the concrete can accelerate corrosion of steel bars, especially in areas where deicing salts are usually applied to concrete structures [9, 12]. Furthermore, freeze-thaw cycles of water in cracks, which can increase crack width, and leakage of water to supporting structures may destroy RC structures and reduce their service life [1]. Therefore, RC structures have a widely-recognized problem that influences the durability of concrete structures: the corrosion of steel.

Damage of bridges is defined as either functionally obsolete or structurally deficient. According to 2013 ASCE Report Card [13], just one in nine, or just below 11%, of the nation's bridges was classified as structurally deficient. The number of bridges defined as functionally obsolete has also declined, with currently 24.9% of the nation's bridges in 2012. However, while billions have been spent annually on bridge construction, rehabilitation, and repair in the last twenty years, current funding levels are not enough to repair or replace the nation's large-scale, urban bridges, which carry a high percentage of the nation's traffic. At the state level, 22 states have a higher percentage of structurally deficient bridges than the national average, while five states have more than 20% of their bridges defined as structurally deficient. Pennsylvania tops the list with 24.4%, while Iowa and Oklahoma are not far behind, each having just over 21% of their bridges classified as structurally deficient. When looking at the highest percentage of deficient bridges (combined structurally deficient and functionally obsolete bridge categories), the nation's capital tops all 50 states, with 77%, or 185 of 239, of bridges in the District of Columbia falling into at least one of these categories.

Based on 2013 ASCE Report Card for Missouri [14], when considering recent strides to improve the condition of Missouri's bridges, more than one in four of the state's bridges are considered deficient and one in seven is considered structurally deficient. The recently completed Safe Sound Bridge Improvement Program has made great progress in dealing with those in the worst condition, but considering the large number of bridges in the state inventory, similar programs must be implemented to prevent losing those gains.

Special concern should be put to concrete bridge decks reinforced with steel bars, especially in the regions of high use of deicing salts in United States. Bridge decks commonly require major repair or replacement every 15 to 20 years, while most other components remain in service for 40 or more years [15]. A key reason that reduces the service life of the RC deck is that the concrete deck is exposed to deicing salts, the chlorides from salts then infiltrates the concrete through cracks and initiates corrosion of the steel reinforcement. When steel bars corrode, their volume will increase, and then the properties of steel will decrease. The increase in volume will cause stresses in the concrete and de-bonding between concrete and reinforcement. Therefore, there is the temperature and shrinkage reinforcement applied to limit crack width. The Missouri Department of Transportation (MoDOT) details a typical reinforcement layout when using temperature and shrinkage reinforcement that is located closest to the top of the bridge deck. Therefore, chloride ions, oxygen, and moisture can reach first the secondary reinforcement to corrode steel bars through cracks, which affects the durability of the concrete deck and structural integrity. There are multiple techniques that are used to prevent corrosion of steel bars including epoxy-coated reinforcement, galvanized steel reinforcement, and cathode protection. However, these methods have illustrated only to delay corrosion of reinforcement in the deck [15]. The epoxy-coated reinforcement has produced some problems due to faulty construction techniques therefore a reinforcement that is resistant to corrosion is the best viable option for the future.

The use of fiber reinforced polymer (FRP) bars for temperature and shrinkage reinforcement in RC bridge decks may improve corrosion of steel due to their higher resistance to corrode. Today FRP reinforcement systems have been applied to concrete bridge decks, along with the overall bridge structure. The Morristown Bridge in Vermont, for example, spans over Ryder Brook and has a steel free concrete deck slab that was completely reinforced with GFRP [16]. GFRP reinforcing bars were also used in some demonstration projects like the Southview Bridge and the Walker Street Bridge in Rolla, Missouri. In other states like Texas, bridges like the Serrita de la Cruz creek bridge have implemented GFRP bars for embedded reinforcement. These GFRP reinforcements in these demonstration project are monitored in this study to investigate their field-based long-term durability as opposed to simulated laboratory studies.

In the last decade, as externally bonded composite material, carbon and glass fiber reinforced polymer strengthening systems to reinforce the flexural or shear strengthening of concrete structures in situ are increasingly being used for repair and rehabilitation (R&R) of existing structures [17-19]. These existing civil infrastructure projects do not need to be replaced due to the development and use of new innovative FRP strengthening systems. Therefore, R&R can provide significant economic advantages for the construction and maintenance industry. FRP laminates, as one rehabilitation method, are applied to concrete beams, columns, walls, slabs, and pipes to strengthen their load-carrying capacity. The increasing requirements for their applications create a significant need to understand the short and long-term behavior of this strengthening system under varying loading configurations and environmental conditions [20]. According to the 2013 ASCE Report Card, a number of RC civil infrastructures that needs to repair or rehabilitate because they are either functionally obsolete or structurally deficient in U.S.A. This should be related to the demand for higher load-carrying capacity, degradation of structural or materials, or change in use [21]. Recently, a new technique for repair, steel reinforced polymers (SRP), is a promising system as they can be applied to concrete bridges to strengthen flexural load-carrying capacity and they are much less expensive composites than carbon fiber reinforced polymer (CFRP). However, studies on the long-term durability performance of SRP application are very limited particularly the assessment of SRP system subjected to field exposure. Therefore, it is necessary to study the long-term properties and behaviors of concrete elements externally reinforced with SRP system.

1.2. SCOPE, OBJECTIVES AND SIGNIFICANCE OF THIS WORK

This research involves three topics:

1) Long-term durability of concrete panels reinforced with steel and glass reinforced polymer (GFRP),
2) Durability of concrete elements reinforced with Steel Reinforced Polymer (SRP),
3) Assessment of existing FRP bridge structures exposed to field conditioning.

1.2.1. Objectives and Significance of Topic 1. There are two phases for this topic. The objectives of this study are to (1) examine the appropriateness of the ACI 440 1R-06 [22] "Guide for the Design and Construction of Concrete Reinforced with FRP Bars" requirements for secondary reinforcement by comparing final cracking patterns and crack widths of these panels; (2) investigate the mechanical property of the GFRP bars; (3) observe the secondary crack development of these panels and investigate the previous recommendations; and (4) compare the maximum probable crack width equation of ACI 440 1R for FRP-reinforced members.

Even if the appropriate shrinkage and temperature (Sh&T) reinforcement ratio was properly proportioned for several years, the current code basis of the Sh&T reinforcement ratio was based on anecdotal observed field behavior of RC members using steel rather than FRP. Until now, there is no experimental long-term study to support ACI 440.1R expression for FRP bars serving as secondary reinforcement. This research, therefore, will provide the long-term behaviors and properties of GFRP bars used as secondary reinforcement in real-time natural environment.

The work will also yield results on GFRP bars extracted from reinforced concrete elements that have seen multiple years of field exposure. This data is extremely limited in the current literature and reported to be a limiting reason why FRP reinforced bridge elements have not seen wider implementation into today's bridge and infrastructure inventory.

1.2.2. Objectives and Significance of Topic 2. SRP has been applied to concrete members for externally bonded reinforcements to repair and retrofit bridges such as Bridge P-962 in Dallas County, Missouri. However, the non-galvanized SRP (i.e. an earlier generation) utilized to strengthen girders of this bridge showed signs of rust in many places. This was especially prevalent in locations where water was able to drain from the deck to the girders [23]. The durability study of SRP, therefore, is imperative to better understand the long-term implications of using said system in the field. Furthermore, there are current ACI (and other international) design guides for FRP systems to strengthen concrete structures. However, there are no current standards or guidelines for the design and construction of externally bonded SRP systems for strengthening concrete structures. Therefore, the objectives of this project are to (1)

assemble database of current durability test results for ACI 440.9R-15 [24] “Guide to accelerated conditioning protocols for durability assessment of internal and external fiber reinforced polymer (FRP) reinforcement for concrete”; (2) investigate whether galvanized and non-galvanized steel wires in epoxy matrix systems will corrod and study/understand the reason of corrosion under different environmental conditionings; (3) analyze the environmental reduction C_E factor for ACI 440.2R-08 [25] “Guide for the Design and Construction of Externally Bonded FRP Systems for Strengthening Concrete Structures”. The significance of this research is to provide a through durability study of SRP to supplement ACI 440 standards.

1.2.3. Objectives and Significance of Topic 3. There are limited results whether GFRP bars deteriorate after long-term field exposure in concrete since laboratory durability studies cannot duplicate synergistic in-situ exposure conditions and loading cycles. As a result, these field based durability studies are critical to understanding the properties of GFRP bars extracted from concrete structures. In addition, the long-term bond performance of FRP strengthening systems have not been investigated in the state of Missouri and elsewhere. Therefore, the objectives of this topic are to (1) further illustrate whether the properties of GFRP bars will change after several years of exposure in concrete due to the environment, (2) investigate the durability of FRP externally strengthening system. Its significance is to provide a direction or guideline of long-term performance of FRP system so that this system can be applied widely to civil engineering.

1.3. LAYOUT OF THE DISSERTATION

Section 1 involves the background information, and scope, objectives, and significance of this research.

Section 2 introduces a literature review. In Section 2.1, restrained shrinkage cracking of GFRP panels including the cracking of concrete due to shrinkage and prediction of cracking behavior for restrained concrete members is discussed. The deterioration of GFRP systems involving field and laboratory research of GFRP bars that are exposed to concrete environment is detailed in Section 2.2. And durability behavior

of concrete members reinforced with composite material laminates including FRP and SRP sheets is discussed in Section 2.3.

Section 3 describes Topic 1 including introduction, the properties of materials, test setups, testing results and discussions, theoretical analysis and calculations, and summary.

Section 4 details Topic 2 including introduction, the properties of materials, test setups, testing results and discussions, comparison and discussion with CFRP strengthening system, and summary.

Section 5 consists of Topic 3 including introduction, the properties of materials, test setups, testing results and discussions, and summary.

Section 6 summarizes the conclusions of these three topics.

2. LITERATURE REVIEW

2.1. RESTRAINED SHRINKAGE CRACKING OF GFRP PANELS

The formation of cracks is inevitable in reinforced concrete (RC) structures. Different types of cracks that develop in RC include: (1) direct tension cracks, (2) flexural cracks, (3) shear cracks, (4) torsion and shear cracks, (5) bond cracks, (6) concentrated load cracks, (7) heat-of-hydration cracks, and (8) effect of corrosion cracks. Significant and/or severe cracking of reinforced concrete is an important concern for the durability and design life of bridge decks. Crack widths are of concern for three key reasons: appearance, leakage and corrosion [26]. Therefore, it is used to minimize loss in durability and design life that crack width can be controlled.

Shrinkage is a main reason of cracking when the concrete hardens and internal free moisture evaporate. Direct tension cracks are the cracks when the tensile stresses induced by shrinkage exceed the tensile capacity of concrete as the concrete member is restrained. Shrinkage of concrete is the reduction of volume caused by loss of water during the drying process (drying shrinkage) and also by chemical reactions of hydration of cement paste (endogenous shrinkage or autogenous shrinkage).

Drying shrinkage is defined as the contracting of a hardened concrete mixture due to the loss of capillary water. It is dependent upon several factors. These factors include the properties of the components, proportions of the components, mixing manner, amount of moisture while curing, dry environment, and member size. Concrete cured under normal conditions will undergo some volumetric change. Drying shrinkage happens mostly because of the reduction of capillary water by evaporation and the water in the cement paste. The higher amount of water in the fresh concrete, the greater the drying shrinkage affects. The shrinkage potential of a particular concrete is influenced by the amount of mixing, the elapsed time after the addition of water, temperature fluctuation, slumping, placement, and curing. The makeup of concrete is also very important. Each aggregate and cement type has distinctive characteristics, each contributing to concrete shrinkage. The amounts of water and admixtures used during mixing also have direct and indirect effects on drying shrinkage of concrete. Concrete shrinkage occurs mostly due to the evaporation of the mixing capillary water. The severity of this shrinkage depends on

the physical properties of the concrete including size of the structure, location of the structure, and the surrounding temperature.

Autogenous shrinkage is a volume change resulting when there is no moisture transfer to the surrounding environment. It occurs when a concrete can self-desiccate during hydration or water is consumed by the chemical reactions in concrete. Autogenous shrinkage is an important phenomenon in young concrete. At low water/cement ratios, less than about 0.42, all the water is rapidly drawn into the hydration process and the demand for more water creates very fine capillaries. The surface tension within the capillaries causes autogenous shrinkage (sometimes called chemical shrinkage or self-desiccation) which can lead to cracking. Autogenous shrinkage can be important when in situ concrete is placed over older concrete as in various forms of hybrid construction. Drying shrinkage is the principal form of shrinkage. Concrete structure is free to contract if shrinkage is not restrained. As a result, shrinkage has little consequence. However, this is rarely situation in concrete structures. The bonded reinforcement in concrete structures provides restraint to shrinkage. The reinforcement imposes a tensile force on the concrete at the level of the reinforcement when the concrete shrinks. At the same time, the reinforcement produces an equal and opposite tensile force on the concrete at the level of the reinforcing bars. This internal tensile restraining force is often important enough to cause cracking of concrete members. In addition, connections provide restraint to shrinkage if a concrete member is connected to other parts of the structure or to the foundations. The tensile restraining force can develop rapidly with time at the restrained ends of the member, which results in cracking of the concrete member. Thin floor slabs and walls in buildings and deck slabs of bridges are particularly prone to significant cracking resulting from restrained shrinkage and temperature changes [27].

It is impossible to effectively eliminate the cracking of concrete structures. The most effective way to deal with cracking of reinforced concrete structures is to account for it during the design stage, and to use appropriate techniques during the construction period. In general, steel bars in concrete members are often corroded by some harmful elements that can penetrate into concrete through cracks. In order to decrease the corrosion problem of conventional reinforcing steel, non-metalic glass fiber reinforced polymer (GFRP) bars have been applied to some concrete structures to address this issue.

Their comparable cost (to epoxy coated steel), higher tensile capacity, and lower weight make it a promising material. GFRP bars, however, have relatively lower modulus of elasticity than steel bars, which can result in wider cracks in concrete structures reinforced with GFRP bars. Temperature and shrinkage reinforcement, therefore, are often utilized in concrete members to limit crack width.

Shrinkage cracks perpendicular to a concrete member span are restricted by flexural reinforcement. Thus, shrinkage and temperature reinforcement that is specified in ACI 318-11 Section 7.12 [28] – Shrinkage and Temperature Reinforcement is only required in the direction perpendicular to the span. ACI 318-11 requires:

1) A minimum steel reinforcement ratio of 0.0020 when slabs are reinforced with Grade 40 or 50 deformed steel bars,
2) The reinforcement ratio of 0.0018 when slabs are reinforced with Grade 60 deformed bars or welded reinforcement (deformed or smooth),
3) Slabs with steel reinforcement that yield stress exceeds 60,000 psi (414 MPa) measured at a yield strain of 0.35 percent to gross area of concrete should be at least $0.0018\times 60/f_y$, where f_y is in ksi, but not less than 0.0014.

This code also requires that the spacing of shrinkage and temperature reinforcement not exceed five times the member thickness or 18 inches (500 mm). The amounts specified given for deformed steel bars and welded fabric are empirical but have been utilized satisfactorily for several years.

To date, there are no experimental data that are available for the minimum FRP reinforcement ratio for shrinkage and temperature. Shrinkage and temperature reinforcement for FRP is detailed in ACI 440.1R “Guide for the Design and Construction of Structural Concrete Reinforced with FRP Bars”, specifically Section 10-Temperature and Shrinkage Reinforcement. ACI 440.1R followed the same method for determining shrinkage and temperature reinforcement that was expressed by ACI 318. The stiffness and the strength of shrinkage and temperature for FRP reinforcement can be incorporated in this formula ($0.0018\times 60/f_y$). Therefore, deformed FRP shrinkage and temperature

reinforcement is used, the amount of reinforcement should be determined by using Equation (1) [22]

$$\rho_{f,ts} = 0.0018 \cdot \frac{60,000}{f_{fu}} \cdot \frac{E_s}{E_f} \tag{1.1}$$

It is recommended that the ratio of temperature and shrinkage reinforcement given by Equation (1.1) be taken not less than 0.0014, the minimum value specified by ACI 318 for steel shrinkage and temperature reinforcement. The engineer may consider an upper limit for the ratio of temperature and shrinkage reinforcement equal to 0.0036, or compute the ratio based on calculated strain levels corresponding to the nominal flexural capacity rather than the strains calculated using Equation (1). Spacing of shrinkage and temperature FRP reinforcement should not exceed three times the slab thickness or 12 inches, whichever is less [22]. Due to limited experience, however, this equation is only a recommended expression. Therefore, it is necessary to perform more experiments to examine its appropriateness.

In the original experimental study completed by Branham and Myers [29] from August 31st, 2005 through March 22nd, 2006, one steel (Panel P-1) and five GFRP reinforced panels (Panel P-2 through Panel P-6) with varying widths were fabricated. They were exposed to an in-situ field environment in Rolla, Missouri. At different time periods, cracking for these six panels were recorded. At the same time, the crack widths were measured. Based on this first study, the FRP secondary reinforcement ratio Equation (1) was reported to be overly conservative in estimating the amount of secondary reinforcement needed to control the effects of temperature and shrinkage.

The second stage of this study was performed by Myers and Golden [30] at an age of 762 days, when both the original and new crack widths for each panel at that time were measured and recorded. The cracking patterns of these panels were also reported and studied. According to the report regarding FRP as reinforcement, ACI Committee 440.1 R-06 referred to the Canadian Standards Association (1996) limits for allowable crack widths: *for structures such as bridges (exterior exposure), the maximum allowable crack width is set at 0.013 inch. (0.3 mm).* With a maximum crack width of 0.039 inch (0.9

mm), Panel P-2 failed this specification. (Panel P-2 also had a damaged center support which may have skewed the results). However, all of the other four GFRP reinforced panels passed with maximum crack widths of 0.010 to 0.012 inch (0.25 to 0.30 mm).

Reinforced concrete (RC) structures with high surface-to-volume ratios such as bridge deck slabs, concrete pavements, and parking garages form transverse cracks easily due to restraint and the shrinkage of concrete. Because bridge deck slabs are typically much longer in one direction than the other, volumetric changes of concrete due to shrinkage and thermal changes are more pronounced in the longitudinal direction. In slab-on-girder bridges, the girders and continuity of slabs restrain the movement of deck slabs due to shrinkage and thermal changes, which induces stresses that result in transverse cracks [8-31]. Shrinkage is greatest at the surface of a concrete member when exposing to drying environment, and decreases gradually towards the interior of the member. The resulting differential shrinkage across the member's cross section produces tensile stresses near the drying surface that may lead to surface cracking [27]. In restrained concrete members, cracks generally penetrate over the full depth of members' cross sections. Full-depth cracks are generally considered the most severe form of bridge deck slab cracking. The width of a crack depends on the quantity, orientation, and distribution of the reinforcing bars crossing the crack. The bond characteristics between concrete and reinforcement bars also can influence the width of the crack.

Early-age cracking (transverse cracking) of concrete bridge deck slabs, typically resulted from autogenous shrinkage, drying shrinkage, and thermal changes, could produce several disadvantageous influences on long-term behavior and durability. As water was consumed by the ongoing hydration process, the voids empty, and capillary stresses were generated resulting in a volumetric shrinkage. Autogenous shrinkage was the concrete volume change occurring without moisture transfer to the environment [32]. There was enough water in concrete voids to provide hydration reaction, and stresses associated with autogenous shrinkage did not develop when the ratio of water to cement or cementitious material (w/cm) exceeded 0.42 [33]. In this study, w/cm of the concrete was 0.5, the autogenous shrinkage, therefore, was not major reason to cause the concrete panels volume change.

Thermal changes of concrete from hydration processes could increase early-age cracking tendency of freshly placed concrete bridge decks. Higher thermal stresses in fresh concrete would produce when increasing placement and curing temperature. The early-age cracking of bridge deck concrete would occur when the thermal stresses exceeded its tensile strength [34]. The ambient temperature and humidity variations controlled mainly the shrinkage of concrete. Transverse cracking of concrete bridge deck slabs commonly occurred in bridge superstructures after concrete hardens [8]. In addition, reinforcement bars created internal restraint and could limit transverse crack width as shrinkage and thermal changes generated tensile stress in concrete that exceeded the tensile strength of concrete. However, the internal restraint of reinforcement could be ignored or negligible compared with external restraints like adjoining members or the continuity of concrete bridge deck slabs that could cause restrained shrinkage cracking [35].

Restrained shrinkage cracking of concrete bridge deck slabs reinforced with steel bars had become a common problem in the United States (U.S.). Restraint to shrinkage could lead to cracking that is time-dependent, and gradually destroyed the positive influences of tension stiffening of concrete. Consequently, it made existing cracks be wider in concrete members [36]. According to a study carried out by Krauss and Rogalla [8], more than 100,000 bridges in the U.S. faced early-age shrinkage cracking problems.

Qiao *et al.* [37] studied the main factors of the early-age cracking in the bridge decks reinforced with steel bars. According to previous studies [38-40] these causes included low humidity and hot weather, low water-cementitious material ratio, improper mix design with high cement content or high quantity of water, restraint from deep longitudinal girders and their connections, low tensile strength of concrete, high modulus of elasticity of concrete, low creep properties, temperature differential between the newly-placed deck and supporting girders with different shrinkage rates, and high curing temperatures. In order to evaluate the causes that affected restrained shrinkage cracking of concrete, they conducted restrained shrinkage ring tests. Finally, shrinkage-reducing admixture (SRA) was recommended to minimize early-age shrinkage cracking. In addition, larger sizes of aggregates in concrete were also proposed to reduce shrinkage.

Gilbert [41] considered shrinkage cracking in fully restrained reinforced concrete (RC) members subjected to direct tension force resulted from dry shrinkage. The mechanism of shrinkage tension cracking was discussed. Some common misconceptions concerning the behavior of restrained concrete members were exposed. A reasonable analytical model was developed by Gilbert. He proposed equations (2) through (7) to determine the average crack width, spacing of cracks, and final stresses in reinforcing bars in crack.

$$s_0 = \frac{d_b}{10\rho} \tag{1.2}$$

where s_0 is that stresses in concrete and reinforcing bars are no longer affected directly by the presence of this crack, d_b is the bar diameter, ρ is the reinforcement ratio. The final tensile force, $N(\infty)$ due to shrinkage and temperature changes was given by

$$N(\infty) = -\frac{n^* A_s}{C_2}(\sigma_{av} + \varepsilon_{sh}^* E_e^*) \tag{1.3}$$

where $N(\infty)$ is the final tensile force, $n^* = E_s / E_e^*$, A_s is the area of reinforcement, σ_{av} is estimate of the average concrete stress in the period after first cracking, ε_{sh}^* is the final shrinkage strain, E_e^* is final effective modulus for concrete.

$$\sigma_{s2}^* = \frac{N(\infty)}{A_S} \tag{1.4}$$

where σ_{S2}^* is final stress of steel bar at the crack.

$$s \le \frac{2s_0(1+\xi)}{3\xi} \tag{1.5}$$

$$\xi = \frac{-n^* \rho(\sigma_{av} + \varepsilon_{sh}^* E_e^*)}{n^* \rho(\sigma_{av} + \varepsilon_{sh}^* E_e^*) + f_t} \tag{1.6}$$

where s is crack spacing, f_t is the tensile strength of concrete, ρ is the reinforcement ratio, the distance s_0 is that stresses in concrete and reinforcing bars are no longer affected directly by the presence of this crack.

$$w = -\left[\frac{\sigma_{c1}^*}{E_e^*}(s - \frac{2}{3} s_0) + \varepsilon_{sh}^* s \right] \tag{1.7}$$

where w is the final average crack width, σ_{c1}^* is final concrete stress away from the crack, $N(\infty)(1+C_2)/A_c \le f_t$. He gave some numerical examples. The predicted results were in accordance with observed cracking in restrained members.

Nejadi and Gilbert [42] found that shrinkage made transition zone between steel and concrete be deteriorative. As a result, the bond at the steel-concrete interface lessened gradually with time. Finally, the distance s_0 on each side of the crack, which the concrete and steel stresses were no longer affected by the occurrence of the crack, increased progressively with time. Therefore, for long-term study of shrinkage cracking, the value of s_0 should be multiplied by 1.33.

Nejadi and Gilbert [27] built eight longitudinally restrained concrete slabs reinforced with steel bars with different reinforcement layouts. The slabs were anchored at their ends by concrete blocks. These concrete blocks provided the restraint to shrinkage of slabs. They were considered to be immovable previously. These concrete members, however, also shrank with time. Therefore, a relative movement (Δu) of supports was considered in theoretical analysis. The ultimate average crack width, spacing of cracks, final stress of reinforcement in crack, and ultimate concrete stress away from crack were measured. Finally, they were compared with the theoretical results using the analytical model developed by Gilbert. They found that the final crack width, the crack spacing, and steel stress at each crack reduced with an increase in the steel area, and the concrete stress away from a crack increased with increasing the reinforcement ratio of concrete slabs.

The experimental and theoretical values were similar. However, they considered that crack width and crack spacing could not be predicted with any great accuracy using an analytical model because cracking in restrained reinforced concrete members was extremely variable.

There are some different methods to restraint the corrosion of steel reinforcement within concrete. They include (1) reducing the permeability of the concrete, (2) increasing the concrete cover outside the reinforcement, (3) using epoxy-coated steel reinforcement, (4) using the fiber reinforced polymer (FRP) reinforcing bars to replace the conventional steel reinforcement, etc. FRP has been applied to civil engineering due to corrosion resistance of FRP. The use of fiber reinforced polymer (FRP) bars can improve corrosion of steel due to their higher resistance to corrode. Ghatefar *et al.* [43] performed an experimental study on effect of different longitudinal reinforcement ratio (0.30, 0.50, 0.70, and 1.1%) on transverse early-age cracking of GFRP-RC bridge deck slabs (98.4 in. long x 30.1 in. wide x 7.1 in. thick [2,500 x 765 x 180 mm]). These slabs were fixed at their ends by 58.0 in. x 39.4 in. x 47.2 in. (1,473 x 1,000 x 1,200 mm) concrete blocks, which were fastened to the laboratory strong floor before casting. Crack width and strains in GFRP bars and concrete were measured. At the same time, a published model that Gilbert predicted restrained shrinkage cracking was utilized to calculate ultimate GFRP bar stress at the crack and crack width. They found that the average crack width at mid-span and strain in GFRP bars and concrete decreased when increasing reinforcement ratio. The measured final shrinkage crack width and stresses in GFRP bars were compared with the results of Gilbert analytical model. The errors were within 16%. The author's recommended that the coefficient of s_0 should be modified to 0.8 instead of 1.33 when GFRP bars replaced steel.

Ghatefar *et al.* [44] focused on the effect of different environmental conditions on early-age restrained shrinkage cracking of GFRP-RC bridge deck slabs with the reinforcement ratio of 0.7% recommended by the Canadian Highway Bridge Design Code 2006 [46, CHBDC 2006] for concrete bridge deck slabs reinforced with GFRP bars. The same dimension of concrete slab as that of Ghatefar *et al.* [43] was used. Two slabs reinforced with GFRP and steel bars were investigated under the laboratory condition. And two specimens reinforced with GFRP bars were experimented under

freezing-thawing and wetting-drying conditions. Crack widths, spacing of cracks, and strains in concrete and reinforcing bars were measured. Ultrasonic pulse velocity (UPV), Rapid chloride permeability (RCPT) tests and microstructural analysis were used to investigate degradation of concrete exposed to cyclic conditions. They found that the minimum reinforcement ratio of 0.7% satisfied the serviceability requirements. The results of material tests showed that there was some degradation of concrete exposed to cyclic conditions. At the same time, the theoretical model developed by Gilbert was used to predict crack widths and stresses in GFRP bars. The results illustrated that the experimental results were similar with those predicted by Gilbert analytical model within 17% error.

Although numerous researchers to study behavior of shrinkage cracking of concrete elements reinforced with steel and GFRP bars, their studies focused on early-age cracking behavior of GFRP concrete members. There are extremely limited data to evaluate restrained shrinkage cracking of FRP-RC members under long-term exposure to field environment. Further study, therefore, is needed in this area. This paper contributed an experimental study that investigated the effect of low longitudinal (secondary) GFRP reinforcement ratio on shrinkage cracking over 2400 days in fully restrained concrete element exposed to natural environment. This was the longest and one of only very few cracking studies on GFRP found in available literature. At the same time, a model that was developed by Gilbert initially was modified to predict the cracking behavior for GFRP panels.

2.2. THE DETERIORATION OF GFRP SYSTEMS

Early-age cracking of bridge deck slabs can increase penetration of harmful elements like chloride ions from deicing salts that result in corrosion of steel bars in concrete. The corrosion of steel reinforcement is a major problem with traditional steel reinforcement used in bridge decks. Although steel's natural tendency is to undergo corrosion reactions, the alkaline environment of concrete (pH of 12 to 13) provides steel with a period of corrosion protection. At high pH, a thin oxide layer forms on the steel and prevents metal atoms from dissolving. This passive film does not actually stop corrosion; it reduces the corrosion rate to an insignificant level. For steel in concrete, the

passive corrosion rate is typically 0.1 μm per year. Without the passive film, the steel would corrode at rates at least 1,000 times higher [45]. Due to the use of deicing salts, the chlorides penetrate the concrete and reach the steel reinforcement through cracks. They will attack the concrete surrounding the reinforcing bars, which makes the pH value of the concrete drop to around 10 or 11. They serve as the catalyst that breaks down the protective alkalinity layer around the reinforcing bars and allow oxygen and moisture to initiate the corrosion process. The corrosion of steel reinforcement can cause some undesirable consequences for reinforced concrete. First, the mechanical properties of steel will reduce like lower yield stress, and lower modulus of elasticity, which makes an engineer overestimate the capacity of reinforced concrete element. Second, the cross-sectional area of steel will decrease, and the corrosion by-product will expand. The expansion in volume will result in spalling of the concrete, which allows for more undesirable elements to penetrate the concrete and can cause safety problems.
FRP bars are applied to some concrete structures like deck slabs of bridges due to their performance of non-corrosion. Although GFRP bars cannot be corroded like steel bars, concrete structures reinforced with GFRP bars may be still susceptible to other forms of deterioration due to harsh environments involving deicing chemicals, sulfate salts and alkalis, which can readily infiltrate concrete through cracks [46]. A number of researchers, therefore, are paying close attention to the field and laboratory durability performance of FRP system.

In 2004, a major study by ISIS Canada was launched to obtained field data with respect to the durability of GFRP in concrete exposed to natural environment. This was the first reported field study and to date the only major longer-term field study outside of the work conducted herein jointly with the University of Miami. Concrete cores containing GFRP were removed from several 5- to 8-year-old exposed structures, and the GFRP was analyzed for its physical and chemical composition at the microscopic level. Direct comparisons were conducted between the control GFRP rods and in-service GFRP samples. Through the microscopic analysis, there is no any sign to indicate that in-service GFRP samples were corroded [47]. However, they did not perform experimental work on the bars mechanical properties.

Phelan *et al.* [48] focused on field instrumentation and short-term monitoring of Serrita de la Cruz creek bridge deck. Different types of instrumentation were installed by Texas Tech University on this bridge. The performance of GFRP bars were compared with the performance of the epoxy-coated steel in concrete deck. The short-term tests that were conducted included temperature measurements in the deck during and after a pour, crack mapping under no load and under static live loading, and deflection and strain measurements under static live loading. The GFRP-reinforced concrete decks showed very good short-term performance. The reported emphasized the importance to examine the long-term properties of FRP bars.

Chen *et al.* [49] researched accelerated aging tests of durability performance of FRP reinforcing bars. The authors conducted tensile strength testing of GFRP bars that were embedded in normal concrete, and then immersed in tap water solution at 20℃ and 60℃, respectively for 90 days duration in a laboratory setting. The loss in tensile strength were 10% and 39%, respectively.

Robert *et al.* [50] analyzed performance of GFRP bars embedded in moist concrete in a laboratory setting. They immersed mortar-wrapped GFRP bars in tap water. The conditioning used in the study was closer to field conditions because the FRP material is embedded in concrete which is the actual situation in the field. The specimens were completely immersed at three different temperatures (23, 40, and 50℃) and were removed from the water after 240 days duration. Tensile test was conducted. It can be seen that the losses of strength were 9%, 10%, and 16% at 23, 40, and 50℃, respectively.

Davalos *et al.* [51] studied the durability of GFRP embedded in concrete beams in a laboratory setting. Concrete beams with GFRP bars were immersed in tap water at different temperatures (20, 40, 50, and 60℃) to accelerate the attack of concrete environment on the beams. The tensile capacity retentions of GFRP bars embedded in concrete were about 93%, 80%, 68%, and 61% at 20, 40, 50, and 60℃, respectively after duration of 90 days. And the strength retentions of GFRP bars were about 85%, 68%, 50%, and 45% at the elevated temperatures above, respectively after 270 days exposure.

Dejke *et al.* [52] researched the performance of GFRP bars embedded in concrete as well, in a laboratory setting. The bars came from different manufacturers, and were embedded in concrete for up to approximately 600 days. Dejke found that the tensile

strength decreases with the increase of time and temperature. For one manufacturer, he reported that GFRP bars embedded in concrete and exposed to 68°F and 140°F (20℃ and 60℃) exhibited approximately 25 and 42% loss in tensile strength after 520 days. The authors also reported that another manufacturer's GFRP bars tested lost about 15 and 56% of their tensile strength after 528 days of embedment in concrete when the concrete beams were exposed to 68°F and 140°F (20℃ and 60℃), respectively.

Mukherjee *et al.* [53] focused on the properties of GFRP bars embedded in concrete beams in tropical environments. The beams with GFRP reinforcing bars were immersed in a 140°F (60℃) water tank for 3, 6, and 12 months. The GFRP bars contained E-glass and vinyl ester, the surface had a helically-wrapped E-glass and sand coating. In addition, some specimens reinforced with GFRP bars were also kept in the natural weather that a temperature range was from 50°F and 100°F (10℃ to 38℃) for 18 and 30 months duration. As a result, the reinforcing bars in concrete beams conditioned outdoors for 18 and 30 months lost their tensile strength by 34.6 and 38.6% respectively.

Trejo *et al.* [54] analyzed the long-term properties of GFRP bars embedded in concrete. These specimens were exposed to a natural environment for about 7 years. These GFRP-reinforced samples were made in 2000 and exposed to a mean annual temperature of 23℃. The minimum and maximum average daily temperatures were 41°F and 90°F (5℃ and 32.2℃) (in College Station, TX), respectively. Three different bar types (P, V1, and V2) with diameters of 0.625 in. (15.9 mm) and 0.75 in. (19.1 mm) were performed tensile tests. Bar type P was made with a polyethylene terephthalate Polyester matrix and E-glass fibers. Bar type V1 contained E-glass fiber embedded in a vinyl ester resin. This bar was made with external helical fiber wrapping and the surface of the bar was coated with fine sand. Bar type V2 was composed of E-glass fibers embedded in a vinyl ester resin and had a circular cross section coated with coarser sand. All of these GFRP samples lost their tensile strengths compared with the original those.

Dai *et al.* [55] studied the influence of moisture on the bond behavior of FRP sheets to concrete interfaces. Specimens underwent WD cycling in various exposure period. Two series of specimens were tested using direct pull-off bond test method. One series had dry concrete substrates treated with a normal primer FR-NS. The other had wet concrete substrates treated with a hydrophobic primer FP-WE7. It was seen that, before

exposure, both series exhibited similar interfacial tensile bond strength in spite of each having different initial moisture contents. Therefore, a conclusion can be obtained that initial moisture content of a concrete substrate may not be a major issue. There was a clear and rapid decrease in the tensile bond strength of FRP-to-concrete interfaces after eight months of exposure. However, further exposure of up to two years did not result in greater reductions in the bond strength between concrete and FRP.

2.3. DURABILITY BEHAVIOR OF CONCRETE MEMBERS REINFORCED WITH COMPOSITE MATERIAL SHEET

Over two hundred million trips are taken daily across deficient bridges in the nation's 102 largest metropolitan regions. In total, one in nine of the nation's bridges are rated as structurally deficient, while the average age of the nation's 607,380 bridges is currently 42 years. The challenge for federal, state, and local governments is to increase bridge investments by $8 billion annually to address the identified $76 billion in needs for deficient bridges across the United States. However, with the overall number of structurally deficient bridges continuing to trend downward, the grade improved to C+ (*The infrastructure in the system or network is in fair to good condition; it shows general signs of deterioration and requires attention. Some elements exhibit significant deficiencies in conditions and functionality, with increasing vulnerability to risk*). The percentage of bridges that are either functionally obsolete or structurally deficient has been declining slowly over the last decade as states and cities have increased efforts to prioritize repairs and replacements. In 2013, one in nine, or just below 11%, of the nation's bridges was classified as structurally deficient. However, while billions have been spent annually on bridge construction, rehabilitation, and repair in the last twenty years, current funding levels are not enough to repair or replace the nation's large-scale, urban bridges, which carry a high percentage of the nation's traffic. To illustrate, the nation's 66,749 structurally deficient bridges make up one-third of the total bridge decking area in the country, showing that those bridges that remain classified as structurally deficient are significant in size and length, while the bridges that are being repaired are smaller in scale [13].

Approximately one in seven of Missouri's 24,334 bridges are considered structurally deficient meaning load carrying members have been found in poor condition or the adequacy of the waterway opening is considered extremely insufficient. This ranks Missouri 41st in the percentage for this category and at 3,528 bridges ranks 47th in overall number. In addition, a similar percentage is considered functionally obsolete which indicates their design is outdated considering current standards. These categories combine to approximately 28% or 6,893 of the overall bridges are defined as deficient (structurally deficient or functionally obsolete) [14].

It was discovered that the majority of concrete bridges require repair within the first 11 to 20 years of their service lives. Only 50% of concrete repairs are deemed successful, with a 25% failure rate. This high failure rate is presumably due to the frequent use of concrete surface repair for a vast array of deterioration problems, regardless of whether the patch is appropriate. The same survey discovered that the concrete surface repair was successful only 45% of the instances for which it was implemented [56].

Fiber reinforced polymer (FRP) has become an avenue of repairing structurally deficient bridges. The advantages associated with such a repairing system over conventional strengthening techniques are (1) expected long-term durability, (2) short construction times, and (3) negligible traffic disturbances. In addition, the durability and lightweight properties of FRP materials have led to their implementation in new bridge construction [23].

There are some current composite strengthening techniques available that are used to repair structurally deficient bridges. They include manual FRP lay-up, pre-cured laminate plates, near surface mounted (NSM) bars, steel reinforced polymer (SRP), and mechanically fastened FRP. These strengthening methods have their own advantages and shortcomings.

Huang *et al.* [57] studied the properties and application of steel reinforced polymer (SRP). First of all, the mechanical properties of SRP were evaluated experimentally and compared to micromechanical equations to determine a suitability of these equations for the prediction of materials constants. The properties of SRP can be accurately predicted by mechanics of materials using micromechanics models. Second,

the tests on the effectiveness of SRP reinforcement in concrete beams of existing structures were performed in Clayton, MO. Four strips (beams) were cut out of the deck of a parking garage. There was no strengthening on the surface of Beam 1. For Beam 2, there were two plies of CFRP reinforcement in positive moment region. Beam 3 had two plies of CFRP reinforcement in both the positive and negative moment regions. For Beam 4, one ply of SRP reinforcement and two plies of CFRP reinforcement were applied to negative moment region and positive moment region, respectively. The research illustrated that both CFRP and SRP strengthening systems increased the ultimate capacity of the beams. The flexural stiffness of the beams was also significantly improved.

Wobbe *et al.* [21] analyzed the flexural capacity of RC beams reinforced with steel reinforced polymer (SRP) and steel reinforced grout (SRG) in the lab. Four beams were cast including two SRP specimens, one SRG specimen, and one control beam. Four-point beading test was conducted. The load, mid-span deflection, and strain of matrix were measured. When in comparison with the control specimen, all three specimens strengthened by the SRP and SRG presented a much higher level of ultimate strength. This research proved that this strengthening technology has great potential for the improvement of existing reinforced concrete structures.

Lopez *et al.* [58] studied the field performance of a reinforced concrete bridge (P-0962) reinforced with steel reinforced polymer (SRP). A comprehensive study addressing analysis, design, installation, load rating and monitoring of this bridge strengthened with this technology was reported. Load tests were performed to evaluate the bridge structural behavior before and after the strengthening. Deflections were measured at several locations. There is a decrease in deflection after the application of the SRP strengthening system. This illustrated an initial good performance of this technology. However, the long-term performance needs to be monitored.

Myers *et al*. [23] summarized and studied long-term strengthening performance of five bridges in the state of Missouri (i.e. T-0530, X-0495, X-0596, P-0962, and Y-0298). Table 2.1 illustrates the type, amount, placement location and flexural capacity gained by adding the strengthening reinforcement to the girders of the load tested spans.

Table 2.1. Composite strengthening on tested spans

Bridge & tested span	Girder	Flexural reinforcement description	Analytical capacity increase
X-596 span 2	Interior	Manual lay-up: 4 plies 20-in. wide (4) NSM bars	42%
	Exterior	None	N/A
T-530 span 2	Interior	1 laminate plate: 12-in. wide	29%
	Exterior	1 laminate plate: 12-in. wide	15%
X-495 span 2	Interior	Manual lay-up: 5 plies 20-in. wide	40%
	Exterior	None	N/A
P-962 span 1 & 2	Interior	Manual lay-up: 5 plies 16-in. wide (4) NSM bars	56%
	Exterior	Manual lay-up: 3 plies 16-in. wide	25%
P-962 span 3	Interior	SRP 3 x 2: 3plies 16-in. wide	54%
	Exterior	SRP 3 x 2: 3plies 16-in. wide	49%
Conversion Units: 1 in. = 25.4 mm			

Load testing represented an imperative step in validating the effectiveness of FRP composites in the field. The first series of load tests began in July of 2003 and have been conducted semi- annually since, once each fall and each spring with the final series of testing taking place during the spring of 2008. The deflection of the girders from each pass was determined by taking the difference between the baseline and the recorded stop elevations. Because the temperature increase resulted in a thermal camber of the bridge, which was apparent in subtracting the elevation of the final no load test from the initial no load test, temperature readings were recorded with a temperature gun. Some conclusions can be drawn from this research: (1) The apparent increase in stiffness achieved by adding FRP strengthening is primarily attributed to the restraint of concrete cracks from opening, (2) There was a decrease in deflection and a subsequent apparent increase in stiffness for bridges T-530 and P-962 due to strengthening, (3) For Bridges X-495 and X-596, it is difficult to quantify the apparent increase in stiffness due to strengthening with load testing. This is due to a lack of flexural strengthening of the exterior girders, and (4) based on the visual inspections to date, the SRP system exhibited signs of steel corrosion and was the worst observed strengthening deterioration for any system used.

Phillis *et al.* [59] used CFRP U-Wraps and CFRP Near Surface Mounted (NSM) bars to study the shear strength of PC bridge tee-girders and compare the two systems to

each other. The CFRP U-Wraps were attached by externally bonding strips to the web of the girder. The NSM bars were installed by cutting grooves in the web of the girders and embedding the bars in epoxy paste. According the testing results, both the U-Wrap and NSM bar shear-strengthened girders showed a capacity equal to or exceeding that of sufficient girders. This would give engineers confidence to use the two strengthening systems in field application.

Laboratory tests and field applications have illustrated that externally bonded composite materials can efficiently improve load-carry capacity of existing structures. Short-term behavior of composite strengthening system has been studied. However, research of the long-term performance of these composite strengthening systems is incomplete. The problems of durability remain unanswered.

Gartner *et al.* [60] analyzed tests methods used to bond between FRP composites and concrete. The objectives of this research were to develop a test method that (1) can be used to evaluate the durability of the FRP-concrete bond (adhesion failure mode); (2) facilitate multiple replicate for statistical validation; (3) is simple to conduct; and (4) provides comparative results that are easy to interpret. By summarizing and analyzing the shortcomings of single shear, direct tension, peel test, and double shear test, it was decided that a small beam test modeled after the ASTM flexural strength test method would be the best compromise. The standard test configuration was adopted for the CFRP test beam. Three main changes were (1) a saw cut was added in the tension side of the beam at midspan; (2) a strip of CFRP composite was added to the tension face of the beam; (3) three-point bending test was conducted. Based on the test results, some characteristics were found to be the most suitable for use in the bond test: (1) Loading: three-point loading over a 12 inches (305mm) span; (2) Beam size: 4 inches x 4 inches x 14 inches (100mm x 100mm x 356mm) with a half-depth saw cut at midspan. (3) If the durability of the FRP composite bond is being evaluated, then an adhesive failure mode would be desirable.

Deng *et al.* [19] studied the durability performance of concrete beams externally strengthened by carbon fiber reinforced polymer (CFRP). Plain concrete beams were cast. A half-depth, 0.125 inch (3 mm) wide saw-cut at the middle of a beam was cut. This saw-cut simulated a wide flexural crack, maximized environmental exposure at the point

of maximum moment, and focused the location of failure. CFRP laminate strips with dimensions of 8 inches x 1 inch (200 x 25 mm) were bonded to the beam using different types of resins. The external strengthening system was centered on the tension side of the flexural specimen. Five CFRP composite systems (A, B, C, D, and E) were used. These specimens were subjected to different environmental conditions including elevated-temperature water, different relative humidity levels, wet-dry cycles, and real-time exposure for several days, and then three-point bending test was conducted. In all tests, performance of CFRP strengthening systems deteriorated with time. However, greater strength loss occurred as the exposure temperature increased.

Ekenel *et al.* [61] focused on the fatigue performance of RC beams reinforced with CFRP under environmental conditioning and sustained load. Two groups CFRP specimens were fabricated. The first group specimens were stored in the lab. The second group specimens were put into an environmental chamber. One pair of samples was maintained in the chamber conditioned four environmental cycles. A second pair of specimens was conditioned similarly except for eight environmental cycles. One cycle was made up of 50 freeze and thaw cycles between -18 and 4°C; 60 extreme temperature cycles between 27 and 49°C; 120 relative humility cycles between 60% and 100%; and UV light exposure during high-to-low temperature cycles. Test results indicated that fatigue resistance of RC beams is improved by strengthening with CFRP fabrics, and environmental conditioning and sustained load significantly affected the flexural stiffness of these specimens.

3. STUDY OF TOPIC 1

3.1. GENERAL

This section discusses the completion of a long-term Missouri University of Science and Technology (Missouri S&T)-University of Missouri-Rolla (UMR) shrinkage cracking study on panels reinforced with steel and GFRP bars. A numerical model of shrinkage cracking was built. Then, smaller panels were cut from the original panels in non-cracked regions. At same time, the longitudinal properties of the GFRP rebars that were extracted from these panels were evaluated. Microscopic examinations including digital microscope investigations, scanning electron microscopy (SEM), and energy dispersive X-ray spectroscopy (EDS) analyses were examined to investigate whether GFRP rebars were deteriorative in concrete from the in-situ environmental conditioning. It should be noted that the stress level in these bars were higher than traditional GFRP stress levels due to the low reinforcement ratio in this secondary reinforcement study. In addition, NO salts or chlorides were every applied to the surface of the panels. This was essentially a long-term field study with higher than traditional stress level in the bars (i.e. representative of secondary reinforcement stress levels with high restraint level) and highly varying thermal and moisture conditions. A highly unique study both in terms of conditions and longevity.

3.2. OUTLINE

This project was originally initiated under the Center for Infrastructure Engineering Studies (CIES) and the Department of Civil, Architectural, and Environmental Engineering at Missouri University of Science and Technology. One steel and five GFRP reinforced concrete panels with varying widths of panels were constructed by Branham and Myers in 2005. The first specimen (Panel P-1) was reinforced with Grade 40 steel reinforcement. The other five specimens (Panels P-2 through P-6) were reinforced with 110 ksi (758.4 MPa) embedded GFRP reinforcement. The panels ID with reinforcement and panels' size details are described in Table 3.1.

Table 3.1. Panel dimension and reinforcement ratio [29]

Panel ID	Rein. Type	Rein. Area (in.^{2})	Length (in.)	Width (in.)	Depth (in.)	Rein. Ratio (%)
P-1	Steel	0.22	360	24.44	5	0.18
P-2	GFRP	0.261	360	29.04	5	0.18
P-3	GFRP	0.261	360	23.76	5	0.22
P-4	GFRP	0.261	360	15.84	5	0.33
P-5	GFRP	0.261	360	11.88	5	0.44
P-6	GFRP	0.261	360	9.51	5	0.55
Conversion Units: 1 in. = 25.4 mm, 1 in.^{2} = 645.16 mm^2						

The first stage of this study was completed by Branham and Myers in 2006 [29]. The shrinkage cracking behaviors, patterns, and crack widths of six panels were analyzed for one year. The second phase of this research was finished by Myers and Golden in 2007 [30]. The shrinkage cracking patterns and crack widths of the six GFRP-reinforced concrete panels were summarized for two years.

The panels were fabricated at a span length of 30 feet (9.1 m) consisting of four spans of 7.5 feet (2.3 m) and a depth of 5 in. (127 mm). Interior supports consisted of three roller supports, while the two ends of the panel were fixed by two concrete blocks to restrain the axial movement with respect to the panels. All panels were constructed outside and exposed to the ambient environment to investigate shrinkage and temperature crack development over time. Figure 3.1 illustrates the profile view of a panel. Figure 3.2 shows the cross section and reinforcement placement for panel.

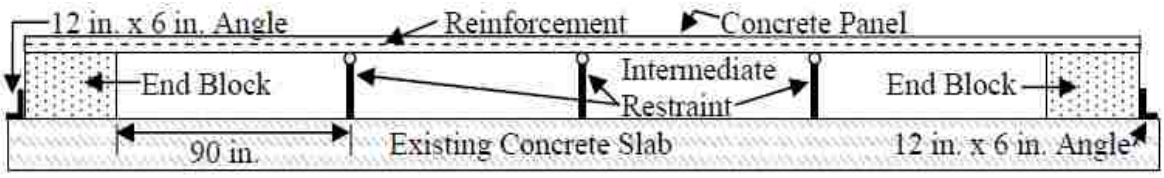

Conversion Units: 1 in. = 25.4 mm

Figure 3.1. Profile view of a panel [29]

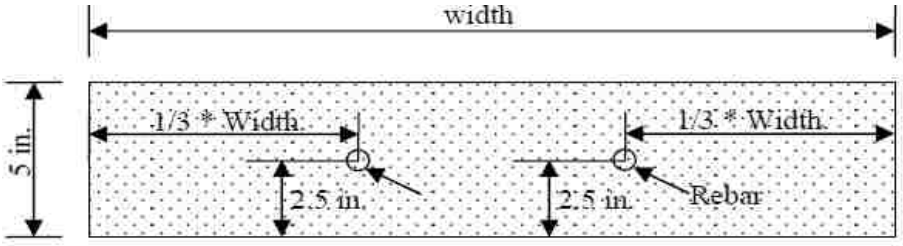

Conversion Units: 1 in. = 25.4 mm

Figure 3.2. Cross section for panels [29]

Steel and GFRP bars used for shrinkage and temperature reinforcement were investigated under this project, including:

1) Long-term shrinkage behavior of GFRP-reinforced panels. The objectives of this part are to investigate shrinkage and temperature crack development of panels, and determine a theoretical model based on Gilbert analytical model to estimate the cracking behavior of fully restrained concrete members reinforced with FRP bars for long-term exposure to field environment.

2) This section includes a uniaxial longitudinal tensile strength test of GFRP bars. Its objectives are to evaluate the residual capacity after long-term exposure to natural environment and analyze whether the physical characteristics of GFRP bars changed in any discernible fashion with time when exposed to field environment.

3) Microstructural analysis of samples with GFRP bars extracted from panels exposed to an exterior environment and seasonal thermal changes for almost eight years. It includes optical microscopic images analysis, scanning electron microscope (SEM) analysis, and energy dispersive X-ray spectroscopy (EDS) analysis. The objective of this section is to investigate whether the GFRP rebars deteriorated when exposed to an exterior environment in concrete.

Within the study, the research team examined crack development over time relative to varied reinforcement ratios to address the issue of developing a minimum temperature and shrinkage reinforcement for FRP reinforced members in the ACI 440 design code. The study also exposed a new reinforcement material, GFRP, to outdoor conditioning and seasonal changes over multiple years, serving as a test bed for exposing

the GFRP bars to real-world field thermal exposure in the presence of minimal live loading.

3.3. PREVIOUS WORKS OF THIS STUDY

In this original project, a 4,000 psi (27.58 MPa) conventional concrete mix design was used to fabricate these concrete reinforced panels as illustrated in Table 3.2. The ratio of water to cement was 0.5. The average slump of concrete was 4.5 in. (114.3 mm).

Table 3.2. The mix design of concrete used in this study [29]

Components of Concrete	Mix Design (lb/yd^3)
Type I Portland Cement	564
Coarse Aggregate	1678
Fine Aggregate	1340
Water	282
Conversion Units: 1 in. = 25.4 mm, 1 lb/yd^3 = 16 kg/m^3	

The concrete compressive strength tests were determined at different ages as shown in Table 3.3. The ready-mixed concrete was delivered and placed on site during fabrication.

Table 3.3. The compressive strength of concrete at different time [29]

Concrete Ages (days)	Average Compressive Strength (psi)
1	1840
7	3530
14	3560
21	3820
28	3850
Conversion Units: 1 psi = 0.0069 MPa	

Although a fully fixed-fixed condition was a challenge to achieve under field conditions (i.e. the highest restraint level physically possible), the best efforts were taken to create continuity and fixed end conditions to simulate the highest level of panel

restraint. Each fixed end-support was a concrete block that was consisted of 2 feet wide (0.610 m), 3 feet long (0.914 m), and 2 feet deep (0.610 m). Each panel consisted of four reinforcement bars. Two reinforcement bars made up the reinforcement section for each side of the panel. The reinforcement was space at 1/3 the width and 1/2 the depth of the beam. The reinforcement was spaced 1 in. (25.4 mm) from the back of the end block and had a splice length of 4 feet 2 in. (1.3 m) at the mid-span of the panel. No. 3 reinforcing bars were used. Tables 3.4 and 3.5 illustrate the properties of reinforcement bars. The panels were monitored for shrinkage cracking throughout the duration of the study. The crack widths were measured with a crack scope.

Table 3.4. Steel reinforcement material properties [29]

Bar Number	Diameter (in.)	Area ($in.^2$)	Grade	f_y (psi)	f_u (psi)
3	0.375	0.11	40	50,019	75,343
Conversion Units: 1 in. = 25.4 mm, 1 $in.^2$ = 645.16 mm^2, 1 psi = 6.895 kPa					

Table 3.5. Aslan 100 GFRP rebar reported design properties [29]

Bar Number	Diameter (in.)	Area (in^2)	f_{fu} (psi)	E_f (psi)
3	0.375	0.1307	110,000	5.92×10^6
Conversion Units: 1 in. = 25.4 mm, 1 $in.^2$ = 645.16 mm^2, 1 psi = 6.895 kPa				

The initial phase of this study (from Day 1 to Day 203) was completed by Branham and Myers [29]. During the initial study period, the first sign of cracking was observed at day 13. There were four panels (panels P-2, P-4, P-5, and P-6) cracked 13 days after casting. Each panel appeared one crack that extended the full width of the panel and propagated over the full depth of the panel. The cracks in panels P-2, P-4, and P-5 were located at the exterior support. The crack widths were 0.0085 in. (2.159 mm), 0.0046 in. (0.01684 mm), and 0.00197 in. (0.05004 mm), respectively. The crack in panel P-6 was located 13.5 in. (342.9 mm) from the support and measured 0.00197 in. (0.05004 mm) in width. The crack in panel P-1 was first observed 28 days after casting and measured 0.000656 in. (0.01666 mm) in width. The crack in P-1 was located at the exterior support and was a full depth crack that extended approximately 1/3 of the width

in from each side, leaving the middle third of the panel uncracked. The first crack in panel P-3 was observed 19 days after casting. The crack was a full depth full crack located 1.5 in. (38.1 mm) from the exterior support. This crack width was 0.00394 in. (0.100076 mm). Panel P-6 developed a second crack at 64 days on the opposite side of the first crack. This second crack in panel P-6 measured 0.00197 in. (0.05004 mm). A second crack was observed in panel P-3 at 203 days from casting. This crack had a width of 0.00197 in. (0.05004 mm). At 203 days, a second crack was also observed in panel P-5, the width was 0.00197 in. (0.05004 mm). This second crack in panel P-5 was on the opposite side of its first crack.

The GFRP panels at tested reinforcement ratios yielded maximum and average percentages of crack areas that were larger than the steel reinforced panel. P-2 (GFRP, ρ=0.18%) had a maximum crack width 225% and an average percentage crack area 282% greater than the steel control. P-3 (GFRP, ρ=0.22%) had a maximum crack width 100% and an average percentage crack area 312% greater than the steel control. P-4 (GFRP, ρ=0.33%) had a maximum crack width 125% and an average percentage crack area 335% greater than the steel control. P-5 (GFRP, ρ=0.44%) had a maximum crack width 100% and an average percentage crack area 210% greater than the steel control. P-6 (GFRP, ρ=0.55%) had a maximum crack width 75% and an average percentage crack area 345% greater than the steel control panel [29].

During the second study period (at 762 days), two new cracks in panel P-2 were observed at second intermediate roller support and near right fixed end block, respectively. Panel P-4 appeared a new crack that was closed to the left exterior support. Panel P-5 developed a new crack near the third intermediate roller restraint. There were no new cracks in other panels. Average crack widths of these panels in this stage were greater than those in the first phase study. The maximum average crack width was 0.0237 in. (0.602 mm) that was observed in panel P-2. The minimum average crack was observed in panel P-5, the crack width was 0.0053 in. (0.135 mm), as illustrated in Table 6. During the original study period, crack measurements ranged in width from 0.00026 in. (0.0066 mm) to 0.0085 in. (0.216 mm). Crack widths for the second study period ranged from 0.004 in. (0.102 mm) to 0.039 in. (0.991 mm), a 93.3% and 78.3% increase from the original minimum and maximum, respectively [30].

3.4. CURRENT STUDY OF THIS RESEARCH

This section focuses on the study of cracking behavior in concrete panels and physical and microstructural analyses of GFRP samples extracted from these panels.

3.4.1. Long-term Shrinkage Cracking Behavior in Concrete Panels.

Shrinkage of concrete is the reduction of volume caused by loss of water during the drying process (drying shrinkage) and also by chemical reactions of hydration of cement paste (endogenous shrinkage or autogenous shrinkage). Concrete structure is free to contract if shrinkage is not restrained. As a result, shrinkage has little consequence, but this is hardly the situation in concrete structures. The bonded reinforcement in concrete structures provides restraint to shrinkage. The reinforcement imposes a tensile force on the concrete at the level of the reinforcement when the concrete shrinks. At the same time, the reinforcement produces an equal and opposite tensile force on the concrete at the level of the reinforcing bars. This internal tensile restraining force is often significant enough to cause cracking of concrete members. In addition, connections provide restraint to shrinkage if a concrete member is connected to other parts of the structure or to the foundations. The tensile restraining force can develop rapidly with time at the restrained ends of the member, which results in cracking. Thin floor slabs and walls in buildings are particularly prone to significant cracking resulting from restrained shrinkage and temperature changes [27].

In addition, reinforced concrete (RC) structures with high surface-to-volume ratios such as bridge deck slabs, concrete pavements, and parking garages form easily transverse cracks due to restraint to shrinkage of concrete. Because bridge deck slabs are typically much longer in one direction than the other, volumetric changes of concrete due to shrinkage and thermal changes are more pronounced in the longitudinal direction. In slab-on-girder bridges, the girders and continuity of slabs restrain the movement of deck slabs due to shrinkage and thermal changes, which induces stresses that result in transverse cracks. Shrinkage is greatest at the surface of a concrete member when exposed to a dry environment and decreases gradually towards the interior of the member. The resulting differential shrinkage across the member's cross section produces tensile stresses near the drying surface that may lead to surface cracking [27]. In restrained concrete members, cracks generally penetrate over the full depth of members'

cross sections. The width of a crack depends on the quantity, orientation, and distribution of the reinforcing bars crossing the crack. The bond characteristics between concrete and reinforcement bars also can influence the width of the crack.

Full-depth cracks are generally considered the most severe form of bridge deck slab cracking. Due to the use of deicing salts, the chlorides penetrate the concrete and reach the steel reinforcement through cracks. They will attack the concrete surrounding the reinforcing bars, which makes the pH value of the concrete drop. They serve as the catalyst that breaks down the protective alkalinity layer around the reinforcing bars and allows oxygen and moisture to initiate the corrosion process. The corrosion of steel reinforcement can cause some undesirable consequences for reinforced concrete. Therefore, non-metallic and non-corrodible glass fiber reinforced polymer (GFRP) bars have been developed due to their comparable cost (to epoxy coated steel), higher tensile capacity, and lower weight to decrease the corrosion problem of conventional reinforcing steel. GFRP bars, however, have relatively lower modulus of elasticity than steel bars, which can result in wider cracks in concrete structures reinforced with GFRP bars. Although GFRP bars cannot be corroded like steel bars, GFRP-RCs are still susceptible to other forms of deterioration due to harsh environments involving deicing chemicals, sulfate salts, and alkalis, which can readily infiltrate concrete through cracks [46].

The availability of data on long-term restrained shrinkage cracking in RC members is extremely limited. The final purpose of this research, therefore, is to examine the crack width and observe the development patterns of the cracks in concrete panels reinforced with GFRP bars over seven years, investigate the effect of different sizes of panels with low GFRP longitudinal reinforcement ratio on long-term shrinkage cracking under field environment, find a more reasonable reinforcement ratio of GFRP-reinforced concrete for shrinkage and temperature reinforcement, and predict crack width using a published analytical model [41].

Although numerous researchers have studied the behavior of shrinkage cracking of concrete elements reinforced with steel and less so with GFRP bars, their studies focused on early-age cracking behavior of steel and GFRP concrete members. There is no reported long-term data (> 2 years) to evaluate restrained shrinkage cracking of FRP-RC

members under long-term exposure to field environments. Further study, therefore, is needed in this area.

This section contributes an experimental study that investigated the effect of low longitudinal (secondary) GFRP reinforcement ratio on long-term shrinkage cracking in fully restrained concrete elements exposed to natural environment. At the same time, a numerical model that was initially developed by Gilbert was modified to predict the cracking behavior for GFRP panels.

3.4.1.1 Data acquisition. The final crack widths were measured with a crack scope (CS-100 Crack Scope manufactured by PEAK). The crack scope had a 25x magnification, and measured to an accuracy of 0.004 in. (0.1 mm). The lens of the crack scope stood 1 in. (25.4 mm) from the surface of the concrete, and had manual focus for better clarity in viewing the crack. On the top of the panels, five measurements were taken along the length of each crack. The five measurements were then averaged for the final average crack width.

3.4.1.2 Experimental results and discussion. This section exhibits the crack patterns and crack widths of all panels.

3.4.1.2.1 Crack patterns of the panels. Because there were three times as much concrete that tended to shrink in the longitudinal direction than in the transverse direction [31], restrained shrinkage cracks developed in the transverse direction of the panels in order to relieve the larger tensile stress due to restrained end blocks in the longitudinal direction. Cracks propagated over the full depth of the panels when observing cracking in the panels after exposure of seven-year field environment. These cracks appeared at or near restrained end supports or intermediate supports, as can be seen in the following figures. Also, the majority of the cracks appeared in the original and second study period (762 days); only three new cracks were observed in panels P-3, P-4, and P-6, respectively in final study phase. There was still only one crack in panel P-1 during these years. When observing the crack patterns for these panels, it should be noted that the center support for panel P-2 was damaged, which may have affected the results. The following Figures 3.3 through 3.8 illustrate the various crack patterns and locations of the cracks observed in the last stage.

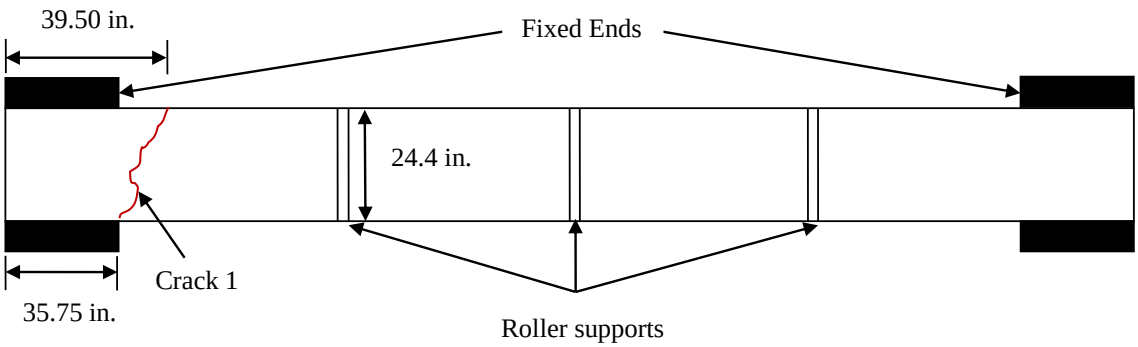

Conversion Units: 1 in. = 25.4 mm

Figure 3.3. Panel P-1 (Steel, ρ=0.18%)

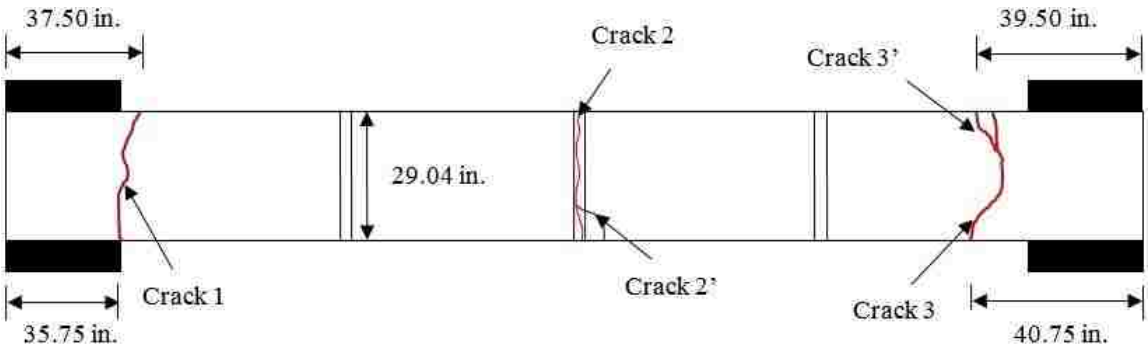

Conversion Units: 1 in. = 25.4 mm

Figure 3.4. Panel P-2 (GFRP, ρ=0.18%)

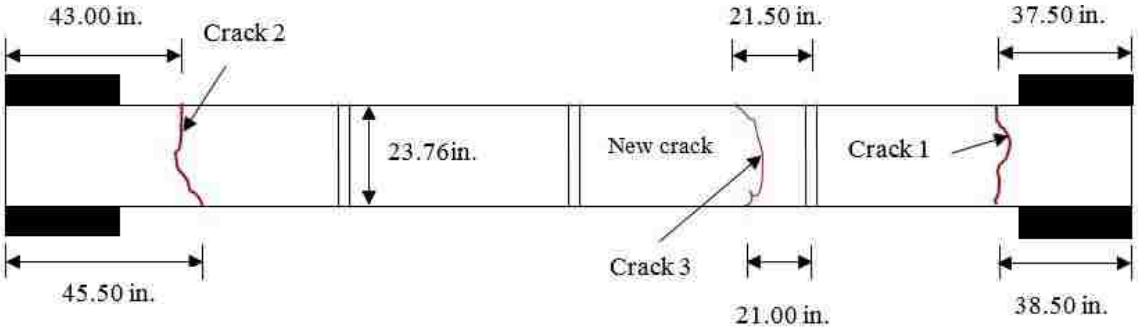

Conversion Units: 1 in. = 25.4 mm

Figure 3.5. Panel P-3 (GFRP, ρ=0.22%)

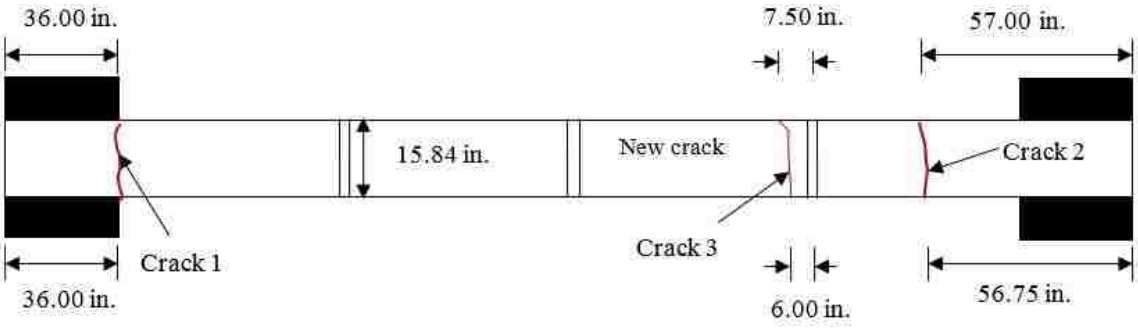

Conversion Units: 1 in. = 25.4 mm

Figure 3.6. Panel P-4 (GFRP, ρ=0.33%)

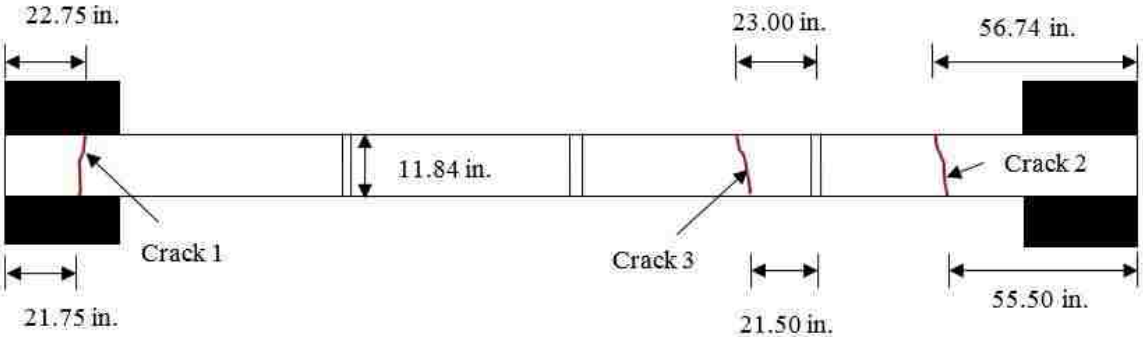

Conversion Units: 1 in. = 25.4 mm

Figure 3.7. Panel P-5 (GFRP, ρ=0.44%)

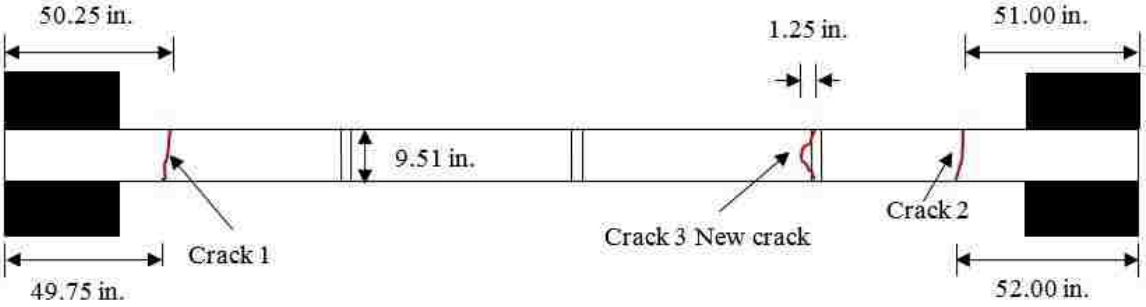

Conversion Units: 1 in. = 25.4 mm

Figure 3.8. Panel P-6 (GFRP, ρ=0.55%)

Because this study involved GFRP reinforced concrete panels at the secondary reinforcement level (low levels of reinforcement), the GFRP bars in panels 2 through 6 were subjected to sustained stress levels throughout the exposure conditioning due to the dead load weight of the panels. The maximum positive and negative moments due to the self-weight of concrete and cracking moments of these panels are illustrated in Table 3.6. The distributed moment and shear stresses were maximum values at the restrained concrete supports and interior roller supports on these panels, the maximum tensile stresses occurred at the interior and exterior supports, and were equal. In addition, axial restraining forces N(t) induced by the restrained shrinkage and temperature changes of these concrete panels caused the highest level of tensile stress at the exterior support of the panel. This helps to explain that all six of the tested panels cracked at or near the exterior and interior supports. Sustained stress, moisture and temperature are among the three exposure conditions that are reported to affect GFRP durability behavior most significantly [136].

Table 3.6. Sustained maximum moments due to self-weight and cracking moments

GFRP Panel	Max. Negative Moment (in-lb.)	Max. Positive Moment (in-lb.)	Cracking Moment (in-lb)
Panel 2	-8,505	4,252	56,309
Panel 3	-6,959	3,479	46,071
Panel 4	-4,639	2,320	30,714
Panel 5	-3,479	1,740	22,958
Panel 6	-2,782	1,391	18,440
Conversion Units: 1in. = 25.4 mm; 1 lb = 0.454 kg			

It should be noted from Table 3.6 that the self-weight of these GFRP panels cannot alone induce cracking of concrete because the cracking moments are greater than the maximum moments caused by self-weight. It can be concluded that these panels were not subjected to significant bending in which restraint was provided to the longitudinal movement induced by shrinkage and temperature changes. In general, these cracks are called direct tension cracks because they were induced by axial tension force rather than flexural tension. Restrained drying shrinkage, therefore, was a major factor inducing

cracking of these panels. When the concrete panels shrank, the axial tensile restraining forces developed with time. As a result, cracks formed in these concrete panels due to the restraint of end concrete blocks that restrained free volumetric changes of the panels when the concrete stress caused by N(t) at a particular cross section first reached the direct tensile strength of concrete.

3.4.1.2.2 <u>Crack widths and changes over time.</u> During the final observation, the average crack widths for panels P-1 through P-6 were higher than the values measured in the second study period. The maximum average crack was formed in panel P-2, the width was 0.0587 in. (1.491 mm). Panel P-5 appeared the minimum average crack of 0.0289 in. (0.734 mm). Table 3.7 illustrates the ultimate average crack widths and crack numbers in different study period.

Table 3.7. Average crack width and crack numbers at different time

Panel	At 203 days		At 762 days		At 2400 days	
	Ave. crack width (in.)	Crack No.	Ave. crack width (in.)	Crack No.	Ave. crack width (in.)	Crack No.
P-1	0.00197	1	0.0076	1	0.0308	1
P-2	0.00394	1	0.0237	3	0.0587	3
P-3	0.00295	2	0.0070	2	0.0350	3
P-4	0.00328	1	0.0074	2	0.0351	3
P-5	0.00295	2	0.0053	3	0.0289	3
P-6	0.00263	2	0.0066	2	0.0357	3
Conversion Units: 1 in. = 25.4 mm						

Panel P-1 (steel, width = 24.4 in.) appeared a relatively small final crack width when comparing these results for these six panels, as shown in Table 3.7 and Figure 3.9. Due to higher stiffness of steel reinforcing bars than GFRP reinforcement, higher internal tensile stresses in panel P-1 will develop due to internal restraint against concrete shrinkage or temperature variations, which leads to a relatively small ultimate average crack width in panel P-1. At the same time, panel P-2 illustrated the maximum average crack width compared with those results of panels P-3, P-4, P-5, and P-6. The reason is that the dimension for panel P-2 is the biggest, and the reinforcement ratio of this panel is the smaller than those counterparts of the other GFRP panels.

The maximum crack widths measured for panels P-1 through P-6 in the initial (at 203 days), second (at 762 days), and final studies (at 2,400 days) are shown in Table 3.8. Figures 3.9 and 3.10 illustrate the comparisons of the final average crack widths and maximum crack widths from panel P-1 to panel P-6 at the different stages of inspection.

Table 3.8. The maximum crack widths at different time (in.)

Panel	1-203 (day)	762 (day)	2,400 (day)
P-1	0.00263	0.016	0.039
P-2	0.00853	0.039	0.087
P-3	0.00525	0.012	0.067
P-4	0.00591	0.012	0.055
P-5	0.00525	0.010	0.043
P-6	0.00459	0.010	0.073
Conversion Units: 1 in. = 25.4 mm			

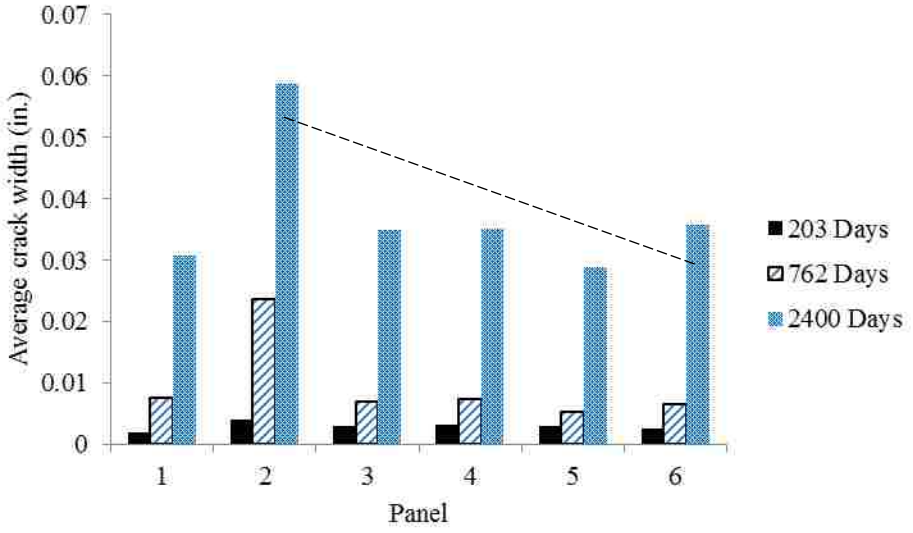

Conversion Units: 1 in. = 25.4 mm

Figure 3.9. The comparison of total average crack widths

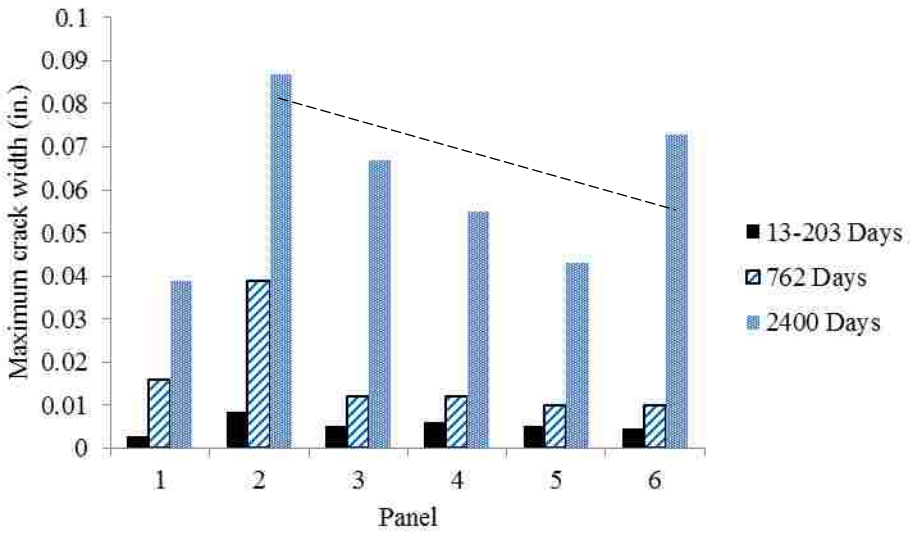

Conversion Units: 1 in. = 25.4 mm

Figure 3.10. The comparison of maximum crack widths

From Tables 3.7 and 3.8, panel P-1 (steel, ρ=0.18%) shows the final average and maximum crack widths increase of 1463% and 1383% from the original measurement to ultimate value, respectively. The final average and maximum crack widths in panel P-2 (GFRP, ρ=0.18%) have increased 1390% and 920% in ultimate study stage, respectively. Panel P-3 (GFRP, ρ=0.22%) has an average crack width of 1086% and a maximum crack width of 1176% when comparing the ultimate measurement with the initial result. Panel P-4 (GFRP, ρ=0.33%) illustrates that the ultimate average crack and maximum cracking value have increased 970% and 831%, respectively. The increases of the final average and maximum crack width in panel P-5 (GFRP, ρ=0.44%) are 880% and 719%, respectively. Average crack width in panel P-6 (GFRP, ρ=0.55%) has increased 1257%, and the maximum crack width increases 1490% in the final measurement. Therefore, it can be concluded that the rate of crack width development is the lowest in panel P-5.

According to the Figures 3.9 through 3.10, the final average crack width and maximum crack width are the smallest in panel P-5 (GFRP, ρ = 0.44%) at 2400 days when the panels are reinforced with GFRP bars. This can illustrate that the reinforcement ratio of panel P-5 may be of a reasonable shrinkage and temperature one.

In addition, it should be noted that crack widths increase constantly with time. It may be explained by the following:

(1) GFRP bars are susceptible to attack under exposures to moisture, alkaline solutions and elevated temperature. In addition, it is well known that the coefficients of thermal expansion (CTE) of FRP bars are different in the longitudinal and transverse directions. The longitudinal CTE, depending on fibers, is lower than that of concrete, while the transverse CTE, depending on matrix, is about 3-6 times larger than that of concrete [62]. GFRP can experience an expansion of 4-6 times greater than that of concrete in the transverse direction due to temperature variations. As a result, an increase in temperature produces bursting stresses within the concrete surrounding the reinforcement, which may cause splitting cracks or debonding of GFRP bars from concrete. This fact involves a degradation of the bond between concrete and reinforcement, affecting the structural response [63]. Moreover, under freezing-thawing cycles, ice formation at the interface between GFRP and concrete leads to further loss of the FRP bond to concrete and increase existing crack width under sustained loads (self-weight) [64]. Additionally, volume changes may result in material fatigue and debonding of reinforcement due to repetitive shrinkage and swelling when the concrete surrounding GFRP bars subject to wetting-drying conditions in the vicinity of the main crack [65, 66]. These appear as micro-cracks generally naked to the eye. Their stiffness will decrease greatly. In addition, cracks are the easiest location for moisture and aggressive chemicals to accelerate the deterioration of reinforcement as well as to reduce the service life of concrete structures [44]. The cracks on the panels extended through the height and width of the panels. This creates more exposed surface areas leading to increased shrinkage and creep over several years. Therefore, the crack width will be bigger and bigger with time.

(2) The fixed-fixed end supports of these panels, which provide the restraint to shrinkage, are not immovable, but are adjacent parts of the concrete panels that are themselves prone to shrinkage. If the exterior supports of the panels produce a relative movement, at the same time, these panels also create drying shrinkage that is restrained by exterior supports. As a result, the crack width increases gradually.

(3) Due to the self-weight (sustained load) of these panels, which cannot be ignored even if flexural cracking cannot be induced by self-weight directly because of

their larger cracking moments compared to moments caused by self-weight for these panels; the moment and shear stresses are maximum values at the exterior restrained supports and interior roller supports on these panels that can also contribute.

3.4.1.2.3 <u>Theoretical versus experimental results.</u> There are limited studies that predict cracking characteristics especially long-term cracking behaviors such as average crack width, average crack spacing of fully restrained concrete deck slabs reinforced with GFRP bars, and stress distribution in reinforcing bars at cracking locations due to restrained drying shrinkage. Gilbert [41] analyzed shrinkage cracking characteristics of a direct tension concrete member reinforced with steel bars that were fully restrained and developed theoretical formulas to estimate the crack spacing and final average width of fully restrained concrete slab by using equations (2) through (7) in Section 2.

In this model, the longitudinal movement of reinforced concrete member that is caused by changes of temperature and drying shrinkage of concrete is restrained by fully fixed-fixed end supports. These equations were proposed by Gilbert based on concrete slab reinforced with steel bars. Some factors, therefore, should be investigated and modified for FRP-reinforced members. Ghatefar et al. [43, 44] studied early-age restrained shrinkage cracking of concrete deck slabs reinforced with GFRP bars. They modified the coefficient of s_0 (reinforcement stress transfer length at cracking location) that was used by Gilbert's model on each side of the crack. Finally, they predicted reasonably average crack spacing and crack width by using the modified s_0 and Gilbert's model. In this section, the Gilbert's model was used. The coefficients for s_0 and s (average crack spacing) were modified and calibrated according to the experimental results. In order to evaluate the average crack width and cracking spacing for each panel by using Gilbert's analytical model, the ACI 209.2R-08 [67] guideline was used to determine ultimate shrinkage strain (ε^*_{sh}) and ultimate creep coefficient ($\emptyset^*$). Table 3.9 illustrates the parameters that were used to predict the final average crack width and average crack spacing.

At crack location, the reinforcing bars completely carried the direct tension force due to shrinkage and temperature changes because crack that extended the full width of the panel and propagated over the full depth of the panel. The distance s0, over which the concrete and reinforcing bars stresses vary considerably in the region adjacent to the

crack, needs to be known. It was proposed originally by Favre et al. [68] for a concrete member reinforced with deformed steel bars or welded wire mesh. Nejadi and Gilbert [27] found that s0 may be calculated using Eq. (1) at first cracking. However, this value of s0 should be multiplied by a coefficient of 1.33 for final or long-term calculation. Ghatefar et al [43] revised this coefficient. It was varied from 0.1 to 1.6 in 0.1 increments until a reasonable agreement. They obtained a coefficient of 0.8.

Table 3.9. Values used to predict average crack spacing and final average crack width

Panel	A_c (in.^{2})	f_f (ksi)	d_b (in.)	A_f (in.^{2})	E_c (ksi)	E_f (ksi)	$f_c^{'}$ (ksi)	ϕ^*	ε_{sh}^*
P-2	145.2	110	0.374	0.262	3605	5920	3.9	1.585	-5.10×10^{-4}
P-3	118.8	110	0.374	0.262	3605	5920	3.9	1.602	-5.15×10^{-4}
P-4	79.2	110	0.374	0.262	3605	5920	3.9	1.641	-5.25×10^{-4}
P-5	59.4	110	0.374	0.262	3605	5920	3.9	1.678	-5.33×10^{-4}
P-6	47.6	110	0.374	0.262	3605	5920	3.9	1.712	-5.41×10^{-4}

Two coefficients of 1.33 and 0.8 that were considered as the coefficient value for s_0 in this paper resulted in substantial differences between experimental results and theoretical calculations. The value, therefore, was adjusted from 0.1 to 1.0 in 0.01 increments for each panel. However, it was noted that average cracking spacing for each panel caused still high inconsistency between experimental and analytical results. The coefficient values for s_0 and s were varied simultaneously from 0.1 to 1.0 in 0.01 increments until relatively small errors were obtained. These adjusted values were regressed to obtain the regression equations for s_0 and s. It was concluded that these equations were related to reinforcement ratios of each panel. The regression equation of coefficient value (α) for s_0 was expressed as

$$\alpha = \frac{1}{-993.4\rho + 6.708} \tag{3.1}$$

where α is coefficient of s_0, ρ is reinforcement ratio. It was found that coefficient value (β) for s kept a constant of 0.95, which yielded reasonable agreement between experimental results and theoretical predictions, when the reinforcement ratios of these panels were equal to or more than 0.0044. Therefore, the regression equation of coefficient value (β) of panels P-2, P-3, P-4, and P-5 for s was given by

$$\beta = 232.04\rho - 0.0746 \tag{3.2}$$

where β is coefficient of s. This value for panel P-6 was 0.95. Table 3.10 illustrates the coefficients of each panel that were adjusted and regressed for s_0 and s.

Table 3.10. The coefficients of each panel for s_0 and s

Panel	ρ	Coefficient for s_0	α	Coefficient for s	β
P-2	0.0018	0.20	0.203	0.34	0.343
P-3	0.0022	0.21	0.221	0.44	0.436
P-4	0.0033	0.28	0.292	0.69	0.691
P-5	0.0044	0.45	0.428	0.95	0.95
P-6	0.0055	0.80	0.804	0.95	0.95

Table 3.11 provides a comparison between the final crack width calculated by using the coefficients of α and β and final average crack width measured in ultimate study period. Average crack spacing using β adjusted is illustrated Table 3.12.

Table 3.11. Final average crack widths (in.)

	P-2	P-3	P-4	P-5	P-6
Theoretical	0.0729	0.0503	0.0391	0.0321	0.0380
Experimental	0.0587	0.035	0.0351	0.0289	0.0357
Percentage (%)	24.17	43.62	11.29	10.94	6.43
Conversion Units: 1 in. = 25.4 mm					

Table 3.11 shows that the measured crack widths due to shrinkage and temperature changes for panel P-2, P-4, P-5, and P-6 agree with the values of theoretical prediction based on Gilbert's model [41] with an error that is less than 25% error except panel P-3. The difference between experimental and analytical values of crack width for panel P-3 may be resulted from an error of measurement or a contingency because there is only one panel for each type of panels. Comparisons between the experimental data and results predicted by the theoretical model for average crack spacing of these panels are illustrated in Table 3.12. The measured average crack spacing for each panel agrees with the value of analytical model with the largest error of 22%.

Table 3.12. Average crack spacing (in.)

	P-2	P-3	P-4	P-5	P-6
Theoretical	142.2	135.6	133.5	152.5	175.5
Experimental	176.9	174.0	169.5	176.3	164.9
Percentage (%)	19.62	22.07	21.24	13.50	6.43
Conversion Units: 1 in. = 25.4 mm					

3.4.1.3 Conclusions. The main purpose of this study was to investigate long-term shrinkage cracking behavior in fully restrained concrete panels reinforced with GFRP bars. One reinforced concrete panel and five GFRP panels with end-restrained supports were experimented under field environments in Rolla, Missouri for seven years (2400 days). Gilbert's model that was initially proposed for concrete members reinforced with steel bars was applied to GFRP concrete panels to estimate crack behavior. Suggested modifications to the two coefficients for s_0 and s were proposed for GFRP panels. According to experimental data and theoretical predictions in this research, the following conclusions can be drawn:

1) As axial restraining forces induced by the restrained shrinkage and temperature changes of these concrete panels caused the highest level of tensile stress at the exterior support of the panel; in addition, the distributed moment and shear stresses were maximum values at the restrained concrete supports and interior roller supports on these panels. The cracks appeared at or near exterior or

intermediate supports. When comparing the cracking moments with maximum positive and negative moments caused by self-weight for these panels as illustrated in Table 3.6, the cracking moments were greater. The restrained shrinkage, therefore, should be a major factor to induce cracking for each panel.

2) Panel P-5 was observed that the average and maximum crack width increased 880% and 719%, respectively, when compared to the results of original measurement. These increasing percentages of panel P-5 are the lowest among the GFRP panels.
3) When comparing the measured average shrinkage crack width and cracking spacing for each GFRP panel with the results that were calculated by using Gilbert modified analytical model [41], the errors for average crack width and cracking spacing were within 25% and 22.07%, respectively. This was accomplished by modifying the coefficients of s_0 and s that were related to the reinforcement ratio of the GFRP panel. However, the coefficient for s should be 0.95 after reinforcement ratio reaches 0.0044. the error is comparable to the error found by both Gilbert (steel reinforced RC) and Ghatefar et al (GFRP reinforced RC) in their early-age studies, however, this work was undertaken over a much longer sever-year period of study and presents refined factors for later-age cracking using GFRP reinforcement.

3.4.2. The Uniaxial Longitudinal Properties of the GFRP Bars. Four GFRP bars of the longitudinal tensile properties prepared in accordance to ASTM D7205/D7205M-06 (Reapproved 11) [72] were tested using a Tinius Olsen L240 machine that is illustrated in Figure 3.11.

The GFRP specimens used in this study were cut to a length of 39 in. (991 mm) and grouted with a resin mixture (EPON Resin 828 and EPIKURE 3140 Curing Agent, 1:1 by weight) inside 12 in. (305 mm) long threaded steel tubes at both ends, as shown in Figure 3.12.

The peak loads, ultimate tensile stresses, and modulus of elasticity were recorded using a data acquisition system. The tested properties of extracted bars from autopsied panels are summarized in Table 3.13.

Figure 3.11. Tinius Olsen L240

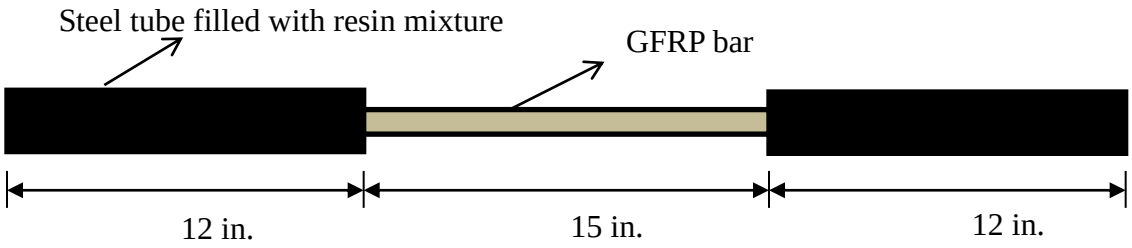

Conversion Unit: 1 in. = 25.4 mm

Figure 3.12. Details and dimensions of GFRP tensile testing specimen

Table 3.13. GFRP reinforcement testing properties

GFRP rebar	Diameter (in.)	Area (in^2)	f_{fu} (psi)	E_f (psi)	Peak Load (lb)
Rebar 1	0.375	0.1307	86,284	880,368	11,277
Rebar 2	0.375	0.1307	89,079	972,912	11,643
Rebar 3	0.375	0.1307	95,263	934,489	12,451
Rebar 4	0.375	0.1307	84,050	941,461	10,986
Average	0.375	0.1307	88,669	932,308	11,590
Conversion Units: 1in. = 25.4 mm, $1in.^2 = 645.2\ mm^2$ 1psi = 6.9 kpa, 1 lb = 0.454 kg					

The utmost care was taken to extract the bars without inducing any damage. A picture of the failed specimens is shown in Figures 3.13 and 3.14.

Figure 3.13. Failed specimens of GFRP Bars

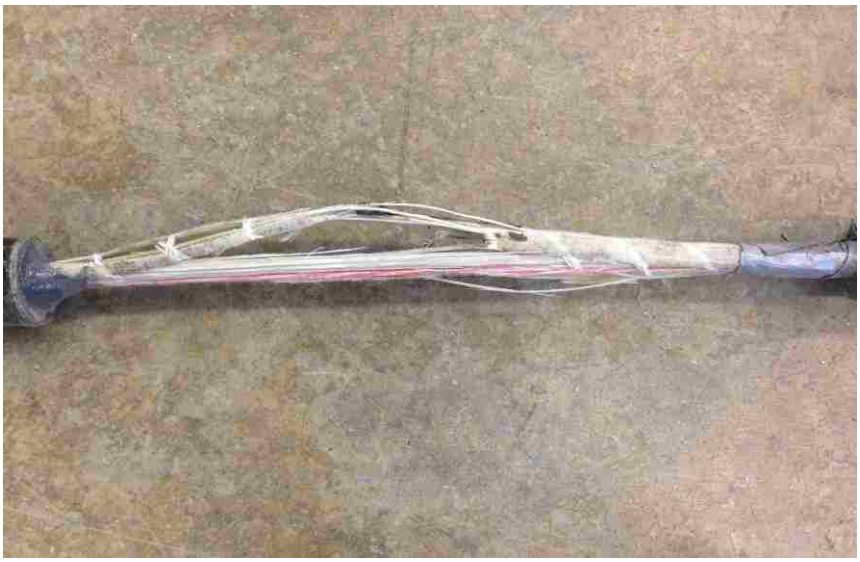

Figure 3.14. Typical failure mode of GFRP bar subjected to tensile test

Like all other FRP rebars, the GFRP bars present linear elastic behavior until ultimate failure. These specimens failed through the rupture of the glass fibers. The failure was accompanied by the delamination of glass fibers and resin as illustrated in Figures 3.13 and 3.14. No chemical deposit was observed on the surface of the GFRP bars before tensile testing. In Table 3.13, it should be noted that the tested bar properties, on average, were 80.6 % of the manufacturer reported properties in Table 3.5 at the time of manufacture. No experimental tensile test was undertaken on the GFRP bars at the time of construction on a virgin GFRP bar to benchmark the base GFRP bar properties. Because this study involved GFRP reinforced concrete panels at the secondary reinforcement level (i.e., low levels of reinforcement), the bars on panels 2 through 6 were subjected to sustained stress levels throughout the exposure conditioning due to the dead load weight of the panels. These generated maximum positive and negative moments as illustrated in Table 3.14.

Table 3.14. Sustained maximum moments on GFRP panels due to self-weight

GFRP Panel	Maximum negative moment (in-lb)	Maximum positive moment (in-lb)	Peak negative sustained bar stress (ksi)	Peak positive sustained bar stress (ksi)	Maximum sustained stress % of tested f_{fu}
Panel 2	-8505	4252	13.37	6.68	15.1
Panel 3	-6959	3479	10.97	5.48	12.4
Panel 4	-4639	2320	7.35	3.68	8.3
Panel 5	-3479	1740	5.54	2.77	6.2
Panel 6	-2782	1391	4.45	2.23	5.0
Conversion Units: 1in. = 25.4 mm, $1in.^2$ = 645.2 mm^2,1psi = 6.9 kpa, 1 lb = 0.454 kg					

Table 3.14 also details the resulting sustained stress levels in the bars at critical moment locations due to the dead load self-weight and estimates a stress level of 15.1 % of the autopsied tested f_{fu}. While this estimated sustained stress level is below the widely-reported creep rupture level of many GFRP bars, this stress level does not include the seasonal exposure conditions. For example, additional stresses that may occur due to positive or negative thermal gradients due to seasonal temperature changes are absent. Due to the end restraint, these thermal induced stresses are more significant than an

unrestrained member. Additionally, nonpermanent loads due to snow and ice also accumulated on the panels in the winter months, increasing the stress levels in the bars for certain periods of time. While there was no physical evidence that any creep rupture of the GFRP reinforcing bars occurred due to the seasonal effects, it is consistent with laboratory studies [137] that higher sustained stress levels on the GFRP bars could result in long-term degradation of the GFRP properties. In addition, the micro-structure of GFRP bars should be observed to investigate whether there are damages on the surface of the fibers or more voids inside the bar, which could result in lower experimental values than the manufacturer's results.

3.4.3. Microstructural Analysis of GFRP Reinforcing Bars. For the microstructure portion of the study, full cross sections of the samples were performed. The six additional panel samples were cut and subdivided into six small specimens sized 1.5 x 1.5 x 1.5 in. (38 x 38 x 38 mm) using a diamond bit concrete saw. Within the center of each of these specimens was a steel bar or GFRP bar.

3.4.3.1 Optical microscopic images analysis. For the Digital Microscope investigations, these specimens were ground carefully using five different level grits (1200, 800, 600, 240, and 180) of sandpaper that were installed in a grinding and polishing equipment to guarantee that the surface of specimens was flat enough in order for the HIROX KH-87 Digital Microscope shown in Figure 3.15, to observe the surface of these specimens clearly.

Figure 3.15. HIROX KH-87 Digital Microscope

This part focuses on the observation of the concrete specimens with reinforcing rebars to investigate whether their surfaces had any deterioration or evidence of any debonding between concrete and reinforcing. Figures 3.16 through 3.21 show images from samples taken from panels P-1 through P-6, respectively.

Figure 3.16. Sample of P-1

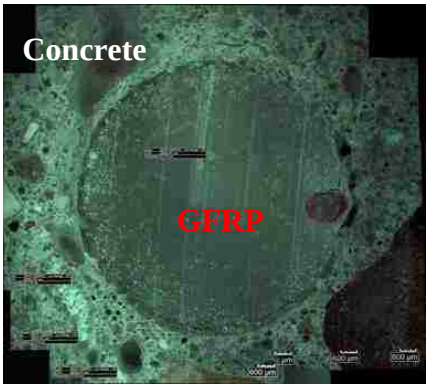

Figure 3.17. Sample of P-2

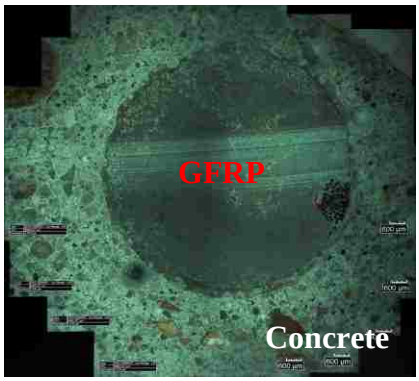

Figure 3.18. Sample of P-3

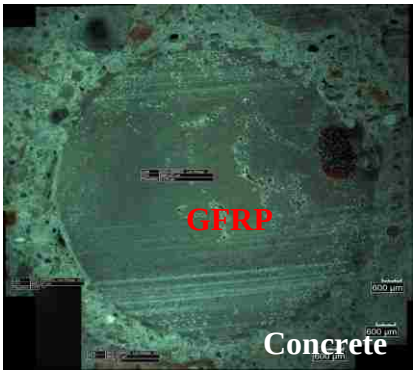

Figure 3.19. Sample of P-4

Figure 3.20. Sample of P-5

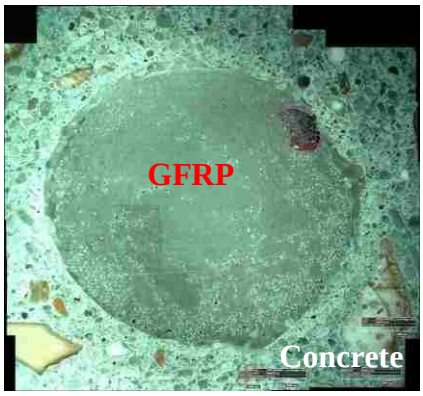

Figure 3.21. Sample of P-6

The pore structure of the concrete including the air void network is visible in these images, as well as the reinforcing bars themselves. From this optical imaging, there is no visible deterioration or debonding within the transition zones of concrete and reinforcing bars of these specimens after long-term exposure. Therefore, the investigators decided to use a Scanning Electron Microscope (SEM) to obtain a higher level of imaging.

3.4.3.2 Scanning electron microscope (SEM) analysis. For the initial step of the SEM experiment, the specimens were first more finely cut as smaller samples of size 1/16 x 3/4 x 3/4 in. (1.59 x 19 x 19 mm) using the diamond saw once again. Using the same method as 3.4.3.3, these smaller specimens were ground. Then 8 in. (203.2 mm) micro cloth PSA 702-3 was used to grind these samples. Finally, these five samples were ground by using 0.3 μm MicroPolish. For the second step, the five GFRP specimens were placed into an oven to dry, then coated using an ion sputtering device for specimen preparation prior to SEM examination. Figure 3.22 illustrates the specimens of SEM before and after coating.

Finally, an S-4700 model SEM (10 KV 12.0 mm x 60 SE [M]) was used to conduct SEM analysis at different levels of magnification. The images were taken at random locations, as shown in Figure 3.23, and the specimens were examined for possible deterioration and/or debonding between the concrete and reinforcing bar. The

specimens were also examined for glass fibers damaged during the exposure to the concrete environment.

(a) Before coating (b) after coating

Figure 3.22. GFRP samples of SEM

Figure 3.23. S-4700 model SEM (10 KV 12.0 mm x 60 SE (M)

The typical images of panel P-2 are illustrated in Figures 3.23 through 3.26. Images of panels P-3, P-4, P-5, and P-6 are available in Appendix A. The goal of the SEM investigations of panel P-2 was to examine the transition zones from different

directions between the reinforcement and concrete materials, as illustrated in Figure 3.24. Through these SEM images, possible debonding between the concrete and reinforcing materials could be examined.

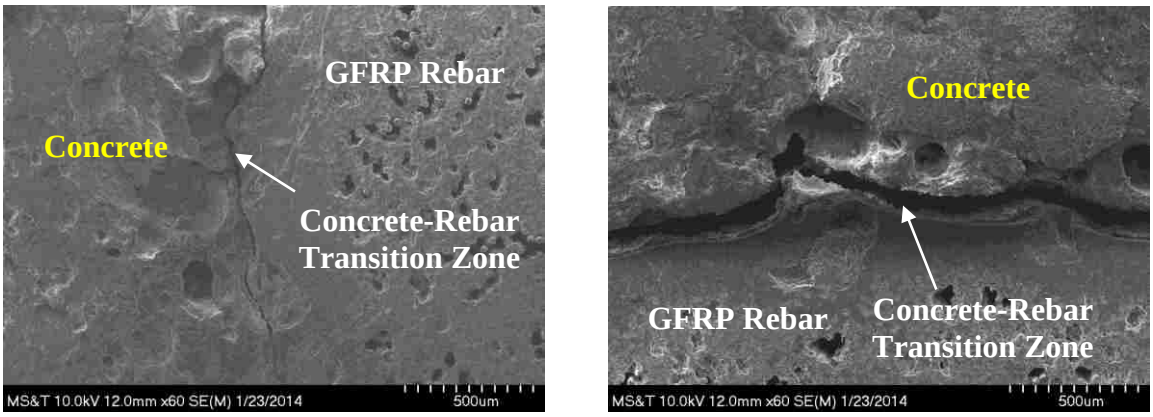

(a) (b)

Figure 3.24. Images of transition zone from different directions for Panel P-2

The images of these five GFRP samples indicate that the FRP reinforced specimens appear to exhibit different levels of debonding between the concrete and GFRP bars. From these images it may be concluded that some level of debonding between the concrete and FRP reinforcement exits. While the number of samples was limited, FRP samples with the lowest reinforcement ratio (i.e., resulting in the highest stressed bars) appeared to have a more significant level of debonding (i.e. panel P-2 > P-6). The immediate cause of the observed level of debonding is currently unknown, but it may be theorized. Possible causes could be related to a) the long-term seasonal environmental conditioning of the panels and/or b) unintended damage caused during the aforementioned specimen preparation. Since care was taken during the specimen preparation, it is more likely that the damage may have been caused by the environmental conditioning. Other studies [47] with field obtained samples have indicated that there was no discernible fiber damage in the GFRP bars within concrete after a similar time frame (5 to 8 years) of field exposure. In this cited work, the authors did observe interfacial

damage, but attributed it to the drying process in the SEM chamber. Certainly, more field-based sampling of specimens under varying field exposure conditions and time frames are needed to more definitively address this durability issue. It should be noted that these specimens were subjected to much higher sustained bar stress levels as secondary reinforcement than a typical bridge deck GFRP application where the bar stress level is much lower.

In addition, the results of the longitudinal properties of GFRP rebars in Section 3.4.2 show that the average tensile strength was lower than the value that the manufacturer reported. The reason may be the degradation of the glass fibers due to chemical attack in a concrete environment, or the GFRP rebars were not centered inside the two steel tubes precisely. Thus, there was bending moment while conducting the tensile test. These SEM images were observed to find whether there was some glass fiber that was damaged due to long-term exposure of GFRP bars to concrete. The typical voids in the cross section of panel P-2 at different magnifications are illustrated in Figure 3.25. Figure 3.26 illustrates the representative images of the fibers of panel P-2 at magnification levels. The image of a single fiber is shown in Figure 3.27.

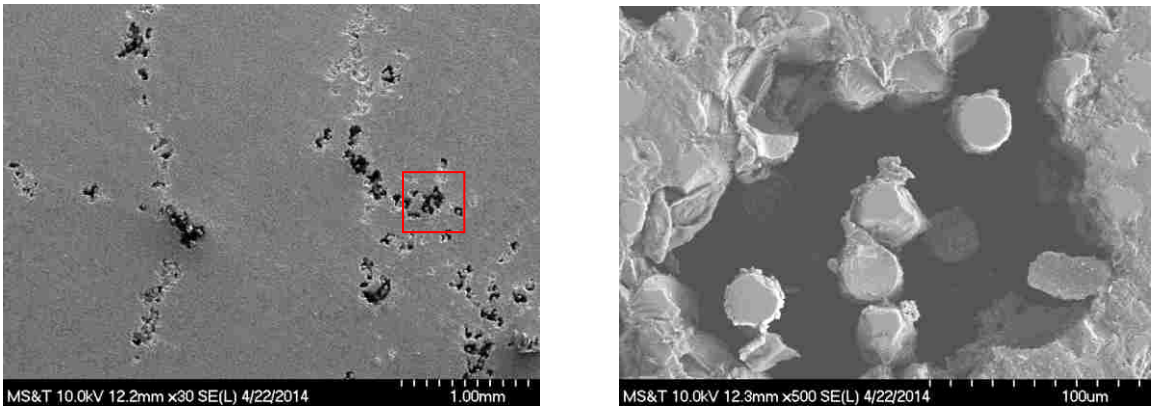

Figure 3.25. The voids of panel P-2 at magnification levels of 30 (left) and 500 (right)

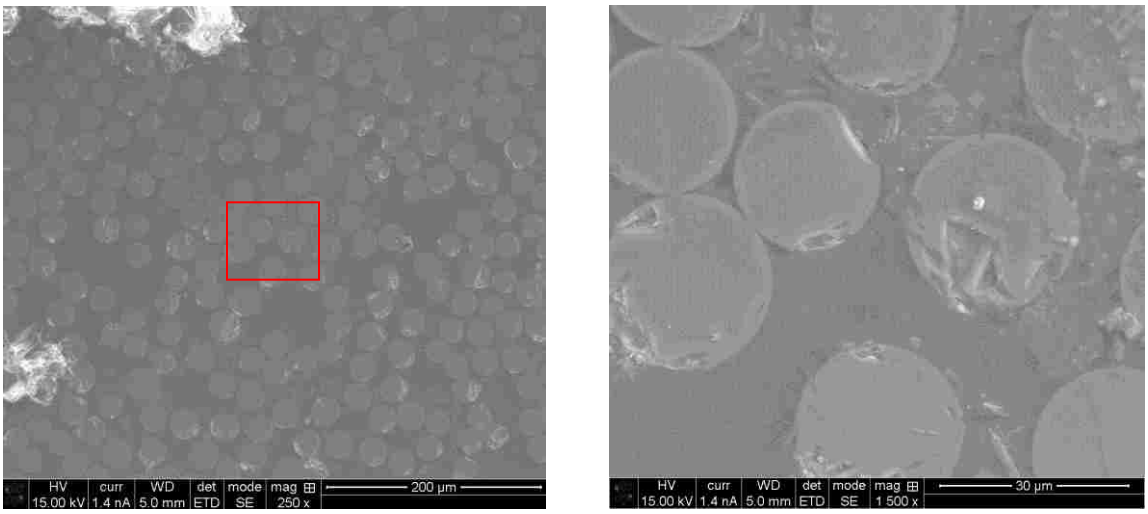

Figure 3.26. Images of the fibers at magnification levels of 250 (left) and 1500 (right)

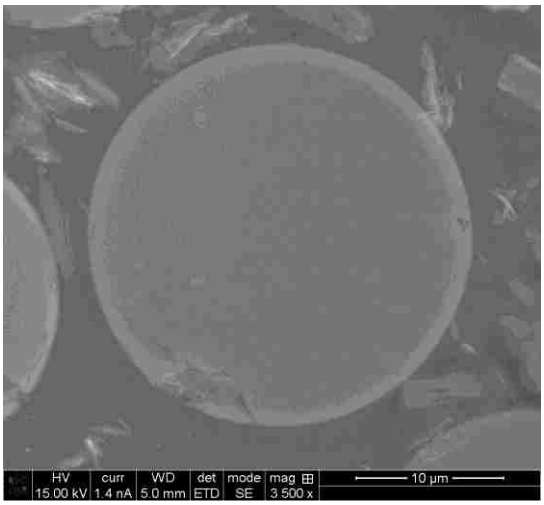

Figure 3.27. Image of a single glass fiber

SEM analysis approved that there was no sign of deterioration in the GFRP rebars. Some voids exist in the cross section of panel P-2 when observing the higher magnification level of Figure 3.25, which means that there were some losses of resin matrix due to the deficiency when the GFRP bars were produced by the manufacturer.

Glass fibers were intact without loss of any cross-sectional area. They were surrounded by the resin matrix. However, it should be noted that there was some damage to the glass fibers, as shown in Figures 3.26 and 3.27. They should be induced due to the specimen preparation stages.

3.4.3.3 Energy dispersive X-ray spectroscopy (EDS) analysis. The same SEM samples were utilized to perform this test using a Helios NanoLab 600, as illustrated in Figure 3.28. Random locations were selected to identify existing chemical elements in GFRP samples.

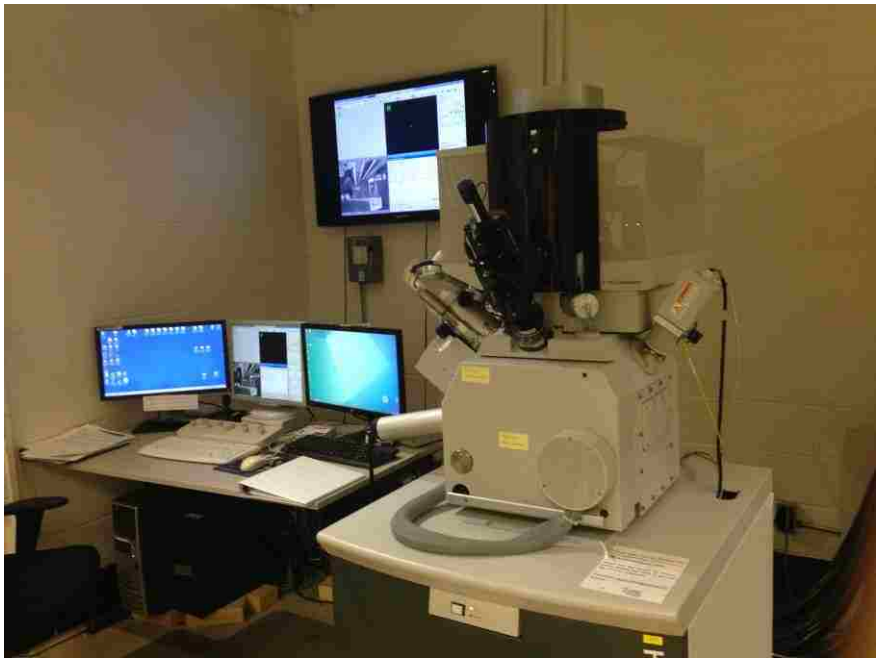

Figure 3.28. Helios NanoLab 600

The typical results of glass fibers and resin of panels P-2 and P-3 are illustrated in Figures 3.29, 3.30, and 3.31, where the Y-axis corresponds to the count (number of X-rays received and processed by the detector) and the X-axis presents the energy level of those counts. The results of panels P-4, P-5, and P-6 are illustrated in Appendix A.

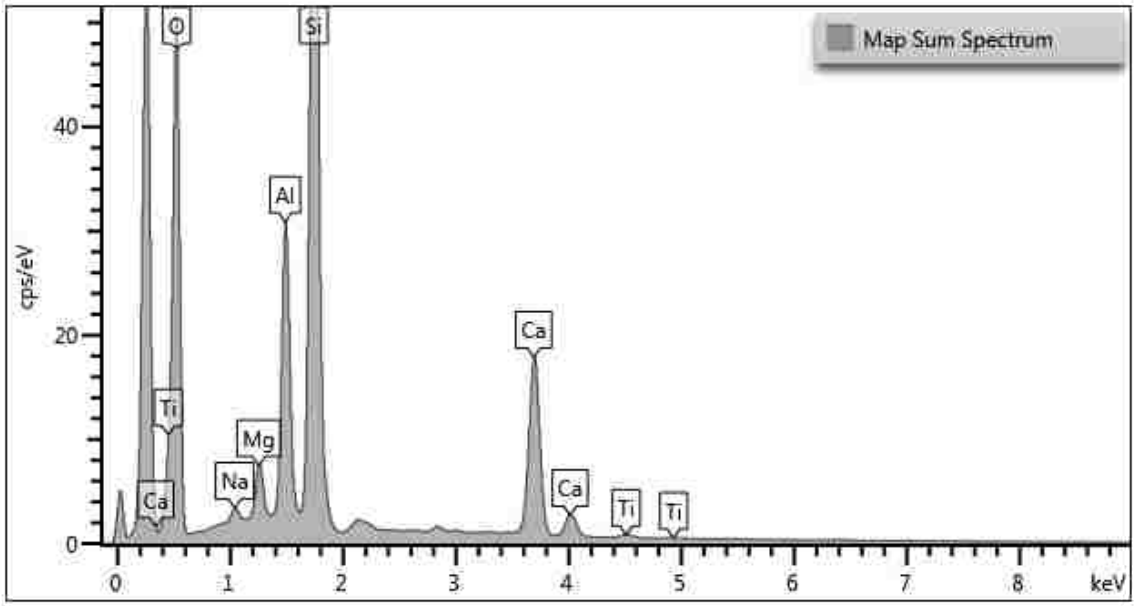

Figure 3.29. Results of the EDS analysis performed on P-2 after 7 years

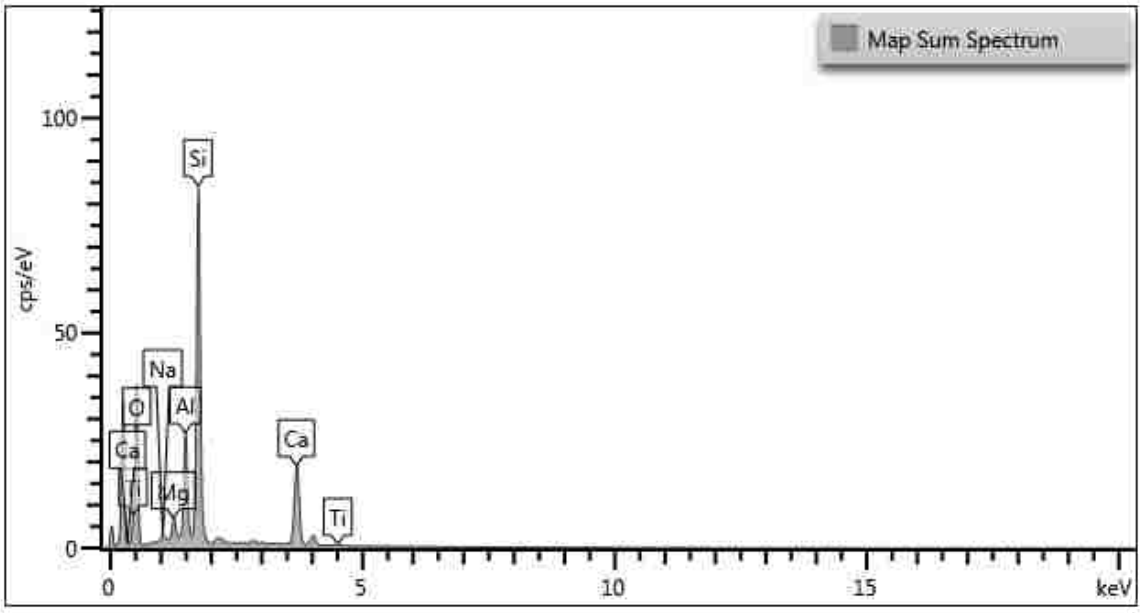

Figure 3.30. Results of the EDS analysis performed on P-3 after 7 years

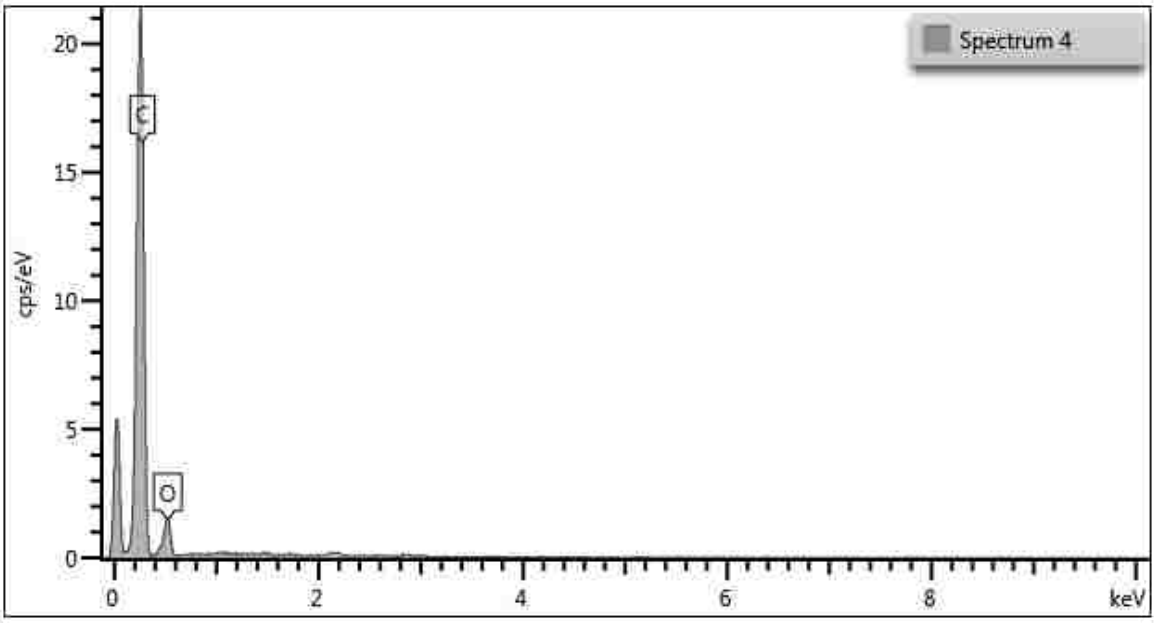

Figure 3.31. Typical resin result of EDS analysis

Si, Al, Ca, Mg (from the glass fibers), and C (from the resin) were the predominant chemical elements in these GFRP samples, as shown in Figures 3.29 through 3.31. The presence of Na and Ti in these samples was not a sign of degradation or alkaline attack. It may be due to contamination and elements of coating during sample preparation. This result was also presented in the report from the University of Miami.

Backscattered electron images are provided to display compositional contrast of existing chemical elements and their distribution in fibers and resin matrix. The images of panels P-2 and P-3 were taken randomly, and results are illustrated in Figures 3.32 and 3.33.

Comparing the results of EDS analyses performed on panels P-2 and P-3 showed the same chemical compositions of fiber and resin matrix. The silica was not dissolved in the alkaline environment of concrete. The EDS results of GFRP rebars for the other panels are available in Appendix A.

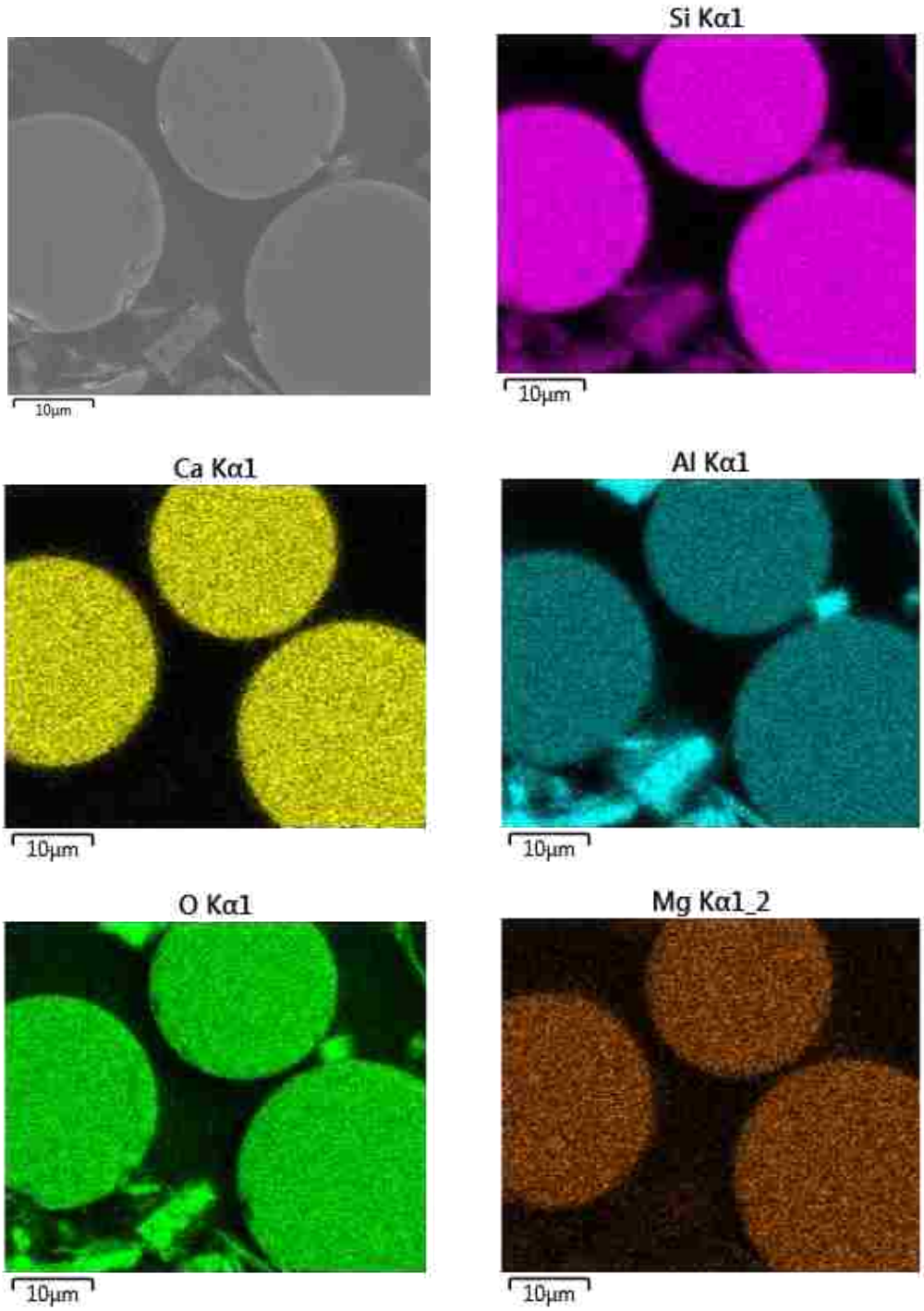

Conversion Units: 1 µm = 3.94 x 10^{-5} in.

Figure 3.32. Elemental scatter in GFRP rebar of P-2

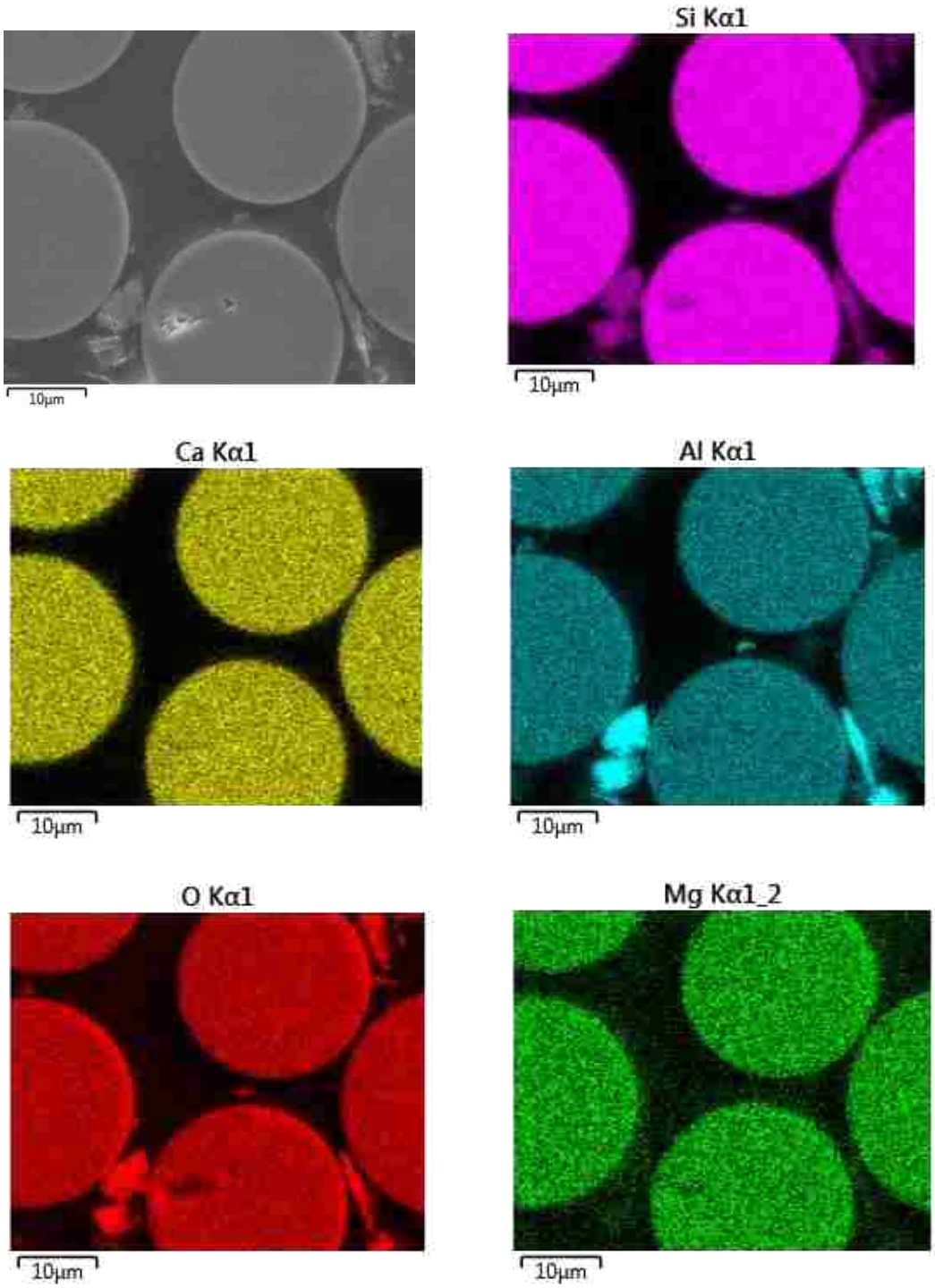

Conversion Units: 1 µm = 3.94 x 10^{-5} in.

Figure 3.33. Elemental scatter in GFRP rebar of P-3

3.4.3.4 Conclusions. There was no observable damage in the GFRP bars from the optical microscopic images, as shown in Figures 3.15 through 3.20. There was no discernable definitive deteriorative symptom in the SEM images due to long-term harsh environmental exposure other than evidence of varying cracks in the interfacial zones between the bars and paste matrix. Through the analyses of SEM and EDS revealed no evidence of GFRP degradation. There was no sign that the glass fibers lost any cross-sectional area; the matrix was intact and no damage was observed. Some voids were observed in GFRP rebars, as shown in Figure 3.25, due to the deficiency of the original process from manufacture in the early 2000's and use of polyester resin rather than the attack of alkaline in concrete environment. Today's general use of vinylester resins in the manufacturing process has essentially eliminate voids in the matrix produced during manufacturing.

Some studies [47] with field-obtained samples have indicated that their samples revealed no discernible fiber damage in the GFRP bars within concrete after a similar time frame (5 to 8 years) of field exposure. The authors did observe interfacial damage (i.e., cracking within the outer bar coating), but attributed it to the drying process in the SEM chamber. The SEM micrographs from other researches [44] that studied early-age restrained shrinkage cracking of GFRP-RC bridge deck slabs illustrate that the specimen subjected to wetting-drying conditions in the vicinity of the main crack had high intensity of micro-cracks and internal damage. There was debonding between concrete and GFRP bars.

Certainly more field based in-situ sampling of specimens under varying field exposure conditions and time frames are needed to more definitively address the microscopic imaging observations and physical and chemical investigations such as short beam shear (SBS) testing of GFRP bars, transition glass temperature (T_g) for GFRP samples, and chloride content of concrete, to know for certain if damage could be related due to specimen preparation or long-term exposure. Limited results are available to date from field-extracted samples, and more autopsied samples from field applications are the focus of the Missouri S&T research team in the final aspect of this research investigation.

3.5. SUMMARY

Axial restraining force induced by the restrained shrinkage and temperature changes of these GFRP-reinforced panels caused the highest level of tensile stress at the fixed-fixed supports. The cracks occurred at or close to external supports or interior roller supports on the panels. The restrained shrinkage should be a major element that induced the cracking of panels.

Using Gilbert's analytical model approach, the numerical model of shrinkage cracking in fully restrained concrete members reinforced with FRP bars that were exposed to natural environment for seven years was established based on the modification of the coefficients of s_0 and s.

There was no sign to observe that glass fibers were damaged, and the resin matrix in GFRP rebars deteriorated due to long-term exposure to the alkaline concrete environment, based on the observation of SEM images and DES analysis. There were some voids that were observed in GFRP samples, which were attributed to the resin used in the original process of manufacture rather than the attack of alkaline in concrete environment.

4. STUDY OF TOPIC 2

4.1. GENERAL

Externally bonded fiber reinforced polymer (FRP) composites are more commonly utilized in civil engineering to strengthen and rehabilitate reinforced concrete (RC) structural members such as girders, columns, decks, beams, etc. The long-term durability of FRP is frequently considered the principal limitation for the widespread application of this material. However, the durability of composite materials depends on the selection of component materials, method and conditions of processing, and surrounding environmental conditions that they experience in their service lives. Even though some previous studies demonstrate the advantages of using FRP to strengthen concrete members or repair existing concrete structures, several concerns related to the lack of clear understanding of the long-term characteristics of FRP-based renovations are obstructing their widespread application. One of the main issues for the implementation of the composite materials is the long-term bond performance between concrete and FRP sheet under harsh environments such as high and low temperature and humidity cycles, freezing and thawing cycles, water, seawater, etc. [75].

The objective of this study is to investigate the influence of harsh environmental exposure on the long-term bond behavior of steel reinforced polymer (SRP) composite, and provide a methodology for evaluation of durability-related strength loss of this bonded system. In this section, plain concrete beams externally strengthened with SRP were prepared. Despite the proven advantages of using SRP (for example, the price of SRP is similar to glass fiber reinforced polymer [GFRP], and the mechanical properties are comparable to carbon fiber reinforced polymer [CFRP]), the greatest disadvantage to its application is the limited knowledge of 1) the long-term bond behavior between concrete and SRP strengthening systems and 2) mechanical properties of SRP after being exposed to harsh weather. Therefore, this study will experimentally investigate the bond behavior of SRP-to-concrete systems and the variation of mechanical properties in terms of tensile strength of the SRP strips when they are exposed to various environmental conditionings.

Concrete beams reinforced with a SRP strengthening system and SRP coupon specimens were maintained in several environmental conditions including environmental chamber, tap water (3,000 hours), hot potable water at 140 °F (60 °C) (4,000 hours), salted tap water (1,500 and 4,000 hours), and real-time weather and solar exposure (1 year). Flexural bending load tests (three-point load tests) and direct pull-off tests were performed after being exposed to each environmental condition to evaluate the bond performance between SRP and concrete substrate. Meanwhile, tensile coupon tests for SRP strips exposed to the environmental conditions above were conducted to investigate the mechanical properties. In addition, the durability performance of concrete beams reinforced with the SRP strengthening system was compared with that of concrete beams reinforced with CFRP.

4.2. OUTLINE

Currently, there are several composite application technologies to repair and retrofit deficient and aging concrete members in existing buildings and bridges. These technologies involve manual FRP lay-up, pre-cured laminate plates, near surface mounted (NSM) bars, mechanically fastened FRP, and SRP.

SRP strengthening systems are similar in nature to FRP strengthening systems. The main difference is that SRP contains high strength steel fibers other than carbon, glass, or aramid fibers. The wires are now produced in both galvanized and non-galvanized configuration. SRP is applied in a similar way as the FRP strengthening system. The non-galvanized configuration has been installed to an existing concrete bridge, Bridge P-0962, that is located on Highway B and spans Dousinbury Creek in Dallas County, Missouri. The SRP strengthening system was utilized to reinforce the girders and deck of this bridge that showed signs of rust in many locations after several years in service. This was especially dominant in places that were able to drain from the deck to the girders or bents [23]. Figure 4.1 exhibits the corrosion of a transverse girder of Bridge P-0926. This new generation of the galvanized version of the high strength wire is a dominate feature of study in this work not investigated previously.

Figure 4.1. Corrosion of a transverse girder of Bridge P-0926 [23]

For the externally bonded SRP strengthening system of this bridge, 3x2 steel cords with a micro-fine brass coating were used. The worst strengthening deterioration occurred when rusting of SRP system was observed on bridges. If the epoxy bonding matrix cannot protect the Hardwire® and the system rusts even slightly, then the complete SRP strengthening system could be ruined due to the overall small area of the steel wires. The following reasons may result in the corrosion of SRP system:

1) The epoxy that was utilized may not sufficiently resist moisture or rainwater (i.e. provide a durable barrier to the wires) after long-term exposure to wet enviornments. Therefore, applicable selection of highly durable epoxy resin and appropriate installation of high strength steel wires should be significant concerns for application of this strengthening system.

2) Installation deficiency may cause the corrosion when the SRP strengthening system was installed.

4.2.1. Hardwire® Tapes (High Strength Steel Reinforcement). Hardwire® is a family of reinforcements made from ultra-high strength twisted steel wires. The steel can be molded into thermos-set, thermoplastics, or cementitious resin systems with never-before-seen ease. It occupies a new reinforcement niche between fibers and steel rebar. This creates a new class of reinforcements called micro-rebar that will work with composite, plastic, and cement-based processes. Further, Hardwire® can be used to

upgrade steel, wood, or concrete structures in both new construction and retrofit applications. Composites made from Hardwire® are up to 70% thinner and 25% lighter than composites made with glass fibers. The price of Hardwire® is like glass, but it performs like carbon at a fraction of the cost. Hardwire® composite reinforcements are used in different applications such as flooring reinforcement, historical building restorations and retrofits, laminates in the boating industry, and strengthening bridges and buildings. Hardwire® unidirectional tapes can be specified with wire cord counts from 4 to 20 wires per inch. The strengths range from 1.1 to 8.0 kips per in. (4.9 to 35.6 kN per mm) [76].

In this study, Hardwire® tapes of 5 wires per inch were utilized with 3x2-G Hardwire® (*a new galvanized coated wire version*) and 3x2 Hardwire® applied individually to study the durability performance of concrete members reinforced externally with composite materials made from Hardwire® and epoxy (SRP). They are illustrated Figure 4.2, respectively. The 3x2-G Hardwire® has yet to be implemented in a field application and the only non-galvanized use of Hardwire® used in the field to date known to the author was as described in Section 4.2 in Missouri.

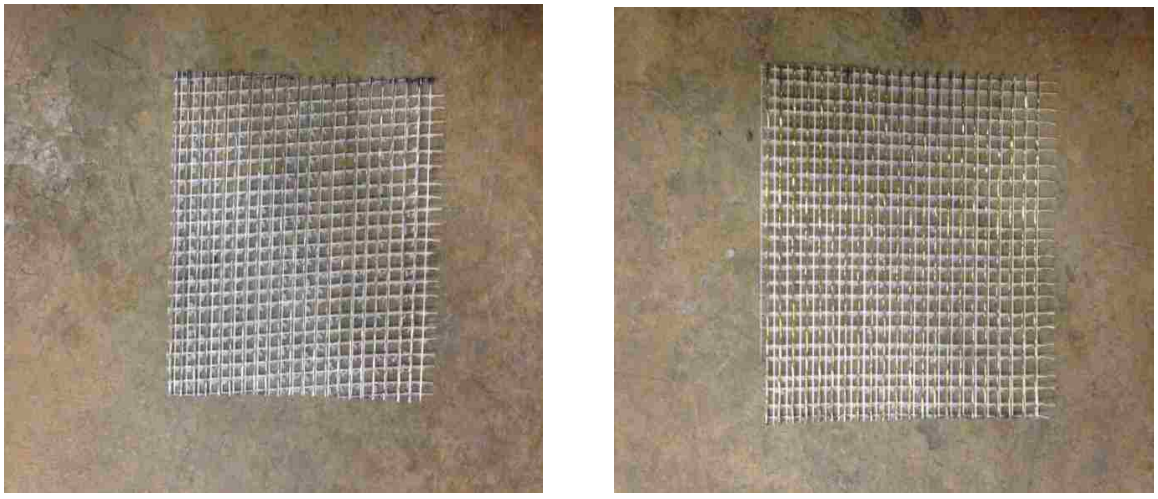

Figure 4.2. 3x2-G Hardwire (left) and 3x2 Hardwire (right)

Both the 3x2-G Hardwire® and the 3x2 Hardwire® are high carbon steel cords, but the 3x2 Hardwire® has a micro-fine galvanized coating and the 3x2 Hardwire® has a micro-fine brass coating. The 3x2 wire cord is made by twisting five individual wire filaments together-three straight filaments wrapped by 2 filaments at a high twist angle. Figure 4.3 shows details of 3x2 cords.

Figure 4.3. 3x2 cords [76]

The properties for 3x2 Hardwire® that was used in this research include the following [76]:

1) Excellent mix of engineering properties-up to 8 kips/in. (35.6 kN/mm).
2) Great stiffness, instant wettability, and excellent conformability.
3) Ability to work in all types of resins.
4) Asymmetric shape acts like a screw and gives mechanical bonding characteristics.
5) Excellent fatigue properties in tension and in high-flex situations.
6) Great choice for extrusion and pultrusion applications.

In addition to the above list of properties, 3x2-G Hardwire® has a property of corrosion resistance in exterior applications. The properties of these two types of Hardwire® are illustrated in Table 4.1.

These Hardwire® tapes are 12 in. (305 mm) wide (12 in. of steel fiber, 12 ½ in. grids) [76]. In this research, the Hardwire® tapes were manufactured and provided by Hardwire LLC. The strengthening systems that Hardwire® tapes impregnated with epoxy resin are named after SRP systems.

Table 4.1. The properties of Hardwire® tapes [76]

Hardwire®	Cord Type	Cord Dia. (in)	Standard Cord Coatings	Tape Density (wire/in)	Tensile Load (kips/in)	Laminate density (lbs/ft^3)	Sheet stress (ksi)	Effective modulus (msi)
3x2-4-G	3x2-G	0.037	Galvanized	4	1.42	85.4	22.9	2.1
3x2-4	3x2	0.035	Brass	4	1.38	89	28.8	2.35

4.2.2. Epoxy Resin. In this study, Sikadur® 330, which consists of Sikadur® 330 US Part A (component A) and Part B (component B), was used. It was manufactured by Sika Corporation. It is a two-component, solvent-free, moisture-tolerant, high strength, and high modulus structural epoxy adhesive. It has long pot life; long open time; high strength and modulus adhesive; excellent adhesion to concrete, masonry, metal, wood, and most structural materials; high temperature resistance; and high abrasion and shock resistance. It is also easy to mix; tolerant of moisture before during and after cure; fully compatible and developed specially for the SikaWrap® systems, and solvent-free, VOC compliant [77]. Components A and B were mixed to form epoxy that was utilized in this research. The mixture ratio of this compound was 4:1 by weight. The mechanical properties of this epoxy for seven days are illustrated in Table 4.2.

Table 4.2. The mechanical properties of Sikadur® 330 (7 days) [77]

Compressive strength (73 °F) (psi)	Tensile strength (psi)	Elongation break	Flexural strength (psi)	Flexural modulus (psi)
11,200	4,900	1.2%	8,800	5.06×10^5
Conversion Units: 1 psi = 0.0069 MPa, 1°F = 1.8°C + 32				

4.2.3. Specimen Exposure Conditions and Experimental Design. Durability of SRP-bonded concrete beams have not been studied extensively. According to previous research, major environmental factors that influence external bond durability of composite material-to-concrete are moisture, temperature, chemical elements in water, UV radiation, and so on [78]. In addition, Green et al. [79] reported the influence of

freeze-thaw cycles on the bond performance between concrete and FRP plates, and found very little damage when the FRP specimens were exposed to freeze-thaw cycles. Therefore, following experiments were designed to evaluate the bond durability of the SRP-to-concrete systems under various environmental exposures:

1) Perform the experiment in an environmental chamber with a combination of freeze and thaw, temperature, and humidity cycles.

2) Conduct the experiment in tap water (laboratory temperature).

3) Conduct the experimental in hot potable water (122°F (50°C)).

4) Conduct the experiment in NaCl solution (laboratory temperature).

5) Conduct the experiment in field environment.

6) Experiment with the tensile coupon testing for SRP specimens and direct tensile testing (pull-off testing) for the SRP strengthening system.

SRP was applied to the surfaces of concrete beams using the wet lay-up method. The SRP specimens were exposed to varying environmental conditions to study the durability behavior of concrete beams reinforced with the SRP strengthening system. The flexural bending tests (three-point load testing) were performed after these specimens were taken out of these environmental conditions at different periods to investigate the flexural strength and failure modes of SRP-to-concrete systems. At the same time, direct pull-off tests of SRP-concrete beams were also conducted to evaluate the tensile strength and failure modes after exposure to different environmental conditions. Both of the experiments were considered as the evaluation of long-term bond performance of SRP-to-concrete systems. Finally, tensile coupon tests of SRP strips that were also subjected to the environmental conditions mentioned above were conducted to investigate the mechanical properties of SRP laminate specimens. The exposure utilized to condition the SRP specimens are summarized in Table 4.3. These environmental conditions provided controlled accelerated aging exposures and real-time weather and solar exposure.

4.2.4. Concrete Design. Plain concrete beams and cylinders with a compressive strength of 6010 psi (41.4 MPa) at Day 28 were cast in material's laboratory using several batches. A 6000 psi (41.4 MPa) to 7000 psi (48.3 MPa) compressive strength was targeted to be representative of RC bridges in Missouri of the age and compressive strength commonly strengthened based on past field studies. Concrete beams were

demolded after 24 hours and maintained in the laboratory. Cylinders were kept in the moisture room. Table 4.4 shows the concrete mix design used to produce the concrete beams. The same mix design was used for all experiments in this study.

Table 4.3. Summary of exposure conditions used to weather the specimens

Exposure condition	Temp. (°F)	Exposure times	Number of specimens
Environmental chamber	Variable	82 days	12 (sustained load), 10 (unloaded)
Tap water	Lab	3,000 hours	6
Hot water	122	4,000 hours	10
Salt water 1	Lab	1,500 hours	10
Salt water 2	Lab	4,000 hours	10
Outdoor	Variable	1 year	12 (sustained load), 10 (unloaded)
Control	Lab	82 days, 4,000 hours, 1 year	18
Conversion Units: °F = 1.8°C + 32			

Table 4.4. Concrete mix design

Materials	Mix design (lb/yd^3)
Coarse aggregate	1755
Fine aggregate	1134
Type I Portland cement	611
Water	306
Water/Cement ratio	0.50
Slump	5.5 in.
Conversion Units: 1 in. = 25.4 mm, 1 lb/yd^3 = 16 kg/m^3	

The compressive strength of concrete was tested according to ASTM C39/C39M-16b [80] specification. The cylinders were tested using sulfur capping as the capping method in Tinius Olsen L240, as shown in Figure 3.11. The compressive strength was measured at certain time intervals throughout this study. Table 4.5 illustrates the average compressive strengths at different periods.

Table 4.5. The average compressive strength at different time

Concrete age (days)	Average strength (psi)
7	5460
28	6010
1 year	7260
Conversion Units: 1 psi = 0.0069 MPa	

4.2.5. Preparation of Flexural Bending Specimens. The dimension of the flexural specimen was 6 in. (width) x 6 in. (height) x 24 in. (length) (152.4 x 152.4 x 609.6 mm). The specimen preparation included two major steps: fabrication of concrete beams and application of SRP laminates.

4.2.5.1 Fabrication of concrete beams. An important variable that influences the bond behavior between FRP strengthening system and concrete substrate is the coarseness of the concrete substrate surface that the FRP system will be applied to. When the surface is too smooth, it may develop a poor bond between FRP and concrete, but if the surface is too coarse, putty has to be used and placed under the epoxy to provide a level repair surface, which increases cost of materials and labor. Consequently, an appropriate level of surface coarseness should be necessary to ensure proper bonding of the epoxy resin to the concrete surface and improve the bond behavior between the concrete and composite material [81].

Methods to obtain the roughness include manual tools, sandblasting, water jetting, etc. In this study, a concrete grinder was utilized to make the concrete surface coarse. First, the tension surfaces of concrete beams were ground. All loose particles and other contaminations on the tension side were removed to attain proper surface roughness in order to increase the contact area, obtain an appropriate bond, and improve the mechanical interlock between the concrete and SRP strengthening system. Secondly, a concrete saw was used to make saw cuts with a width of approximately 0.125 in. (3.18 mm) on the tension side of the beam at mid-span. The depth of saw cuts was 2 in. (50.8 mm). This process follows the ACI 440.9R-15 [24] protocols. The representative specimens ground with the saw cuts are illustrated in Figure 4.4.

Figure 4.4. The specimens ground with the saw-cuts

The saw cut simulates a wide flexural crack and focuses on the location of failure. The saw cut will cause a crack to develop at the center of the tension side of the SRP specimen and extend up to the compressive surface when performing the three-point load tests.

4.2.5.2 Application of SRP laminates. Two layers of steel laminate strips were utilized with 1 in. (25.4 mm) width for the first ply and 0.75 in. (19.05 mm) width for second ply. The selected Hardwire® reinforcement sheets, 3x2-G Hardwire® and 3x2 Hardwire®, consisted of five cords. The external reinforcement sheet was centered on the tension surface of concrete using Sikadur® 330 epoxy resin. The 12 in. (304.8 mm) long strips had a development length of 6 in. (152.4 mm) on each side of the saw cut based on previous research [60, 82] and ACI 440.9R-15. First of all, the first layer epoxy was applied to the tension surface as the primer, and to cover the voids on the surface of concrete, and first ply steel sheet with dimensions of 12 x 1 in. (304.8 x 25.4 mm) was applied and pressed into the epoxy, then brushed the second layer resin. The second ply steel fibers with dimensions of 12 x 0.75 in. (304.8 x 19.1 mm) were then staggered to apply to first steel ply to decrease the interval between steel fibers, which can increase the tensile strength of the SRP strengthening system, and pressed this steel strip into the

epoxy. The air voids contained in the resin were dispersed by using a small steel plate. Finally, the third layer of epoxy was brushed to cover the steel wires completely. Additional epoxy of 0.5 in. (12.7 mm) and 0.25 in. (6.35 mm) was applied to each longitudinal and transverse sides of the SRP, respectively, in order to decrease corrosion of the steel fibers in the epoxy resin, resulting in a total length of 12.5 in. (317.5 mm) and a width of 2 in. (50.8 mm) for the SRP strengthening system. Micro-fine galvanized coating and micro-fine brass coating steel fibers were used to prepare the SRP specimens, respectively. The representative SRP specimens are shown in Figure 4.5.

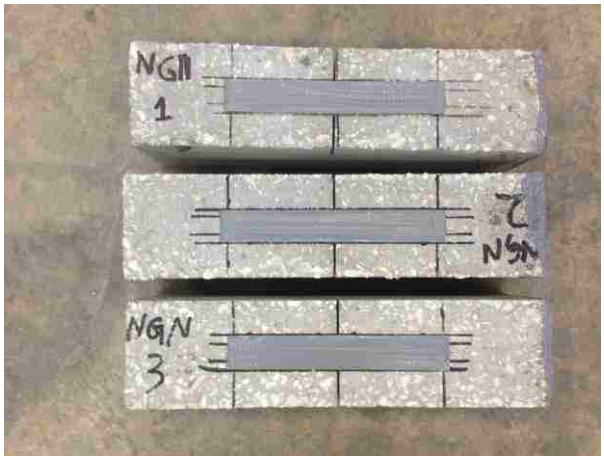

Figure 4.5. The typical SRP specimens

4.2.6. Fabrication of Direct Pull-off Specimens. The important bond behavior between composite material and concrete substrate can be investigated by several methods including both non-destructive and destructive methods. Acoustic sounding, chain dragging and thermographic imaging are considered nondestructive methods. The destructive methods include differential scanning calorimetry and direct tensile testing (Pull-off testing) [83]. Since the pull-off testing method is one of the most common methods to evaluate the bond behavior between concrete and FRP strengthening system and is the only avenue that is standardized ASTM D7522/D7522M-15 [84], this method is used in a research capacity and also recommended as a useful tool for quality control

during construction [85]. Therefore, this test was performed in all tasks of this study. This method determined the greatest direct tension force that was applied perpendicular to the SRP surface. According to ACI Committee 440 L, pull-off specimens were prepared. The pull-off specimen preparation included two main steps: fabrication of SRP specimens and construction of direct pull-off specimens.

4.2.6.1 Fabrication of SRP pull-off specimens. The procedure of preparation of concrete surface was the same as that of the flexural bending specimens. One layer of epoxy was brushed onto the roughened surface, and then a 5.5 x 5.5 in. (140 x 140 mm) steel sheet was applied. The second layer resin was applied to the first ply steel sheet and epoxy. Another 5.0 x 5.0 in. (127 x 127 mm) steel fabric square was performed in the exact same manner as the first steel ply. These two steel squares were also staggered to put together. The air voids inside were dispersed using the same method as that of the preparation of flexural bending specimen. Finally, the third layer of epoxy was applied to cover the two-ply steel fibers completely. Micro-fine galvanized coating and micro-fine brass coating steel fibers were used to prepare the SRP specimens, respectively. A typical pull-off specimen is illustrated in Figure 4.6.

Figure 4.6. A typical SRP pull-off specimen

4.2.6.2 Construction of direct pull-off bond specimens. The concrete blocks with the SRP sides were maintained after the flexural bending tests to construct the specimens of direct pull-off testing. A concrete saw was used to cut the side of the block without the SRP system to make this side balanced for tensile tests. First, the surface of SRP was ground to guarantee a flat SRP surface, which makes the surface drill cores easily. A diamond bit (see Figure 4.7) was used to drill the cores to separate the adhesion fixture from the surrounding SRP. The process of drilling the cores is shown in Figures 4.8 and 4.9.

Figure 4.7. The diamond bit

Figure 4.8. The detailed process of drilling core

According to ASTM D7522, the depth of core drilling into the SRP specimen should be between 0.25 in. (6 mm) and 0.5 in. (12 mm). In this research, the SRP specimen was drilled until ground fine concrete particles extruded from the core drill bit. The depth of the core was consistently around 0.25 in. (6 mm). There were two cores that were drilled for each SRP specimen, resulting in a total of three pull-off replicates per specimen. The powders of epoxy, steel, and concrete were vacuumed while SRP sample was drilled. Then, the surfaces of the specimen and aluminum disk (dolly) were cleaned by using acetone before the dollies were applied to the surface of SRP specimen. Figure 4.10 shows a typical cleaned specimen.

Figure 4.9. The process of drilling core

The aluminum disk (dolly) with a 2 in. (50.8 mm) diameter, which was adhered with a 5-minute, 3200 psi (22.1 MPa), two-part, LOCTITE Instant-Mix epoxy, was bonded to the SRP testing surface. The dolly contained a threaded hole in the center that allowed for attachment of the fixed alignment adhesion testing device (pull-off tester)

using a pull pin. Figures 4.11 and 4.12 illustrate a typical dolly with a pull pin and a representative pull-off specimen, respectively.

Figure 4.10. The sample with two cores

Figure 4.11. A typical dolly with a pull pin

Figure 4.12. A typical pull-off specimen

4.2.7. Preparation of Tensile Coupon Specimens. According to ASTM D3039/D3039M-14 [86], tensile coupon specimens were fabricated. Tensile specimens were used to investigate the material properties of the SRP laminates and evaluate whether they degraded under various environmental conditions compared to the control specimens. The method and procedure of preparation were the same as those of flexural bending test specimens. The tensile coupon specimen preparation includes two main steps: fabrication of SRP strips and production of tensile coupon specimens. Two specimen geometries were performed, including tabbed strips and dog bone shaped specimens. Tabbed strips failed in the grips of the testing machine or at the tab-lamina interface, while the dog bone shaped specimens greatly decreased the occurrence of the mentioned above. Therefore, the dog bone shaped geometry was chosen for this study.

4.2.7.1 Fabrication of SRP strip. All tensile coupon specimens were fabricated on an aluminum plate. A 0.75 in. (19.1 mm) x 12 in. (305 mm) and another 0.5 in. (12.7 mm) x 12 in. (305 mm) unidirectional steel plies were applied. They were also staggered together. The application of two-layer steel fibers and epoxy and the fabrication procedure of tensile coupon specimens were in the same manner as those of flexural bending specimens. Finally, the resin layer was brushed to cover the steel fibers completely. Micro-fine galvanized coating and micro-fine brass coating steel fibers were used to prepare the specimens, respectively. The dimension of a typical SRP specimen for tensile coupon test was 1 in. (width) x 12 in. (length) (25.4 x 305 mm). Figure 4.13 illustrates the SRP strips.

Figure 4.13. The typical original tensile coupon specimens

4.2.7.2 Production of tensile coupon specimens. In order to decrease the stress concentrations in specimens when performing this test, the dog bone shaped geometry was molded to produce the tensile specimens. First of all, the surface of the SRP specimen was ground by using sandpaper to make sure that the surface was flat. Second of all, four aluminum tabs of 1 in. wide by 2.5 in. long (25.4 x 63.5 mm) were attached to the ends of the respective specimen, using a 5-minute, 3200 psi (22.1 MPa), two-part, LOCTITE Instant-Mix epoxy. Finally, a grinder was used to cut the epoxy to make a dog bone shape. Tensile coupon specimens reinforced with micro-fine galvanized and brass coating steel fibers are illustrated in Figures 4.14.

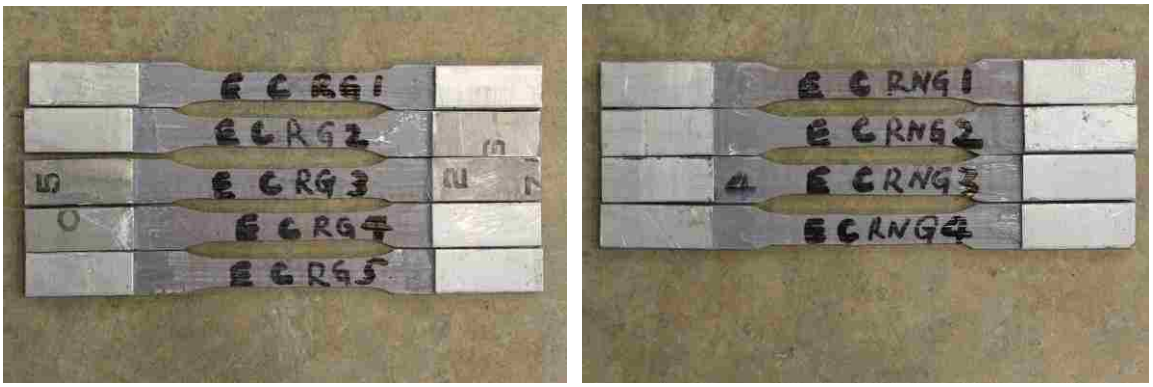

Figure 4.14. The samples with galvanized (left) and brass coating (right) steel fibers

4.3. THE EXPERIMENT IN ENVIRONMENTAL CHAMBER

Concrete structures externally reinforced with FRP composite systems are often in contact with temperature cycles and other environmental conditions like freeze-thaw cycles and humidity that degrade the expected bond durability of this system. Bond degradation is considered a common source of premature failure in concrete structures reinforced with FRP. Environmental conditions are related to such failures. Al-Mahmoud et al. [75] studied the bond strength of concrete members reinforced with FRP under freeze-thaw cycles and found that the failure mode of conditioned specimens was the same as that of the control specimen. However, the load capacity was decreased when

compared to the control specimens. Wolff [87] concluded that a combination of time, temperature, stress, chemical, cyclic loads, and moisture influenced durability of FRP composites. In addition, Grace and Singh [88] reported that reinforced concrete beams reinforced with CFRP plates illustrated a loss of load capacity after 10,000 hours of 100% humidity exposure.

In order to investigate the bond characteristics of SRP-to-concrete system under a harsh environment, the concrete beams reinforced with a SRP strengthening system that were loaded and unloaded, and SRP strips for tensile coupon tests were maintained in an environmental chamber that simulated the exterior weather of Rolla, MO. These SRP specimens experienced a series of freeze-thaw, temperature, and humidity cycles to experimentally investigate the influence of the accelerated aging environmental condition on bond performance between SRP strengthening system and concrete substrate. Flexural bending tests and direct pull-off bond tests were performed to evaluate the long-term bond performance of SRP-to-concrete interfaces.

4.3.1. Sustained Loading and Environmental Conditioning. Twenty-eight flexural SRP specimens were fabricated in the laboratory for this test. The test specimens were divided into three groups: Group I specimens were maintained in laboratory conditions with three samples reinforced with micro-fine galvanized coating steel fibers (RG) and three specimens reinforced with micro-fine brass coating steel sheet (RNG) as control specimens. Group II included six RG specimens and six RNG samples that were subjected to environmental conditions and sustained loading of 20% and 40% of ultimate tensile capacity, respectively. Pairs of back-to-back specimens were subjected to the sustained three-point flexural load in the vertical orientation using a spring-loaded fixture. This fixture consisted of clamps that were made of steel plates and beams, long threaded bolts with nuts, and springs, as shown in Figure 4.15. The sustained loads were controlled by frequently checking the spring length while tightening the bolts. The spring was located at the mid-span positions on the surfaces of two specimens without SRP strengthening systems. The span between two supports was 18 in. (457.2 mm). The spring had a free length of 5 in. (127 mm) and was compressed 0.28 in. (7.1 mm) for 20% of ultimate capacity and 0.56 in. (14.2 mm) for 40% of ultimate load to subject the samples to sustained loads of 700 lb (3.1 kN) and 1,400 lb (6.2 kN), respectively. The

lengths of these springs were examined to investigate if relaxation of the springs occurred during the conditioning. Group III SRP samples (five RG specimens and five RNG samples) were only subjected to environmental conditioning.

The purpose of this research was to investigate the bond behavior between SRP strengthening systems and concrete under freeze-thaw cycles, varying temperatures and humidity. Following the application of load, these specimens were exposed to an environmental chamber for one complete environmental cycle plus 50 additional freeze-thaw cycles. Based on the exterior weather conditions in Rolla, MO, including the annual average high and low temperature and annual humidity, the environmental conditioning regime was developed. The data collected was from the National Weather Service [89] and National Climatic Data Center [90] during a time frame from 1980 to 2013 was used to determine a suitable weather conditioning regime. In this study, one complete conditioning cycle was made up of 50 freeze-thaw cycles, 150 extreme temperature cycles, 150 relative humidity cycles, and 50 additional freeze-thaw cycles. Table 4.6 illustrates details of each conditioning cycles. The exposure regime of the environmental chamber is illustrated in Figure 4.16.

Figure 4.15. Spring-loaded fixture and the testing samples in environmental chamber

4.3.2. Flexural Bending Testing (Three-Point Load Testing). To evaluate the influence of a combination of freeze-thaw, temperature, and humidity cycles on bond performance between the FRP strengthening system and concrete substrate, several methods can be used, including the direct tension pull-off test, the single and double

direct shear tests [91-93], the peel test [91, 92], and the three or four-point bending test [17, 94, 95]. In this part, three-point load tests were used to examine the bond durability of the SRP-to-concrete substrate.

Table 4.6. Temperature and RH range for each conditioning cycles

Condition Type	Freeze and Thaw	Temp.	1st RH	2nd RH	3rd RH
Temp./RH Range	-4 to 50°F @ 40% RH	68 to 122°F @ 40% RH	60% to 95% RH @ 68°F	60% to 95% RH @ 77°F	60% to 95% RH @ 104°F
Conversion unit: 1°F = 1.8°C + 32					

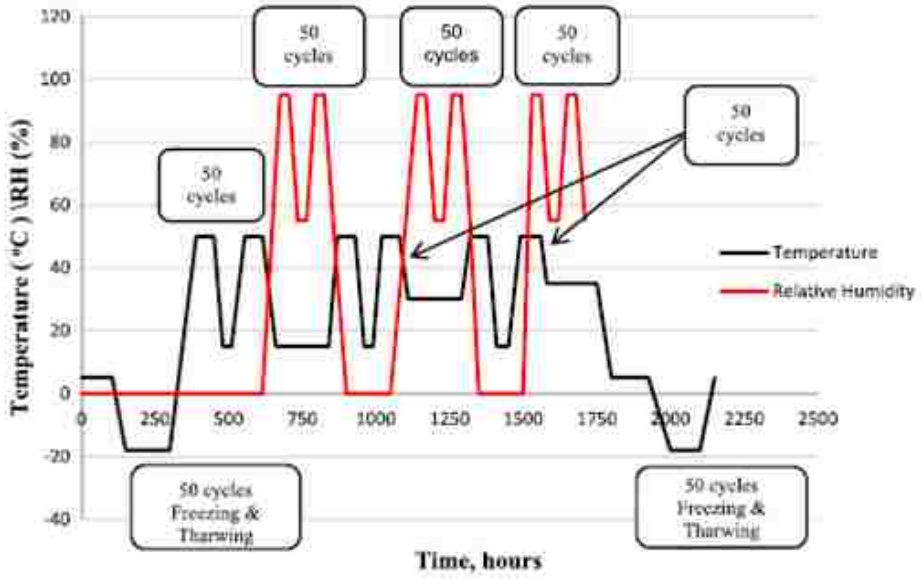

Conversion Units: 1°F = 1.8°C + 32

Figure 4.16. Environmental chamber regime

4.3.2.1 The setup of the experiment. The standard test method to determine the flexural tensile strength of plain concrete beam [73] was chosen as an example test method. This standard calls for four-point bending with three equal intervals between support and load points. The four-point bending produces an area in the middle third of the concrete beam with zero shear and maximum moment, which creates a state where

only the normal stresses exist. However, the four-point load testing setup results in a plateau in the moment diagram. This plateau will cause bending cracking that will probably interrupt the development length of the SRP strengthening system, and perhaps lead to additional variability of the testing results. In contrast to this, the maximum moment for three-point bending will occur at mid-span of the tested beam. The maximum moment and the weakening of the section from the saw cut guarantee that a single flexural crack will occur at the tip of the saw cut and the complete available development length of the SRP strengthening system is activated. In addition, the three-point bending test shows that the shear strength in the cross section of concrete is less than that of the four-point load test when the same moment is applied, which can decrease the possibility of a concrete shear failure. Therefore, the three-point load bending test was selected for this research.

A span length of 18 in. (457.2 mm) was used to perform this test. Composite dimensions were 2 in. (50.8 mm) wide and 12.5 in. (317.5 mm) long. The detailed dimension of the specimen for the flexural bending test is illustrated in Figure 4.17. The tension surface of the SRP sample is exhibited in Figure 4.18 per ACI 440.9R-15.

All SRP-reinforced concrete beams were loaded using an MTS 880 to conduct the flexural bending tests. Load was applied at a constant rate of 0.005 in./min (0.127 mm/min) to cause failure of the specimens in 9 to 10 minutes. The deflections of both sides at the mid-span of the SRP specimen were measured by using two linear variable displacement transducers (LVDTs) with 0.5 in. (12.7 mm) extension. Figure 4.19 illustrates the three-point loading test configuration.

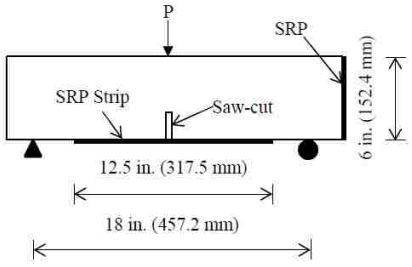

Conversion Units: 1 in. = 25.4 mm

Figure 4.17. The setup of bending test

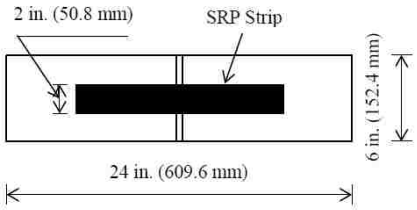

Conversion Units: 1 in. = 25.4 mm

Figure 4.18. The tension side of specimen

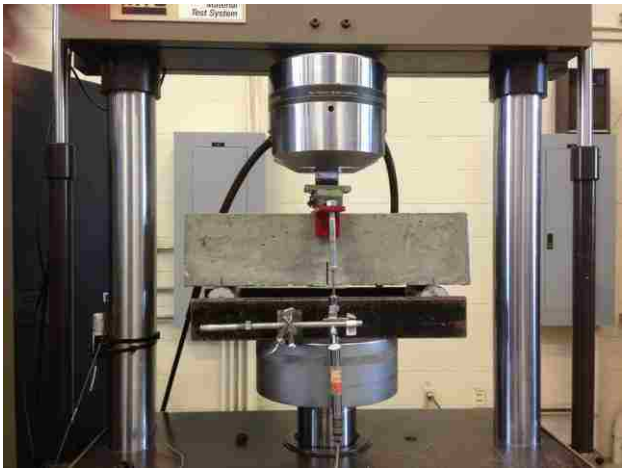

Figure 4.19. Three-point loading test configuration

4.3.2.2 Experimental results and discussion. Flexural strength reductions of SRP specimens quantify the degradation in bond due to exposure to the environmental chamber and/or failure mode mechanism. This section presents the testing results and analysis of the results for peak and failure load and maximum deflection. The concrete cover area on the fracture SRP strip was analyzed after flexural bending tests. Meanwhile, failure modes of SRP specimens were also observed, which provided qualitative insight into bond degradation between SRP and concrete. In externally bonded SRP reinforcement design, there should be five types of failure modes:

1. Cohesive Failure Mode (substrate failure): This failure mode is typically assumed, which is where the fracture SRP surface passes completely through the concrete substrate and some concrete and aggregate remains adhered to the SRP sheet.
2. Adhesive Failure Mode: Rupture initiates between the concrete surface and SRP strips. The SRP failure surface is clean or covered with a thin layer of concrete paste.
3. Mixed-Failure Mode: partial cohesive and adhesive failure mode.
4. SRP strip rupture Failure Mode: Steel fibers rupture due to less tensile capacity of steel wires than the flexural strength of concrete beam. It is considered an invalid test result.
5. Shear Failure of concrete beam: Diagonal crack occurs on the end of the concrete block. However, SRP sheet remains intact and completely adhered to the concrete beam. This mode is also considered an invalid result.

According to ACI 440.9R-15, a cohesive bond failure is typically assumed. The intent of the experiment after exposure to environmental chamber is to investigate the bond performance (degradation of adhesive strength) between the SRP strengthening system and concrete. As a result, a failure mode change from Failure Mode 1 in the control specimens to Failure Mode 2 or Mode 3 in the specimens after being exposed to the environmental chamber provides a principal sign of degradation of bond strength for the SRP strengthening system.

The SRP specimens were tested with a displacement-controlled testing machine (MTS 880) under three-point loading. The control specimens failed in Failure Mode 1. Failure modes for the conditioned SRP specimens were Failure Mode 3 after the exposure to freezing and thawing, temperature, and humidity cycles for 82 days. The crack occurred at the tip of the saw cut. Figure 4.20 shows a typical concrete cracking.

The flexural crack extended up towards the compressive face of the beam. There was progressive slip at the interface of the SRP sheet and concrete due to delamination after the crack width increased steadily. Finally, the SRP specimen failed when the debonding reached the end of the SRP strip. Figure 4.21 shows the failed specimen.

Figure 4.20. A typical cracking at the tip of saw-cut

Figure 4.21. A typical failed SRP specimen

Once the cracking moment of the concrete prism was exceeded crack propagation initiated in the notch. The tensile stress in the concrete was transferred to the SRP strengthening system, which resulted in the first peak load. This also caused a peak tensile stress in the SRP sheet at the intersection with the saw cut (i.e. notch). This peak tensile stress in the SRP strip was then transferred to the concrete at both sides of the saw cut by the bond shear stress or interfacial shear stress. The debonding between the concrete and the SRP sheet initiated when the peak tensile stress in the concrete and the

SRP strip exceeded the interfacial shear stress. This debonding between the concrete and the SRP strengthening system occurred initially in the middle of the SRP strip (the intersection with saw cut) due to the weakening of the cross section of saw cut and the highest bending moment at the mid-span of the specimen, and then extended out through the end of the SRP system until the specimen failed. The typical load-deflection characteristics of the loaded, unloaded, and control specimens reinforced with galvanized and brass coating steel fibers under three-point loading are illustrated in Figure 4.22 and 4.23.

It can be seen in Figures 4.22 and 4.23 that the SRP control specimen (RG 11 and RNG 5) had a greater ultimate deflection than the conditioned specimens that were exposed to the environmental chamber. Therefore, the control specimens exhibited higher deformation ductility than those of the conditioned specimens. This is an indication that it maintained the bond between the SRP and concrete substrate longer under increasing loading. The saw tooth changes in the loading after cracking also indicates bond slip. It should also be noted that the ultimate strength losses of the conditioned RG and RNG specimens were observed when compared to the control samples. At the beginning of the flexural bending test, the load-deflection behaviors of the control and conditioned specimens were roughly linear until the cracking moment of the concrete prism was exceeded. The flexural load in the SRP specimens dropped considerably once the cracking moment capacity of the concrete prism was exceeded. These points demonstrated that the SRP strips bridged the tensile crack in the concrete. For the control specimens, they experienced several peak loads until failure. In contrast, there were only two and three peak loads in all conditioned SRP specimens. In some cases, only one peak load represented the relationship between load and deflection. They failed at lower loads with lower deflections. Therefore, results support that the bond strength of the conditioned RG and RNG specimens deteriorated by the combination of freeze-thaw cycles, temperature, and humidity cycles. The stiffness of the control and conditioned specimens was almost the same even though the bond characteristics of the control specimens were much better than those of the conditioned samples.

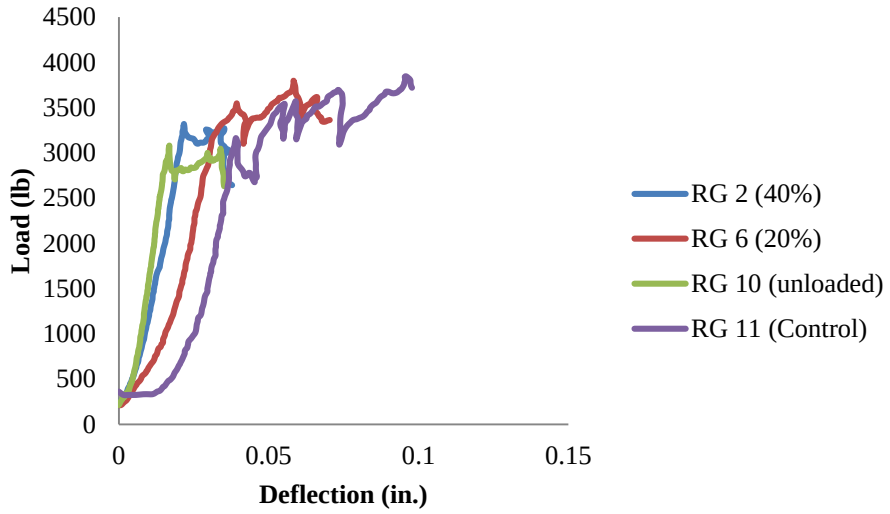

Conversion Units: 1 in. = 25.4 mm, 1 lb = 0.0044 kN

Figure 4.22. Load-deflection characteristics of the RG specimens

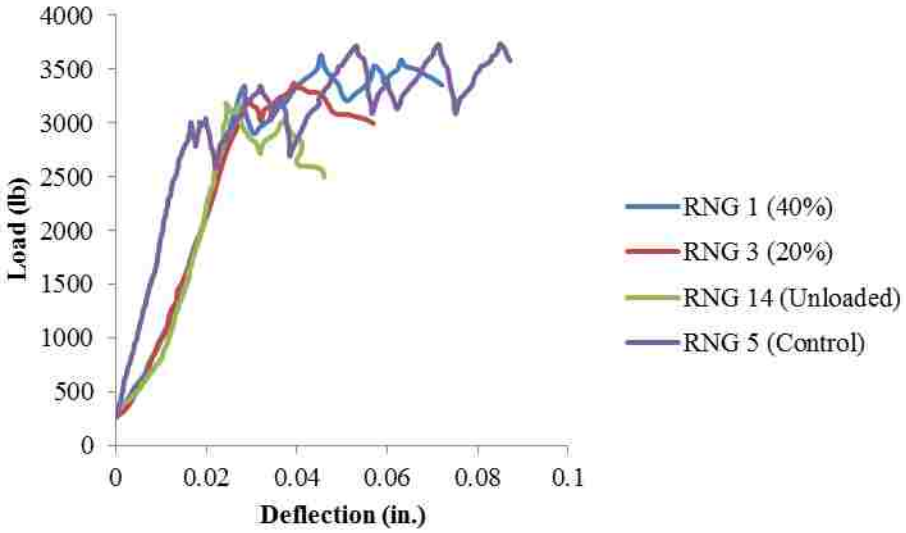

Conversion Units: 1 in. = 25.4 mm, 1 lb = 0.0044 kN

Figure 4.23. Load-deflection characteristics of the RNG specimens

The fracture SRP surface of the control specimens after the bond failure revealed the curved fracture lines (see Figure 4.24). In the contrast to this, the surface of the SRP

strips showed few or no curved lines. Figure 4.25 illustrates the samples of SRP sheet. Pellegrino et al. [96] obtained the similar results in a non-related durability study.

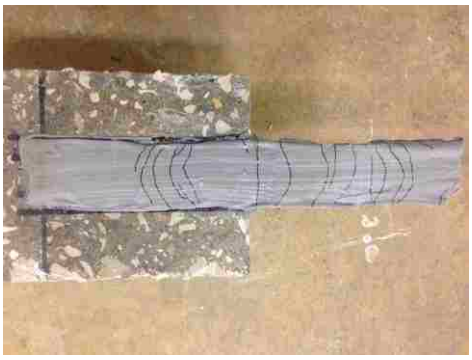

Figure 4.24. SRP sheet with curved lines in control specimen

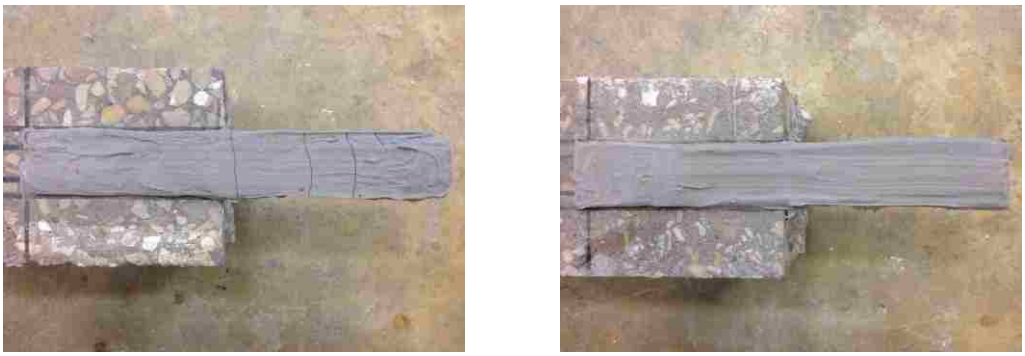

Figure 4.25. SRP sheets in conditioned sample

As shown in Figure 4.24, the distance between the curved lines was not always the same, but despite the inconstant spacing of the fracture lines, these lines were always curvilinear for all control SRP specimens. This indicates that the deformation of SRP strengthening system was not constant along the transverse axis. It was a maximum value in the middle of the bonded area and a minimum value at the edges of the SRP sheet. Therefore, it can be concluded that the delamination began in the middle of the SRP

strengthening system and then extended continuously to the lateral areas of the SRP strip. There were few or no curved lines on the surface of SRP sheets for the conditioned specimens (see Figure 4.25). This also suggests that bond performance was deteriorative when the SRP specimens were subjected to the freezing and thawing, temperature, and humidity cycles in the environmental chamber.

The specimens exposed to the environmental chamber were in Failure Mode 3. The control specimens were in Failure Mode 1. Figure 4.26 and 4.27 illustrate the SRP sheets with some concrete of a typical conditioned specimen (RG 1) and a representative control specimen (RG 7) reinforced with micro-fine galvanized coating steel fibers, respectively. The failure modes of SRP specimens, including conditioned (RNG 2) and control specimens (RNG 6) reinforced with micro-fine brass coating steel fabrics, are shown in Figure 4.28 and 4.29. The failure modes of the other specimens are illustrated in Appendix B.

For the control RG and RNG specimens, it was observed that the fracture surface of the SRP strengthening system (Figures 4.27 and 4.29) passed almost completely through the concrete into the concrete substrate and included some hardened paste and aggregate after the beams failed. However, there was only small amount concrete to partially cover the surface of the SRP strips for the conditioned specimens. It can be concluded that the bond behavior between concrete and the SRP strengthening system was degraded by the conditioning in the environmental chamber. The concrete substrate area that was covered on the surface of the fractured SRP sheet was calculated by using the IMAGE J (see Table 4.6 and 4.7). From Figure 4.25 and 4.27, the percentage of concrete substrate area of RG 1 was 57.8%. In the contrast to this, RNG 2 had a concrete substrate area of 29.4%. Therefore, the exposed specimens were in Failure Mode 3. The percentages of concrete substrate area for RG 7 and RNG 6 were 92% and 90.1%, respectively. Consequently, the control RG and RNG specimens were in Failure Mode 1 based on the definition of the failure modes before, as illustrated in Figure 4.27 and 4.29. In addition, there were no signs to demonstrate that the steel fibers in the epoxy resin were corroded when the SRP specimens were exposed to the environmental chamber. This indicates that the epoxy resin can protect the micro-fine galvanized and brass

coating steel fibers considerably. It could also indicate that these two types of steel fibers can resist the corrosion greatly.

Figure 4.26. The failure mode of a typical conditioned specimen reinforced with galvanized coating steel fibers (RG 1, Failure Mode 3)

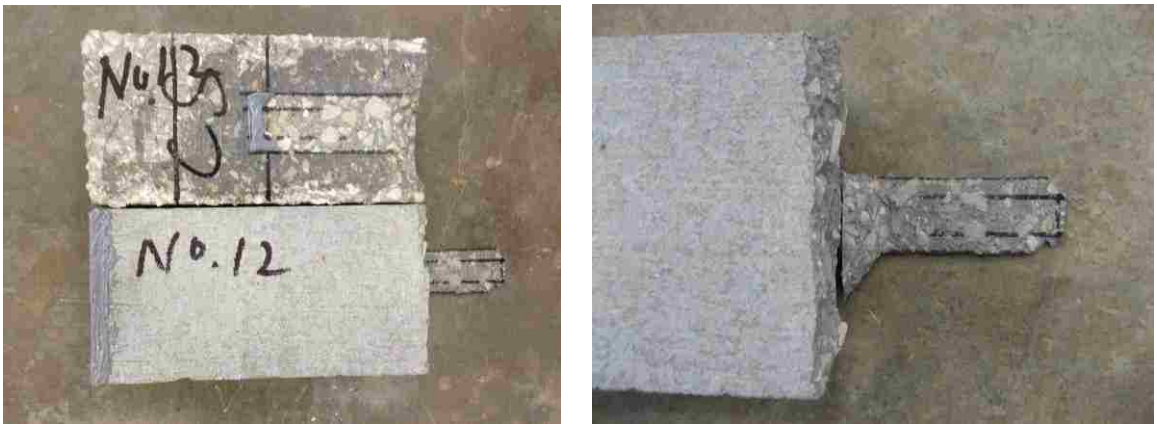

Figure 4.27. The failure mode of a representative control specimen reinforced with galvanized coating steel fibers (RG 7, Failure Mode 1)

Figure 4.28. The failure mode of a typical conditioned specimen reinforced with brass coating steel fibers (RNG 2, Failure Mode 3)

Figure 4.29. The failure mode of a typical control specimen reinforced with brass coating steel fibers (RNG 6, Failure Mode 1)

Tables 4.7 and 4.8 illustrate mechanical properties such as the ultimate loads, peak loads, first peak loads, and maximum deflections; failure modes; and percentages of concrete-covered substrate areas for the control and conditioned specimens reinforced with micro-fine galvanized and brass coating steel wires.

Table 4.7. SRP specimens reinforced with galvanized coating steel fibers

Specimens (40%)	Ultimate Load (lb)	Max Def. (in.)	First Peak load (lb)	Peak Load (lb)	Failure Mode	Concrete (%)
RG 1	3027.4	0.0518	3221.4	3404.1	Mode 3	57.8
RG 2	2647.0	0.0379	3321.2	3325.8	Mode 3	58.1
RG 5	3318.4	0.0529	3124.4	3788.3	Mode 3	48.8
Average	2997.6	0.0475	3222.3	3506.1		54.9
Specimens (20%)	Ultimate Load (lb)	Max Def. (in.)	First Peak load (lb)	Peak Load (lb)	Failure Mode	Concrete (%)
RG 3	3150.5	0.0580	3116.9	3590.6	Mode 3	34.5
RG 4	2919.3	0.0491	3333.3	3333.3	Mode 3	43.5
RG 6	3359.4	0.0707	3557.1	3795.8	Mode 3	56.6
Average	3143.1	0.0593	3335.8	3573.2		44.9
Unloaded	Ultimate Load (lb)	Max Def. (in.)	First Peak load (lb)	Peak Load (lb)	Failure Mode	Concrete (%)
RG 8	2389.6	0.0443	3038.6	3038.6	Mode 3	13.9
RG 9	2923.0	0.0677	3307.2	3348.2	Mode 3	22.9
RG 10	2628.3	0.0399	3075.9	3075.9	Mode 3	52.1
RG 12	3116.9	0.0434	3005.0	3366.8	Mode 3	38.3
RG 14	3094.6	0.0517	3217.6	3288.5	Mode 3	83.9
Average	2830.5	0.0494	3128.9	3223.6		42.2
Control	Ultimate Load (lb)	Max Def. (in.)	First Peak load (lb)	Peak Load (lb)	Failure Mode	Concrete (%)
RG 7	3318.4	0.0618	3392.9	3795.8	Mode 1	92
RG 11	3710	0.0979	3109.5	3836.8	Mode 1	92
RG 13	3385.5	0.0785	3042.3	3780.9	Mode 1	98.6
Average	3471.3	0.0794	3181.6	3804.5		94.2
Conversion units: 1 in. = 25.4 mm, 1 lb = 0.0044 kN						

Note: “RG” indicates the specimens reinforced with galvanized coating steel fibers, “RNG” indicates the specimens reinforced with brass coating steel fibers. “Concrete %” indicates the percentage of the failure mode within the concrete substrate.

As shown in Table 4.7, all the three control specimens resulted in an ultimate deflection more than the SPR specimens that were exposed to the environmental chamber. The average ultimate deflection of the control specimens was 0.0858 in. (2.18 mm). The average ultimate displacements of the specimens stressed by 40% of the ultimate load, 20% of the ultimate load, and unloaded were 0.0475 in., 0.0593 in., and 0.0494 in. (1.25 mm, 1.51 mm, and 1.25 mm), respectively. These displacements

decreased by 44.6%, 30.9%, and 42.4%, respectively, compared to the control specimens. Consequently, it can be concluded that the bond performance of the SRP-to-concrete system deteriorated after exposure of the environmental condition. All SRP specimens failed due to the debonding between the concrete and the SRP strengthening system. Figures 4.25 and 4.26 illustrate two representative RG specimens.

The average percentage of concrete-covered substrate area for the control specimens was 94.2%. In contrast to this, the percentages of concrete-covered substrate area of loaded (40% and 20%) and unloaded specimens decreased by 41.7%, 52.4%, and 55.0%, respectively, when compared to the control specimens. Therefore, the three control RG specimens were in Failure Mode 1. However, the exposed specimens illustrated Failure Mode 3. Therefore, the bond durability of the specimens was degraded after being exposed to the environmental chamber.

The control specimens failed at higher loads. The average peak loads of the three control specimens were also higher than those of the SRP specimens after exposure to the environmental chamber. However, there was no substantial difference between the average first peak loads of the control and conditioned RG specimens, which suggests that the initial cracking of SRP specimens on the tension side was not affected by the conditioning in the environmental chamber. In other words, the tensile strength of concrete was not degraded by the environmental conditioning.

As shown in Table 4.8, the average ultimate deflection of 0.0748 in. (1.90 mm) was much higher for all the three control specimens than those of the SPR specimens that experienced the freeze-thaw, temperature, and humidity cycles. The average ultimate displacements of the conditioned specimens stressed by 40% of the ultimate load, 20% of the ultimate load, and the unstressed samples were 0.0631 in. (1.60 mm), 0.0566 in. (1.44 mm), and 0.0511 in. (1.30 mm), respectively. They decreased by 15.6%, 24.4%, and 31.7%, respectively, compared to that of control specimens. Consequently, it can be concluded that the bond performance of the SRP-to-concrete system was deteriorated after exposure to environmental conditions. All SRP specimens failed due to the debonding of different concrete-covered substrate areas between the concrete and the SRP strengthening system. Figures 4.25 through 4.28 show typical failed samples.

Table 4.8. SRP specimens reinforced with brass coating steel fibers

Specimens (40%)	Ultimate Load (lb)	Max Def. (in.)	First Peak load (lb)	Peak Load (lb)	Failure Mode	Concrete (%)
RNG 1	3389.2	0.0722	3333.3	3631.7	Mode 3	37.1
RNG 2	3818.2	0.08	3120.7	4004.7	Mode 3	29.4
RNG 7	2326.2	0.0372	2475.4	2475.4	Mode 1	98.9
Average	3177.9	0.0631	2976.5	3370.6		55.1
Specimens (20%)	Ultimate Load (lb)	Max Def. (in.)	First Peak Load (lb)	Peak Load (lb)	Failure Mode	Concrete (%)
RNG 3	3027.4	0.0571	3228.8	3378.0	Mode 3	52.0
RNG 4	2934.2	0.0559	3176.6	3176.6	Mode 3	41.2
RNG 8	2941.6	0.0567	2676.8	3225.1	Mode 3	46.5
Average	2967.7	0.0566	3027.4	3259.9		46.6
Unloaded	Ultimate Load (lb)	Max Def. (in.)	First Peak load (lb)	Peak Load (lb)	Failure Mode	Concrete (%)
RNG 9	3146.8	0.0582	3340.7	3538.4	Mode 3	32.4
RNG 10	2699.2	0.0529	3012.5	3068.4	Mode 3	20.4
RNG 11	3098.3	0.0560	3333.3	3370.6	Mode 3	24.7
RNG 13	3020.0	0.0434	3187.8	3187.8	Mode 3	33.5
RNG 14	2486.6	0.0449	3197.5	3197.5	Mode 3	26.2
Average	2890.2	0.0511	3214.4	3272.5		27.4
Control	Ultimate Load (lb)	Max Def. (in.)	First Peak load (lb)	Peak Load (lb)	Failure Mode	Concrete (%)
RNG 5	3609.3	0.0878	3023.7	3739.8	Mode 3	30.5
RNG 6	3739.8	0.0830	3527.2	4291.9	Mode 1	90.1
RNG 12	2658.2	0.0537	2826.0	3184.1	Mode 1	97.8
Average	3335.8	0.0748	3125.6	3738.6		72.8
Conversion units: 1 in. = 25.4 mm, 1 lb = 0.0044 kN						

Note: “RG” indicates the specimens reinforced with galvanized coating steel fibers, “RNG” indicates the specimens reinforced with brass coating steel fibers. “Concrete %” indicates the percentage of the failure mode within the concrete substrate.

The control specimens failed at higher loads. The average peak load of the three control specimens was much higher than that of the SRP specimens after exposure to the environmental chamber, but there was no substantial difference between the average first peak loads of the control and conditioned specimens after exposure to the environmental chamber. This indicates that the combination of freeze-thaw cycles, temperature, and humidity cycles in the environmental chamber did not influence the initial cracking of

concrete, meaning there was no loss of tensile strength of concrete observed for the conditioned specimens.

The average percentage of concrete-covered substrate area of the SRP sheet for the control specimens was 72.8%, which was much higher than those of conditioned specimens. In contrast to this, the percentages of concrete-covered substrate area of loaded (40% and 20%) and unloaded specimens decreased by 24.2%, 36.0%, and 62.3%, respectively, when compared to the control specimens. Therefore, the three control specimens were in Failure Mode 1, except RNG 5, which failed in Failure Mode 3. However, the exposed specimens illustrated Failure Mode 3, except RNG 7, which exhibited Failure Mode 1. Therefore, the bond durability of the RNG specimens degraded after exposure to the environmental chamber.

It should be noted in Tables 4.7 and 4.8 that ultimate loads of the specimens that were stressed illustrated some difference to those of unloaded samples. Because the concrete and epoxy resin have their own thermal properties (different coefficient of thermal expansion), this difference will result in the thermal incompatibility between the epoxy and the base concrete when these specimens experience the freeze-thaw, temperature, and humidity cycles [97]. When the temperature in the environmental chamber changes, the concrete volume will expand or shrink. Meanwhile, the expansion or shrinkage of the SRP strengthening system will also occur. However, the SRP strip will expand or shrink differently than the concrete due to different thermal expansion coefficients, so it will be restrained by the interfacial bond. Consequently, the excess bond shear stress in the SRP sheet will degrade the interfacial bond performance. The SRP strip is tensioned as the SRP specimen is bent by the spring-loaded fixture, which counteracted partially the bond shear stress in the strip. As a result, this tension in the SRP sheet may improve the bond performance between the concrete substrate and the SRP strengthening system. Subsequently, the ultimate loads of the stressed specimens are higher than those of unloaded SRP samples.

According to the percentage of concrete-covered substrate area and ultimate loads of conditioned SRP specimens, all of the conditioned specimens (except RNG 7) failed in Failure Mode 3 when they were exposed to an aggressive environment. In contrast to this, the control specimens were in Failure Mode 1, which is the target failure mode based on

the ACI 440.9R-15. Consequently, it should be concluded that the bond performance of the SRP-to-concrete systems degraded under the varying temperatures and humidity.

According to the ultimate loads of the control and exposed specimens that are listed in Tables 4.7 and 4.8, the environmental reduction factors (C_E) of 0.81 and 0.87 were acquired for conditioned RG and RNG specimens, respectively. The condition of environmental chamber may be defined as "air environments" with exposure of 100% RH for sustained periods of time based on Deng *et al.* [19] definition of the design environments. It is a less-severe exposure where water or moisture can simply accumulate on the boundary between the SRP strengthening system and concrete substrate. A C_E of 0.81 is therefore recommended for SRP-to-concrete systems subjected to an "air environment" with low UV radiation. This value may be a conservative estimate based on the relative bond durability of the SRP strengthening system under the accelerated aging environmental condition.

The failure loads and percentages of concrete-covered substrate areas of control and conditioned SRP specimens are summarized in Figures 4.30 and 4.31.

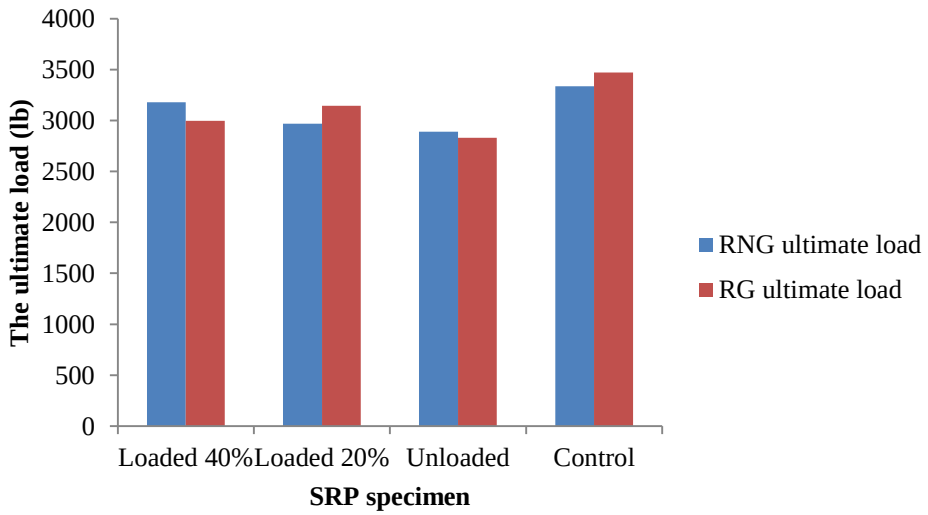

Conversion Units:1 lb = 0.0044 kN

Figure 4.30. Failure loads for RNG and RG specimens

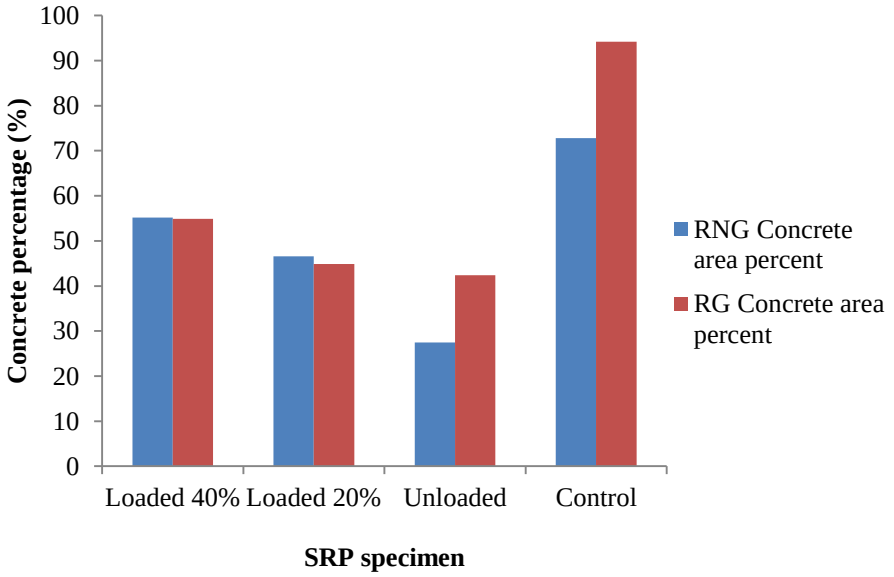

Figure 4.31. The percentage of concrete substrate area for RNG and RG specimen

It should be noted from Figure 4.30 that there were no high deviations for the ultimate loads between the RG and RNG specimens. The conditioned specimens failed at lower loads with lower percentages of concrete-covered substrate areas. For the specimens reinforced with micro-fine galvanized coating steel fibers, the average ultimate loads of the conditioned specimens decreased by 13.6% (loaded 40%), 9.5% (loaded 20%), and 18.5% (unloaded), respectively, when compared to the control specimens. For the RNG specimens, the average ultimate loads of the conditioned specimens decreased by 4.7% (loaded 40%), 11.0% (loaded 20%), and 13.4% (unloaded), respectively, when compared to that of the control RNG specimens. This suggests that the combination of the freeze-thaw, temperature, and humidity cycles degraded the bond performance between the SRP sheet and concrete substrate.

In addition, the average final capacity of loaded (40% and 20%) specimens reinforced with these two types of steel fibers were similar of the unloaded samples for this specific exposure condition. This finding is different than traditional CFRP and GFRP externally bonded FRP system [103]. In contrast, the tension in loaded specimens

may partially counteract the additional shear in SRP strip. Consequently, the final loads of the unloaded samples were lower when compared to the loaded specimens.

It can be seen in Figure 4.31 that no major difference of the concrete-covered substrate areas on the fracture SRP strips was observed for the stressed RG and RNG specimens. The concrete-covered substrate areas for the unloaded specimens were similar when compared to those of the stressed samples. The concrete-covered substrate areas of the control RG and RNG specimens were much higher than those of conditioned SRP-to-concrete systems because their bond characteristics were not degraded after exposure to the laboratory.

The results from the flexural bending test have suggested that the combination of freeze-thaw cycles, varying temperature, and humidity cycles resulted in considerable loss of the load carrying capacity or bond shear strength between the concrete and the SRP strengthening system. The failure mode shifted from Failure Mode 1 in the specimens without environmental cycling to Failure Mode 3 in conditioned SRP specimens.

4.3.3. Direct Pull-Off Test. Tensile pull-off tests are generally applied to Investigate the adhesion of a coating to a stiff substrate such as metal, concrete, or wood. Such tests are commonly utilized to evaluate the bond quality in situ. The tensile pull-off bond stress is also an important bond performance factor for FRP-to-concrete interfaces [98]. Previous studies have evaluated the pull-off bond behavior of FRP-to-concrete systems. Malvar et al. [99] investigated the influence of moisture and chloride content on the CFRP bond to concrete by using the direct pull-off test. CFRP specimens were exposed to saltwater and marine conditions for 48 months. The results showed that application of primer improved the bond between CFRP and concrete. Carrillo [100] evaluated the bond performance of CFRP-to-concrete systems when exposed to various environmental conditions like salt water and wet-dry and freeze-thaw cycles. The results indicated that various failure modes were obtained, and there were some discrepancies. No significant pattern was found when comparing the conditioned specimens to the control ones. Benzarrti et al. [101] studied the bond behavior between CFRP and concrete under hygrothermal and accelerated aging for several months. The testing results illustrated that there was an apparent decrease in the pull-off bond strength when the

specimens were subjected to hygrothermal aging. The initial failure mode was cohesive within the concrete substrate. However, the mixed or adhesive failure modes were found over time. Myers et al. [81] evaluated the effect of different surface coarseness and concrete strength on the pull-off bond strength of the concrete reinforced with CFRP sheet. The failure mode was cohesive within the concrete substrate for all the specimens. The pull-off results had a large scatter and variation. There was no necessary relation between the bond strength and surface roughness. No signification difference was found between the average pull-off values for the 3000 psi (20.7 MPa) and the 4000 psi (27.6 MPa) concrete.

In addition, the direct pull-off test is a direct, simple, and standardized method when compared to the other methods. Therefore, it was applied to this study to evaluate the pull-off bond strength, discuss failure modes, and compare the results to the flexural bending tests of SRP-strengthened concrete systems under the combination of environmental cycling. The concrete blocks with SRP sides were maintained after the three-point bending tests. A concrete saw was used to cut the sides without SRP to make sure that the pull-off specimens were balanced.

4.3.3.1 The test setup of this experiment. In order to isolate the adhesion fixture of 1.81 in. (46 mm) in diameter that was attached to the surface of the SRP pull-off specimen (see Figure 4.32), a diamond bit was used to drill the SRP into the concrete to a target depth of 0.25 in. (6.4 mm). Next, one type of epoxy was utilized to glue the dolly to the surface of the core. After this adhesion fixture cured for four or five days to guarantee the epoxy's strength, the DYNA Z Pull-Off Tester with digital manometer (shown in Figure 4.33) was used to pull the dolly with a pull pin off in direct tension. The test setup is illustrated in Figure 4.34. Finally, a peak tension value was recorded by the pull-off tester to evaluate the bond performance of the SRP-concrete interface.

4.3.3.2 The experimental results and discussion. According to ASTM D7522 [102], there are seven types of failure modes. They are defined in Table 4.9. The bond between concrete and SRP strips was evaluated by tensile stress at failure and the percentage of concrete-covered substrate area attached on the surface of SRP.

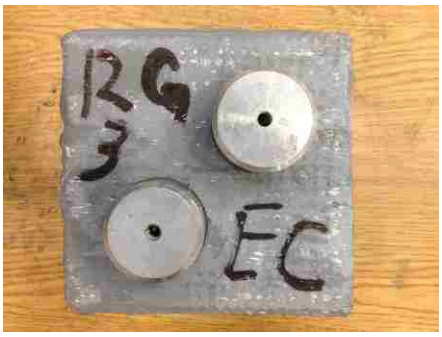

Figure 4.32. A typical adhesion fixture

Figure 4.33. The DYNA Z pull-off tester

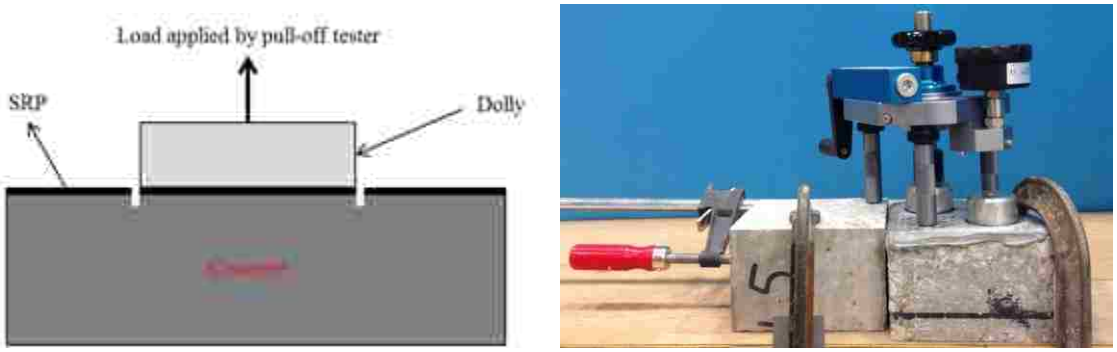

Figure 4.34. The test setup for the pull-off bond test

Table 4.9. The types of Failure Modes of pull-off bond test [102]

Failure Mode	Detailed Description
A	Bonding adhesive failure at loading fixture
B	Cohesive failure in FRP laminate
C	Adhesive failure at FRP/adhesive interface
D	Cohesive failure adhesive
E	Adhesive failure at FRP/concrete interface
F	Mixed Mode E and Mode G
G	Cohesive failure in concrete substrate

Pull-off tests with failure modes A through F are considered to be premature failures, and failure Mode G is the expected failure mode. In this section, the pull-off bond strength (or concrete strength) was calculated by the following equation:

$$\sigma = \frac{4F_p}{\pi D^2} \tag{4.1}$$

where σ is the pull-off bond strength (psi [MPa]), F_p is the pull-off force (lb [N]), and D is the diameter of the loading fixture (in. [mm]).

The final failure loads of twenty-two conditioned specimens (ten for micro-fine galvanized coating steel fiber and ten for micro-fine brass coating steel fibers) and five control specimens were measured (three for micro-fine galvanized coating steel fiber and two for micro-fine brass coating steel fibers). Meanwhile, the bond strengths of these specimens were calculated and compared. The test results of all specimens are summarized in Table 4.10.

Table 4.10. The ultimate loads and bond strengths for the pull-off specimens

Specimen	Ultimate load (#1) (lb)	Failure Mode (#1)	Ultimate load (#2) (lb)	Failure Mode (#2)	Bond strength (#1) (psi)	Bond strength (#2) (psi)
Conditioned specimens						
RG 1	885	Mode G	1059	Mode G	343.2	410.6
RG 2	832	Mode G	1024	Mode G	322.6	397.1
RG 3	1211	Mode G	821	Mode F (87.9%)	469.6	318.4
RG 4	937	Mode G	1106	Mode G	363.3	428.9
RG 5	1379	Mode G (95.2%)	797	Mode F (76.9%)	534.7	309.1
RG 6	728	Mode G	N/A	N/A	282.3	N/A
RG 8	233	Mode G	1019	Mode G (94.7%)	90.4	395.1
RG 9	960	Mode G	873	Mode G	372.3	338.5
RG 10	955	Mode G	989	Mode G	370.3	383.5
RG 12	1193	Mode G (96.9%)	1013	Mode G	462.6	392.8
RG 14	1273	Mode G	N/A	N/A	405.4	N/A
RNG 1	693	Mode G	995	Mode G	268.7	385.8
RNG 2	1170	Mode G	995	Mode G	453.7	385.8
RNG 3	861	Mode G	576	Mode G	333.9	223.4
RNG 4	902	Mode G	687	Mode G	349.8	266.4
RNG 7	960	Mode F (83.2%)	501	Mode F (76.7%)	372.3	194.3
RNG 8	914	Mode G	722	Mode G	354.4	280.0
RNG 9	1071	Mode G	1030	Mode G	415.3	399.4
RNG 10	658	Mode G	576	Mode G (95.6%)	255.2	223.4
RNG 13	664	Mode G (96.1%)	698	Mode G	257.5	270.7
RNG 14	646	Mode G	599	Mode G	250.5	232.3
Control specimens						
RG 7	733	Mode G	943	Mode G	284.2	365.7
RG 11	786	Mode G	576	Mode G	304.8	223.4
RG 13	861	Mode G	1024	Mode G	333.9	397.1
RNG 6	424	Mode G	279	Mode G	164.4	108.2
RNG 12	1065	Mode G	594	Mode G	413.0	230.3
Converse units: 1 lb = 0.0044 kN, 1 psi = 0.0069 MPa						

Note: RG means the specimens reinforced with galvanized coating steel fibers, RNG means the specimens reinforced with brass coating steel fibers. % means the percentage of concrete substrate area when compared to the area of SRP core.

It may be noted in Figure 4.35 that control specimens failed in Mode G. The explanation is that the control specimen was maintained in the laboratory. Therefore, the bond performance between the SRP and the concrete substrate was not affected and the direct pull-off bond strength of SRP system was higher than the tensile strength of concrete. The majority of the conditioned specimens failed in Mode G. It seemed that the bond durability for SRP-to-concrete systems using the direct pull-off test was not degraded by the environmental cycling. However, according to the results of flexural bending tests, the bond performance showed deterioration. Therefore, it is possible that the tensile strengths of the pull-off specimens were higher than the tensile strength of concrete even though the bond characteristics may have had some level of degradation after exposure to environmental cycling, simply not captured based on the weak link in the failure mode. It should be noted that the failure modes of RG 3 (core #2), RG 5 (core # 2), and RNG 7 (cores #1 and #2) were Mode F. This may be due to the non-homogenous characteristic of the concrete, applied load rate using hand method, or the inconsistency in specimen preparation.

The average bond stresses, standard deviations, and coefficient of variation (COV) of conditioned and control RG and RNG specimens are summarized in Table 4.11 and Figure 4.38.

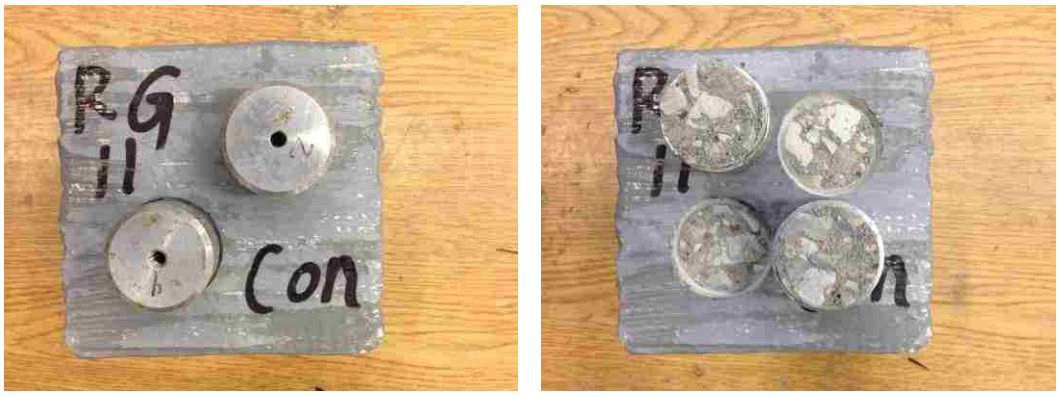

Figure 4.35. A typical control specimen with failure Mode G

Figure 4.36. Pull-off specimens reinforced with galvanized coating steel fibers (Mode F)

Figure 4.37. Pull-off specimens reinforced with brass coating steel fibers (Mode F)

Table 4.11. The average bond strength and standard deviation

SRP specimen	Average bond stress (psi)	Standard deviation	COV (%)
Conditioned RG	369.5	88.9	24.1
Conditioned RNG	308.6	75.7	24.5
Control RG	318.2	61.7	19.4
Control RNG	229.0	132.4	57.8
Converse Units: 1 psi = 6.9 kPa			

High standard deviations and coefficient of variations of the control and conditioned specimens were observed in Table 4.11 and Figure 4.38. For all of the pull-off test results illustrated a higher COV when compared to that of ASTM C 39 (10%) [80]. It should be noted that the highest COVs are control specimens reinforced with brass coating steel fibers, which had only four replicate specimens tested. This test method is known to produce large variation. There was a large degree of scatter and variation, indicating the variability of this test method.

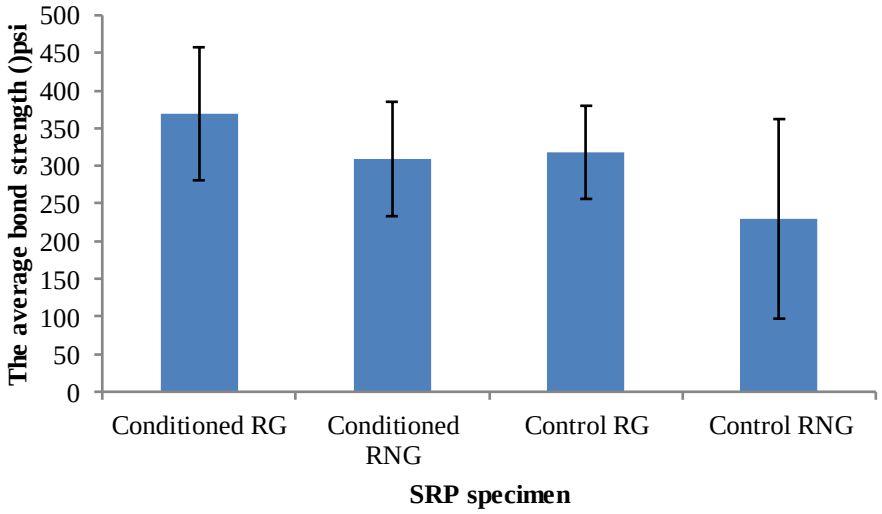

Conversion Units: 1 psi = 6.9 kPa

Figure 4.38. Average pull-off test results for conditioned and control specimens

In addition, there was no interfacial bond strength loss of the conditioned RG and RNG specimens observed when compared to the control specimens. Their failure modes were Mode G (cohesive failure in concrete substrate). The higher temperature exposures in the environmental chamber could have resulted in added post-curing of the epoxy, which caused the pull-off bond strength or concrete strength to be higher when compared to the control specimens.

It should be noted that the results of the flexural bending tests were opposite when compared to those of pull-off tests. The conditioned RG and RNG specimens failed in

Failure Mode 3 when performing the flexural bending tests, which means that there was only a few concrete to attach on the fracture SRP sheet. However, the failure modes were observed mainly in the concrete substrate (Mode G) for the conditioned pull-off specimens. Possibly due to the moisture or humidity concentration in the concrete substrate that was close to the edges of the SRP strip. Ouyang and Wan [104] and Au and Büyüköztürk [91] suggested that the moisture concentrated in the concrete substrate next to the primer layer was a main factor to deteriorate the interfacial bond performance between the concrete and FRP. For this research, no indication of corrosion of steel fibers in the epoxy was observed on SRP strengthening systems under the environmental cycling. It should be concluded that the moisture did not penetrate and diffuse into the epoxy to corrode steel fibers, therefore the epoxy was highly effective to protect the steel wires. The adhesion of two materials is related to several mechanisms including absorption, mechanical interlocking, diffusion, and electrostatic mechanisms [105]. Even if it is unclear how moisture affects each single mechanism above, it can be revealed that primer-to-concrete boundary was the weakest link [55]. The moisture infiltrated easily into the interface near the SRP-to-concrete boundary in this study. Therefore, the bond performance was degraded by the moisture diffusion in the area near this boundary. This is possibly due to the flexural bending specimens failing in Failure Mode 3. However, the moisture for pull-off bond testing did not easily reach the locations of drilled cores. As a result, the bond performance of SRP systems may not be influenced by the moisture in those areas, resulting in no bond strength loss. Additionally, the direct tension bond strength was higher than the tension strength of concrete, leading to Mode G presented in pull-off specimens.

4.4. THE EXPERIMENT IN TAP WATER (AMBIENT TEMPERATURE)

Moisture is absorbed when an FRP strengthening system is exposed to a moist environment, which may cause plasticization of FRP through hydrolysis. As a result, the glass transition temperature (T_g) will decrease, which induces relaxation in the polymer matrix. This can result in the loss of mechanical properties of the FRP system, ultimately leading to a fiber-matrix or adhesive bond failure. Therefore, moisture has been considered one of the most important deleterious issues to influence the bond durability

of FRP strengthening systems and concrete substrates. Aiello et al. [106] and Tu and Kruger [107] reported that water submersion resulted in bond strength degradation between concrete and epoxy. Wan et al. [108] concluded that CFRP composite systems were immersed into water, leading to an adhesive failure along the primer-concrete interface.

In order to evaluate the effects of moisture or water on the bond performance of SRP-to-concrete systems, the SRP specimens were submerged completely in tap water at ambient temperature for 3,000 hours. Six specimens (three for micro-fine galvanized coating steel fibers, three for micro-fine brass coating steel fibers) were prepared as mentioned above. Meanwhile, ten SRP tensile coupon specimens (five for micro-fine galvanized and five for micro-fine brass coatings steel fibers) were also maintained in tap water, as illustrated in Figure 4.39.

According to ACI Committee 440.9R-15, ASTM C78, and ASTM D7522, the three-point bending and direct tensile pull-off tests were performed to evaluate the long-term bond durability of SRP-to-concrete systems in tap water.

Figure 4.39. SRP specimens in tap water

4.4.1. Flexural Bending Tests (Three-Point Load Tests). In this section, the bond performance between the SRP strengthening system and concrete substrate was investigated by flexural bending tests. The SRP specimens were maintained in the laboratory for one week in order to dry them after the immersed exposure of 3,000 hours.

The flexural bending tests were performed. The test setup was the same as that of the experiment in the environmental chamber. All SRP-reinforced concrete members were loaded by using an MTS 880 to conduct the flexural bending tests. Load was applied at a constant rate of 0.005 in./min (0.127 mm/min) to cause failure of the specimens in 9 to 10 minutes. The deflections of both sides at the mid-span of the SRP specimen were measured by using two linear variable displacement transducers (LVDTs) with ±0.5 in. (12.7 mm). Figure 4.40 illustrates a representative three-point loading test configuration.

Figure 4.40. A typical flexural bending test configuration

The specimens were tested under a Displacement-controlled machine under three-point loading. This section exhibits the bending test results and analysis of the results for peak and failure loads and maximum deflection. The concrete-covered substrate area on the fracture SRP strip was analyzed for each specimen after beam flexural testing, and the failure mode of the SRP specimen was also investigated, which provided qualitative insight into bond degradation between the SRP strengthening system and concrete substrate.

The crack occurred at the tip of the saw cut. Debonding between concrete and SRP sheet initiated when the peak tensile stress in concrete and SRP strip exceeded the interfacial shear bond stress. The debonding occurred initially in the middle of the SRP strip (the intersection with the saw cut) due to the weakening of the cross section of the saw cut and the highest bending moment at the mid-span of the specimen, and then

extended out through the end of the SRP system until the specimen failed. The load-deflection characteristics of the conditioned and control RG and RNG specimens reinforced under three-point loading are illustrated in Figure 4.41.

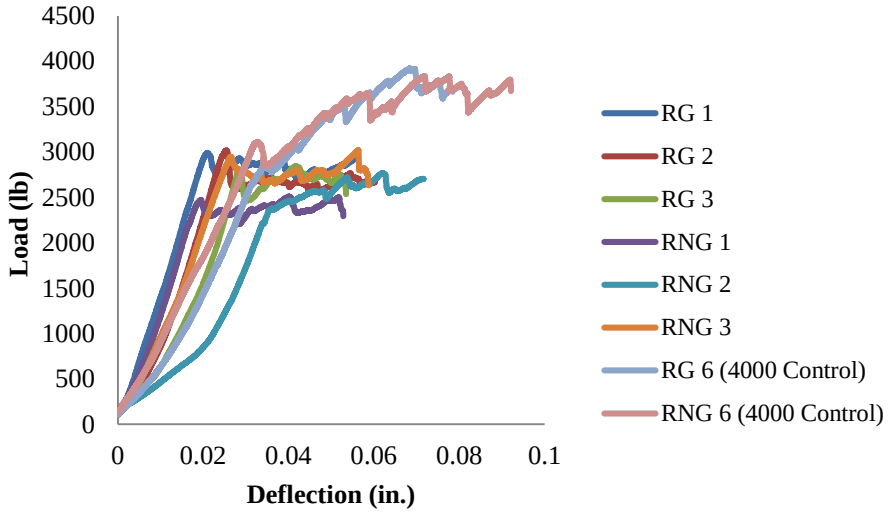

Conversion Units: 1 in. = 25.4 mm, 1 lb = 0.0044 kN

Figure 4.41. Load-deflection characteristics of the SRP specimens reinforced with galvanized and brass coating steel fibers

It can be seen in Figure 4.41 that the SRP control specimen (RG 6 and RNG 6) had a larger ultimate deflection than the conditioned specimens that were exposed to tap water. Ultimate ductility of the control specimens was higher than those of the conditioned specimens. It should be noted that a considerable decrease in ultimate load capacity occurred for the SRP sheet strengthened specimens that were subjected to tap water. However, no significant difference when the cracking moment occurred between the conditioned and control specimens. At the beginning of the flexural bending test, the load-deflection behaviors of the control and conditioned specimens were almost linear until the cracking moment of the concrete prism was exceeded. The flexural strength in the SRP specimens dropped at the start of the tension cracking in the concrete. These points demonstrated that the SRP strips bridged cracking in the concrete. The load

capacities of the control specimens continued to increase significantly until failure after the first peak loads occurred. In contrast to this, there was no an apparent degree of increase after the first peak loads for conditioned RG and RNG specimens. For the control specimens, they experienced several peak loads until failure. The conditioned specimens failed at lower loads with lower deflections. Therefore, it can be concluded that the bond durability of the conditioned specimens was degraded by tap water. The bond strength between the SRP sheet and the concrete decreased considerably. The stiffness of these SRP specimens, however, was almost the same even if the bond characteristics of the control specimens were much stronger than those of the conditioned samples, as shown in Figure 4.41.

The control specimens failed in Failure Mode 1. The conditioned SRP specimens failed in Failure Mode 3. Figures 4.42 and 4.44 show the typical failed specimens. No steel corrosion on the SRP strengthening systems was observed for the conditioned specimens. The results for other failed specimens immersed in tap water are available in Appendix B.

For the control specimens reinforced with micro-fine galvanized and brass coating steel fibers that were maintained in the laboratory for 4,000 hours, it was observed that the fracture surface of the SRP strengthening system (Figure 4.44) passed almost completely through the concrete and included some hardened paste and aggregate after the beams failed. However, there was only a small amount of concrete to cover the surface of the SRP strip for the specimens immersed in tap water. It should be concluded that the bond behavior between the concrete and the SRP system was significantly affected by tap water. Because there was a sufficient amount of water to penetrate the interface of the SRP-to-concrete system through the boundary between the SRP and concrete substrate to deteriorate the bond performance. In addition, no corrosion of steel fibers was observed. It can be concluded that the epoxy resin utilized in this research showed perfect moisture-tolerant behavior to protect the steel fibers. The concrete substrate area that was covered on the fractured SRP sheet was calculated by using the IMAGE J (see Tables 4.12). Shown in Figures 4.42 and 4.43, the percentages of the concrete substrate area were only 10.6% and 14.1%, respectively. In contrast to this, the control specimen (see Figure 4.44) had a concrete substrate area of 95.3% that failed in

Failure Mode 1. Therefore, all conditioned specimens except RNG 3 (Failure Mode 2) failed in Failure Mode 3 except based on ACI 440.9R-15.

Figure 4.42. A typical failed specimen reinforced with galvanized coating steel fibers under tap water (3,000 hours)

Figure 4.43. A representative failed specimen reinforced with micro-fine brass coating steel fibers under tap water (3,000 hours)

Table 4.12 and 4.13 illustrate mechanical properties such as the ultimate loads, peak loads, first peak loads, and maximum deflections; failure modes; and percentages of the concrete-covered substrate area for the control and conditioned specimens reinforced with micro-fine galvanized and brass coating steel wires.

Figure 4.44. A typical failed control specimen (4,000 hours)

In Table 4.12, all control specimens deformed more than the SPR specimens that were subjected to tap water. The ductility for each control specimen was higher than the conditioned specimens. The average deflections of the control RG and RNG specimens were 0.0826 in. (2.10 mm) and 0.0806 in. (2.05 mm), respectively. In contrast to control specimens, the average displacements of the conditioned RG and RNG specimens were 0.0535 in. (1.50 mm) and 0.0602 in. (1.53 mm), respectively. For the conditioned RG and RNG specimens, the average final deflection decreased by 35.2% and 25.3%, respectively, when compared with those of control specimens. Subsequently, it should be concluded that the bond performance of the SRP-to-concrete system deteriorated after exposure of tap water. All SRP specimens failed due to the debonding between the concrete and SRP strengthening system. Figure 4.42 and 4.43 illustrate two representative conditioned specimens reinforced with micro-fine galvanized and brass coating steel fabrics, respectively.

The control specimens failed at higher ultimate loads. The average peak loads of the control specimens were much higher than those of SRP specimens after exposure to tap water. There was no significant degree of variation observed in mechanical properties and maximum deflections between the conditioned RG and RNG specimens and between the control RG and RNG samples respectively. There was little difference observed for the first peak loads between control and conditioned specimens. This indicates that tap water did not influence the initial cracking of concrete, which means no loss of the concrete's tensile strength observed for the conditioned specimens.

Table 4.12. SRP specimens reinforced with galvanized and brass coating steel fibers

Specimens immersed into tap water for 3,000 hours						
Specimen	Ultimate load (lb)	Max. def. (in.)	First peak load (lb)	Peak load (lb)	Failure mode	Concrete (%)
RG 1	2927.3	0.0560	2991.3	2991.3	Mode 3	14.1
RG 2	2665.0	0.0602	3019.4	3019.4	Mode 3	13.4
RG 3	2535.5	0.0535	2808.9	2844.7	Mode 3	15.2
Average	2709.3	0.0566	2939.9	2951.8		14.2
RNG 1	2292.9	0.0528	2472.5	2508.5	Mode 3	10.6
RNG 2	2700.7	0.0717	2574.9	2767.5	Mode 3	16.3
RNG 3	2632.5	0.0588	2947.1	3020.5	Mode 2	6.8
Average	2542.0	0.0602	2664.8	2765.5		11.2
Control specimens for 4,000 hours						
Specimen	Ultimate load (lb)	Max. def. (in.)	First peak load (lb)	Peak load (lb)	Failure mode	Concrete (%)
RG 6	3663.6	0.0785	2866.0	3921.5	Mode 1	95.1
RG 7	3946.1	0.0823	3046.1	4269.2	Mode 1	82.1
RG 8	3514.5	0.0871	2912.6	3759.8	Mode 1	94.3
Average	3708.1	0.0826	2941.6	3983.5		90.5
RNG 6	3670.9	0.0921	3091.4	3834.9	Mode 1	95.3
RNG 7	3433.0	0.0690	3046.1	3593.4	Mode 1	95.7
Average	3551.9	0.0806	3068.8	3714.1		95.5
Conversion Units: 1 in. = 25.4 mm, 1 lb = 0.0044 kN						

Note: “RG” indicates the specimens reinforced with galvanized coating steel fibers, “RNG” indicates the specimens reinforced with brass coating steel fibers. “Concrete %” indicates the percentage of the failure mode within the concrete substrate.

The average percentages of concrete-covered substrate areas for the control RG and RNG specimens were 90.5% and 95.5%, respectively. However, for the conditioned specimens, there was only a little concrete attached to the fractured SRP strips near the saw cut area due to more epoxy close to this zone when preparing the specimens. The average percentages of concrete-covered substrate areas for the conditioned RG and RNG specimens were 14.2% and 11.2%, respectively. Therefore, the conditioned specimens failed in Failure Mode 3. It should be noted that RNG 3 failed in Failure Mode 2 (adhesive failure). The preparation of this specimen could be a possible explanation. It indicates that the bond durability of the specimens immersed in tap water decreased

considerably. However, the steel fibers in the epoxy were not corroded by tap water due to the perfect moisture resistance of the epoxy.

According to the failure loads of all RG and RNG specimens listed in Table 4.12, it can be estimated that 0.72 for an environmental reduction C_E factor is suggested in a "wet environment" based on the findings herein. According to the definition of Deng [19], this condition should be that water can continuously accumulate at the boundary between the composite strengthening system and the concrete. This value may be a conservative estimate based on the relative bond durability of SRP strengthening system with micro-fine galvanized and brass coating steel fibers.

The failure loads and the percentages of concrete-covered substrate areas of control and conditioned SRP specimens are presented in Figures 4.45 and 4.46.

From Figure 4.45, it should be noted that there are no high deviations for the average ultimate loads between the conditioned RG and RNG specimens and between the control RG and RNG samples, respectively. The conditioned specimens failed at lower loads with a lower percentage of concrete cover. For the specimens reinforced with these types of steel fibers, the average ultimate loads of conditioned RG and RNG specimens decreased by 26.9% and 28.4% respectively, when compared to the control RG and RNG specimens, therefore suggesting that the bond performance of the SRP-to-concrete system deteriorated after the exposure to tap water for 3,000 hours. The results are the same as those of Aiello et al. [106] and Tu and Kruger [107], where water immersion resulted in the deterioration of bond performance for epoxy-bonded concrete.

It can be seen in Figure 4.46 that the average concrete-covered substrate area on the fracture SRP strips of the conditioned RG specimens was almost the same as that of conditioned RNG specimens. They significantly decreased by 84.3% and 88.2% when compared to the results of control RG and RNG specimens, respectively.

The results from the flexural bending tests have suggested that the specimens immersed in tap water exhibited considerable loss of the load-carrying capacity or bond shear strength between the concrete and the SRP strengthening system. The failure mode shifted from the Failure Mode 1 in the control specimens to Failure Mode 3 in conditioned specimens. Therefore, the long-term bond durability of interface of the SRP-

to-concrete systems was considerably deteriorated after being exposed to tap water for 3,000 hours.

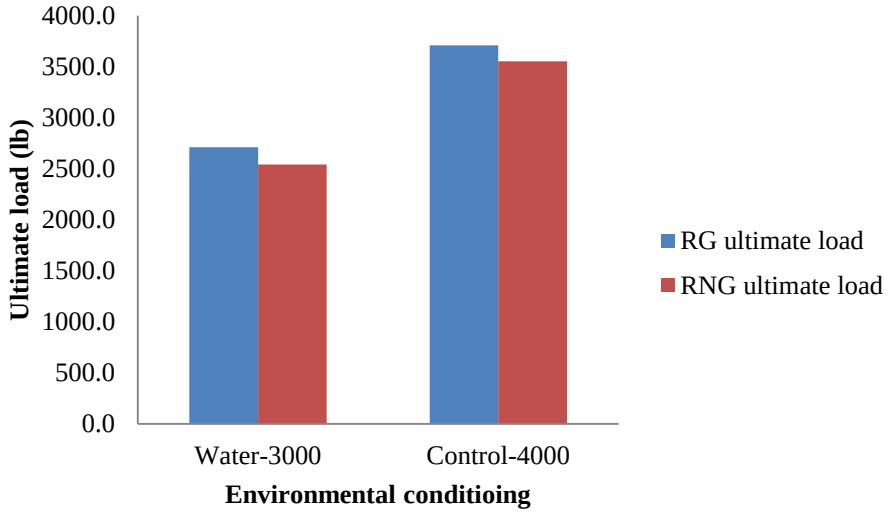

Conversion Units: 1 lb = 0.0044 kN

Figure 4.45. Ultimate loads for RG and RNG specimens under tap water

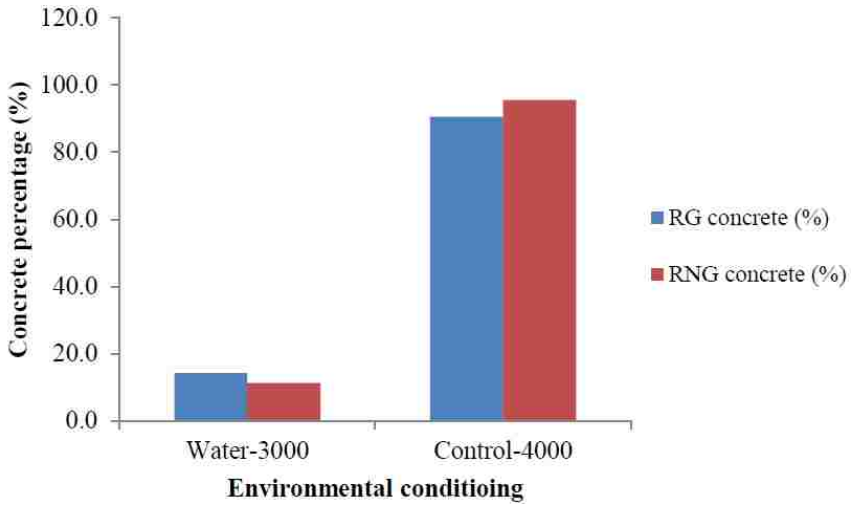

Figure 4.46. The percentage of concrete substrate area for RG and RNG specimens

4.4.2. Direct Pull-Off Test. In this part, the bond strength and failure mode were evaluated and discussed by direct pull-off test, and compared to the results of the flexural bending tests. The specimen preparation was the same as that of the experiment in the environmental chamber. The test setup is illustrated in Figure 4.34.

This test was conducted based on ASTM D7522. And the failure modes were defined by this standard, as shown in Table 4.8. The bond between the concrete and the SRP strengthening system was evaluated by direct tensile stress at failure and the percentage of concrete cover area.

The final failure loads of six conditioned specimens (three for micro-fine galvanized coating steel fiber and three for micro-fine brass coating steel fibers) were measured by the DYNA Z Pull-Off Tester. Meanwhile, the bond strengths of these specimens were calculated. The test results of all specimens subjected to tap water are summarized in Table 4.13.

It can be seen in Table 4.13 that the failure modes of the specimens submerged in tap water were Mode G (the definition in Table 4.8) except core #2 of RNG 1 and cores #1 and #2 of RNG 3. The failure modes of all SRP control specimens were Mode G. The concrete substrate area was measured by IMAGE J. According to Shen's study [103], the percentage of FRP failure was defined: Mode G = 0-15%, Mode F = 15-85%, there were only three cores that were failed in Mode F. No other types of failure modes were observed except Modes G and F. The lowest percentage of concrete cover area was 71.2%. The representative pull-off specimens with discs are illustrated in Figures 4.47 through 4.49. The other failed pull-off specimens that were submerged in water are available in Appendix B.

It should be observed in Figure 4.48 that control specimen (4,000 hours) failed in Mode G. The explanation is that the bond performance of control specimens was not degraded due to the exposure of the laboratory environment. And the direct pull-off bond strength of SRP system was higher than the tensile strength of concrete. The conditioned specimens were failed in Mode G besides core #2 of RNG 1 and cores #1 and #2 of RNG 3. The possible explanation is that the direct bond strength between SRP system and concrete substrate was higher than the tensile strength of concrete even if it was deteriorated after immersion of tap water. However, the failure modes of RNG 1 (core

#2), RNG 3 (core #1 and core #2) were Mode F. The reason may be related to several issues including non-homogenous characteristic of the concrete, applied load rate using hand, or the inappropriateness to prepare the specimens.

Table 4.13. The ultimate loads and bond strengths for the pull-off specimens

Specimen	Ultimate load (#1) (lb)	Failure mode (#1)	Ultimate load (#2) (lb)	Failure mode (#2)	Bond strength (#1) (psi)	Bond strength (#2) (psi)
Conditioned specimens (3000 hours)						
RG 1	1315	Mode G (96.7%)	1240	Mode G	516.3	486.9
RG 2	1030	Mode G	1467	Mode G	404.4	576.0
RG 3	396	Mode G (93.8%)	1117	Mode G	155.5	438.6
RNG 1	1537	Mode G	1304	Mode F (71.2%)	603.5	512.0
RNG 2	1228	Mode G	1019	Mode G (96.8%)	482.2	400.1
RNG 3	1257	Mode F (84.0%)	1560	Mode F (84.1%)	493.5	612.5
Control specimens (4000 hours)						
RG 6	815	Mode G	745	Mode G	320.0	292.5
RG 7	797	Mode G	N/A	Mode G	312.9	N/A
RG 8	797	Mode G	896	Mode G	312.9	351.8
RNG 6	396	Mode G	314	Mode G	155.5	123.3
RNG 7	797	Mode G	978	Mode G	312.9	384.0
RNG 8	1083	Mode G	658	Mode G	425.2	258.4
Converse Units: 1 lb = 4.4 N, 1 psi = 0.0069 MPa						

Note: RG means the specimens reinforced with galvanized coating steel fibers, RNG means the specimens reinforced with micro-fine brass coating steel fibers. % means the percentage of concrete substrate area when compared to the area of SRP core.

The average bond stresses, standard deviations, and COVs of conditioned and control RG and RNG specimens are summarized in Table 4.14 and Figure 4.50.

High standard deviations and coefficient of variations (COVs) of the control and conditioned specimens were observed in Table 4.14 and Figure 4.50. All the pull-off test results illustrated a higher COV when compared to that of ASTM C 39 (10%) [80] except

the result of the control RG specimens. There was a large degree of scatter and variation indicating the variability of this test method.

In addition, the bond performance between SRP and concrete substrate was deteriorative based on the results of flexural bending tests. However, for the pull-off bond testing, the failure modes of conditioned specimens were the Mode G (cohesive failure in concrete substrate), which means the direct tension strength of SRP-to-concrete system was higher than the tensile strength of concrete even if the bond behavior between SRP and concrete was degraded after the exposure to tap water. Additionally, the average interfacial bond strength of the conditioned specimens was much higher than the results of the control specimens. The possible explanation should be that the concrete was post-cured when it was submerged in tap water.

Figure 4.47. RNG 1 (Mode F)

Figure 4.48. RNG 3 (Mode F)

Figure 4.49. RNG 6 (control specimen)

Table 4.14. The average bond strength and standard deviation

SRP specimen	Ave. bond stress (psi)	Standard deviation	COV (%)
Conditioned RG	429.6	147.0	34.2
Conditioned RNG	517.3	80.1	15.5
Control RG	318.0	21.5	6.8
Control RNG	276.6	121.2	43.8
Conversion Units: 1 psi = 0.0069 MPa			

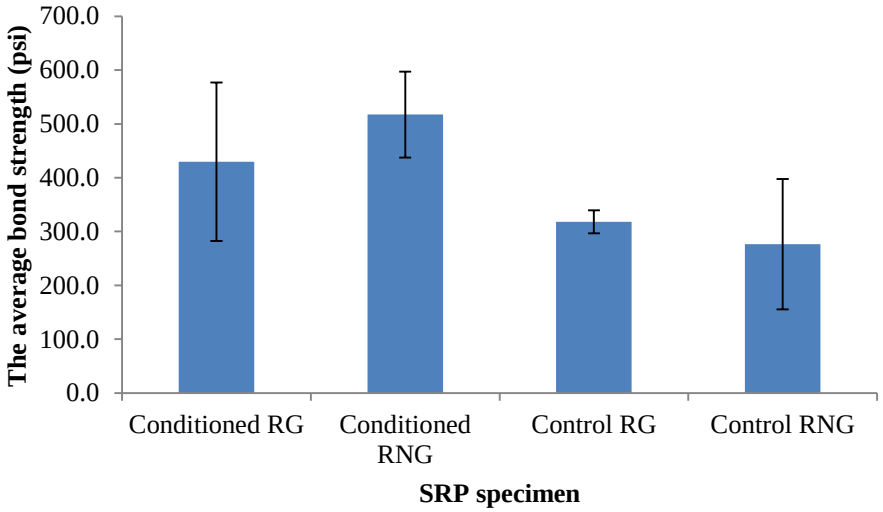

Conversion Units: 1 psi = 0.0069 MPa

Figure 4.50. Average pull-off test results for conditioned and control specimens

4.5. THE EXPERIMENT IN HOT WATER (122 °F [50 °C])

Moisture or water has been proved affecting the durability of SRP bonded concrete in the last two sections. This section combines the effects of temperature and moisture for accelerated aging environment. An overwhelming number of studies report strength loss due to the combination of temperature and moisture. Malvar et al. [99] performed pull-off tests of CFRP concrete and concluded that bond strength of CFRP-to-concrete systems reduced at high temperature and humidity. In addition, Deng et al. [19] studied durability characteristics of CFRP composite systems submerged in elevated-temperature water and found that greater bond strength loss presented as the exposure temperature increased.

In order to investigate the influence of the combination of temperature and moisture on the bond durability of SRP strengthening systems, for this section, the SRP specimens were submerged completely in hot water for up to 4,000 hours at 122°F (50°C) to evaluate the degradation of shear bond strength. A bucket stainless steel heater was used to heat water, and a temperature controller was utilized to control water temperature. They are shown in Figures 4.51 and 4.52, respectively.

Figure 4.51. Stainless steel heater

Figure 4.52. Temperature controller

At the same time, a 291 GPH submersible aquarium pump was used to make the water temperature uniform in the tank as illustrated in Figure 4.53.

Figure 4.53. Aquarium pump

Ten specimens (five for micro-fine galvanized coating steel fibers, five for micro-fine brass coating steel fibers) were prepared. Meanwhile, five RG and five RNG tensile coupon specimens were also maintained into hot water as illustrated in Figure 4.54. The preparation methodology of SRP specimens was mentioned before. The water tank was covered to reduce dissipation of temperature and evaporation of water.

According to ACI Committee 440 L, ASTM C78, and ASTM D7522, the three-point bending and direct tensile pull-off tests were performed to evaluate the long-term bond durability of the SRP-to-concrete systems after the exposure to hot water.

Figure 4.54. SRP specimens in hot water

4.5.1. Flexural Bending Tests (Three-Point Load Tests). In this section, the bond durability between SRP strengthening system and concrete substrate was evaluated by flexural bending tests. The SRP specimens were maintained in laboratory for one week in order to dry them after the exposure of 4,000 hours. The flexural bending tests were performed. The test setup was the same as that of the experiment in environmental chamber. All SRP-reinforced concrete members were loaded by using an MTS 880 to conduct the flexural bending tests. Load was applied at a constant rate of 0.005 in./min (0.127 mm/min) to cause failure of the specimens in 9 to 10 minutes. The deflections of both sides at the mid-span of the SRP specimen were measured by using two linear variable displacement transducers (LVDTs) with ±0.5 inch (12.7 mm). Figure 4.55 illustrates a typical three-point loading test configuration.

Figure 4.55. A typical three-point loading test configuration

The specimens were tested under displacement controlled testing machine under three-point loading. This section exhibits the bending test results and analysis of the results including peak and failure loads, maximum deflections, and failure modes of SRP specimens. The concrete cover area on the fracture SRP strip was analyzed after beam

flexural testing, and failure mode of SRP specimen was also observed, which provided qualitative insight into bond degradation between SRP and concrete substrate.

The crack initiated at the tip of the saw cut. Debonding between concrete and SRP sheet initiated when the peak tensile stress in concrete and SRP strip exceeded the interfacial shear stress. This debonding occurred initially in the middle of the SRP strip (the intersection with saw cut) due to the weakening of the cross section of saw cut and the highest bending moment at the midspan of the specimen, and then extended out through the end of the SRP system until the specimen was failed.

The typical load-deflection characteristics of the conditioned and control RG and RNG specimens under three-point loading are illustrated in Figures 4.56.

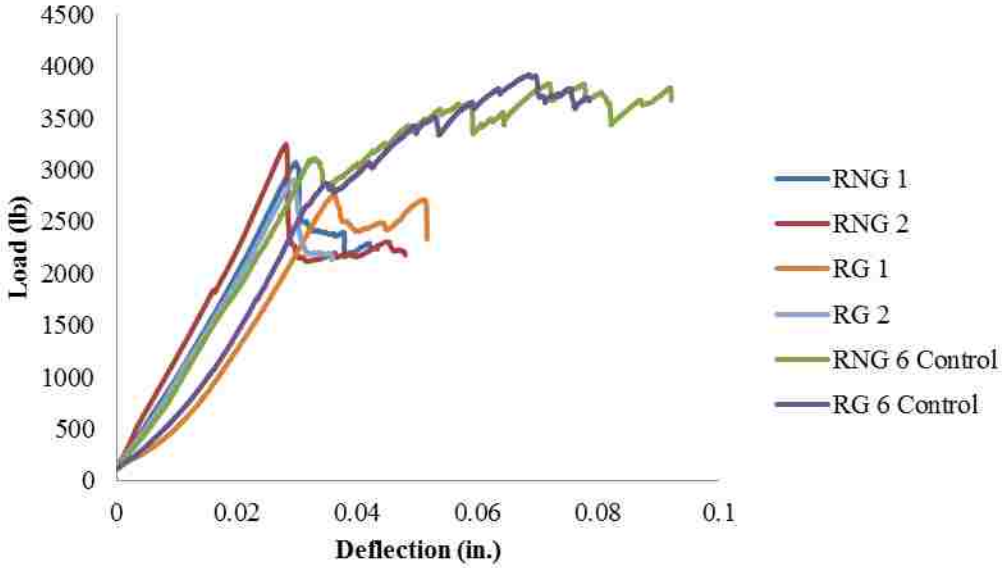

Conversion Units: 1 in. = 25.4 mm, 1 lb = 0.0044 kN

Figure 4.56. Load-deflection characteristics of the RG and RNG specimens

It can be seen in Figures 4.56 that the SRP control specimen (RG 6 and RNG 6) deflected more than the conditioned specimens that were exposed to hot water for 4,000 hours. The control specimens attained the highest ultimate deflection (and deflection-based ductility) compared to those of the conditioned specimens. It should be noted that a

significant decrease in ultimate load capacity of SRP sheet strengthened specimens that were subjected to hot water when compared to the control samples. However, there was not a significant difference when the cracking moment occurred between the conditioned and control specimens. At the beginning of the flexural bending test, the load-deflection behaviors of the control and conditioned specimens were almost linear until the cracking moment of the concrete prism was exceeded. The flexural load in the conditioned SRP specimens considerably dropped at the appearance of the tension cracking in the concrete. The first peak points demonstrated that the SRP strips bridged cracking in the concrete. The load capacities of the control specimens continued to increase significantly until failure after the first peak loads. In contrast to this, there was no an apparent degree of increase after the first peak loads for the conditioned specimens. For the control specimens, they experienced several peak loads until failure. The conditioned specimens failed at lower loads with lower deflections. Therefore, it can be proved that the bond durability of the conditioned specimens was deteriorated after the exposure to hot water. The bond strength between SRP sheet and concrete was decreased. The stiffness of these SRP specimens, however, was almost the same even if bond characteristics of the control specimen were much better than those of the conditioned samples as shown in Figure 4.56.

The control specimens failed in Failure Mode 1. The conditioned SRP specimens failed in Failure Mode 3 after the flexural bending test based on the types of failure modes mentioned before. Figures 4.57 and 4.59 show the typical failed specimens. No steel corrosion on the SRP strengthening system was observed for the conditioned RG and RNG specimens. The other failed specimens immersed in hot water are available in Appendix B.

For the control RG and RNG specimens that were maintained in the laboratory for 4,000 hours, it was observed that the fracture surface of the SRP strengthening system (Figure 4.58) almost completely passed through the concrete and included some hardened paste and aggregate after the beams failed. However, there were only few concrete to cover the surface of the SRP strip for the specimens after being immersed in hot water.

Figure 4.57. Failed RG 1 (4,000 hours)

Figure 4.58. Failed RNG 1 (4,000 hours)

Figure 4.59. Failed control specimen (4,000 hours)

It can be concluded that the bond behavior between concrete and the SRP system was significantly affected by hot water. It can be explained that there was sufficient water to penetrate the interface of SRP-to-concrete system through the boundary between the SRP and concrete substrate to deteriorate the bond behavior. At the same time, high temperature accelerated the penetration into this interface to degrade the bond performance. It was referred to as hygrothermal exposure. Therefore, it can be seen in Figure 4.55 that it was difficult to reach or exceed the first peak load after the cracking of concrete presented.

In addition, no corrosion of steel fibers was observed. It can be concluded that the epoxy resin utilized in this research behaved a perfect moisture-tolerant characteristic to protect the steel fibers. The concrete cover area on the fracture of SRP sheet was calculated by using the IMAGE J (see Tables 4.15). From the Figures 4.56 and 4.57, the percentages of concrete cover areas were only 16.1% and 12.3%, respectively. In contrast to this, the control specimen (see Figure 4.58) had a concrete substrate area of 95.3% that failed in Failure Mode 1. Therefore, the conditioned specimens failed in Failure Mode 3 according on ACI 440.9R-15.

Table 4.15 illustrates the mechanical properties including the ultimate loads, peak loads, and first peak loads; maximum deflections; failure modes; and percentages of concrete cover area on the surface of fracture SRP sheet for the control and conditioned RG and RNG specimens.

In Table 4.15, all control specimens considerably deformed more than the SPR specimens that were immersed in hot water. The average deflections of the control RG and RNG specimens were 0.0826 in. (2.10 mm) and 0.0806 in. (2.05 mm), respectively. In contrast to control specimens, the average displacements of the conditioned RG and RNG specimens were 0.0480 in. (1.22 mm) and 0.0461 in. (1.17 mm), respectively. For the conditioned RG and RNG specimens, the average final deflection decreased by 41.9% and 42.8%, respectively, when compared with the results of control RG and RNG specimens respectively. All SRP specimens failed due to the de-bonding between concrete and SRP strengthening system. Figures 4.56 and 4.57 illustrate two typical SRP specimens reinforced with micro-fine galvanized and brass coating steel fabrics, respectively.

Table 4.15. The results of conditioned and control specimens

Specimens submerged in hot water for 4,000 hours						
Specimen	Ultimate load (lb)	Max. def. (in.)	First peak load (lb)	Peak load (lb)	Failure mode	Concrete (%)
RG 1	2330.5	0.0515	2757.5	2757.5	Mode 3	12.3
RG 2	2129.0	0.0357	2910.7	2910.7	Mode 3	21.2
RG 3	2125.8	0.0460	2762.3	2874.0	Mode 3	22.8
RG 4	2669.7	0.0610	3002.7	3003.9	Mode 3	35.6
RG 5	2461.6	0.0459	3053.0	3091.4	Mode 3	26.4
Average	2343.3	0.0480	2897.2	2927.5		23.7
RNG 1	2233.4	0.0433	3006.7	3072.1	Mode 3	16.1
RNG 2	2177.1	0.0479	3249.8	3249.8	Mode 3	12.6
RNG 3	2083.7	0.0482	2999.0	2999.0	Mode 3	12.9
RNG 4	2610.6	0.0501	2802.0	2813.8	Mode 3	21.7
RNG 5	2161.8	0.0412	2717.3	2717.3	Mode 3	21.0
Average	2253.3	0.0461	2955.0	2970.4		16.9
Control specimens for 4,000 hours						
Specimen	Ultimate load (lb)	Max. def. (in.)	First peak load (lb)	Peak load (lb)	Failure mode	Concrete (%)
RG 6	3663.6	0.0785	2866.0	3921.5	Mode 1	95.1
RG 7	3946.1	0.0823	3046.1	4269.2	Mode 1	82.1
RG 8	3514.5	0.0871	2912.6	3759.8	Mode 1	94.3
Average	3708.1	0.0826	2941.6	3983.5		90.5
RNG 6	3670.9	0.0921	3091.4	3834.9	Mode 1	95.3
RNG 7	3433.0	0.0690	3046.1	3593.4	Mode 1	95.7
Average	3551.9	0.0806	3068.8	3714.1		95.5
Converse Units: 1 in. = 25.4 mm, 1 lb = 0.0044 kN						

Note: “RG” indicates the specimens reinforced with galvanized coating steel fibers, “RNG” indicates the specimens reinforced with brass coating steel fibers. “Concrete %” indicates the percentage of the failure mode within the concrete substrate.

The control specimens failed at higher ultimate loads. The average peak loads of the control specimens were much higher than those of SRP specimens that were exposed to hot water for 4,000 hours. There was no large degree of variation observed in mechanical properties and maximum deflections between the conditioned RG and RNG specimens, and between the control RG and RNG specimens, respectively. There was almost no difference observed for the first peak loads between control and conditioned

specimens. This indicates that hot water did not influence the initial cracking of concrete, which means no loss of tensile strength of concrete observed for the conditioned specimens.

The average percentages of concrete cover areas for the control RG and RNG specimens were 90.5% and 95.5%, respectively. However, for the conditioned specimens, there were only some concrete attached on the surface of the SRP near the saw cut area due to more epoxy closed to this zone when prepared the specimens. The average percentages of concrete-covered substrate areas for the conditioned RG and RNG specimens were 23.7% and 16.9%, respectively. Therefore, the failure modes for the conditioned specimens were the Failure Mode 3. It indicates that the bond durability of the specimens submerged in hot water was deteriorated considerably. However, the steel fibers in the epoxy were not corroded by hot water due to the perfect moisture-resistant epoxy. Figure 4.60 illustrates a typical surface of SRP strip after submersion of hot water.

Figure 4.60. A typical surface of SRP strip

According to the failure loads of all conditioned SRP specimens reinforced with micro-fine galvanized and brass coating steel fibers, it can be estimated that a C_E of 0.6 might be suggested in “wet environment” area with higher temperature. This condition should be considered a long-term exposure to a high temperature wet environment. This

value should be a conservative estimate based on the relative bond durability of SRP strengthening system with galvanized and brass coating steel fibers.

The failure loads and the percentages of concrete-covered substrate areas of control and conditioned SRP specimens are presented in Figures 4.61 and 4.62.

From Figure 4.61, one should be noted that there are no significant deviations for the average ultimate loads between conditioned RG and RNG specimens, and between control RG and RNG specimens, respectively. The conditioned specimens failed at lower loads with lower percentage of concrete-covered substrate area. For the specimens reinforced with micro-fine galvanized and brass coating steel fibers, the average ultimate loads decreased by 36.8% and 36.6%, respectively, when compared to those of the control RG and RNG specimens. The results are the same as those of [78] that hot water immersion at 122°F (50°C) resulted in deterioration of bond performance for epoxy bonded concrete.

It can be seen in Figure 4.62 that the average concrete substrate area on the surface of SRP strip of the conditioned RG specimens was slightly higher than that of conditioned RNG specimens. They significantly decreased by 73.9% and 82.3% when compared to those results of control RG and RNG specimens, respectively.

The results from the flexural bending tests have suggested that the specimens immersed in hot water have exhibited considerable loss of the load carrying capacity or bond shear strength between concrete and SRP strengthening system. The failure mode shifted from the Failure Mode 1 in the control specimens to the Failure Mode 3 in conditioned specimens. Therefore, the long-term bond durability of interface of SRP-to-concrete system was deteriorated considerably by hot water for 4,000 hours at 122°F (50°C).

4.5.2. Direct Pull-Off Test. In this part, the bond strength and failure mode were evaluated and discussed by direct pull-off test, and compared to the results of the flexural bending tests. The specimen preparation was the same as that of the experiment in the environmental chamber. The test setup is illustrated in Figure 4.34.

This test was conducted based on ASTM D7522. And the failure modes were defined by this standard, as shown in Table 4.8. The bond between concrete and SRP

sheet was evaluated by pull-off tensile stress at failure and the percentage of concrete cover area on the surface of SRP sheet.

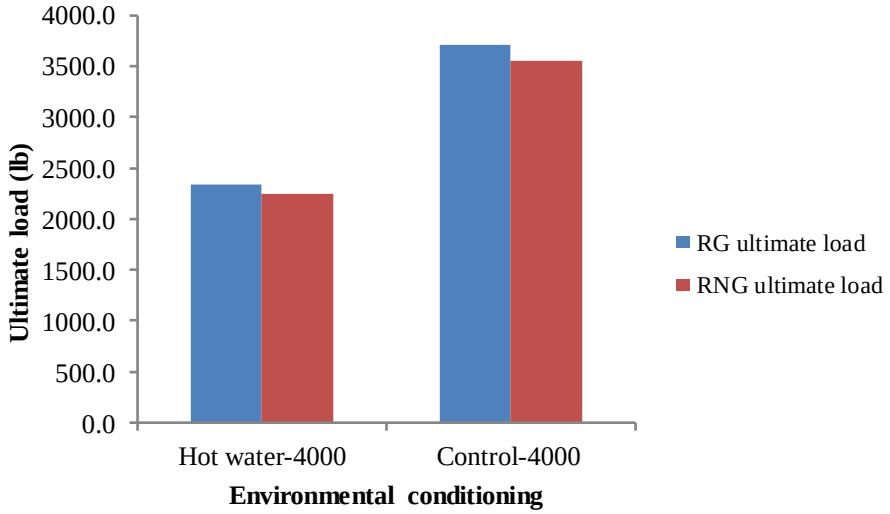

Conversion Units: 1 lb = 0.0044 kN

Figure 4.61. Ultimate loads for RG and RNG specimens under hot water

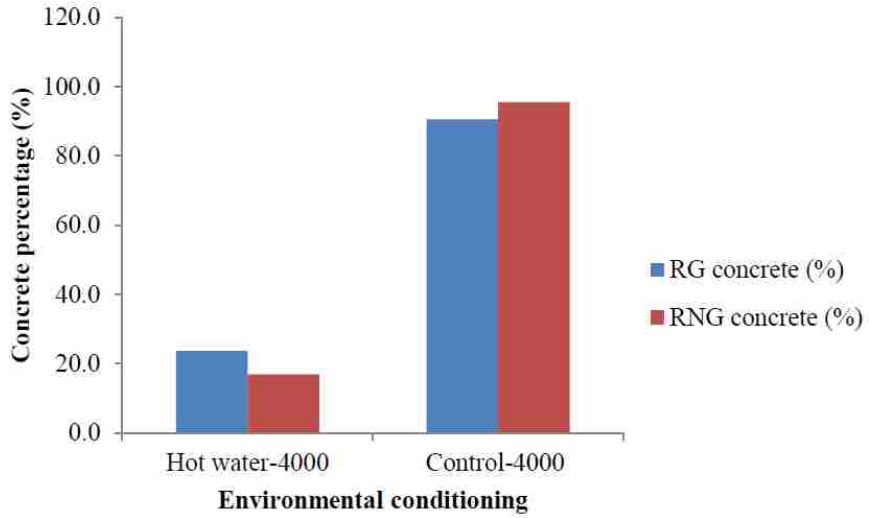

Figure 4.62. The percentage of concrete substrate area for RG and RNG specimens

The final failure loads of ten conditioned specimens (five for micro-fine galvanized coating steel fiber and five for micro-fine brass coating steel fibers) were measured by the DYNA Z Pull-Off Tester. Meanwhile, the bond strengths of these specimens were calculated. The test results of all specimens subjected to hot water are summarized in Table 4.16.

It can be seen in Table 4.16 that the failure modes of the specimens submerged in hot water were Mode G (see Table 4.8) except core #1 of RNG 3. The failure modes of all SRP control specimens were Mode G. The concrete substrate area was measured by IMAGE J. According to Shen's study [103], the percentage of FRP failure was defined as Mode G = 0-15%, Mode F = 15-85%, and only one core failed in Mode F. No other types of failure modes were observed. The lowest percentage of concrete substrate area was 82.3%. The representative pull-off specimens with discs are illustrated in Figures 4.63 through 4.65. The other failed pull-off specimens that were submerged in water are available in Appendix B.

It should be observed in Figure 4.65 that the control specimen (4,000 hours) failed in Mode G. The explanation is that bond performance of the control specimen was not degraded under the laboratory environment, and the direct pull-off bond strength of the SRP system was higher than the tensile strength of concrete. The conditioned specimens also failed in Mode G except core #1 of RNG 3, possibly because is that the direct bond strength between SRP and concrete substrate was higher than the tensile strength of concrete even if the bond strength was deteriorated after exposure to hot water. However, RNG 3 (core #1) failed in Mode F. The reason may be related to several issues, including the nonhomogenous characteristics of the concrete, applied load rate using hand, or the inappropriateness to prepare the specimens.

The average bond stresses, standard deviations, and COVs of conditioned and control RG and RNG specimens are summarized in Table 4.17 and Figure 4.66.

High standard deviations and coefficient of variations (COVs) of the control and conditioned specimens are shown in Table 4.17 and Figure 4.66. All the pull-off test results illustrated a higher COV when compared to that of ASTM C 39 (10%) [80] except the result of the control RG specimens. There was a large degree of scatter and variation, indicating the variability of this test method.

Table 4.16. The ultimate loads and bond strengths for the pull-off specimens

Specimen	Ultimate load (#1)	Failure Mode (#1)	Ultimate load (#2)	Failure Mode (#2)	Bond strength (#1)	Bond strength (#2)
Conditioned specimens (4000 hours)						
RG 1	1024	Mode G	1083	Mode G (86.7%)	397.1	420.0
RG 2	1083	Mode G	1019	Mode G	420.0	395.1
RG 3	681	Mode G	885	Mode G	264.1	343.2
RG 4	850	Mode G	501	Mode G	329.6	194.3
RG 5	861	Mode G	879	Mode G	333.9	340.8
RNG 1	716	Mode G (96.9%)	N/A	Mode G	277.6	N/A
RNG 2	1122	Mode G	1100	Mode G	435.1	426.5
RNG 3	454	Mode F (82.3%)	1059	Mode G	176.0	410.6
RNG 4	1129	Mode G (94.2%)	751	Mode G	437.8	291.2
RNG 5	565	Mode G	1106	Mode G (95.1%)	219.1	428.9
Control specimens (4000 hours)						
RG 6	815	Mode G	745	Mode G	320	292.5
RG 7	797	Mode G	N/A	Mode G	312.9	N/A
RG 8	797	Mode G	896	Mode G	312.9	351.8
RNG 6	396	Mode G	314	Mode G	155.5	123.3
RNG 7	797	Mode G	978	Mode G	312.9	384
RNG 8	1083	Mode G	658	Mode G	425.2	258.4
Converse units: 1 lb = 4.4 N, 1 psi = 0.0069 MPa						

Note: RG means the specimens reinforced with galvanized coating steel fibers, RNG means the specimens reinforced with micro-fine brass coating steel fibers. % means the percentage of concrete substrate area when compared to the area of SRP core.

In addition, the bond performance between the SRP and the concrete substrate was deteriorative based on the results of flexural bending tests. However, conditioned specimens failed in the Mode G (cohesive failure in concrete substrate) during direct tension tests. One possible explanation could be that the direct tension strength of SRP-

to-concrete system exposed to hot water was higher than the tensile strength of concrete because the concrete was post-cured in hot water environment even though the bond behavior of conditioned specimens was degraded.

Figure 4.63. RG 1

Figure 4.64. RNG 3 (Mode F)

Figure 4.65. RNG 6 (control specimen)

Table 4.17. The average bond strength and standard deviation

SRP specimen	Ave. Bond stress (psi)	Standard Deviation	COV (%)
Conditioned RG	343.8	71.6	20.8
Conditioned RNG	344.8	104.0	30.2
Control RG	318.0	21.5	6.8
Control RNG	276.6	121.2	43.8
Conversion unit: 1 psi = 0.0069 MPa			

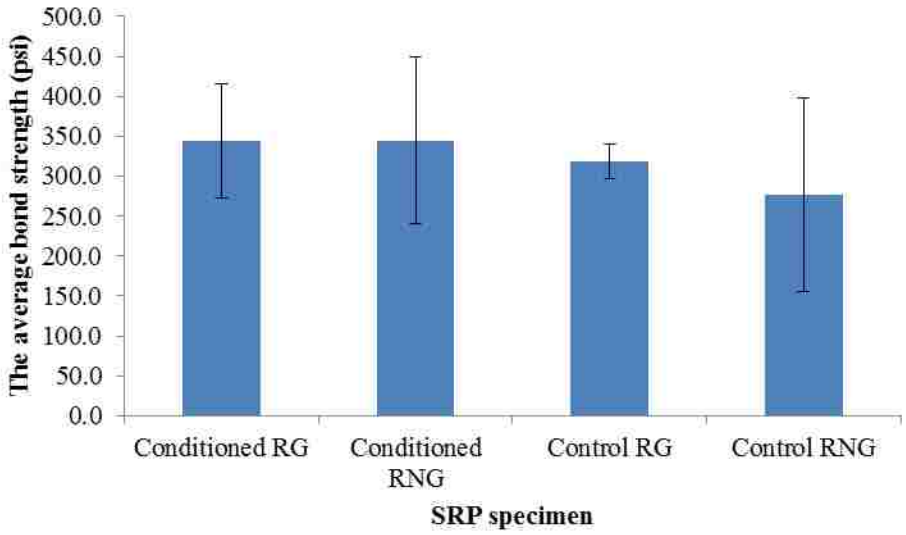

Conversion Units: 1 psi = 0.0069 MPa

Figure 4.66. Average pull-off test results for conditioned and control specimens

4.6. THE EXPERIMENTAL STUDY IN NaCl SOLUTION

Deicing salts are used to mitigate issues of ice formation on bridge decks in a freezing environment. This may affect bond performance for epoxy-bonded concrete members. Al-Mahmoud et al. [75] reported over bond strength of CFRP composite systems under saltwater immersion exposure and found loss of bond strength of concrete specimens reinforced with CFRP sheet after immersion in salt water. Toutanji and Gomez [17] reported that there was some loss in flexural strength when concrete beams reinforced with CFRP and GFRP sheet exposed to salt water. El-Hawary et al. [109]

observed that bond strength of epoxy-bonded concrete had a 25% decrease due to exposure to tidal salt water over 6, 12, and 18 months.

For this section, in order to simulate deicing salts, the SRP specimens were submerged completely in 15% salted tap water for up to 1,500 and 4,000 hours at laboratory temperature. As in the hot water test, a plastic tank was used. A 291 GPH submersible aquarium pump was used to make the salt density uniform in the tank, as illustrated in Figure 4.52. A total of twenty SRP concrete beams (ten for 1,500 hours, including five for RG and five for RNG specimens; ten for 4,000 hours, including five for RG and five for RNG specimens) and twenty SRP tensile coupon specimens (ten for 1,500 hours, including five for RG and five for RNG specimens; ten for 4,000 hours, including five for RG and five for RNG specimens) were prepared for this study. The SRP specimens were prepared as mentioned previously.

According to ACI Committee 440 L, ASTM C78, and ASTM D7522, the three-point bending and direct tensile pull-off tests were performed to evaluate the long-term bond durability of SRP-to-concrete systems in salt water.

4.6.1. Flexural Bending Tests (Three-Point Load Tests). In this section, the bond durability between the SRP strengthening system and concrete substrate was evaluated by flexural bending tests. The SRP specimens were maintained in laboratory for one week in order to dry them after the exposure of 1,500 and 4,000 hours. Figure 4.67 illustrates representative specimens after the exposure of salt water for 1,500 and 4,000 hours.

It can be seen in Figure 4.67 that there was no corrosion or deposition on the surface of the SRP strengthening systems after immersion in salt water. The flexural bending tests were performed. The test setup was the same as that of the experiment in the environmental chamber. All SRP-reinforced concrete members were loaded using an MTS 880 to conduct the flexural bending tests. Load was applied at a constant rate of 0.005 in./min (0.127 mm/min) to cause the specimens to fail after in 9 to 10 minutes. The deflections of both sides at the mid-span of the SRP specimen were measured by using two linear variable displacement transducers (LVDTs) with ±0.5 in. (12.7 mm).

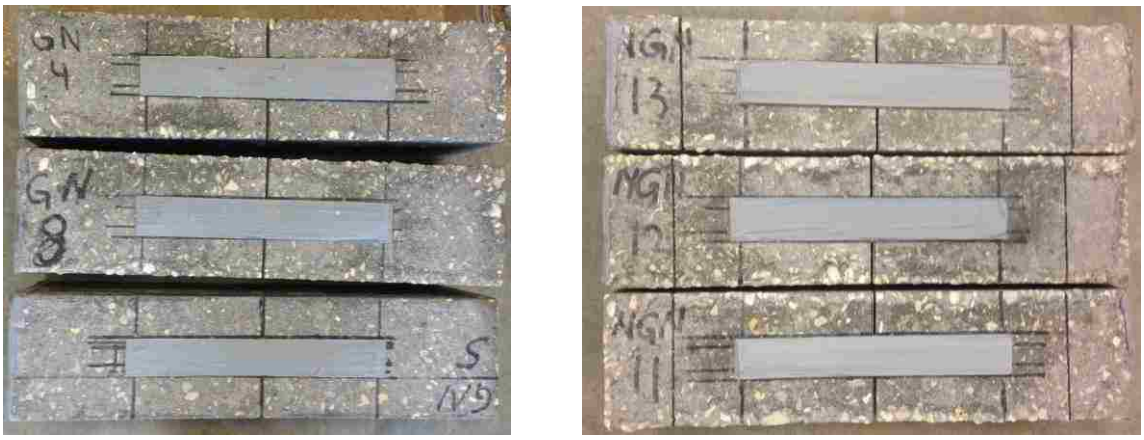

Figure 4.67. The specimens after the exposure of 1,500 (left) and 4,000 (right) hours

The specimens were tested with a displacement-controlled testing machine under three-point loading. This section exhibits the bending test results and analysis of the results for peak and failure loads and maximum deflection. The concrete substrate area that was attached on the surface of the SRP strip was analyzed after beam flexural testing, and failure mode of the SRP specimen was also observed, which provided qualitative insight into bond degradation between SRP and concrete substrate.

The crack occurred at the tip of the saw cut. Debonding between concrete and SRP sheet initiated when the peak tensile stress in the concrete and SRP strip exceeded the interfacial shear stress. This de-bonding occurred initially in the middle of the SRP strip (the intersection with the saw cut) due to the weakening of the cross section of the saw cut and the highest bending moment at the mid-span of the specimen, and then extended out through the end of the SRP system until the specimen failed. The typical load-deflection characteristics of the conditioned (1,500 and 4,000 hours) and control RG and RNG specimens (4,000 hours) reinforced under three-point loading are illustrated in Figure 4.68.

It can be seen in Figure 4.68 that the SRP control specimen (RG 6 and RNG 6) significantly deflected more than the conditioned specimens that were exposed to salt water for 1,500 and 4,000 hours. Ultimate ductility of the control specimens was higher than that of the conditioned specimens. It should be noted that a significant decrease

occurred in ultimate load capacity of SRP sheet-strengthened specimens that were immersed in salted tap water when compared to the control samples. However, no significant difference when the cracking moment occurred between the conditioned and control specimens.

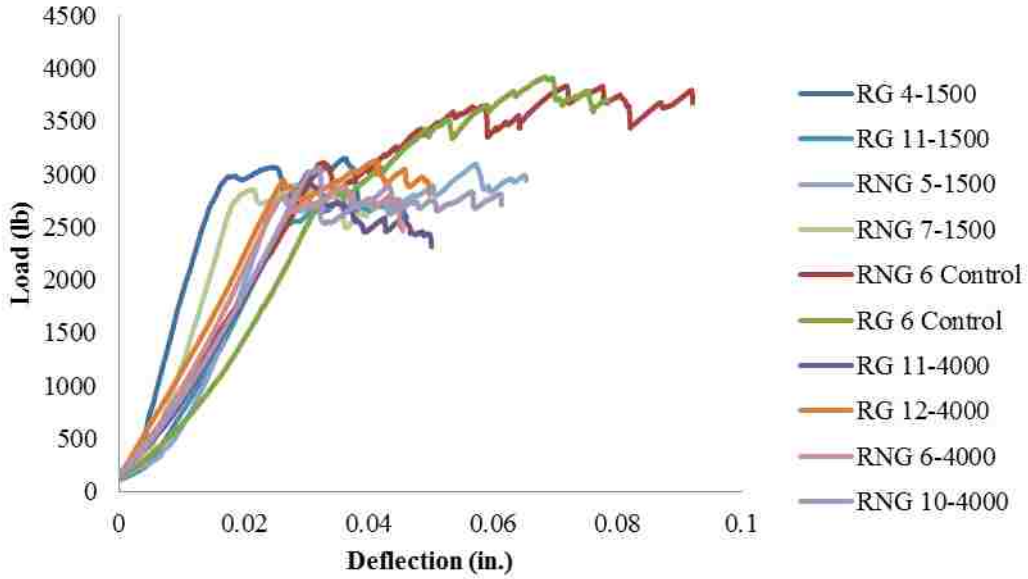

Conversion Units: 1 in. 25.4 mm, 1 lb = 0.044 kN

Figure 4.68. Load-deflection characteristics of the SRP specimens reinforced with galvanized (RG) and brass (RNG) coating steel fibers

At the beginning of the flexural bending test, the load-deflection behaviors of the control and conditioned specimens were almost linear until the initial cracking in the concrete beams. The flexural load in the conditioned RG and RNG specimens dropped at the start of the tension cracking in the concrete. These first peak points demonstrated that the SRP strips bridged cracking in the concrete. The load capacities and deflections of control specimens continued to increase significantly until failure after the first peak loads occurred. In contrast to this, there was no apparent load capacity increase after the first peak loads for conditioned specimens. The conditioned and control specimens experienced several peak loads until failure. The conditioned specimens failed at lower

loads with lower deflections. Therefore, it can be concluded that the bond durability of the conditioned specimens was deteriorated after submersion in salt water, which caused the bond strength of the SRP-to-concrete system to decrease. The stiffness of these SRP specimens, however, was almost the same even if bond characteristics of the control specimens were much better than those of the conditioned samples, as shown in Figure 4.68.

The control specimens failed in Failure Mode 1. The conditioned SRP specimens failed in Failure Mode 3 except RG 5, RG 6, and RNG 8 (1,500 hours), and RG 10, RG 11, RNG 10, and RNG 13 (4,000 hours) according to the types of failure modes mentioned previously. Figures 4.69 through 4.73 show some typical failed specimens. No steel corrosion was observed on the fracture SRP strengthening system for the conditioned specimens. The other failed specimens immersed into salted tap water are available in Appendix B.

After the control RG and RNG specimens were exposed to the laboratory for 4,000 hours, it was observed that the fracture surface of the SRP strengthening system (Figure 4.73) passed almost completely through the concrete and included some hardened paste and aggregate after the beams failed. However, there was little concrete to cover the fractured SRP strip for the specimens immersed into salt water, even though some specimens exhibited Failure Mode 2. It can be concluded that the bond behavior between concrete and the SRP system was significantly affected by salt water, most likely because there was sufficient water to penetrate the interface of the SRP-to-concrete system through the boundary between the SRP and concrete substrate to deteriorate the bond behavior. Therefore, it can be seen in Figure 4.68 that no apparent increases of load capacities were observed after the initial cracking presented.

In addition, no corrosion of steel fibers was observed on the fractured SRP sheets. It can be concluded that the epoxy resin utilized in this research exhibited a perfect moisture-tolerant behavior and resistance of chloride to protect the steel fibers. The concrete cover area was calculated by using the IMAGE J (see Table 4.18). From Figure 4.68 and 4.69, the percentages of concrete substrate areas were only 13.2% (Failure Mode 3) and 8.5% (Failure Mode 2) for RG and RNG specimens respectively, after exposure of 1,500 hours. Figure 4.71 and 4.72 illustrate that there was only 5.0% of

concrete for the RG specimen and 4.8% of concrete for the RNG specimen (both in Failure Mode 2) after exposure of 4,000 hours. In the contrast to this, the control specimen (see Figure 4.72) had a concrete substrate area of 95.3% that failed in Failure Mode 1.

Table 4.18 illustrates the mechanical properties for the RG and RNG specimens, including the ultimate loads, peak loads, and first peak loads; maximum deflections; failure modes; and areas of concrete that covered the surface of the fractured SRP sheet.

Figure 4.69. A typical failed RG specimen under salt water (1,500 hours)

Figure 4.70. A failed RNG specimen under salt water (1,500 hours) (Mode 2)

Figure 4.71. A typical failed RG specimen under salt water (4,000 hours)

Figure 4.72. A representative failed RNG specimen under salt water (4,000 hours)

Figure 4.73. A failed control RG specimen (4,000 hours)

Table 4.18. The results of conditioned and control specimens

Specimens submerged in salted tap water for 1,500 hours						
Specimen	Ultimate load (lb)	Max. def. (in.)	First peak load (lb)	Peak load (lb)	Failure mode	Concrete (%)
RG 4	2381.0	0.0464	2921.5	2921.5	Mode 3	17.6
RG 5	2980.3	0.0654	2818.6	3096.0	Mode 2	8.5
RG 6	2436.6	0.0630	2892.6	2892.6	Mode 2	9.1
RG 7	2752.3	0.0397	2852.2	2905.6	Mode 3	15.9
RG 8	2839.9	0.0492	2852.4	2852.4	Mode 3	19.4
Average	2678.2	0.0527	2867.5	2933.6		14.1
RNG 4	2744.8	0.0481	2922.7	3151.1	Mode 3	18.2
RNG 5	2240.4	0.0697	2736.4	2736.4	Mode 3	13.2
RNG 7	2551.0	0.0544	2933.4	2933.4	Mode 3	15.3
RNG 8	2752.3	0.0724	2728.7	2934.6	Mode 2	7.0
RNG 11	2595.3	0.0462	2518.4	2760.2	Mode 3	12.8
Average	2576.7	0.0582	2767.9	2903.1		13.3
Specimens submerged in salted tap water for 4,000 hours						
Specimen	Ultimate load (lb)	Max. def. (in.)	First peak load (lb)	Peak load (lb)	Failure mode	Concrete (%)
RG 9	2645.8	0.0538	2591.0	3069.9	Mode 3	15.7
RG 10	2995.5	0.0633	2964.5	3161.8	Mode 2	4.8
RG 11	2312.5	0.0516	3023.0	3023.0	Mode 2	7.6
RG 12	2805.9	0.0498	2943.6	3132.1	Mode 3	14.3
RG 13	2680.2	0.0535	3172.9	3181.3	Mode 3	11.7
Average	2688.0	0.0544	2939.0	3113.6		10.8
RNG 6	2744.8	0.0455	2782.5	2884.7	Mode 3	14.7
RNG 9	2559.1	0.0478	2677.9	2803.4	Mode 3	21.4
RNG 10	2707.1	0.0614	3020.3	3059.9	Mode 2	5.0
RNG 12	2585.8	0.0537	2874.3	2934.6	Mode 3	11.5
RNG 13	2759.9	0.0567	2901.7	3169.9	Mode 2	4.2
Average	2671.3	0.0530	2851.3	2970.5		11.4
Control specimens for 4000 hours						
RG 6	3663.6	0.0785	2866.0	3921.5	Mode 1	95.1
RG 7	3946.1	0.0823	3046.1	4269.2	Mode 1	82.1
RG 8	3514.5	0.0871	2912.6	3759.8	Mode 1	94.3
Average	3708.1	0.0826	2941.6	3983.5		90.5
RNG 6	3670.9	0.0921	3091.4	3834.9	Mode 1	95.3
RNG 7	3433.0	0.0690	3046.1	3593.4	Mode 1	95.7
Average	3551.9	0.0806	3068.8	3714.1		95.5
Converse Units: 1 in. = 25.4 mm, 1 lb = 0.0044 kN						

Note: RG means the specimens reinforced with galvanized coating steel fibers, RNG means the specimens reinforced with micro-fine brass coating steel fibers.

In Table 4.18, all control specimens considerably deformed more than the SPR specimens that were subjected to salted tap water. The average deflection of the control RG and RNG specimens was 0.0826 in. (2.10 mm) and 0.0806 in. (2.05 mm), respectively. For the specimens submerged in salt water for 1,500 hours, the average displacements of the RG and RNG specimens were 0.0527 in. (1.34 mm) and 0.0582 in. (1.48 mm), respectively. The average deflections of conditioned specimens were 0.0544 in. (1.38 mm) and 0.0530 in. (1.35 mm) after exposure of 4,000 hours. No large difference of deflections was observed between conditioned specimens after exposure of 1,500 and 4,000 hours. The deflections of conditioned RG and RNG specimens that were immersed in salt water for 1,500 hours were decreased by 36.2% and 27.8%, respectively, when compared to the control specimens. For RG and RNG conditioned specimens after exposure of 4,000 hours, the deflections were decreased by 34.1% and 34.2%, respectively, compared to the results of the control specimens. All SRP specimens failed due to the de-bonding between the concrete and SRP strengthening system. Figures 4.68 through 4.71 illustrate four typical conditioned RG and RNG specimens.

The control specimens failed at higher ultimate loads. The average peak loads of the control specimens were higher than the results of SRP specimens after exposure of 1,500 hours and 4,000 hours. There was no large degree of variation observed in mechanical properties between the conditioned RG and RNG specimens immersed in salted tap water for 1,500 and 4,000 hours respectively. The average percentages of concrete cover areas for the control RG and RNG specimens were 90.5% and 95.5%, respectively. However, for the conditioned specimens, there was only some concrete attached to the surface of the SRP near the saw-cut area due to more epoxy close to this zone when preparing the specimens. The average percentages of concrete substrate areas for the conditioned RG and RNG specimens exposed to salt water for 1,500 hours were 14.1% and 13.3%, respectively. For the conditioned specimens after exposure of 4,000 hours, the average percentages of concrete of RG and RNG specimens were 10.8% and 11.4% respectively. There was a large decrease of concrete substrate areas for the conditioned specimens compared to the results of control samples. Therefore, it indicates that the bond performance of the SRP-to-concrete systems was degraded considerably after exposure to salted tap water.

According to the failure loads of all conditioned SRP specimens reinforced with galvanized and micro-fine brass coating steel fibers, it can be estimated that an environmental reduction C_E factor of 0.7 might be suggested for "wet environments" with freezing weather in winter where deicing salts are often used. This condition should be considered as a long-term exposure to this environment condition. This value should be a conservative estimate based on the relative bond durability of SRP strengthening system with galvanized and brass coating steel fibers.

The failure loads and the percentages of concrete cover areas of control and conditioned SRP specimens are presented in Figures 4.74 and 4.75.

From Figure 4.74, it should be noted that there are no large deviations for the average ultimate loads between conditioned RG and RNG specimens after exposure of 1,500 hours. The result of the conditioned RG specimens had no difference with that of conditioned RNG specimens after exposure of 4,000 hours. In addition, no difference was also seen between conditioned specimens immersed in salted tap water for 1,500 and 4,000 hours. The conditioned specimens failed at lower loads with lower percentages of concrete cover areas. For the conditioned RG and RNG specimens (1,500 and 4,000 hours), the average ultimate loads decreased by 27.8% and 27.5% (for 1,500 hours), and 24.8% and 27.5% (for 4,000 hours), respectively, when compared to those of the control specimens.

It can be seen in Figure 4.75 that the average area of concrete on the surface of the SRP strip of the conditioned specimens (1,500 hours) was slightly higher than the results of the conditioned specimens after exposure of 4,000 hours. For the RG specimens, the concrete substrate areas of conditioned specimens exposed to salt water for 1,500 and 4,000 hours decreased by 84.4% and 88.1%, respectively. For the RNG specimens, the results of conditioned specimens exposed to salt water for 1,500 and 4,000 hours decreased by 86.1% and 88.1%, respectively when compared to those results of control RG and RNG specimens.

The results from the flexural bending tests have suggested that the specimens immersed into salt water have exhibited considerable loss of the load-carrying capacity or bond shear strength between the concrete and the SRP strengthening system. The failure mode shifted from Failure Mode 1 in the control specimens to the Failure Modes 2 and 3

in conditioned SRP specimens. Therefore, the long-term bond durability of the SRP-to-concrete system interface was considerably deteriorated by salted tap water.

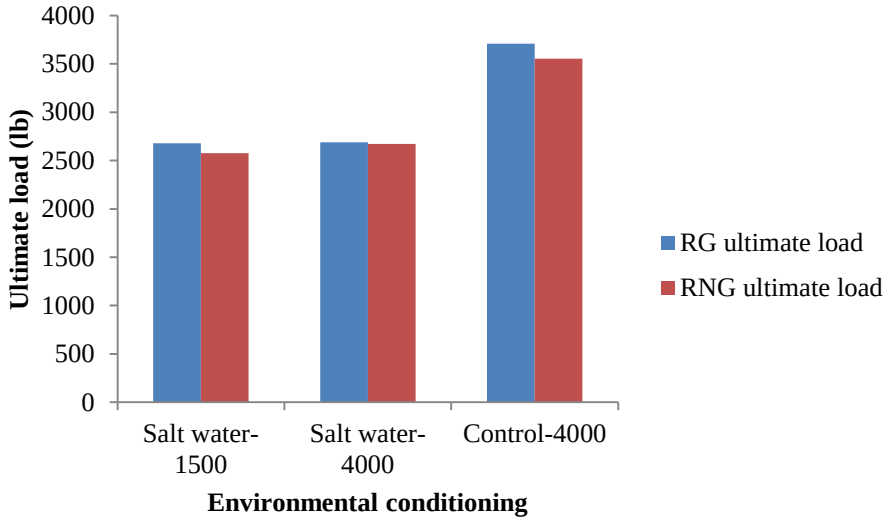

Conversion Units: 1 lb = 0.044 kN

Figure 4.74. Ultimate loads for RG and RNG specimens under salt water

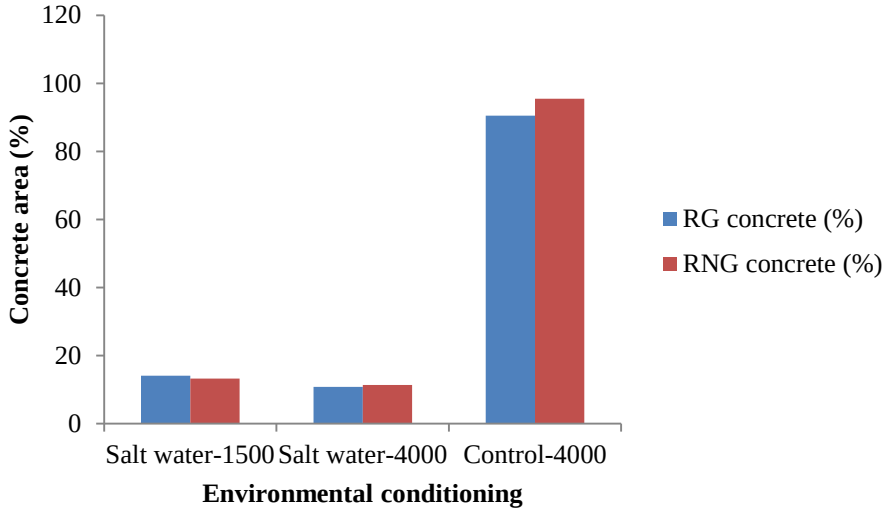

Figure 4.75. The percentage of concrete substrate area for RG and RNG specimens

4.6.2. Direct Pull-Off Test. The bond strength and failure mode were evaluated and discussed by direct pull-off test, and compared to the results of the flexural bending tests. The specimen preparation was the same as that of the experiment in the environmental chamber. The test setup is illustrated in Figure 4.34.

This test was conducted based on ASTM D7522, and the failure modes were defined by this standard, as shown in Table 4.18. The bond between the concrete and the SRP sheet was evaluated by pull-off tensile stress at failure and the percentage of concrete substrate area attached to the surface of SRP.

The final failure loads of 40 conditioned pull-off cores (20 for 1,500 hours and 20 for 4,000 hours) were measured by the DYNA Z pull-off tester. Meanwhile, the bond strengths of these specimens were calculated. The test results of all specimens subjected to salt water are summarized in Table 4.18.

For the conditioned specimens exposed to salt water for 1,500 hours, it can be seen in Table 4.18 that the failure modes were Mode G (see Table 4.8). All conditioned specimens failed in Mode G except core #2 of RG 11 and core #1 of RNG 12 and RNG 13 after exposure of 4,000 hours. The failure modes of all SRP control specimens (4,000 hours) were Mode G (see Table 4.19). The concrete substrate area was measured by IMAGE J. No failure modes other than Mode G and F were observed. The lowest percentage of concrete cover area was 72.1% (Mode F). The representative pull-off specimens with discs are illustrated in Figures 4.76 through 4.79. The other failed pull-off specimens that were submerged in water are available in Appendix B.

The majority of the conditioned specimens (1,500 and 4,000 hours) failed in Mode G. One possible explanation is that the direct bond strength of the SRP-to-concrete system was higher than the tensile strength of concrete even if the bond strength was deteriorated by salted tap water. Therefore, they failed in concrete. However, core #2 of RG 11, and cores #1 of RNG 12 and RNG 13 (4,000 hours) failed in Mode F, possibly due to several issues including non-homogenous characteristics of the concrete, applied load rate by hand, or the improper preparation of the specimens.

The average bond stresses, standard deviations, and coefficient of variation of conditioned (1,500 and 4,000 hours) and control RG and RNG specimens (4,000 hours) are summarized in Table 4.20 and Figure 4.80.

Table 4.19. The ultimate loads and bond strengths for the pull-off specimens

Specimen	Ultimate load (#1) (lb)	Failure Mode (#1)	Ultimate load (#2) (lb)	Failure Mode (#2)	Bond strength (#1) (psi)	Bond strength (#2) (psi)
Conditioned specimens (1,500 hours)						
RG 4	891	Mode G (86.0%)	1234	Mode G (97.6%)	345.7	478.7
RG 5	1141	Mode G (90.4%)	832	Mode G	442.7	322.8
RG 6	1438	Mode G (93.4%)	1310	Mode G	557.9	508.2
RG 7	1187	Mode G	1315	Mode G	460.5	510.2
RG 8	1531	Mode G	1030	Mode G	594.0	399.6
RNG 4	1024	Mode G (94.7%)	955	Mode G (95.2%)	397.3	370.5
RNG 5	1298	Mode G (94.8%)	1129	Mode G	503.6	438.0
RNG 6	1141	Mode G	1199	Mode G	442.7	465.2
RNG 7	1263	Mode G	1502	Mode G	490.0	582.7
RNG 8	1100	Mode G	1246	Mode G (93.8%)	426.8	483.4
Conditioned specimens (4,000 hours)						
RG 9	1286	Mode G (97.5%)	1717	Mode G	498.7	665.8
RG 10	1019	Mode G (93.0%)	64	Mode G (92.4%)	395.1	24.8
RG 11	1246	Mode G (86.1%)	1438	Mode F (72.1%)	483.2	557.6
RG 12	995	Mode G (92.0%)	925	Mode G (91.1%)	385.8	358.7
RG 13	1135	Mode G (86.0%)	1205	Mode G (96.2%)	440.1	467.3
RNG 6	1473	Mode G	1315	Mode G	571.2	509.9
RNG 9	1083	Mode G	1106	Mode G	420.0	428.9
RNG 10	1036	Mode G	1129	Mode G	401.7	437.8
RNG 12	1473	Mode F (80.9%)	1409	Mode G	571.2	546.4
RNG 13	1804	Mode F (76.8%)	1403	Mode G	699.5	544.0
Converse units: 1 lb = 4.4 N, 1 psi = 0.0069 MPa						

Note: RG means the specimens reinforced with galvanized coating steel fibers, RNG means the specimens reinforced with micro-fine brass coating steel fibers. % means the percentage of concrete substrate area when compared to the area of SRP core.

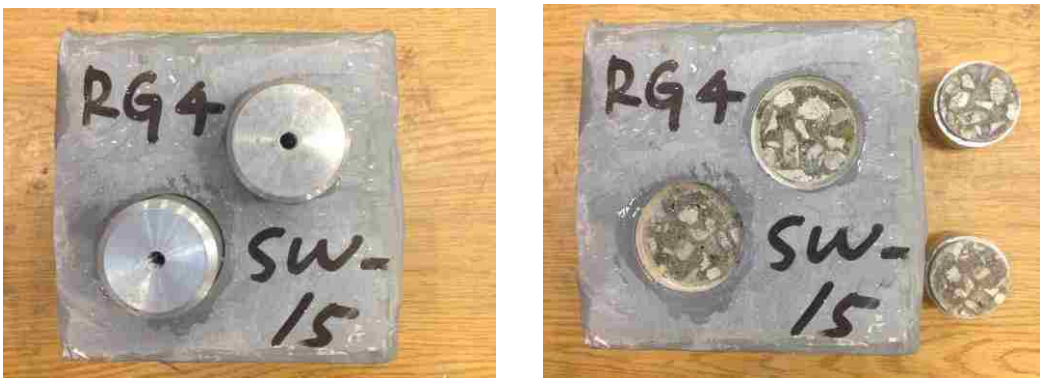

Figure 4.76. RG 4 (1,500 hours)

Figure 4.77. RG 11 (4,000 hours)

Figure 4.78. RNG 2 (4,000 hours)

Figure 4.79. RNG 13 (4,000 hours)

High standard deviations and coefficient of variations (COVs) of the control and conditioned specimens were observed in Table 4.20 and Figure 4.80. All the pull-off test results illustrated a higher COV when compared to that of ASTM C 39 (10%) [80] except the result of the control RG specimens. There was a large degree of scatter and variation, indicating the variability of this test method.

Table 4.20. The average bond strength and standard deviation

SRP specimen	Ave. Bond stress (psi)	Standard Deviation	COV (%)
Conditioned RG (1,500)	462.0	87.3	18.9
Conditioned RNG (1,500)	460.0	59.9	13.0
Conditioned RG (4,000)	427.7	167.8	39.2
Conditioned RNG (4,000)	513.1	92.7	18.1
Control RG (4,000)	318.0	21.5	6.8
Control RNG (4,000)	276.6	121.2	43.8
Conversion unit: 1 psi = 0.0069 MPa			

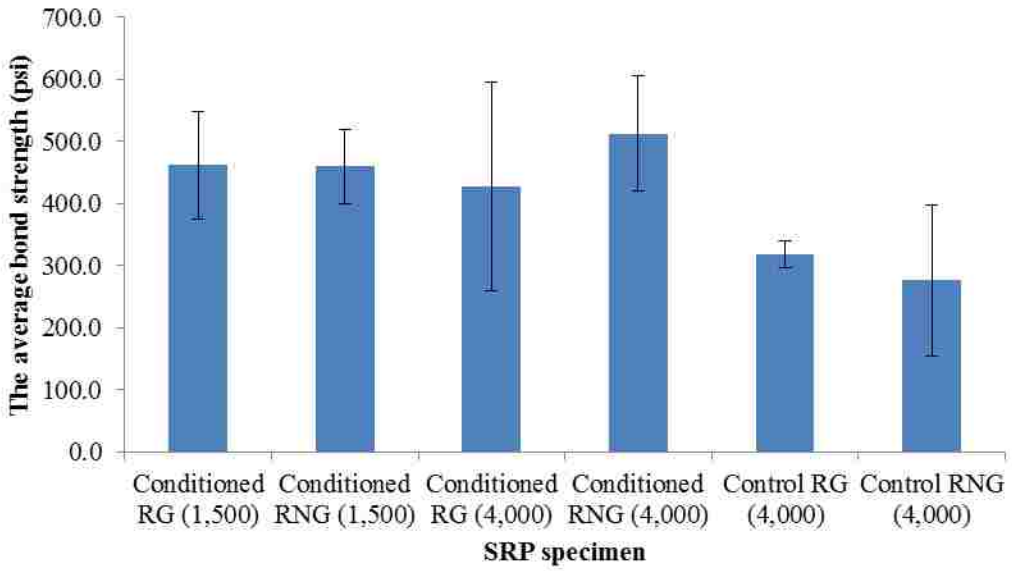

Conversion Units: 1 psi = 0.0069 MPa

Figure 4.80. Average pull-off test results for conditioned and control specimens

In addition, the bond performance between the SRP and concrete substrate was deteriorative based on the results of flexural bending tests. However, the conditioned specimens failed in the Mode G (cohesive failure in concrete substrate) except core #1 of RG 11 and core #1 of RNG 12 and RNG 13 (4,000 hours). It can be concluded that the direct tension strength of the SRP-to-concrete systems was higher than the tensile strength of concrete even if the bond behavior between SRP and concrete was degraded after the environmental exposure. Additionally, the average interfacial bond strength of all conditioned specimens was much higher than the results of the control specimens, possibly because the concrete was post-cured when concrete was submerged in salted tap water.

4.7. THE EXPERIMENT STUDY IN FIELD ENVIRONMENT

There is limited available data to exhibit the influence of real-time seasonal weather on the bond performance between SRP strengthening systems and concrete. Deng et al. [19] evaluated durability performance of concrete beams reinforced with

CFRP sheet under real-time weather and solar exposure, and found flexural strengths showed a 45% loss. The failure modes were also changed from substrate to interfacial. Direct pull-off tension strength decreased after 18 months of real-time exposure. Liau and Tsent [110] reported that that cracks occurred when CFRP specimens were exposed to the UV, finally reducing the strength due to stress concentrations.

In order to investigate the effects of field exposure on the bond performance of concrete beams reinforced with SRP, they were subjected to real-time weather and solar exposure in Rolla, MO for 12 months (from October 2015 to September 2016). A total of 22 SRP specimens, including 12 specimens loaded and 10 specimens unloaded, were maintained in outdoor weather in Rolla, which has moderate UV radiation with various freeze-thaw, and variable temperature, and moisture conditions. These SRP specimens were tested in three-point loading. At the same time, direct pull-off tension tests were conducted after 12 months of exposure. The average monthly weather conditions during this research in Rolla, MO are illustrated in Table 4.21. The data was collected from the National Weather Service.

Table 4.21. Monthly temperature and average relative humidity (RH)

Month	Max. (°F)	Min. (°F)	Ave. RH (%)
15-Oct	83	60	64.3
15-Nov	75	58	68.8
15-Dec	69	60	75.4
16-Jan	68	45	71.3
16-Feb	75	52	64.8
16-Mar	83	59	67.3
16-Apr	83	64	65.3
16-May	88	65	72.5
16-Jun	97	77	71.4
16-Jul	98	77	78.6
16-Aug	96	76	79.8
16-Sep	93	75	74.8
Converse unit: °F = °C x 1.8 +32			

4.7.1. Sustained Loading. The SRP specimens, including six galvanized coating and six brass coating steel fiber samples, were subjected to real-time seasonal exposure and sustained loading of 20% and 40% of ultimate capacity (six specimens for 20% and six specimens for 40%), respectively. The ten SRP specimens exposed to field environment were unloaded including five RG and five RNG specimens. Pairs of back-to-back specimens were subjected to the sustained three-point flexural load in the vertical orientation using a spring-loaded fixture. This fixture consisted of clamps that were made of steel plates and beams, long threaded bolts with nuts, and springs, as shown in Figure 4.81. More detailed information of the fixture and loading process can be found in Section 4.3.1.

Figure 4.81. Spring-loaded fixture and the testing samples under the real-time exposure

4.7.2. Flexural Bending Testing (Three-Point Load Testing). The bond durability between SRP strengthening system and concrete substrate was evaluated by flexural bending tests. The SRP specimens were maintained in field environment for one year, then moved to the laboratory to perform the tests. All SRP-reinforced concrete

beams were loaded by using an MTS 880 to conduct the flexural bending tests. Load was applied at a constant rate of 0.005 in./min (0.127 mm/min) to cause the specimens to fail in 9 to 10 minutes. The deflections of both sides at the mid-span of the SRP specimen were measured by using two linear variable displacement transducers (LVDTs) with ±0.5 in. (12.7 mm). Figure 4.82 illustrates a typical three-point loading test configuration.

The specimens were tested with a displacement-controlled testing machine under three-point loading. This section exhibits the bending test results and analysis of the results for peak and failure loads and maximum deflections. The concrete cover areas on the fracture SRP strip were analyzed after beam flexural testing, and failure modes of SRP specimens were also observed, which provided qualitative insight into bond degradation between SRP and concrete substrate.

Figure 4.82. A typical three-point loading test configuration

The crack occurred at the tip of the saw cut. Debonding between concrete and SRP sheet initiated when the peak tensile stress in concrete and SRP strip exceeded the interfacial shear stress. This debonding occurred initially at the mid-span of the specimen (the intersection with the saw cut) due to the weakening of the cross section of the saw

cut and the highest bending moment at the mid-span of the specimen, and then extended out through the end of the SRP system until the specimen failed. The typical load-deflection characteristics of the loaded, unloaded, and control RG and RNG specimens are illustrated in Figure 4.83.

It can be seen in Figure 4.83 that the SRP control specimen (RG 14 and RNG 13) experienced higher strength and more ductility than the conditioned specimens that were exposed to field environment. Ultimate ductility of the control specimens was higher than that of the conditioned specimens. It should be noted that a significant decrease occurred in ultimate load capacity of SRP sheet-strengthened specimens after one year of the real-time exposure when compared to the control samples that were maintained in the laboratory for one year. However, no significant difference when the cracking moment occured between the conditioned and control RG and RNG specimens. At the beginning of the flexural bending test, the load-deflection behaviors of the control and conditioned specimens were almost linear until the cracking moment of the concrete prism was exceeded. The flexural load capacities in the conditioned SRP specimens dropped at the start of the tension cracking in the concrete. These first peak points demonstrated that the SRP strips bridged cracking in the concrete. The load capacities of control specimens continued to increase significantly until failure after the first peak loads. In contrast to this, there was no apparent degree of increase after the first peak loads, in other words, the first peak loads were the maximum peak loads for conditioned specimens. The control specimens experienced several peak loads until failure. The conditioned specimens failed at lower loads with lower deflections. Therefore, it can be concluded that the bond durability of the conditioned specimens was deteriorated after one year of real-time seasoning exposure. The bond strength between the SRP sheet and concrete was decreased.

The conditioned and control specimens failed in Failure Mode 3 after the flexural bending test according to the types of failure modes mentioned previously. Figure 4.84 and 4.87 show the typical failed specimens in this section. No corrosion sign was observed on the surface of the SRP strengthening system for the exposed specimens. The other failed specimens immersed into hot water are available in Appendix B.

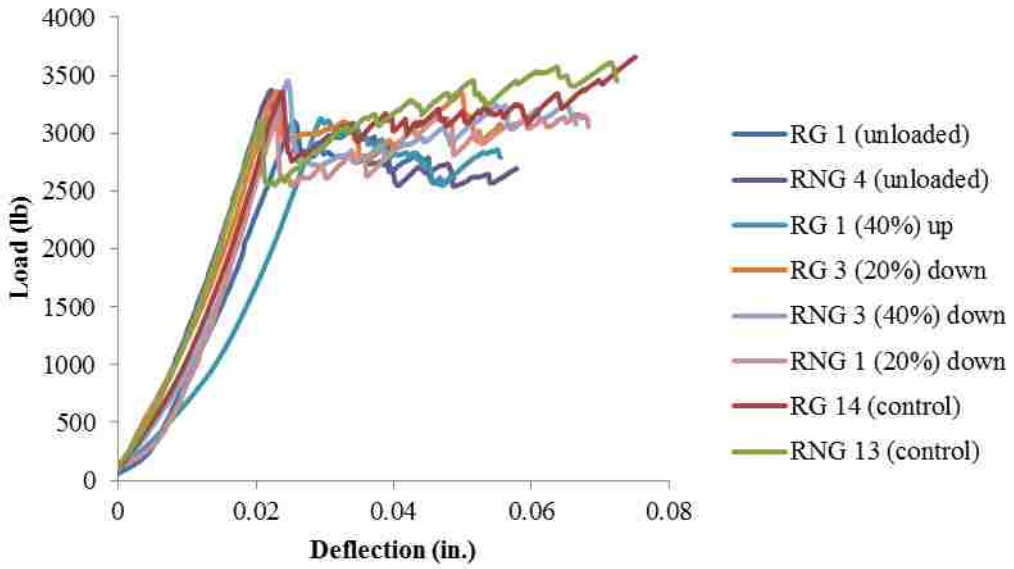

Conversion units: 1 in. = 25.4 mm, 1 lb = 0.0044 kN

Figure 4.83. Load-deflection characteristics of the SRP specimens reinforced with galvanized and brass coating steel fibers

For the conditioned specimens reinforced with galvanized and micro-fine brass coating steel fibers, there was only a small amount of concrete to cover the surface of the SRP strip for the specimens. In addition, the ultimate flexural bending loads of the conditioned specimens were lower than the results of control specimens. Therefore, it can be concluded that the bond behavior between the concrete and the SRP system was significantly degraded after exposure to the natural environment including UV radiation. It can be seen in Figure 4.83 that no apparent increases of load capacities were observed, in other words, the first peak loads exhibited the highest load capacities after the initial cracking of concrete.

It should be noted that there was only partial concrete to cover the fracture SRP sheet for the control specimens when exposed to laboratory conditions for one year. These results were different from those of the control specimens after 82 days and 4,000 hours of exposure, possibly because the concrete strength significantly increased after one year of exposure (see Table 4.5). Consequently, concrete was difficult to attach to the surface of the SRP sheet when conducting the flexural bending tests.

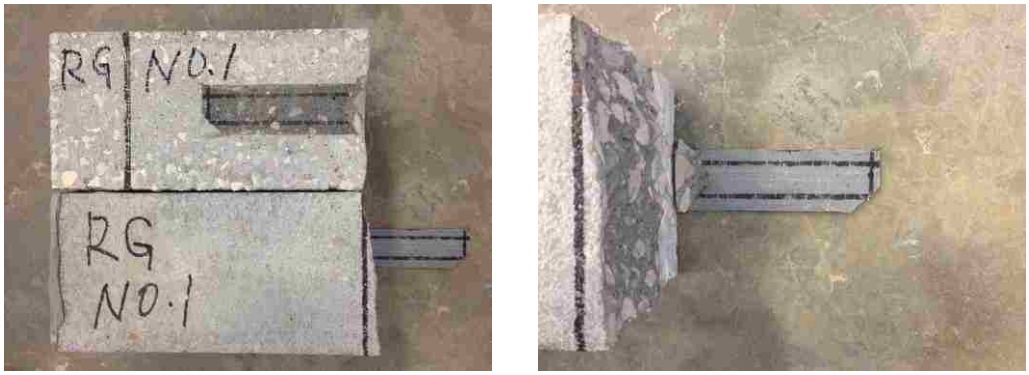

Figure 4.84. A typical failed RG specimen reinforced (unloaded) exposed to field environment

Figure 4.85. A representative failed RNG specimen reinforced (unloaded) exposed to field environment

Figure 4.86. A typical failed RNG specimen reinforced (loaded 20%) exposed to field environment

Figure 4.87. A representative failed control RG specimen reinforced

In addition, no indication of corrosion of steel fibers was observed on the fractured SRP sheets after exposure to this harsh weather. It can be concluded that the epoxy resin utilized in this research exhibited a perfect moisture-tolerant behavior to protect the steel fibers. The concrete cover area was calculated using the IMAGE J. Tables 4.22 and 4.23 illustrate the mechanical properties of the RG and RNG specimens, including the ultimate loads, peak loads, and first peak loads; maximum deflections; failure modes; and percentages of concrete cover area.

In Table 4.22, all the three control specimens considerably deflected more than the SRP specimens that were exposed to natural environment. The average deflection of the control specimens was 0.0706 in. (1.79 mm). The average displacements of the specimens stressed by 40% of the ultimate load, 20% of the ultimate load, and unloaded were 0.0504 in. (1.28 mm), 0.0385 in. (0.98 mm), and 0.0412 in. (1.05 mm), respectively. They decreased by 28.7%, 45.5%, and 41.7% respectively, when compared with that of control specimens. Therefore, it can be suggested that the bond behavior of SRP strengthening system and concrete substrate were degraded after real-time weather and solar exposure. All SRP specimens failed due to the de-bonding between the concrete and the SRP strengthening system. Figure 4.83 illustrates one typical failed RG specimen after the flexural bending test.

Table 4.22. SRP specimens reinforced with galvanized coating steel fibers

Specimens (40%)	Ultimate load (lb)	Max def. (in.)	First peak load (lb)	Peak load (lb)	Failure mode	Concrete (%)
RG 1 (down)	2401.3	0.046	2983.3	2983.3	Mode 3	12.2
RG 1 (up)	2788.3	0.0555	3106.9	3106.9	Mode 3	12.4
RG 2 (up)	2770.5	0.0496	3944.6	3944.6	Mode 3	12.6
Average	2653.4	0.0504	3344.9	3344.9		12.4
Specimens (20%)	Ultimate load (lb)	Max def. (in.)	First peak load (lb)	Peak load (lb)	Failure mode	Concrete (%)
RG 1 (up)	2030.7	0.0232	3277.9	3277.9	Mode 3	14.2
RG 2 (up)	2471.2	0.0367	3222.4	3222.4	Mode 3	40.2
RG 3 (down)	3065.4	0.0555	3361.4	3361.4	Mode 3	16.6
Average	2522.4	0.0385	3287.2	3287.2		23.7
Unloaded	Ultimate load (lb)	Max def. (in.)	First peak load (lb)	Peak load (lb)	Failure mode	Concrete (%)
RG 1	2611.6	0.0488	3111.2	3111.2	Mode 3	15.1
RG 2	2743.2	0.0436	3478.4	3478.4	Mode 3	16.5
RG 5	2120.2	0.0399	3654.2	3654.2	Mode 3	22.9
RG 8	2320.9	0.0336	2898.3	2398.3	Mode 3	23.8
RG 9	2703.5	0.0400	3276.7	3276.7	Mode 3	25.3
Average	2499.9	0.0412	3283.8	3183.8		20.7
Control	Ultimate Load (lb)	Max Def. (in.)	First Peak load (lb)	Peak Load (lb)	Failure Mode	Concrete (%)
RG 12	3123.5	0.0610	3248.3	3365.6	Mode 3	20.9
RG 13	2773.2	0.0757	3540.5	3540.5	Mode 3	45.9
RG 14	3657.2	0.0751	3303.6	3657.2	Mode 3	27.6
Average	3184.6	0.0706	3364.1	3521.1		31.5
Converse units: 1 in. = 25.4 mm, 1 lb = 0.0044 kN						

Note: RG means the specimens reinforced with galvanized coating steel fibers, RNG means the specimens reinforced with brass coating steel fibers. Up means the SRP strip faced to sunlight. Down means the SRP strip faced to ground. % means the percentage of concrete substrate area when compared to the area of SRP core.

The average percentage of concrete cover area for the control specimens was 31.5%. In contrast to this, the percentages of concrete cover area of loaded (40% and 20%) and unloaded specimens decreased by 60.6%, 24.8%, and 34.3% respectively, when compared to the control specimens. The control and conditioned RG specimens failed in Failure Mode 3. For control specimens, the concrete strength increase resulted in

the failure mode. However, the combination of concrete strength increase and the real-time exposure caused the failure mode for the exposed specimens. Therefore, it should be concluded that the bond durability of the specimens was degraded after being exposed to the real-time weather for one year.

The control specimens failed at higher loads. The average peak loads of three control specimens were higher than those of SRP specimens after field exposure. However, there was no large difference between the average first peak loads of conditioned and control RG specimens. This suggests that the initial cracking of concrete on the tension side was not influenced by the real-time solar exposure. In other words, the tensile strength of concrete was not deteriorated by the environmental condition.

As shown in Table 4.23, the average deflection of 0.0697 in. (1.77 mm) for all four control specimens was more than those of the SRP specimens that experienced natural environment for one year. The average displacements of the conditioned specimens stressed by 40% of the ultimate load, 20% of the ultimate load, and the unstressed samples were 0.0474 in. (1.20 mm), 0.0588 in. (1.48 mm), and 0.0455 in. (1.16 mm), respectively. They decreased by 31.9%, 15.6%, and 34.7% respectively, when compared with the results of the control specimens. Therefore, it can be suggested that the bond behavior of the SRP strengthening system and concrete substrate was degraded after real-time weather and solar exposure. All SRP specimens failed due to the debonding of the concrete and SRP strengthening system in different concrete-covered substrate area. Figures 4.84 through 4.85 show typical failed samples reinforced with micro-fine brass steel fibers.

The average percentage of concrete cover-to-SRP sheet for the control specimens was 32.4% which was much higher than those of conditioned specimens. For the exposed specimens, the percentages were decreased by 58.0%, 62.7%, and 59.0% respectively, when compared to the control RNG specimens. The control and conditioned RNG specimens failed in the Failure Mode 3 except RNG 4 (Failure Mode 2). For control specimens, the concrete strength increase resulted in the failure mode. However, the combination of concrete strength increase and the real-time exposure caused the failure mode for the exposed specimens. Therefore, it should be concluded that the bond durability of the specimens was degraded after being exposed to the natural environment

for one year. It should be noted in Tables 4.22 and 4.23 that there was no difference in ultimate loads and the maximum deflections between the control RG and RNG specimens, respectively.

Table 4.23. SRP specimens reinforced with micro-fine brass coating steel fibers

Specimens (40%)	Ultimate Load (lb)	Max Def. (in.)	First Peak load (lb)	Peak Load (lb)	Failure Mode	Concrete (%)
RNG 2 (down)	2401.3	0.0296	3293.0	3293.0	Mode 3	12.6
RNG 3 (down)	3074.6	0.0665	3455.0	3455.0	Mode 3	10.2
RNG 3 (up)	2517.9	0.0462	3564.3	3564.3	Mode 3	18.1
Average	2664.6	0.0474	3437.4	3437.4		13.6
Specimens (20%)	Ultimate Load (lb)	Max Def. (in.)	First Peak Load (lb)	Peak Load (lb)	Failure Mode	Concrete (%)
RNG 1 (down)	3055.3	0.0683	3122.7	3166	Mode 3	12.6
RNG 2 (down)	2603.3	0.0597	3425.2	3425.2	Mode 3	12.4
RNG 1 (up)	2689.7	0.0483	3505.3	3505.3	Mode 3	11.2
Average	2782.8	0.0588	3351.1	3365.5		12.1
Unloaded	Ultimate Load (lb)	Max Def. (in.)	First Peak load (lb)	Peak Load (lb)	Failure Mode	Concrete (%)
RNG 3	2342.2	0.0497	3340.7	3340.7	Mode 3	21.8
RNG 4	2689.7	0.0579	3012.5	3012.5	Mode 2	7.3
RNG 6	2643.6	0.0316	3333.3	3333.3	Mode 3	11.4
RNG 7	2337.4	0.0459	3187.8	3187.8	Mode 3	10.7
RNG 10	2578.5	0.0423	3320.6	3320.6	Mode 3	15.3
Average	2518.3	0.0455	3239.0	3239.0		13.3
Control	Ultimate Load (lb)	Max Def. (in.)	First Peak load (lb)	Peak Load (lb)	Failure Mode	Concrete (%)
RNG 11	3355.1	0.0687	3150.6	3657.1	Mode 3	47.2
RNG 12	3450.8	0.0805	3448.5	3719.2	Mode 3	29.4
RNG 13	3450.9	0.0725	3046.1	3611.5	Mode 3	35.6
RNG 15	2575.4	0.0569	3322.1	3322.1	Mode 3	17.2
Average	3208.1	0.0697	3241.8	3662.6		32.4
Converse units: 1 in. = 25.4 mm, 1 lb = 0.0044 kN						

Note: RG means the specimens reinforced with galvanized coating steel fibers, RNG means the specimens reinforced with brass coating steel fibers. “Up” means the SRP strip faced to sunlight. “Down” means the SRP strip faced to ground. % means the percentage of concrete substrate area when compared to the area of SRP core.

The control specimens failed at higher loads. The average peak loads of the control specimens were much higher than the results of SRP specimens after natural exposure, but there was no large deviation between the average first peak loads of conditioned and control RNG specimens. This indicates that the initial cracking of concrete on the tension side was not influenced by the real-time exposure and solar exposure. In other words, the tensile strength of concrete was not deteriorated by the environmental conditions.

According to the ultimate loads of all RG and RNG specimens that are listed in Tables 4.22 and 4.23, a C_E factor of 0.80 for the environmental reduction is suggested in an aggressive environment with a moderate UV radiation based on the results obtained herein. This value is based on the relative bond durability of SRP strengthening system studied.

The failure loads and the percentages of concrete covered areas of control and conditioned SRP specimens are presented in Figures 4.88 and 4.89.

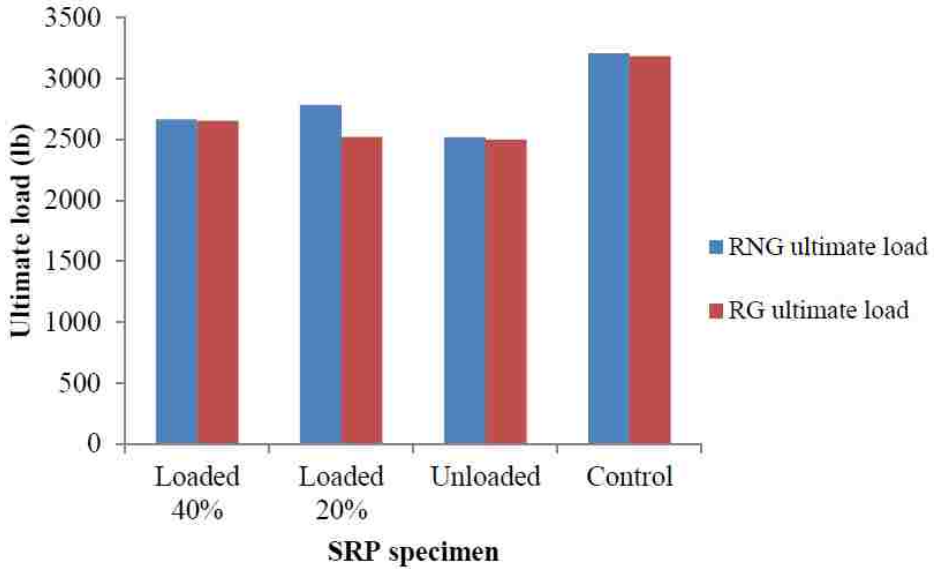

Conversion Units: 1 lb = 0.0044 kN

Figure 4.88. Ultimate loads for RG and RNG specimens

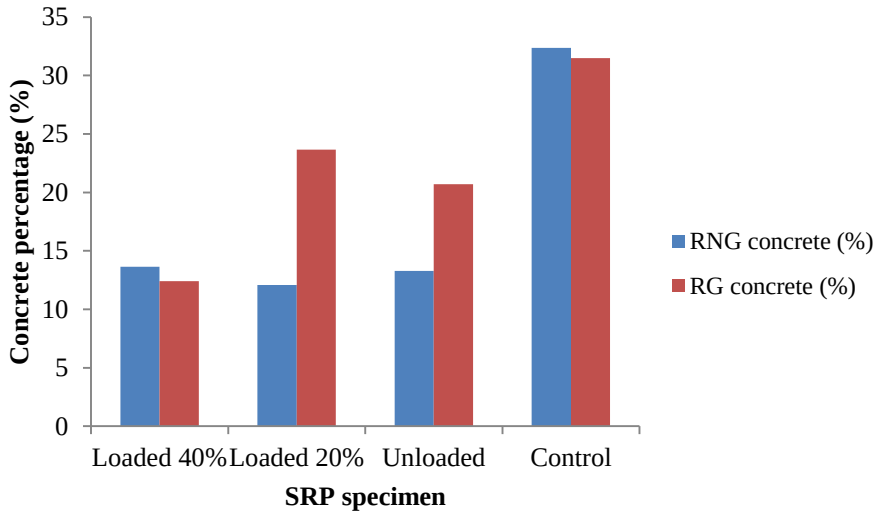

Figure 4.89. The percentage of concrete substrate area for RG and RNG specimens

From Figure 4.88, it should be noted that there are no high deviations for the average ultimate loads between conditioned RG and RNG specimens, and between control RG and RNG specimens. The conditioned specimens failed at lower loads with lower percentages of concrete cover areas. For the RG specimens, the average ultimate loads of conditioned specimens decreased by 16.7% (loaded 40%), 20.8% (loaded 20%), and 21.5% (unloaded) when compared to the average final load of the control RG specimens. For the RNG specimens, the average ultimate loads of the conditioned specimens decreased by 16.9% (loaded 40%), 13.3% (loaded 20%), and 21.5% (unloaded) when compared to the average ultimate load of the control RNG specimens. This suggests that field environment exposure degraded the bond performance between the SRP sheet and concrete substrate.

In addition, it should be noted that the average final capacities of loaded (40% and 20%) specimens reinforced with these two types of steel fibers were much higher than that of unloaded sample. According to a study by Bisby et al. [111], seasonal and daily temperature variations induce numerous expansions and shrinkages of FRP and concrete and freeze-thaw cycles, which results in differential thermal expansion between the FRP and the concrete substrate. Furthermore, the differential thermal expansion causes thermal stresses in FRP laminates[112]. Therefore, additional shear stresses or thermal

stresses in the SRP strips were exposed to seasonal and daily environments with various temperature, solar radiation, and freezing and thawing, which is detrimental to the bond performance of SRP-to-concrete systems. However, the thermal stresses in loaded (40% and 20%) specimens may be partially counteracted by loading of spring-loaded fixture, resulting in higher failure loads.

It can be seen in Figure 4.89 that the average amount of concrete-covered substrate areas of was much higher for the control specimens than the results of conditioned concrete members. There was a large degree of scatter and variation observed for concrete substrate areas except RG loaded 40% and RNG loaded 20% of the ultimate load.

The results from the flexural bending test suggest that harsh weather resulted in considerable loss of the load carrying capacity or bond shear strength between the concrete and the SRP strengthening system. Therefore, the long-term bond durability of the interface of the SRP-to-concrete system was deteriorated considerably after 12 months of real-time exposure to ambient outside conditions. Specimens without environmental exposure were in Failure Mode 3 due to the increase of concrete strength after one year.

4.7.3. Direct Pull-Off Tests. The bond strength and failure mode were evaluated by direct pull-off test and compared to the results of the flexural bending tests. The specimen preparation was the same as that of the experiment in the environmental chamber. The test setup is illustrated in Figure 4.34.

This test was conducted based on ASTM D7522 and the failure modes were defined by this standard, as shown in Table 4.18. The bond between concrete and SRP sheet was evaluated by pull-off tensile stresses at failure and the percentages of concrete cover areas on the fractured SRP strips.

The final failure loads of 22 conditioned specimens (10 for micro-fine galvanized coating steel fiber and 10 for micro-fine brass coating steel fibers) and 7 control specimens were measured (3 for RG specimens and 4 for RNG specimens). Meanwhile, the bond strengths of these specimens were calculated by using the Equation 4.1. The test results of the conditioned and the control specimens are summarized in Tables 4.24 and 4.25, respectively.

Table 4.24. The ultimate loads and bond strengths for the conditioned specimens

Specimen	Ultimate load (lb) (#1)	Failure Mode (#1)	Ultimate load (lb) (#2)	Failure Mode (#2)	Bond strength (psi) (#1)	Bond strength (psi) (#2)
Conditioned specimens						
RG 1 (down 40%)	588	Mode G (93.2%)	955	Mode G (95.3%)	228.0	370.3
RG 1 (up 40%)	821	Mode G	N/A	N/A	318.4	N/A
RG 2 (up 40%)	984	Mode F (79.8%)	1350	Mode G (88.9%)	381.6	523.5
RG 1 (up 20%)	658	Mode F (80.7%)	838	Mode G (95.2%)	255.2	325.0
RG 2 (up 20%)	949	Mode G (95.2%)	1001	Mode F (76.9%)	368.0	388.2
RG 3 (down 20%)	1042	Mode F (71.4%)	1053	Mode G (94.3%)	404.1	408.3
RG 1	1094	Mode F (70.3%)	774	Mode G	424.2	300.1
RG 2	815	Mode G	1053	Mode F (76.3%)	316.0	408.3
RG 5	844	Mode F (69.4%)	844	Mode F (79.7%)	327.3	327.3
RG 8	733	Mode G	1024	Mode F (49.8%)	284.2	397.1
RG 9	1228	Mode F (84.0%)	1036	Mode F (83.3%)	391.1	401.7
RNG 2 (down 40%)	786	Mode G	1269	Mode G	304.8	492.1
RNG 3 (down 40%)	1327	Mode F (68.9%)	1106	Mode G	514.6	428.9
RNG 3 (up 40%)	1030	Mode F (82.3%)	1001	Mode G (90.5%)	399.4	388.2
RNG 1 (down 20%)	978	Mode F (56.7%)	809	Mode G	379.2	313.7
RNG 2 (down 20%)	739	Mode F (84.6%)	937	Mode G (94.1%)	286.6	363.3
RNG 1 (up 20%)	931	Mode G	1077	Mode F (76.7%)	361.0	417.6
RNG 4	995	Mode F (81.6%)	1042	Mode G (95.3%)	385.8	404.1
RNG 10	792	Mode G	809	Mode F (81.4%)	307.1	313.7
Conversion Units: 1 lb = 0.0044 kN, 1 psi = 0.0069 MPa						

Note: RG indicates the specimens reinforced with galvanized coating steel fibers, RNG indicates the specimens reinforced with micro-fine brass coating steel fibers. “Up” indicates the SRP strip faced to sunlight. “Down” means the SRP strip faced to ground.

Table 4.25. The ultimate loads and bond strengths for the control specimens

Specimen	Ultimate load (#1)	Failure Mode (#1)	Ultimate load (#2)	Failure Mode (#2)	Bond strength (#1)	Bond strength (#2)
Control specimens						
RG 12	885	Mode G	757	Mode G	343.2	293.5
RG 13	722	Mode G	1088	Mode G	280.0	421.9
RG 14	1030	Mode G	792	Mode G	399.4	307.1
RNG 11	978	Mode G	652	Mode G	379.2	252.8
RNG 12	850	Mode G	861	Mode G	329.6	333.9
RNG 13	925	Mode G	745	Mode G	358.7	288.9
RNG 15	972	Mode G	896	Mode G	376.9	347.4
Converse Units: 1 lb = 0.0044 kN, 1 psi = 0.0069 MPa						

Note: RG means the specimens reinforced with galvanized coating steel fibers, RNG means the specimens reinforced with micro-fine brass coating steel fibers.

For the conditioned RG specimens, it can be seen in Table 4.24 that 10 cores failed in Mode G and 11 cores failed in Mode F (see Table 4.8) after one year of real-time seasonal weather exposure. For the conditioned RNG specimens, 7 cores failed in Mode F and the others failed in Mode G. Therefore, it should be concluded that the bond performance between the SRP sheet and concrete substrate was deteriorated by the natural environment after 12 months of real-time exposure when conducting the direct tension tests. In contrast, the failure modes of all SRP control specimens were Mode G. No other type of failure mode was observed other than Modes G and F. The minimum percentage of concrete-covered substrate area was 49.8% observed in core #2 of RG 8. The representative pull-off specimens with discs are illustrated in Figures 4.90 through 4.92. The other failed pull-off specimens are available in Appendix B.

The average bond stresses, standard deviations, and COVs of conditioned and control RG and RNG specimens with Failure Mode F and G are summarized in Table 4.26 and Figure 4.93.

Figure 4.90. Pull-off RG specimen under the real-time weather and solar exposure

Figure 4.91. Pull-off RNG specimen under the real-time weather and solar exposure

Figure 4.92. Typical control RG specimen

Table 4.26. The average bond strength, standard deviation, and COV

SRP specimen	Ave. Bond stress (psi)	Standard Deviation	COV (%)
Conditioned RG (Mode G)	344.2	80.5	23.4
Conditioned RG (Mode F)	373.3	49.9	13.4
Conditioned RNG (Mode G)	374.4	61.7	16.5
Conditioned RNG (Mode F)	384.3	75.1	19.5
Control RG (Mode G)	340.9	58.5	17.2
Control RNG (Mode G)	333.4	43.6	13.1
Conversion Units: 1 psi = 0.0069 MPa			

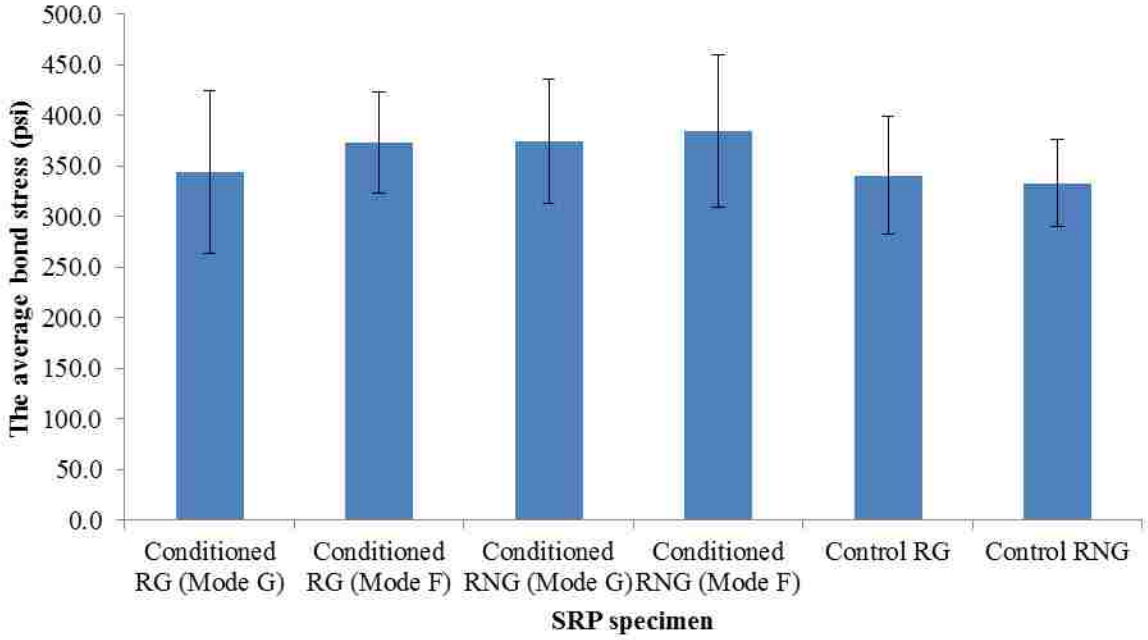

Conversion Units: 1 psi = 0.0069 MPa

Figure 4.93. Average pull-off test results for conditioned and control specimens

High standard deviations and coefficients of variation (COVs) of the control and conditioned specimens are shown in Table 4.26 and Figure 4.93. All the pull-off test results illustrated a higher COV when compared to that of ASTM C 39 (10%) [80]. There was a large degree of scatter and variation, indicating the variability of this test method. The average bond strength of control RG specimens was almost the same as the results of

the control RNG specimens. The average bond stresses of the conditioned specimens that failed in Mode F were higher than the results of the control specimens, possibly because is that the direct tension bond stresses of these conditioned specimens were larger than the concrete tensile strength of the control specimens even if the bond performance was degraded after the real-time environmental exposure. On the other hand, the exposed concrete was greatly post-cured after being exposed to the field environmental conditions, which indicates that the tensile strength of exposed concrete was higher than the pull-off bond strength of SRP-to-concrete system, leading to Mode F in some conditioned specimens.

4.8. THE MECHANICAL PROPERTIES OF SRP LAMINATE

The performance of structural members externally reinforced with FRP composite sheets that are exposed to various environments such as extreme service temperatures, freeze-thaw cycles, underwater conditions, or strong solar radiation is essentially related to either bond durability between the FRP composite laminate and concrete substrate or the mechanical properties of the laminates [113]. Some researchers study the former and report the bond behavior of FRP-to-concrete under varying environmental conditions. However, for mechanical properties of FRP laminates, limited experimental and analytical studies have been performed to study the characteristics of FRP laminates under variable environmental conditions [113-115]. They concluded that some decrease in terms of tensile strength and axial strain GFRP and CFRP laminates was observed under high temperature and higher numbers of freeze-thaw cycles.

4.8.1. Experimental Objectives and Program. The ACI 440 committee has defined the durability of FRP composites as the ability to resist de-bonding, chemical degradation, oxidation, cracking, etc. Daily environmental conditions are not considered harmful to FRP when they are properly fabricated and installed. However, it was not demonstrated whether extreme environmental conditions like underwater, seawater, and freezing and thawing degraded the mechanical properties of FRP sheets. Micro-fine galvanized and micro-fine brass coating steel fibers were used to fabricate the coupon specimens. In order to investigate the mechanical characteristics of SRP laminates under different environmental conditions, the SRP strips were exposed to the environmental

chamber for a complete conditioning cycle plus 50additional freeze-thaw cycles (see Table 4.5 and Figure 4.16), tap water for 3,000 hours at room temperature, hot water for 4,000 hours at 122°F (50°C), salted tap water (15% by weight) for 1,500 and 4,000 hours respectively. In addition, SRP strips were also exposed to the real-time weather and solar exposure to investigate whether daily environmental conditions should be considered detrimental to the mechanical properties of SRP. Finally, they were shaped the dog bones to produce the tensile coupon specimens. The overall length of the coupon specimen was 12 in. (304.8 mm). The configuration of the coupon specimen is illustrated in Figure 4.94.

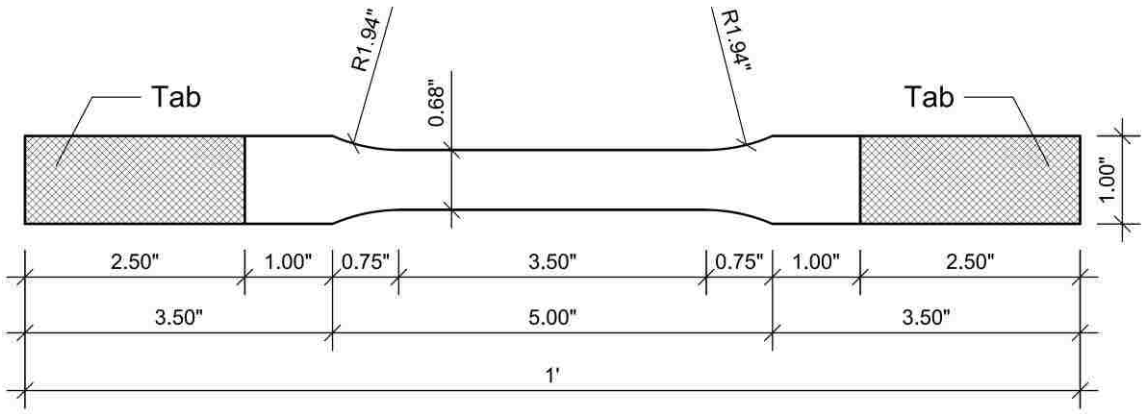

Conversion Units: 1 in. = 25.4 mm, 1 ft. = 304.8 mm

Figure 4.94. Dimensions of the SRP coupon specimen

4.8.2. The Setup of the Experiment. All tensile tests were conducted based on ASTM D3039/D3039M-14 [86]. The longitudinal and transverse strain gauges were applied to the mid-span and mid-width location of the coupon specimen to measure the strains of two directions. The specimens were subjected to uniaxial tension at a displacement rate of 0.05 in./min (1.27 mm/min) using an MTS 880 universal test machine, as shown in Figure 4.95. Mechanical wedge-type grips were utilized to engage the specimens by applying a uniform pressure of approximate 4000 psi (27.6 MPa) directly on the aluminum tabs.

Figure 4.95. The setup of tensile coupon test

4.8.3. The Experimental Results and Discussion. According to ACI 440.9R-15, the environment of Accelerated Conditioning Protocols (ACP) requires continuous immersion in water for 3,000 hours. Therefore, the specimens that were exposed to tap water were taken out from tap water after 3,000 hours of immersion to conduct the tensile coupon tests. However, micro-fine galvanized and micro-fine brass coating steel fibers in epoxy did not exhibit any corrosion after the exposure to tap water. Finally, it was decided that the SRP specimens were submerged in hot water and salted tap water for 4,000 hours before the tests were performed. In addition, tensile strength tests of coupon specimens that were immersed in salt water for 1,500 hours were also conducted to investigate the difference between the tensile capacities of the coupon specimens after exposure of 1,500 and 4,000 hours. Consequently, no any corrosion on the steel fibers of SRP coupon specimens was observed under each accelerated aging regime and field exposure. Figure 4.96 illustrates some representative failure coupon specimens.

Ultimate load capacities of the control and conditioned specimens were recorded. The tensile strengths of these coupon specimens are listed in Tables 4.27 and 4.28. In addition, strength ratios were also illustrated in the two tables. Strength ratio is the average tensile strength of an exposed specimen divided by the corresponding average

tensile stress of control specimens. A ratio of 1.0 indicates that there is no any strength degradation of the SRP coupon specimen.

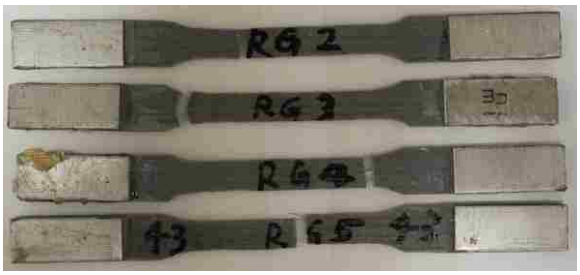

Figure 4.96. Representative tensile failure specimens

It can be seen in Tables 4.27 and 4.28 that no tensile strength loss was observed between the exposed and control specimens. Possible explanations could be the epoxy perfectly protects the micro-fine galvanized and micro-fine brass coating steel fibers, or the duration exposed to the environmental conditions may be not long enough to induce the corrosion of steel fibers in the epoxy resin.

Table 4.27. The mechanical properties of RG specimens

SRP specimen	Ave. ultimate load (lb)	Ave. tensile strength (psi)	Strength ratio	Standard deviation	COV (%)
EC RG	1675.8	17803.9	0.99	2307.1	13.0
W RG	1614.2	17149.4	0.95	1756.4	10.2
HW RG	1642.8	17453.5	0.97	1160.8	6.7
SW-1,500 RG	1611.4	17119.7	0.95	2272.3	13.3
SW-4,000 RG	1556.3	16534.6	0.92	1943.9	11.8
Outdoor RG	1690.1	17955.9	1.00	1847.5	10.3
Control RG	1690.7	17962.7	1.00	2115.5	11.8
Conversion units: 1 lb = 0.0044 kN, 1 psi = 0.0069 MPa					

Note: EC, W, HW, and SW mean environmental chamber, tap water, hot water, and salt water, respectively. RG means the specimens reinforced with galvanized coating steel fibers.

Table 4.28. The mechanical properties of RNG specimens

SRP specimen	Ave. ultimate load (lb)	Ave. tensile strength (psi)	Strength ratio	Standard Deviation	COV (%)
EC RNG	1617.9	17189.1	1.09	1565.0	9.1
W RNG	1802.1	19145.9	1.22	355.5	1.9
HW RNG	1633.8	17357.7	1.11	2034.1	11.7
SW-1,500 RNG	1654.3	17575.8	1.12	1502.9	8.6
SW-4,000 RNG	1579.6	16782.5	1.07	1872.4	11.2
Outdoor RNG	1722.4	18299.7	1.16	1907.3	10.4
Control RNG	1478.5	15708.1	1.00	817.2	5.2
Conversion units: 1 lb = 0.0044 kN, 1 psi = 0.0069 MPa					

Note: EC, W, HW, and SW mean environmental chamber, tap water, hot water, and salt water, respectively. RNG means the specimens reinforced with micro-fine brass coating steel fibers.

4.9. SUMMARY AND CONCLUSIONS

Effective application of externally bonded SRP strengthening systems requires knowledge of their durability under harsh environmental conditions. Long-term bond behavior between SRP composite systems and concrete substrate is associated with the effectiveness of repair or strengthening of concrete members. This study investigates environmental deterioration of SRP bonded to concrete. Ultimate flexural load capacity and direct tensile strength reductions quantify the degradation due to accelerated aging and real-time weather and solar exposure. Meanwhile, observation of failure modes of flexural bending and direct pull-off specimens provides qualitative perception of bond performance of SRP-to-concrete systems. Results indicate that degradation in some environmental conditions is far more serious than current design recommendations. The preparation of specimens reinforced with SRP strengthening system and exposure to environmental conditions provide a foundation for establishing standardized specimens that can be used as a baseline measurement to evaluate the long-term bond deterioration of exposed SRP specimens. Meanwhile, the test results can be utilized as a reference point for the design of concrete members reinforced with SRP composite system.

4.9.1. Three-Point Loading Tests. In this research, specimens of an SRP composite system was exposed to various accelerated aging environmental conditions with different exposure periods, including an environmental chamber, tap water, hot water, salted tap water, and real-time weather and solar exposure, to investigate degradation of SRP bonded to concrete substrate. All test results of flexural bending tests are summarized in Tables 4.29 and 4.30.

Each data point in Tables 4.29 and 4.30 represented an average value of flexural results for at least three composite beams. It can be seen that there was no clear difference in the performance between RG and RNG specimens. Test results of three-point loading tests indicated that the externally bonded SRP strengthening systems illustrated durability performance that can be established by the experiments. The failure modes of all conditioned specimens were Failure Modes 2 and 3. When exposed to real-time weather and EC, RG and RNG specimens performed moderately well. For RG and RNG specimens fully immersed in tap water, hot water, and salted tap water, greater strength losses were exhibited.

When subjected to real-time weather and solar exposure and full immersion of tap water, hot water, and salt water for various periods, the concrete cover areas of the exposed specimens reduced significantly when compared to the counterparts of the control specimens. The degradation should be attributed to loss of adhesion at the bond surface due to the influence of moisture or water and temperature. For the deflections of RG and RNG specimens immersed in tap water and salted tap water, no apparent difference was observed, which means chloride-ion should not further deteriorate the bond performance SRP-to-concrete systems. Therefore, it can be concluded that water or moisture is a major concern to influence on the bond durability between concrete and externally bonded SRP systems rather than deicing salt under the harsh environment. However, for RG and RNG specimens that were immersed in hot water at 122°F (50°C), the losses of deflections were higher than those of the specimens that were submerged in tap water and salted tap water. Consequently, it should be determined that temperature is also a main issue in the bond behavior degradation of SRP-to-concrete systems. This is further confirmed by Deng et al. [19].

Outdoor specimens exhibited higher loss of deflections and less concrete-covered substrate area when compared to SRP beams exposed to EC even though they failed in Failure Mode 3. A possible explanation could be that severer environmental conditions such as UV radiation and more varying temperature and humidity further deteriorated the bond performance between the SRP strengthening system and concrete substrate. Another explanation that should be considered is the increase of concrete strength. The outdoor specimens that were maintained in field environment for one year exhibited higher strength increase due to post-curing of concrete than that of the specimens exposed to EC for 82 days, resulting in the less concrete cover area observed in outdoor specimens. According to the report of Deng et al. [19], Failure Mode 1 (substrate failure) depends primarily on the concrete strength for three-point bending testing, while Failure Mode 2 (adhesive failure) and 3 (partial Failure Mode 1 and partial Failure Mode 2) should mainly depend on the bond strength of SRP composite. However, for Failure Mode 2 and 3, concrete strength should also be considered as a concern for long-term bond performance of the SRP-to-concrete systems based on the results of this research.

It should be noted that there was no clear relationship of deflections between the specimens loaded by 40% of the ultimate load and 20% of the ultimate load. For the exposed RNG specimens, the maximum deflections of unloaded specimens were lowest when compared to the loaded counterparts. However, loaded RG specimens exhibited different results. Therefore, it was not substantial to understand the relationship of deflections between loaded and unloaded specimens. In contrast to this, there was some deviation between the ultimate failure loads of unloaded and stressed specimens. It can be concluded that sustained loading may affect the ultimate load capacity. For ductility and concrete-covered substrate areas, further study will be needed in future work.

The control specimens that were maintained in the laboratory for 1,968 and 4,000 hours illustrated higher deflections and percentages of concrete coverage when compared to the control specimens after one year of exposure. The failure mode switched from Failure Mode 1 to Mode 3, which means that failure mode may change with time. This further demonstrates that Failure Mode 3 should depend on the increase of concrete strength.

Table 4.29. The flexural bending test results of RG specimens

Environmental condition	RG specimen				
	Loading condition	Ultimate load (lb)	Strength ratio	Max def. (in.)	Concrete (%)
OUTDOOR	Specimens (40%)	2653.4	0.83	0.0504	12.4
	Specimens (20%)	2522.4	0.79	0.0385	23.7
	Unloaded	2499.9	0.78	0.0412	20.7
EC	Specimens (40%)	2997.6	0.86	0.0475	54.9
	Specimens (20%)	3143.1	0.91	0.0593	44.9
	Unloaded	2830.5	0.82	0.0494	42.2
WATER-3,000	Unloaded	2709.3	0.73	0.0566	14.2
HOT WATER-4,000 (122°F)	Unloaded	2343.3	0.63	0.0480	23.7
SW-1,500	Unloaded	2678.2	0.77	0.0527	14.1
SW-4,000	Unloaded	2688.0	0.72	0.0544	10.8
C-1,986	Unloaded	3471.3	1.00	0.0794	94.2
C-4,000	Unloaded	3708.1	1.00	0.0826	90.5
C-1 year	Unloaded	3184.6	1.00	0.0706	31.5
Conversion Units: 1 in. = 25.4 mm, 1 lb = 0.0044kN, °F = °C × 1.8 + 32.					

Note: EC, SW, and C represent environmental chamber, salt water, and control, respectively.

The strength ratios in Table 4.29 and 4.30 indicate that a single environmental condition can not define the environmental reduction factor (C_E). Table 4.31 summarizes C_E for SRP system under various exposure conditions.

For exterior exposure subjected to “wet environments”, a C_E of 0.75 could be defined for the SRP strengthening system [25]. For aggressive environments, a C_E of 0.65 is suggested based on the data collected herein. The ultimate load capacities of the specimens under various environmental conditions and real-time weather and solar exposure are exhibited in Figure 4.97.

Table 4.30. The flexural bending test results of RNG specimens

Environmental condition	RNG specimen				
	Loading condition	Ultimate load (lb)	Strength ratio	Max def. (in.)	Concrete (%)
OUTDOOR	Specimens (40%)	2664.6	0.83	0.0474	13.6
	Specimens (20%)	2782.8	0.87	0.0588	12.1
	Unloaded	2518.3	0.78	0.0455	13.3
EC	Specimens (40%)	3177.9	0.95	0.0631	55.1
	Specimens (20%)	2967.7	0.89	0.0566	46.6
	Unloaded	2890.2	0.87	0.0511	27.4
WATER-3,000	Unloaded	2542.0	0.72	0.0602	11.2
HOT WATER-4,000 (122°F)	Unloaded	2253.3	0.63	0.0461	16.9
SW-1,500	Unloaded	2576.7	0.77	0.0582	13.3
SW-4,000	Unloaded	2671.3	0.75	0.0530	11.4
C-1,986	Unloaded	3335.8	1.00	0.0748	72.8
C-4,000	Unloaded	3551.9	1.00	0.0806	95.5
C-1 year	Unloaded	3208.1	1.00	0.0697	37.4
Conversion Units: 1 in. = 25.4 mm, 1 lb = 0.0044kN, °F = °C × 1.8 + 32.					

Note: EC, SW, and C represent environmental chamber, salt water, and control, respectively.

Table 4.31 Reduction factor for SRP system under various exposure conditions

Exposure conditions	Fiber type (steel fiber)	Environmental reduction factor C_E
Interior exposure	Micro-fine galvanized coating	0.95
	Micro-fine brass coating	0.95
Exterior exposure	Micro-fine galvanized coating	0.75
	Micro-fine brass coating	0.75
Aggressive environment (chemical plants and wastewater treatment plants)	Micro-fine galvanized coating	0.65
	Micro-fine brass coating	0.65

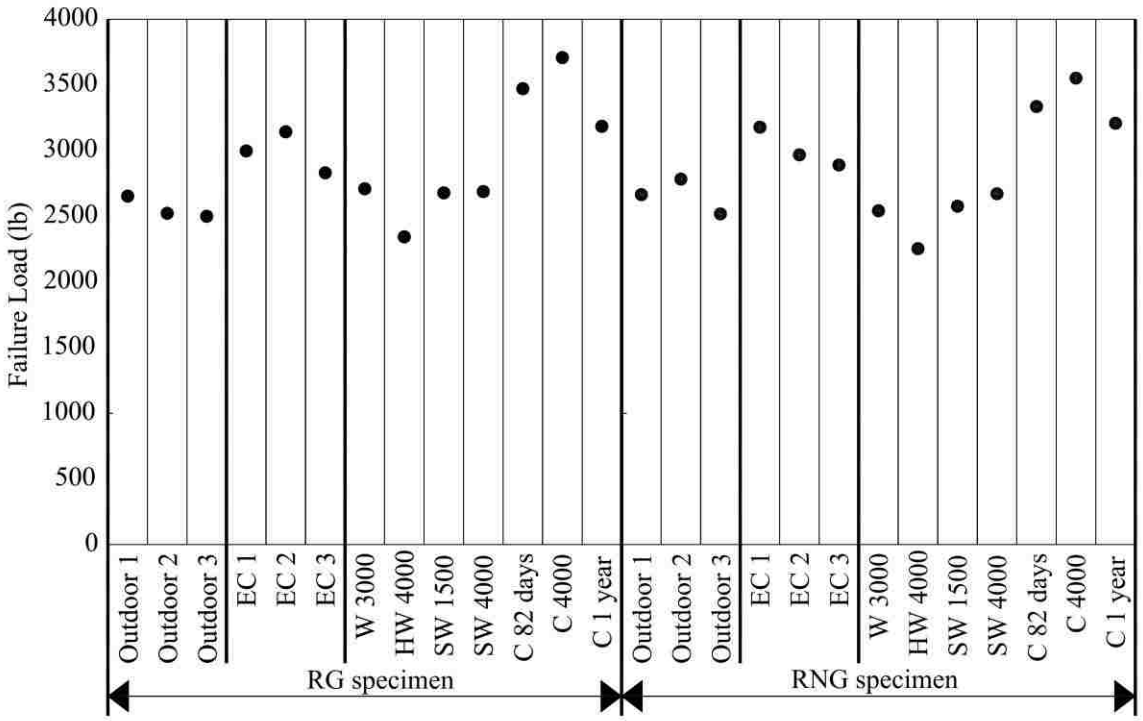

Conversion Units: 1 lb = 0.0044 kN

Figure 4.97. Summary of the flexural test results (Note: Outdoor and EC 1, 2, and 3 means the specimens loaded by 40%, 20% of ultimate load, and unloaded specimens)

It can be seen in Figure 4.97 that significant strength loss of the outdoor specimens and the specimens exposed to full immersion was observed when compared to the control specimens. Therefore, the real-time weather exposure and water considerably influenced the bond durability of the SRP-to-concrete systems. There is no apparent difference in ultimate strength between the RG and RNG specimens. In addition, the specimens exposed to hot water exhibited a strength loss of roughly 37% after 4,000 hours of exposure at 122°F (50°C). This is the most severe strength loss among the results. Thus, the temperature that concrete members reinforced with SRP were exposed to should be another crucial concern to deteriorate the bond performance between the SRP and concrete substrate. Even if water immersion at 122°F (50°C) was considered the most serious aging environmental condition for SRP/concrete application, this exposure

should be considered as indication of long-term characteristics in hot weather and higher humidity.

4.9.2. Direct Pull-Off Tests. Tensile pull-off tests were used to evaluate the bond performance of the SRP-to-concrete system. This method is considered a simple and standardized experimental test. Both flexural bending and pull-off tests were available from a single specimen. Table 4.32 illustrates the test results of pull-off specimens exposed to the various environmental conditions.

According to Table 4.32, the pull-off strength ratios of conditioned RG and RNG specimens exceeded 1.0. The possible explanation is that the concrete exposed to accelerated aging conditions and real-time environment was post-cured due to sufficient moisture or water. It should be noted that the control RG and RNG specimens exposed for one year illustrated higher tensile strength when compared to the control specimens that were exposed to the laboratory for 1,986 and 4,000 hours due to increase of concrete strength after one year of exposure. In addition, the control specimens and the specimens exposed to EC and varying solutions showed a failure Mode G. For the outdoor specimens, some samples failed in Mode G and others failed in Mode F. Furthermore, the results of this test exhibited a large degree of scatter and variation, indicating the variability of this test method. Therefore, direct pull-off tests should be considered as a technology to evaluate the long-term bond performance of SRP-to-concrete systems in the field. However, it may not be an effective avenue.

4.9.3. Comparison with Deng's Study [19]. In order to effectively evaluate the bond durability of the SRP strengthening system, the flexural and direct tensile strengths in this study were compared to Deng's conclusions. The bond performance of CFRP-to-concrete systems that were exposed to varying environmental conditions was investigated in his research. CFRP composite systems A and B were tested. Three-point bending and direct pull-off tests were performed to evaluate the bond durability.

For the flexural bending tests, the failure modes of the control and exposed specimens in this research were the same as those of Deng's study. For the control specimens, the failure mode was Failure Mode 1, and the conditioned specimens showed Failure Modes 2 and 3 in both studies. When the specimens were exposed to water at 122°F (50°C) for 4,000 hours, a strength ratio of 0.63 was obtained in this research. A

ratio of roughly 0.6 was attained for system B in Deng's research. Meanwhile, system A exhibited a lower value than 0.6 in his study. The strength ratios were 0.73 and 0.72 for RG and RNG specimens exposed tap water at room-temperature environment for 3,000 hours, respectively, in this study. Deng obtained strength ratios that were higher than 0.80 for both CFRP system A and B when the specimens were submerged in water for a similar duration. For real-time exposure (12 months), higher strength loss was observed in Deng's study. The strength ratios were roughly 0.60 for both system A and B of Deng's research. In contrast to this, the strength ratios were higher than 0.78 in this study.

Table 4.32. The average bond stress and strength ratio of pull-off test

Environmental condition	RG specimen	RNG specimen	RG specimen	RNG specimen
	Ave. bond stress (psi)		Strength ratio	
OUTDOOR-1 year	358.8	379.4	1.1	1.1
EC	369.5	308.6	1.2	1.3
WATER-3,000	429.6	517.3	1.4	1.9
HOT WATER-4,000 (122°F)	343.8	344.8	1.1	1.2
SW-1,500	462.0	460.0	1.5	2.0
SW-4,000	427.7	513.1	1.3	1.9
C-1,986	318.2	229.0	1.0	1.0
C-4,000	318.0	276.6	1.0	1.0
C-1 year	340.9	333.4	1.0	1.0
Conversion units: 1 psi = 0.0069 MPa, °F = °C x 1.8 + 32				

Note: EC, SW, and C represent environmental chamber, salt water, and control, respectively.

For direct pull-off tests, this study illustrated 5.3% (RG specimens) and 13.8% (RNG specimens) tensile strength increase when the specimens were exposed to real-time weather and solar exposure for 12 months. The failure modes of some samples were Mode G, and the others were failed in Mode F. In contrast to this, direct tension tests of Deng [69] that studied the bond performance of concrete beams reinforced with CFRP

exhibited roughly 20% and 30% strength loss after 12 months of exposure for systems A and B, respectively. The failure modes of the exposed samples switched from Mode G to Mode F when the exposure duration increased based on his study. The RG and RNG specimens immersed in water at 122°F (50°C) for 4,000 hours showed strength ratios of 1.1 and 1.2 respectively, and the failure modes of these two types of specimens were Mode G. However, the ratios of roughly 0.6 (system A) and 0.7 (system B) were demonstrated in Deng's study for the water tests at 122°F (50°C). The exposed specimens failed in Mode F rather than Mode G in his report. The strength ratio of the specimens that were exposed to tap water at room-temperature environment exceeded 1.0. The failure modes were Mode G in this study. However, these ratios that were obtained by Deng's report were less than 1.0 for systems A and B exposed to tap water for the similar duration. Therefore, it can be concluded that SRP may be a more effective repair or strengthening system than CFRP when compared the results of this study to those of Deng's research.

Different results were attained between the flexural bending and direct pull-off tensile tests. Through the results of this research and Deng's conclusions, flexural testing should be recommended because test results of the three-point loading tests can effectively evaluate the long-term bond performance of SRP-to-concrete systems under the real-time weather exposure and immersed environmental conditions. Moreover, a concrete strength of 6,000 psi (42 MPa) is suitable for ascertaining C_E under varying environmental conditions.

5. STUDY OF TOPIC 3

5.1. GENERAL

For RC members, one of the greatest durability issues is the corrosion of reinforcing steel that is subjected to deleterious elements like chloride. Since the late 1990 s there have been a number of bridges in the United States built or rehabilitated using FRP materials due to their chemical inertness. A number of these projects occurred within Missouri between 1999 and 2012. To investigate the long-term durability performance of FRP bars in concrete exposed to a real-time weather environment, some samples with GFRP bars were extracted from Southview Bridge and Walker Bridge in the City of Rolla, MO and Serrita de la Cruz Creek Bridge in TX to examine their performance after a decade or more under field conditions and exposed to varying climates. Physical, chemical, and microstructural analyses of GFRP bars and surrounding concrete were performed to evaluate performance of GFRP bars after several years of service as concrete reinforcement in the decks of these three bridges. To date, very limited data exists, which investigates actual field performance of FRP bars in RC.

5.2. OUTLINE

Long-term durability of FRP reinforcement may be an obstacle for widespread application in concrete members. An overwhelming number of studies have focused on FRP durability with exposure to simulated concrete pore water solution at elevated-temperature environmental conditions. These tests are usually conducted in an alkaline environment because the pH value of a concrete environment is roughly 12 to 13. However, this accelerated aging alkaline environment is different with that presented in field concrete members [116, 117]. Therefore, monitoring the characteristics of existing projects is considered as a real demonstration of FRP reinforcement durability.

The state of Missouri has had a number of FRP projects for both strengthening existing deficient bridges and new FRP bridge construction. Validation of the long-term durability performance and the comprehensive development criteria/guidelines are needed before FRP systems gain widespread acceptance throughout the engineering and civil infrastructure community in the United States. Therefore, many of the Missouri

demonstration projects such as Walker Bridge and Southview Bridge have included ongoing monitoring and load testing to validate these systems and demonstrate their long-term durability performance [118]. A map of FRP RC and rehabilitated bridges in Missouri is illustrated in Figure 5.1.

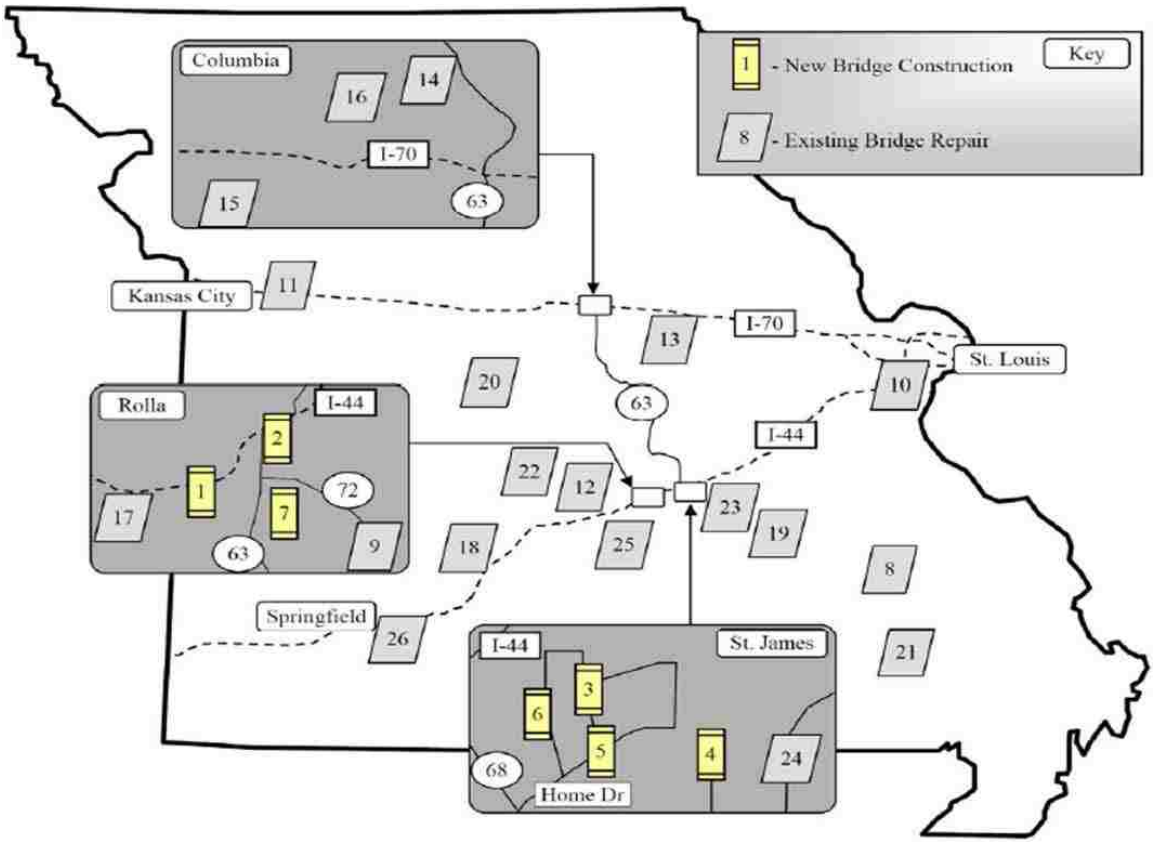

Figure 5.1. Map of FRP RC and rehabilitated bridges in Missouri

In the state of Texas, FRP projects like the Serrita de la Cruz creek bridge (located 25 miles northwest of Amarillo, TX) has been monitored. Several types of instrumentation on this bridge were employed by Texas Tech for comparison of the performance of the GFRP-reinforced concrete decks to the performance of the other decks reinforced entirely with epoxy-coated steel (ECS) [48] when the Serrita de la Cruz creek bridge was constructed. However, this merely consisted of short-term monitoring.

After more than a decade long-term durability performance of FRP reinforcing bars in concrete subjected to real field exposure is a top priority to be studied to aid in wider spread implementation of this technology and answer the question related to concerns about field degradation.

Although GFRP reinforcing bars do not exhibit the traditional corrosion like steel bars, many publications have reported that there is a significant reduction in the tensile capacity of GFRP bars when they are exposed to various environmental conditions in laboratory based studies. Others, however, have reported no sign or minimal signs of GFRP bars degredation through the analysis of microscopic structures of GFRP bars. The obtained results are not enough to prove or disprove that GFRP bars are deteriorative when they are exposed to concrete environments under field conditions. Therefore, Missouri University of Science and Technology in cooperation with The University of Miami and Owens Corning Science and Technology LLC to initiate the first major U.S. study on the long-term performance of FRP bars under field conditions. In this work, several core samples with encapsulated GFRP bars were extracted from Southview Bridge and Walker Bridge in Missouri and the Serrita de la Cruz creek bridge deck in Texas. All of the applied GFRP bars were produced by Hughes Brothers Inc. of Stewart, Nebraska

To date, there is extremely limited data on the behavior of FRP reinforced concrete member that have undergone multiple years of field environmental exposure and service loading. In an effort to document the durability performance of FRP reinforcing bars after years of service, the following two tasks were undertaken in this section:

1: Inspection of Southview and Walker Street bridges in Rolla, Missouri to document any physical damage, including the locations of cracking and measurement of crack widths. 2: Investigate the durability of GFRP bars extracted from in-service FRP reinforced concrete structures (Southview Street and Walker Street bridges, and the Serrita de la Cruz creek bridge).

For the second task, several tests were performed to investigate the durability performance of GFRP reinforcing bars and concrete: (1) scanning electron microscope (SEM) analysis to detect information about the FRP bars' surface topography and composition; (2) energy-dispersive X-ray spectroscopy (EDS) and fourier transform

infrared (FTIR) spectroscopy analyses for the elemental analysis or chemical characterization of FRP bars; (3) short bar shear (SBS) test to evaluate the determination of inter-laminar shear strength; (4) glass transition temperature (T_g) test to detect temperature range of the resin/matrix of GFRP bars, and analyze whether resin is deteriorative; (5) burn-off test to obtain the ignition loss of the GFRP samples or resin content; and (6) concrete tests including: chloride content and pH measurement. The main purpose is to monitor possible changes in chemical behavior of the concrete surrounding the GFRP bars.

5.3. INSPECTION OF SOUTHVIEW AND WALKER STREET BRIDGES

Bridge inspection was undertaken based on FHWA National Bridge Inspection Standards [119]. According to National Bridge Inspections Standards Regulation (NBIS), damage inspection is defined as an unscheduled inspection to evaluate structural damage resulting from environmental influences and human actions. Routine inspection is considered a regularly scheduled inspection composes observations and/or measurements to investigate the physical and functional conditions of the bridge to determine any difference with original or formerly recorded conditions and to confirm whether the bridge can satisfy the current service requirements [119]. Therefore, in order to evaluate the physical damage of these two bridges, the physical conditions of the bridges were observed. The locations of cracks were marked and crack widths were measured.

5.3.1. Investigation for Southview Bridge. This section introduces the bridge including its exiting part and new structures, and its physical inspection.

5.3.1.1 The introduction of the bridge. Southview Bridge is located in Rolla, MO (Southview Drive on Carter Creek). FRP bars and tendons were applied to the new construction of this bridge. The bridge consisted of one lane that was already constructed using conventional four-cell steel RC box culvert. It was composed of a steel RC deck slab about 10 in. (254 mm) thick. The slab deck was continuous over three intermediate reinforced concrete vertical walls, and the overall length of the bridge was roughly 40 ft (12 m). The new deck was constructed on three conventional RC walls, the same as the existing structure. The new construction was completed in 2004 and included the removal of the existing curb from the existing RC slab deck to allow the construction of two new

structures adjacent to the initial slab deck to extend the width of the bridge from 12.8 ft (3.9 m) to 39 ft (11.9 m). The curb-to-curb width of the resulting bridge was 30 ft (9.1 m). The two new structures consisted of a FRP prestressed/reinforced concrete deck and a steel RC deck. Figures 5.2 and 5.3 illustrate the schematic profile and elevation of the whole bridge deck, respectively.

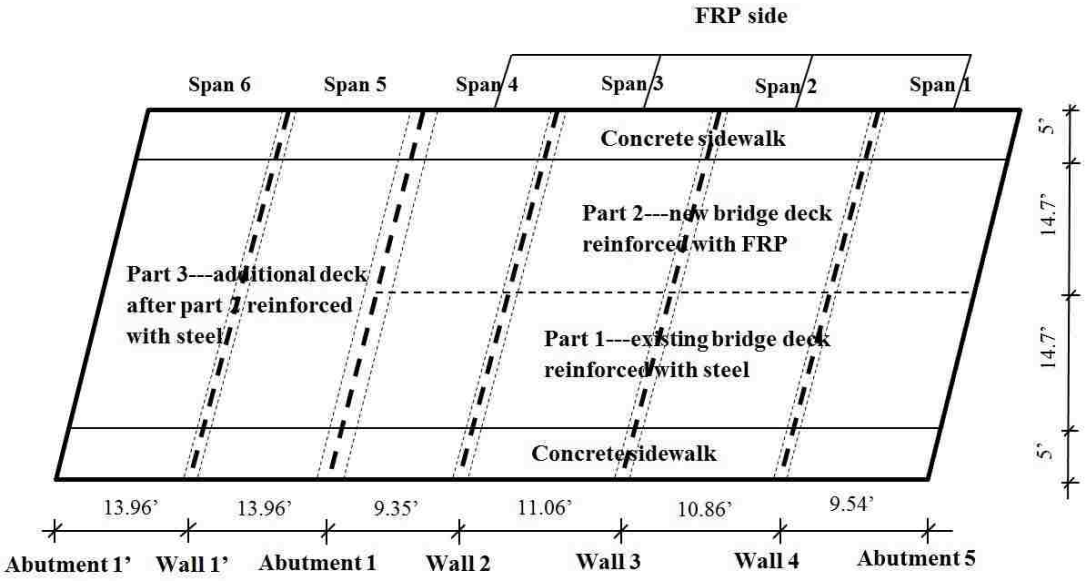

Conversion Units: 1 ft. = 0.305 m

Figure 5.2. A schematic illustration of current Southview Bridge

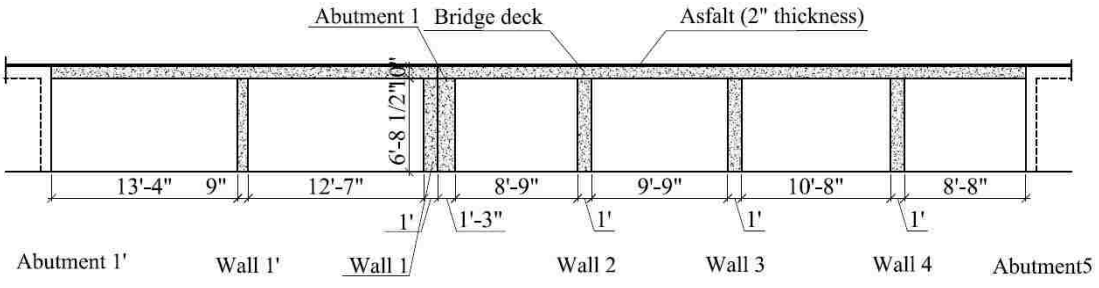

Conversion Units: 1 in. = 25.4 mm, 1 ft. = 0.305 m

Figure 5.3. A schematic elevation of Southview Bridge

The cross section of the deck and the details of internal FRP reinforcement are illustrated in Figures 5.4 and 5.5, respectively.

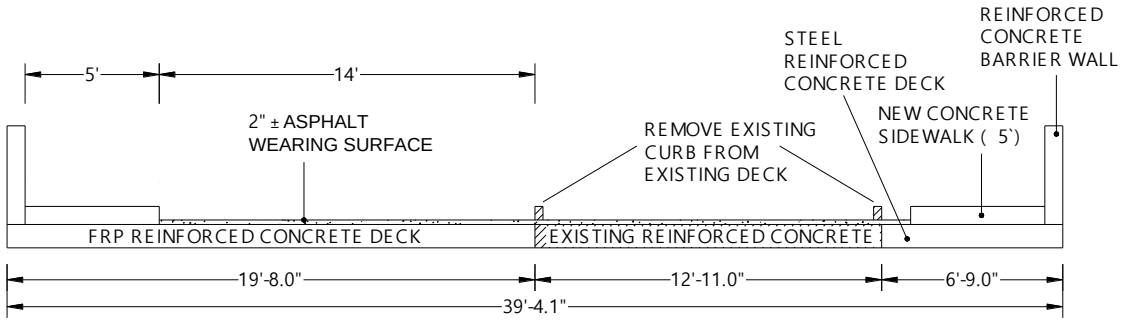

Conversion Units: 1 in. = 25.4 mm, 1 ft. = 0.305 m

Figure 5.4. Cross section of deck for Southview Bridge [120]

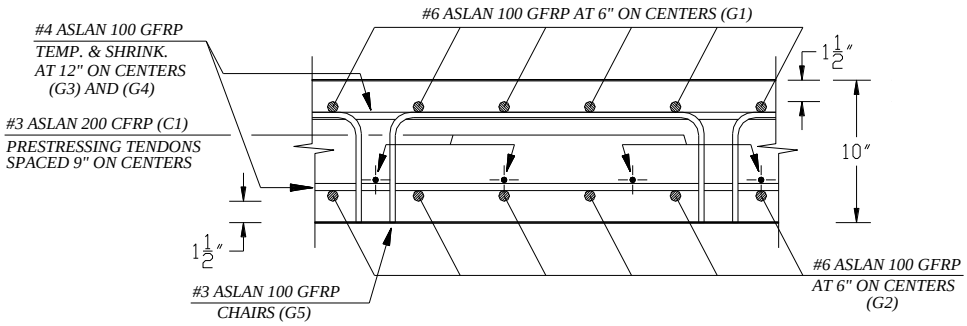

Conversion Units: 1 in. = 25.4 mm, 1 ft. = 0.305 m

Figure 5.5. The details of internal FRP reinforcement [120]

The new construction was completed in October 2004. Figures 5.6 and 5.7 exhibit the existing and the resulting bridge, respectively.

Figure 5.6. View of the existing Southview Bridge [120]

Figure 5.7. View of the new structure

5.3.1.2 The physical inspection. This bridge consisted of three decks: the existing deck reinforced with steel, the deck reinforced with FRP bars, and the additional deck reinforced with steel, as illustrated in Figure 5.2. The bottom of the existing concrete deck exhibited more cracks. Figures 5.8 through 5.13 exhibit the distribution of cracks on the bottom of the decks of each span.

The majority of cracks in spans 1, 2, 3, and 4 were located at the parts of the existing concrete deck. Spans 5 and 6 (additional deck reinforced with steel) showed 4 and 3 cracks, respectively. The most cracks extended the full width of each span. Span 2 showed the highest numbers of cracks. Span 1 had a maximum crack width of 0.1875 in. (4.76 mm). Some mineral efflorescence was observed on the surface of the bottom of decks. Figures 5.14 through 5.19 show representative cracks for each span.

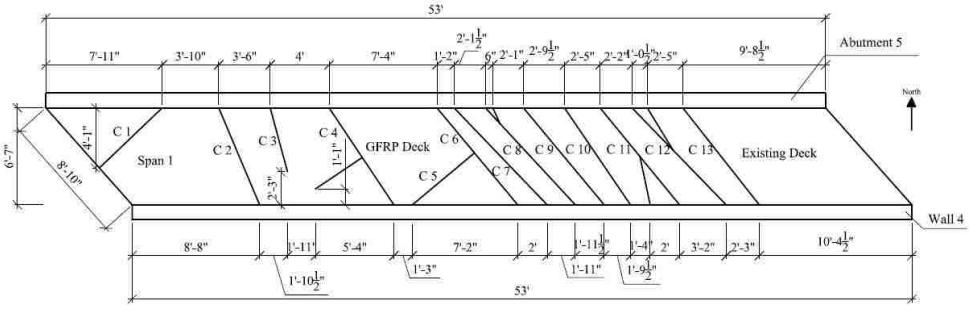

Conversion Units: 1 in. = 25.4 mm, 1 ft. = 0.305 m

Figure 5.8. The locations of cracks of span 1

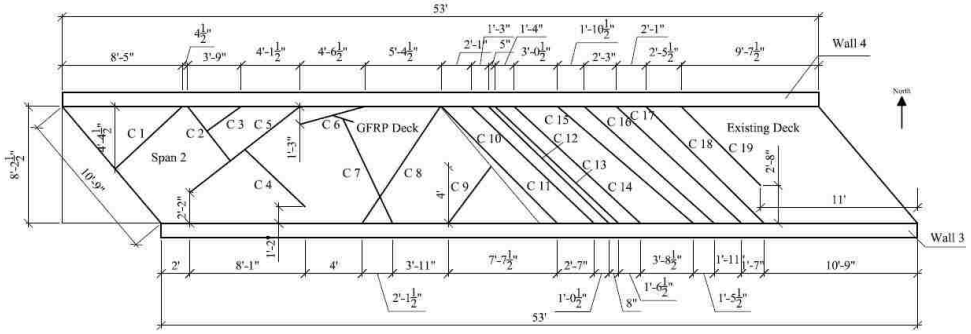

Conversion Units: 1 in. = 25.4 mm, 1 ft. = 0.305 m

Figure 5.9. The locations of cracks of span 2

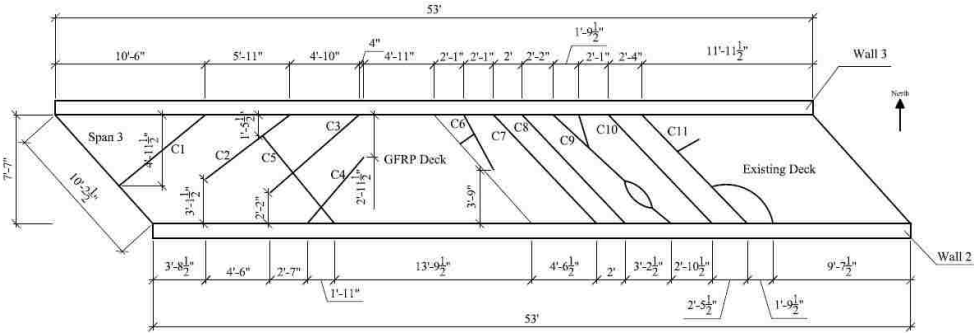

Conversion Units: 1 in. = 25.4 mm, 1 ft. = 0.305 m

Figure 5.10. The locations of cracks of span 3

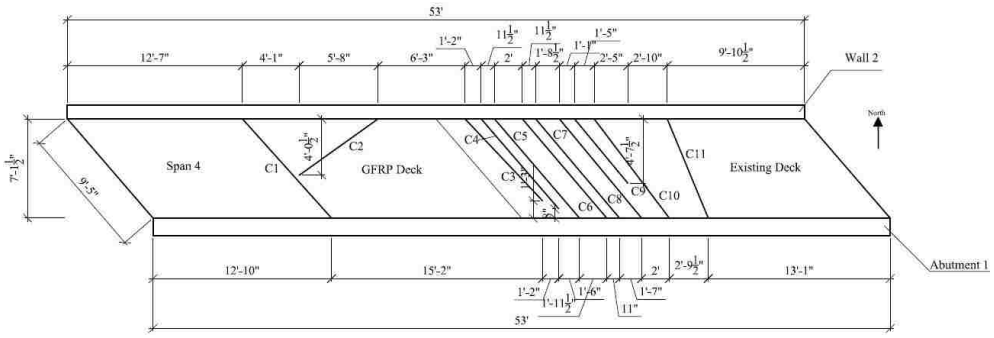

Conversion Units: 1 in. = 25.4 mm, 1 ft. = 0.305 m

Figure 5.11. The locations of cracks of span 4

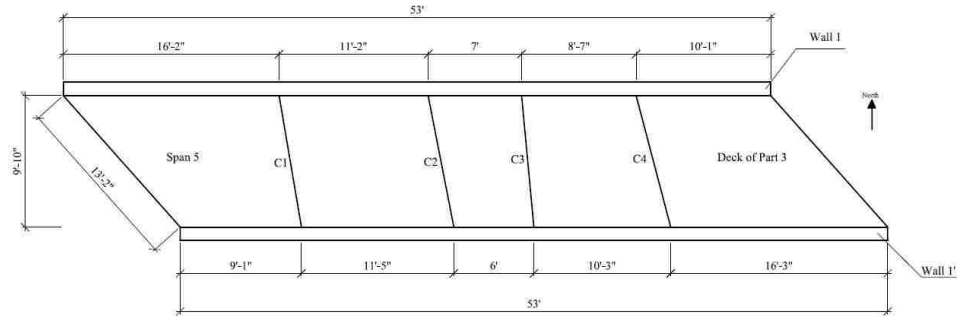

Conversion Units: 1 in. = 25.4 mm, 1 ft. = 0.305 m

Figure 5.12. The locations of cracks of span 5

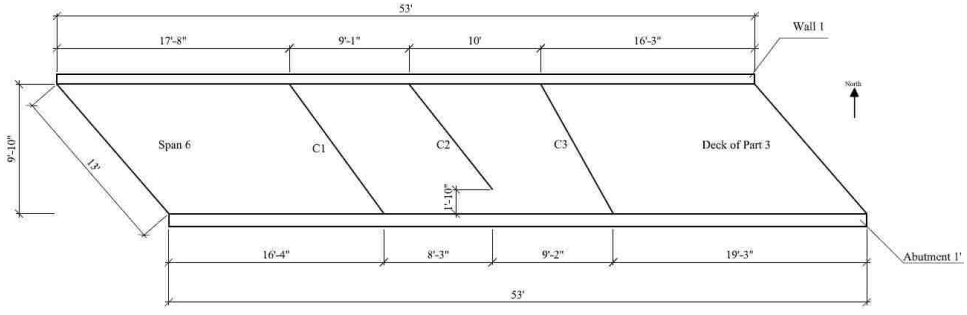

Conversion Units: 1 in. = 25.4 mm, 1 ft. = 0.305 m

Figure 5.13. The locations of cracks of span 6

Figure 5.14. The cracks of span 1

Figure 5.15. The cracks of span 2

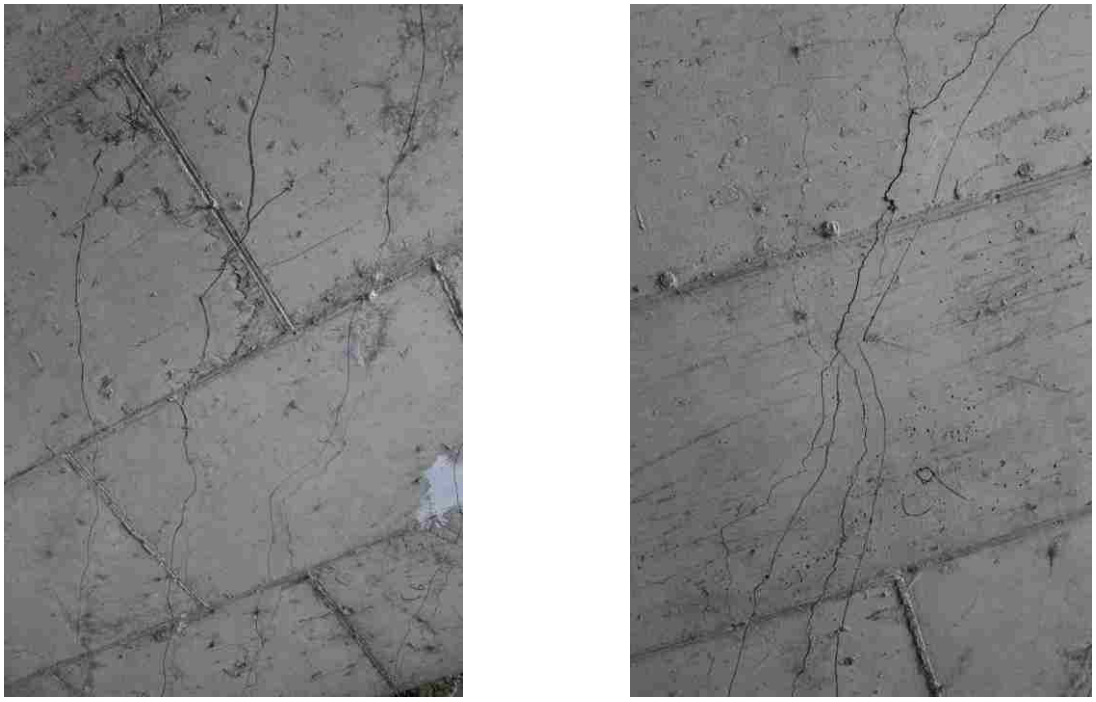

Figure 5.16. The cracks of span 3

Figure 5.17. The cracks of span 4

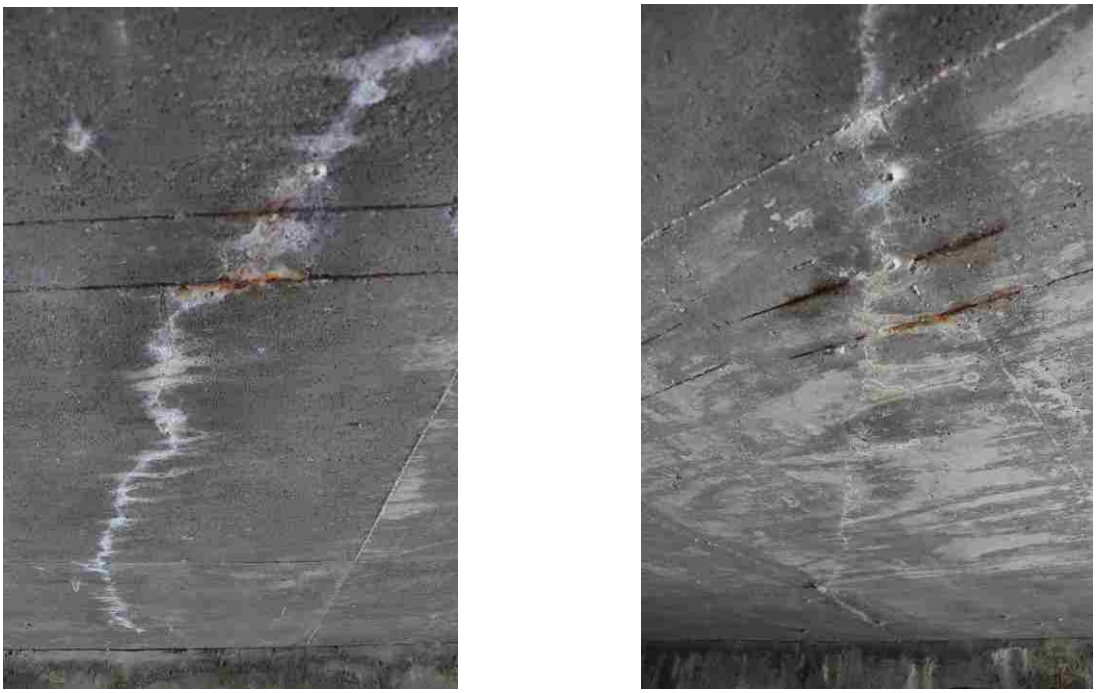

Figure 5.18. The cracks of span 5

Figure 5.19. The cracks of span 6

Tables 5.1 and 5.2 show the crack widths of the decks of spans 1 and 2, respectively. The bottoms of the decks of span 1 and span 2 exhibited 13 and 19 cracks, respectively. The results of the other spans are available in Appendix C.

Table 5.1. Crack widths of span 1

	Crack No.	Ave. crack width (in.)
Span 1	1	0.0040
	2	0.0160
	3	0.0100
	4	0.0160
	5	0.0120
	6	0.1250
	7	0.0320
	8	0.0625
	9	0.0320
	10	0.0625
	11	0.0625
	12	0.0625
	13	0.1875
Conversion Units: 1 in. = 25.4 mm		

5.3.2. Investigation for Walker Bridge. This section included the description of Walker Bridge in Rolla, Missouri, including the old (previous) bridge and rebuilt one, and the physical inspection for this new structure.

5.3.2.1 The introduction of the bridge. Walker Bridge is located on Walker Avenue in Rolla, MO. The existing bridge was composed of three 42 in. (1.1 m) diameter corrugated steel pipes encased in concrete. They were placed transversely on Walker Avenue. The bridge was constructed in the 1970s with an initial roadway width of 16 ft (4.9 m). Because the steel pipes were corroded due to long-term exposure to “wet environment”, the bridge was scheduled for rebuilding during the Fall of 1999 [121]. Figure 5.20 exhibits the old bridge.

Table 5.2. Crack widths of span 2

	Crack	Ave. Crack width (in.)
Span 2	1	0.0600
	2	0.0120
	3	0.0100
	4	0.0140
	5	0.0400
	6	0.0140
	7	0.0140
	8	0.0120
	9	0.0100
	10	0.1250
	11	0.0220
	12	0.1250
	13	0.0625
	14	0.0625
	15	0.0625
	16	0.0625
	17	0.0625
	18	0.0625
	19	0.1250
Conversion Units: 1 in. = 25.4 mm		

Figure 5.20. The old Walker Bridge [121]

According to the hydraulic requirements and the characteristics of the location for this bridge, the box culvert units were selected to build the new bridge. The dimension of one box culvert unit was 5 x 5 ft (1.5 x 1.5 m) with a thickness of 6 in. (152.4 mm). The

internal #2 GFRP reinforcing bars were applied to each box culvert. Figure 5.21 illustrates the details of GFRP bars for a unit and a representative box culvert section.

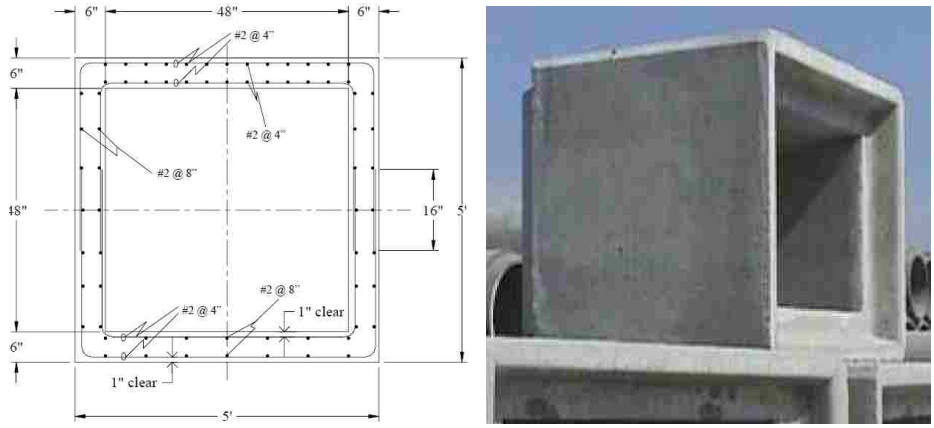

Conversion Units: 1 in. = 25.4 mm, 1 ft. = 0.305 m

Figure 5.21. Details for a box culvert (left) and a representative box section (right) [121]

The new Walker Bridge was 36 ft (11.0 m) wide and composed of 18 pre-cast box culvert units that were arranged in two rows. Each row exhibited nine GFRP-reinforced boxes. The new Walker Bridge was opened to traffic in October 1999. Figure 5.22 presents the new bridge.

Figure 5.22. The view of new Walker Bridge

5.3.2.2 The physical inspection. This bridge consisted of two rows of box culvert units. Figure 5.23 exhibits the numbers and arrangements of the box culverts. Some cracks were observed on the tops and bottoms of these boxes. No cracks were observed on the sides of the boxes.

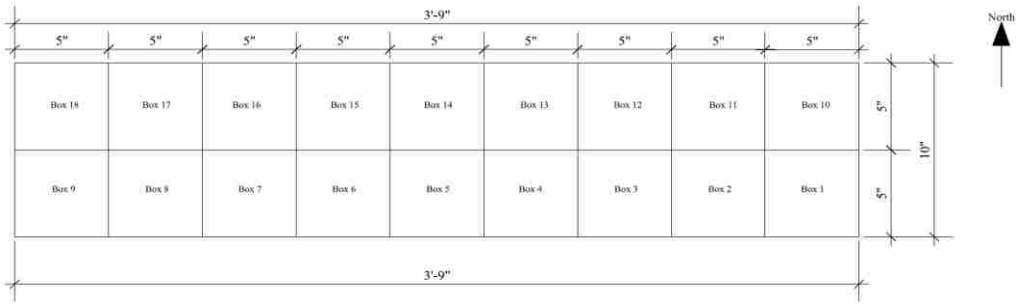

Conversion Units: 1 in. = 25.4 mm, 1 ft. = 0.305 m

Figure 5.23. The numbers and arrangements of the box culverts

Figures 5.24 through 5.26 illustrate the locations of the cracks for Box 1, 2, and 3. The cracks of the other boxes are illustrated in Appendix C.

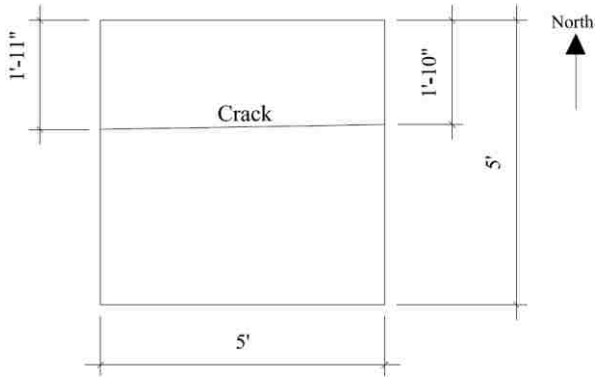

Conversion Units: 1 in. = 25.4 mm, 1 ft. = 0.305 m

Figure 5.24. The location of crack on the top of Box 1

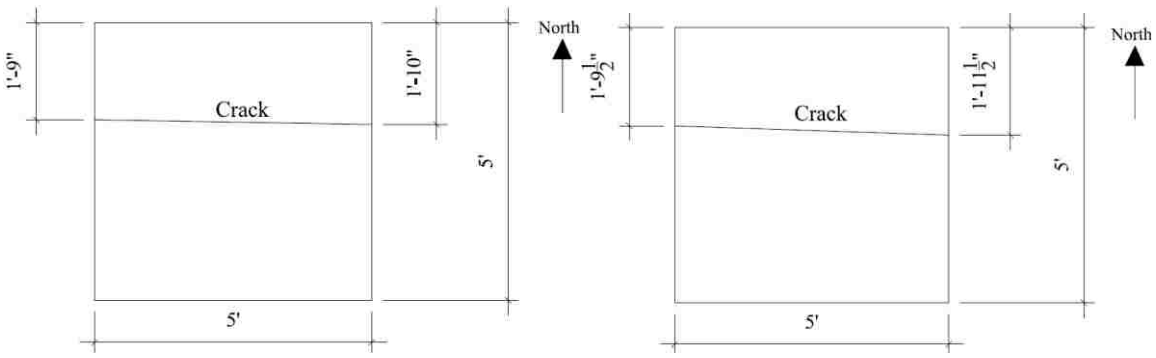

Conversion Units: 1 in. = 25.4 mm, 1 ft. = 0.305 m

Figure 5.25. The locations of cracks on top (left) and bottom (right) of Box 2

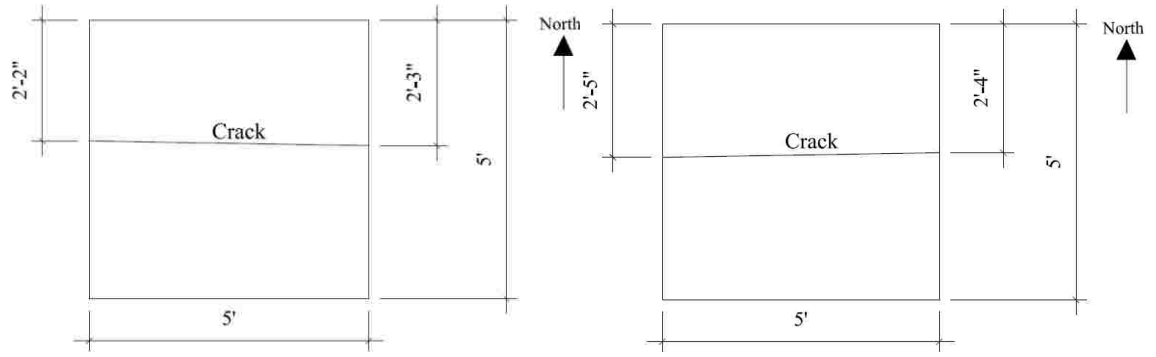

Conversion Units: 1 in. = 25.4 mm, 1 ft. = 0.305 m

Figure 5.26. The locations of cracks on top (left) and bottom (right) of Box 3

Table 5.3 shows the average crack widths of the concrete boxes. The maximum crack width of 0.625 in. (15.90 mm) occurred on the bottom of the Box 16.

Figures 5.27 and 5.28 shows representative cracks for Box 2 and Box 12. The cracks of the other boxes are available in Appendix C.

Table 5.3. Crack widths of Walker Bridge

	Ave. crack width (in.)	
Box No.	Top	Bottom
1	0.0120	0
2	0.0100	0.0260
3	0.0280	0.0320
4	0.0160	0.0280
5	0.0180	0.0260
6	0	0
7	0.0200	0
8	0	0
9	0	0
10	0.0060	0
11	0.0200	0
12	0.0140	0.0240
13	0.0240	0.0120
14	0.0180	0.0220
15	0.0160	0.0220
16	0.0280	0.0625
17	0	0
18	0	0
Conversion Unit: 1 in. = 25.4 mm		

Figure 5.27. The cracks on the top (left) and bottom (right) of Box 2

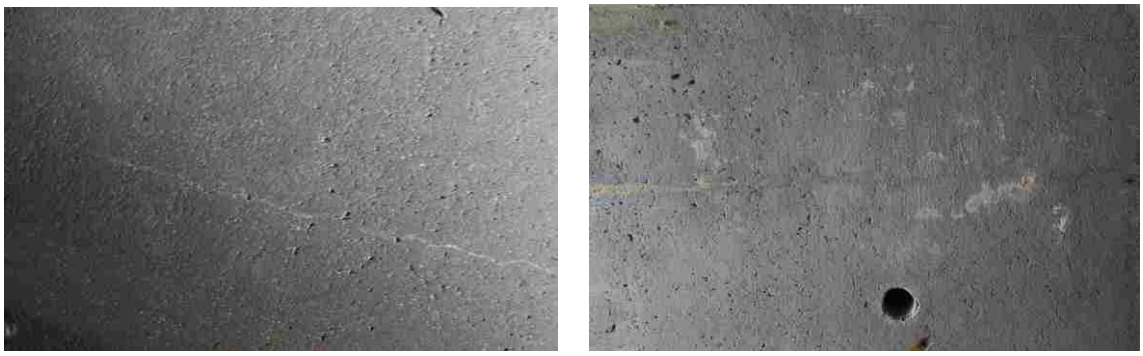

Figure 5.28. The cracks on the top (left) and bottom (right) of Box 12

5.4. LONG-TERM DURABILITY OF GFRP BARS IN CONCRETE

In order to evaluate the long-term performance of GFRP bars in existing concrete structures, SEM, EDS, FTIR Spectroscopy, SBS test, T_g analysis, and burn off testing (i.e. resin) were conducted on GFRP samples to investigate the possible changes in microstructural performance and mechanical characteristics. Meanwhile, chloride content and pH measurements for the samples of concrete cylinders were performed to characterize the concrete environment. In this section, the GFRP bars were the Aslan 100 series manufactured by Hughes Brothers, Inc of Seward, NE. The results of this research were compared to the data that the University of Miami conducted in round robin studies, and the results of some initial production lot quality control testing that Hughes Brothers already maintained.

5.4.1. Sample Extraction. Concrete cores with GFRP bars were extracted from various locations of Southview Bridge and Walker Bridge in October 2015. Meanwhile, these holes from cylinder extraction were repaired using a fast-curing cementitious grout. Two concrete samples were received from the University of Miami.

5.4.1.1 Concrete cores from Southview Bridge. Southview Bridge included three parts. Part 1 was the existing old bridge. The concrete deck was reinforced with steel bars. Part 2 was the “new” bridge with FRP reinforced concrete deck. Part 3 was the additional part after Part 2. The deck was reinforced with steel bars. Ten concrete cores (4 in. [101.6 mm] diameter) with FRP bars were extracted from the deck of Part 2. They

were collected at the midspans from span 1 to span 4 of the FRP side. Figure 5.29 shows the detailed information of this bridge and the locations of core extraction.

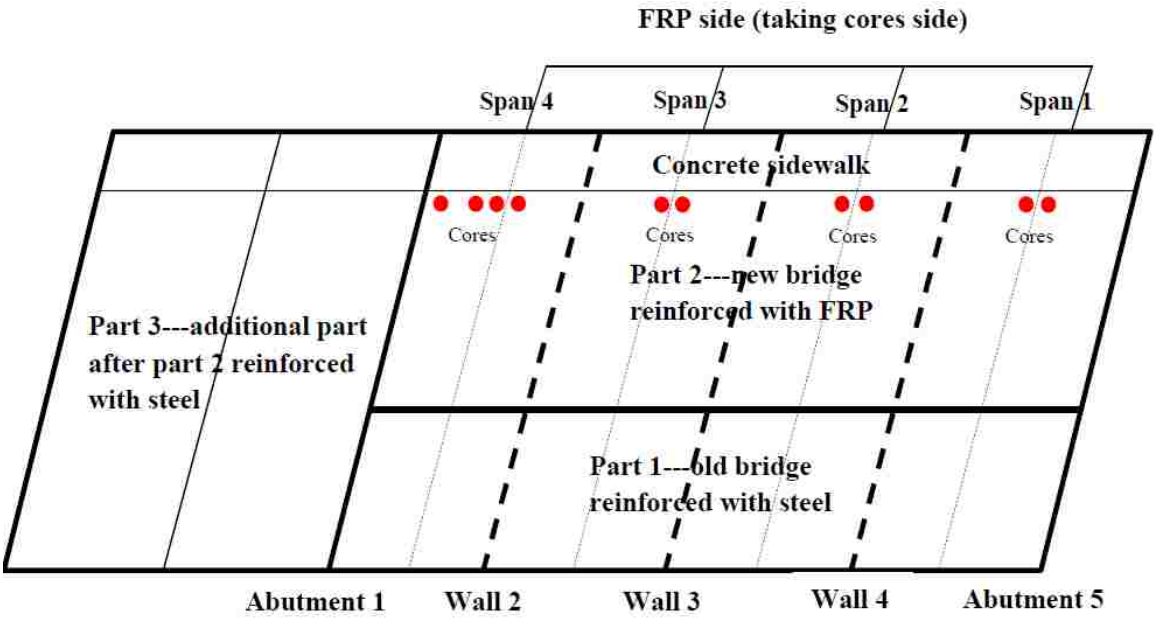

Figure 5.29. The locations of core extraction

The first two cores were taken at the midspan of span 1. The third and fourth cores were extracted from the midspan of span 2. The fifth and sixth samples were from the midspan of span 3. The last four samples were collected at the midspan of span 4. The distance between the center of cores and the side of concrete sidewalk was 9 in. (228.6 mm). Figure 5.30 exhibits the representative of coring process. Table 5.4 illustrates detailed information of these samples.

The representative concrete cores that were extracted from Southview Bridge are shown in Figure 5.31.

Figure 5.30. Concrete core extraction from Southview Bridge

Table 5.4. Summary of the information of cores

Cores ID	Reinforcement (No.)	Span No.	Location
C-1 S-1	GFRP (#6, #4)	Span 1	Mid-span
C-2 S-1	GFRP (2 #6)	Span 1	Mid-span
C-1 S-2	GFRP (#6), CFRP (#3)	Span 2	Mid-span
C-2 S-2	GFRP (#6, #4) , CFRP (#3)	Span 2	Mid-span
C-1 S-3	GFRP (#6, #4)	Span 3	Mid-span
C-2 S-3	GFRP (#6)	Span 3	Mid-span
C-1 S-4	CFRP (#3)	Span 4	Right side of abutment 1
C-2 S-4	GFRP (#6)	Span 4	Near mid-span
C-3 S-4	GFRP (#6)	Span 4	Mid-span
C-4 S-4	GFRP (#6, #4)	Span 4	Mid-span

Note: “C” means core, “S” means span. C-1 S-1 represents this core was first one and from span 1.

Figure 5.31. The representative concrete cylinder extracted from Southview Bridge

5.4.1.2 Concrete cores from Walker Bridge. Six concrete cores (4 in. diameter) with GFRP bars were extracted from the bottom of box culverts. Figure 5.32 illustrates the coring process. Figure 5.33 exhibits the locations of the extracted cores. Table 5.5 presents the detailed information of concrete cores. Figure 5.34 shows a typical concrete core that was extracted through a crack.

Figure 5.32. Concrete core extraction from Walker Bridge

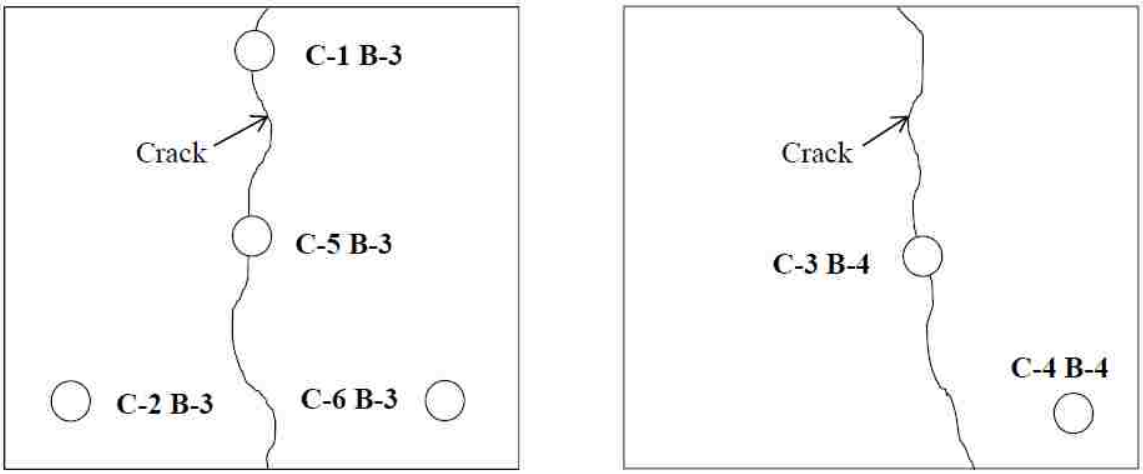

Figure 5.33. The locations of core extraction from No. 3 (left) and No. 4 (right) box culvers

Table 5.5. Summary of the information of cores

Cores ID	Reinforcement (No.)	Box No.	Location
C-1 B-3	GFRP (#2)	3	Cross the crack
C-2 B-3	GFRP (#2)	3	Without crack
C-3 B-4	GFRP (#2)	4	Cross the crack
C-4 B-4	GFRP (#2)	4	Without crack
C-5 B-3	GFRP (#2)	3	Cross the crack
C-6 B-3	GFRP (#2)	3	Without crack

Note: “C” means core, “B” means box. “1” represents the first core, “3” means the No. of box culvert.

Figure 5.34. A representative concrete core with crack

5.4.1.3 Concrete cores from Sierrita de la Cruz Bridge. The Sierrita de la Cruz Bridge was built in 2000 to replace the initial bridge that was considered structurally deficient. It was the first bridge in the state of Texas where GFRP reinforcement was applied to concrete members. This bridge is composed of seven spans 79 ft. (24.1 m) long and 45.3 ft (13.8 m) wide supported by six prestressed Texas type "C" concrete I-beams. Some concrete samples with #5 and #6 GFRP bars were extracted from different locations on the deck of this bridge in 2015. Two of them (cores A and B) were sent to Missouri University of Science and Technology to investigate long-term durability of GFRP reinforcement. Figure 5.35 exhibits core A.

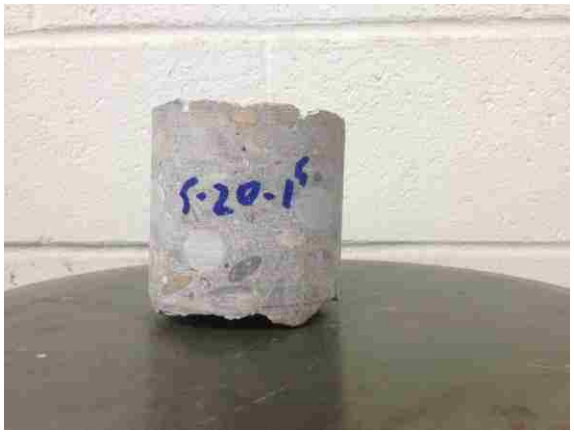

Figure 5.35. Core A from Sierrita de la Cruz Bridge

5.4.2. Preparation of GFRP Samples. Two #6 (0.75 in./19 mm diameter) GFRP bars were extracted from the core C-1 S-2 of Southview Bridge, and two small pieces were sliced from these two bars to prepare the samples of SEM and EDS. The rest of the bars were prepared to perform the other tests. One #5 (0.625 in./16 mm diameter) and one #6 GFRP bars were collected from the core A of Sierrita de la Cruz Bridge, and two small slices that were used for microscopic analyses were cut from the #6 GFRP bar. Meanwhile, the rest of these two bars were utilized for the other evaluation. These four GFRP pieces were cut to an approximate thickness of 0.2 in. (5 mm) by using a diamond

saw, and #2 GFRP bars were applied to Walker Bridge and the diameter was only 0.25 in. (6 mm). If this type of bar without concrete is ground and polished, it would be very difficult to guarantee that the specimen surface is balanced. Therefore, three small concrete pieces with GFRP bars (one from core C-1 B-3 and two from core C-2 B-3) were cut in 0.2 x 0.75 x 0.75 in. (5 x 19 x 19 mm) using the diamond saw once again to prepare samples of SEM and EDS. The rest of the GFRP bars were prepared to perform the other tests. Figures 5.36 and 5.37 illustrate the extracted GFRP bars from different concrete cylinders.

Figure 5.36. The extracted GFRP samples from Southview Bridges (left) and Sierrita de la Cruz Bridge (right)

Figure 5.37. The extracted GFRP samples from core C-1 B-3 (left) and core C-2 B-3 (right) of Walker Bridge

These small samples were ground carefully using five different level grits (1200, 800, 600, 240, and 180) of sand paper that were installed in a grinding and polishing equipment to guarantee that the surface of the specimens was flat. 8-in. micro cloth PSA 702-3 was used to further grind these samples. Finally, fine polishing using 0.3-μm MicroPolish completed the samples preparation. Prior to imaging, these specimens were placed in an oven at 140°F (60°C) for 24 hours to remove moisture produced during the grinding and polishing. An ion sputtering device was used due to the nonconductivity of concrete and GFRP bars for ultimate specimen preparation prior to SEM examination and EDS analysis using Helios NanoLab 600, as exhibited in Figure 3.37. Random locations were selected to identify existing chemical elements in GFRP samples. Figures 5.38 and 5.39 exhibit the prepared GFRP samples for SEM and EDS.

Figure 5.38. Prepared GFRP samples from Southview Bridge (left) and Sierrita de la Cruz Bridge (right) for SEM and EDS

Figure 5.39. Prepared GFRP samples from core C-1 B-3 and core C-2 B-3 of Walker Bridge

5.4.3. The Test Results of GFRP and Discussions. This section includes SBS tests, burn off tests, Tg measurement, SEM analysis, EDS analysis, and FTIR spectroscopy.

5.4.3.1 Short Bar Shear (SBS) tests. An SBS test was performed based on ASTM D4475-02 (Reapproved 2016) [122]. The purpose of this test was to measure the inter-laminar shear properties of GFRP bars and to compare to the values that the manufacturer reported. Shear behavior will change if resin or epoxy in GFRP bars is destroyed or deteriorated under seasonal in-situ field exposure. The Instron 4400 Series Universal Testing Machine (UTM) was used to conduct the test. Figure 5.40 illustrates the test setups that were used in this research and the report of UM [123].

Figure 5.40. The setups of the SBS test in this research (left) and report of UM (right)

This test was conducted in displacement control with the rate of 0.05 in./min (1.27 mm/min). The specimen was center-loaded. The specimens were tested with the span-to-diameter of GFRP bar ratio of 3 based on the ASTM standard. It should be noted in Figure 5.37 that there is some difference between the setups of this study and UM. The setup that UM used is recommended by ASTM D4475-02. This may induce some errors between the results of this study and UM. In this research, #2, #5, and #6 GFRP bars were employed to conduct SBS tests. Therefore, the distance between two supports was

regulated to complete the interlaminar horizontal shear test according to the different sizes of the samples. The ultimate failure loads and failure modes were recorded. Figures 5.41 through 5.44 exhibit the failure samples from these three bridges.

Figure 5.41. Failure #6 GFRP bar from Southview Bridge

Figure 5.42. Failure #5 (left) and #6 (right) GFRP bars from Sierrita de la Cruz Bridge

Figure 5.43. Failure T1 (left) and T3 (right) GFRP bars from C-1 B-3 of Walker Bridge

Figure 5.44. Failure #2 GFRP bars from core C-2 B-3 of Walker Bridge

When the cracks started from the mid-plane under the loading head, failure of the specimens occurred. At the same time, the crack widths also increased gradually. Figures 5.41 and 5.42 illustrate two #6 GFRP specimens, vertical plane of failure (plane of load) with cracks perpendicular to the cross-sections of the rods. The horizontal shear mode of failure was presented by #2 and #5 GFRP bars as shown Figures 5.42 through 5.44. According to the report of UM [123], both #5 and #6 GFRP bars presented the horizontal plane of failure. The reason is unknown. Perhaps different setups were used in this study and the report of UM [123], resulting in different results. Therefore, some additional SBS tests are required to obtain the failure mode of #6 GFRP bar. The results of these three bridges are summarized in Table 5.6.

Table 5.6. The results of SBS tests of the three bridges

Bridge	Walker Bridge (1999)			Sierrita de la Cruz Bridge (2000)		Southview Bridge (2004)
Specimen	NC	S1	S3	S1	S2	S1
Diameter (in.)	0.250	0.250	0.250	0.625	0.750	0.750
Span length (in.)	0.75	0.75	0.75	1.875	2.25	2.25
Max. load (lb)	399	399	354	2882	3281	2913
Conversion units: 1 in. = 25.4 mm, 1 lb = 0.0044 kN						

Note: “NC” represents non-crack, “S” indicates sample.

Due to lack of the original test data prior to construction of Walker Bridge and Southview Bridge, no reference was used to compare the test results of #2 GFRP bars from Walker Bridge. For the results of #6 GFRP bars from Southview Bridge, this section referred to the interlaminar shear strength results for the control specimens reported by Hughes Brothers and UM and in-service specimens from Sierrita de la Cruz Creek Bridge, to serve as a comparison [123]. Table 5.7 illustrates the results of control and extracted GFRP samples.

Table 5.7. The results of the control and in-service samples [123]

Bridge	Sierrita de la Cruz Bridge			
Resource of data	Hughes Brothers (Control, 2000)		UM (In-service, 2016)	
Specimen	10 samples	10 samples	Sample 1	Sample 2
Diameter (in.)	0.625	0.750	0.625	0.750
Max. load (lb)	3009	4664	3143.7	3552
Conversion units: 1 in. = 25.4 mm, 1 lb = 0.0044 kN				

The maximum load of #5 GFRP bar from Sierrita de la Cruz Bridge decreased by 4.2% and 8.3% when compared to the results of control samples and the specimen of UM [123], respectively. The possible explanation is that different setup was employed in this study, leading to small deviations between the result of this research and control samples and UM. The #6 GFRP specimen that was collected from Sierrita de la Cruz Bridge exhibited failure load decreases of 29.7% and 7.6% compared to the values of control samples and the specimen of UM [123]. It should be noted that the results from UM's report [123] decreased by 23% when compared to the average load of the control bars. The setup used in this study may be causing the difference; more SBS tests are needed to explain the change. In addition, the failure load of #6 GFRP from Southview Bridge decreased by 18.0% compared to the results of the in-service specimen from Sierrita de la Cruz Bridge. It should be noted that they were from a different production lot. The chemical composition of fiber/resin, different ratio of fiber and resin, or other parameters may be changed for different production lot, which causes different results for this test. In addition, more #6 GFRP samples need to be tested to evaluate the interlaminar shear

property of this type of bar. For #2 GFRP bars from Walker Bridge, no difference of the failure loads was observed between the bars that were extracted from the cores without crack and with crack.

5.4.3.2 Burn off testing. After the SBS test, the samples were cut to prepare the specimens of burn-off testing. This test was performed following the ASTM D2584 [124]. GFRP bar samples were cut and weighed approximately 0.011 lb (5 g). First, some samples were weighed, then placed on a substrate and reweighed. The samples on the substrates were heated in the muffle furnace at 600°C (1112°F) until all resin had disappeared. Figure 5.45 illustrates the muffle furnace.

Figure 5.45. The muffle furnace

The samples were then cooled and weighed again with the substrate. The change of mass was calculated. The test results were compared with the same test performed in 2000 prior to construction of Sierrita de la Cruz Bridge and the test conducted in UM in 2016 [123]. The purpose of this test is to determine whether epoxy of GFRP bars is deteriorative after long-term field exposure to concrete. Figures 5.46 through 5.50 exhibit the samples of these three bridges before and after this test. Table 5.8 summarizes the results of this test.

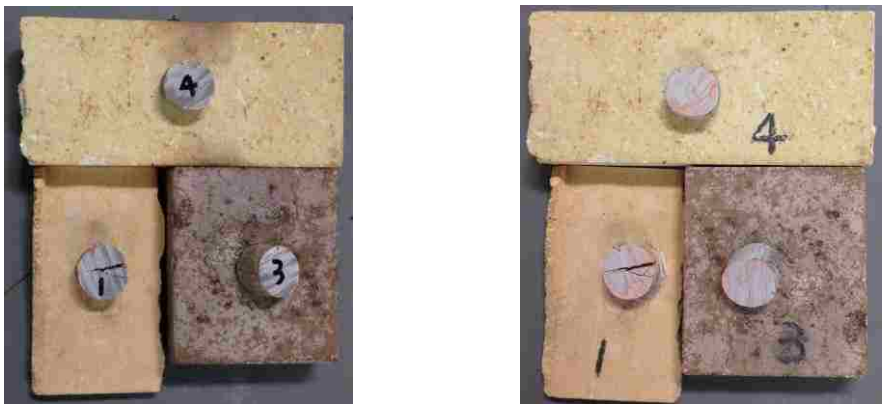

Figure 5.46. The #6 samples of before (left) and after (right) test for Southview Bridge

Figure 5.47. The #2 samples from C-1 B-3 of Walker Bridge before (left) and after (right) test

Figure 5.48. The #2 samples from C-2 B-3 of Walker Bridge before (left) and after (right) test

Figure 5.49. The #6 samples of before (left) and after (right) test for Sierrita de la Cruz Bridge

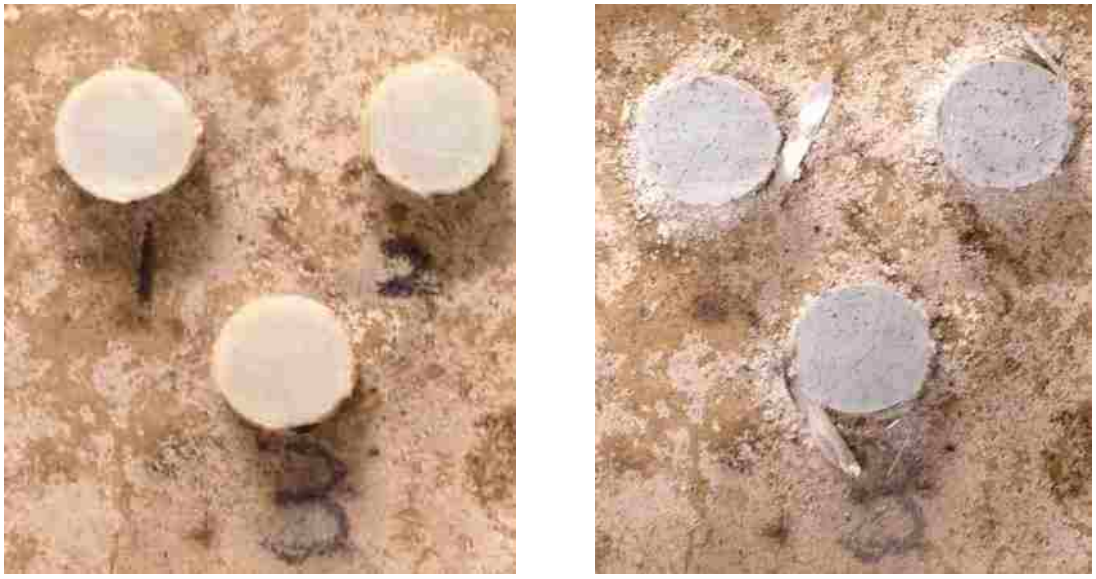

Figure 5.50. The #5 samples of before (left) and after (right) test for Sierrita de la Cruz Bridge

Table 5.8. Illustrates the summary of the results

Diameter (in.)	Bridge		No. of samples	Resin content (%)	Fiber content (%)	Fiber content (%) of control	Fiber content (%) of UM
0.25	Walker Bridge	NC	1	21.9	78.1	N/A	75.7 [138]
		C	2	22.3	77.7	N/A	
0.75	Southview Bridge		4	27.4	72.6	N/A	N/A
0.625	Sierrita de la Cruz Bridge		3	19.9	80.1	75.7	77.9 [136]
0.75			4	17.6	82.4	80.5	79.5 [136]
Conversion Units: 1 in. = 25.4 mm							

Note: “NC” represents concrete core without crack, “C” means concrete core with crack.

Due to lack of the initial test results prior to construction of Walker Bridge and Southview Bridge, there were no references to directly compare the results of #2 and #6 GFRP bars from Walker Bridge and Southview Bridge, respectively. For #2 GFRP samples, no substantial difference was observed between the results of this study and value reported by UM [125]. The average fiber content of #6 GFRP bars from Southview Bridge decreased by 9.8% when compared to the result of control samples prior to the construction of Sierrita de la Cruz Bridge. However, these two types GFRP bars were from a different production lot. This can result in different results for this test, as mentioned before. For the #5 and #6 GFRP bars from Sierrita de la Cruz Bridge, the measured fiber contents in this study were in close agreement with the control samples and in-service samples of UM [123]. The fiber contents of all types of samples in this research were still well above the minimum fiber content requirement of 70% by mass based on AC 454 [126]. The change of the measured fiber contents of #6 GFRP bars from Sierrita de la Cruz Bridge is negligible compared to the results of the original samples, which means that no loss in fiber content was observed after 15 years of real-time weather exposure.

5.4.3.3 Transition glass temperature (T_g). The glass transition temperature (T_g), an important physical characteristic of the matrix, is not only a sign of the thermal stability of the material but also an important indicator of the structure of the polymer and its mechanical performance [47]. The ideal temperature for heat treatment application depends on the thermal behavior of each composite, such as T_g analysis and initial degradation temperature [127]. The T_g, therefore, can successfully be used as a reference to sign the ideal heat treatment for photo-irradiated resin compositions. According to ASTM E1640-13 [128], differential scanning calorimetry (DSC) was used to evaluate the T_g of the resins of the GFRP bars. TA instrument was utilized to perform the T_g measurement, as illustrated in Figure 5.51.

Figure 5.51. TA instrument for T_g measurement

Some small samples were obtained from #2, #5, and #6 GFRP bars that were extracted from these three bridges, to evaluate the thermal behavior of epoxy. They were heated to 392°F (200°C). Moisture in the matrix can reduce T_g of the resin through plastification if the Van der Waals bond between the polymer chains is broken. The swelling stresses are able to result in permanent damage in the epoxy of GFRP bar such as matrix cracking, hydrolysis, and fiber-matrix debonding when the composite material uptakes moisture or alkalis present [47]. Table 5.9 exhibits the test results for these three bridges and the results from the report of UM [123].

Table 5.9. Test results of T_g measurement

Diameter (in.)	Bridge		No. of samples	Ave. (°F) MST	Ave. (°F) control	Ave. (°F) UM
0.25	Walker Bridge	NC	3	183.3	N/A	177.8 [125]
		C	3	186.0	N/A	
0.75	Southview Bridge		6	176.6	N/A	N/A
0.625	Sierrita de la Cruz Bridge		3	187.4	N/A	N/A
0.75			6	187.2	177.9	238.8 [123]
Conversion units: 1 in. = 25.4 mm, °F = 1.8 °C +32						

Note: "NC" represents concrete core without crack, "C" means concrete core with crack.

Due to lack of T_g test results on GFRP samples prior to construction of these three bridges, there are no identical production lot references to compare to the results of Walker Bridge and Southview Bridge. However, T_g measurement of control specimens produced in 2015 that was reported by UM [123] may be considered a reference. It can be seen in Table 5.9 that there is no significant difference between the results of this study and the value from the control GFRP bars [123]. In addition, no substantial difference is observed between the results of this study and the value reported by UM for the samples from Walker Bridge [125]. The GFRP bars in this research and control specimens were from different production lots, resulting in the changes in glass fiber, resin formation, and catalysts of the GFRP bars. The test result of the control GFRP bars does not exactly characterize the initial GFRP samples that were employed in Southview Bridge, Walker Bridge, and Sierrita de la Cruz Bridge. The result of control specimens may be served as a quantitative comparison.

5.4.3.4 Scanning Electron Microscopy (SEM). SEM was utilized to visually evaluate the influence of exposure at a high magnification on the constituent materials of the GFRP bars. Helios NanoLab 600 was used to perform this analysis, as shown Figure 3.37. Two samples from Southview Bridge, three specimens from Walker Bridge (one was from the core with crack, two were from the core without crack), and two GFRP slices from Sierrita de la Cruz Bridge were prepared. They were scanned at different levels of magnification and images were taken at random locations. More attention was focused on the areas in the vicinity of the analyzed GFRP bars and individual glass fibers in the epoxy because possible deterioration due to alkaline attack could start at GFRP-

concrete interface, and the alkaline attack can destroy the integrity of individual glass fibers. Representative SEM micrographs of the GFRP samples from these three bridges are exhibited in Figures 5.52 through 5.59. The other images are available in Appendix C.

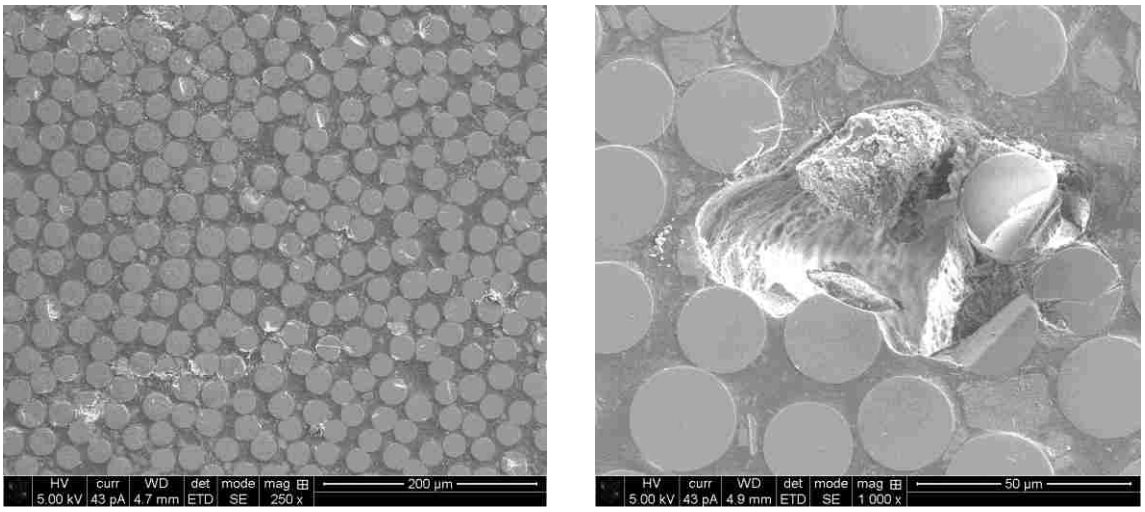

Figure 5.52. SEM images of the fibers and void at magnification levels of 250x (left) and 1000x (right) (Southview Bridge)

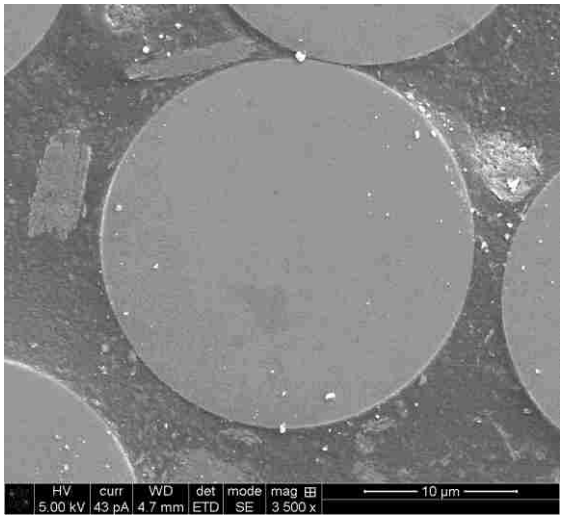

Figure 5.53. SEM image of an individual glass fiber at magnification 3500x (Southview Bridge)

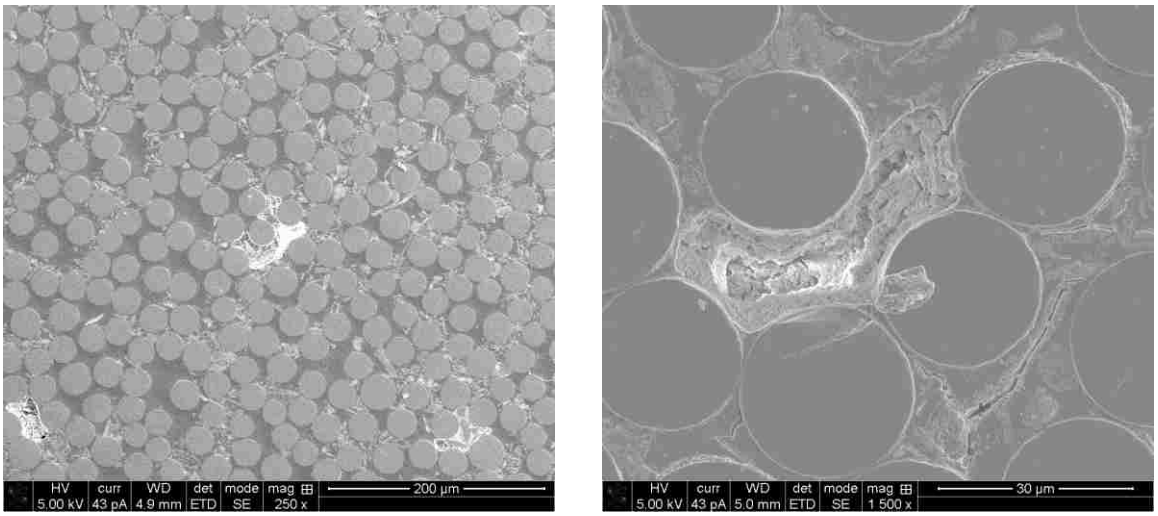

Figure 5.54. SEM images of the fibers at magnification levels of 250x (left) and 1500x (right) (C-1 B-3 of Walker Bridge)

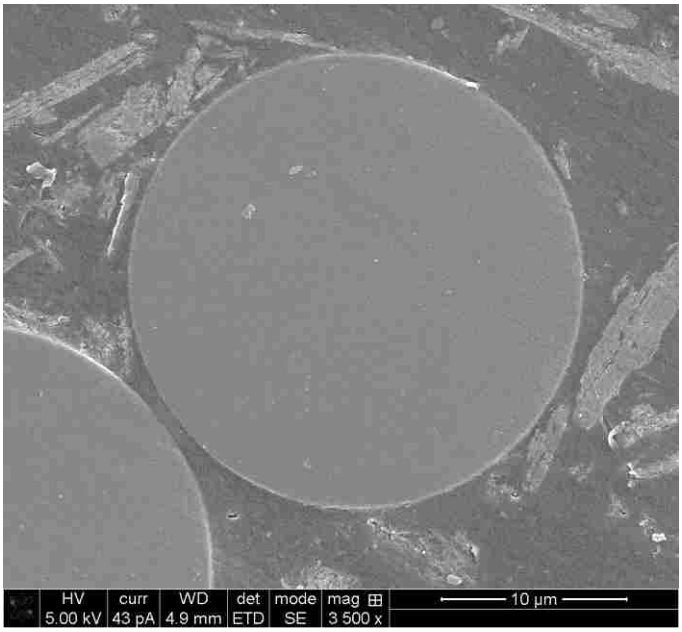

Figure 5.55. SEM image of an individual glass fiber at magnification 3500x (C-1 B-3 of Walker Bridge)

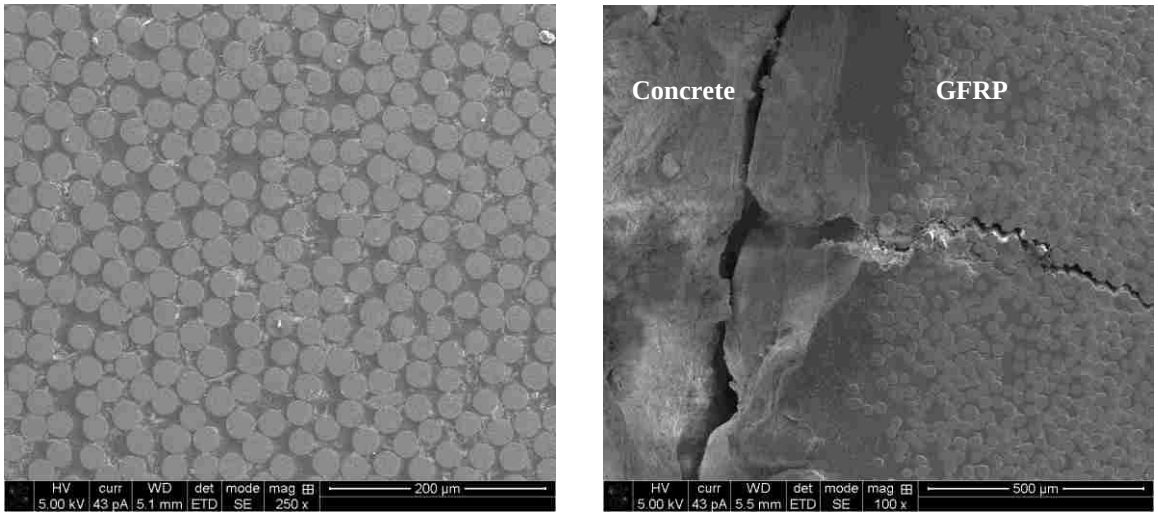

Figure 5.56. SEM images of the fibers and GFRP-concrete interface at magnification levels of 250x (left) and 100x (right) (C-2 B-3 of Walker Bridge)

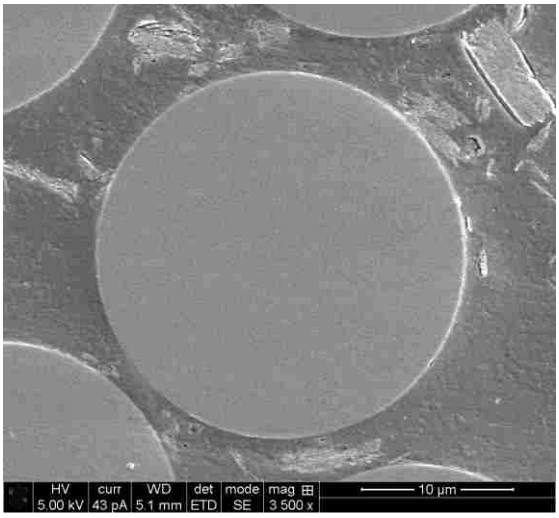

Figure 5.57. SEM image of an individual glass fiber at magnification 3500x (C-2 B-3 of Walker Bridge)

There was no sign of deterioration in the GFRP bars extracted from the Southview Bridge and the Sierrita de la Cruz Bridge. None of the glass fibers lost any cross-sectional area in these two structures. There was no degradation of the fibers observed and glass fibers were intact without any gap between the fibers and the

surrounding resin matrix, indicating no loss of bond between glass fibers and resin. From Figure 5.56, there was a gap between the concrete and the GFRP bar. The sample preparation before the SEM and drying the sample in the SEM chamber may result in the interfacial damage of GFRP-concrete bond [47].

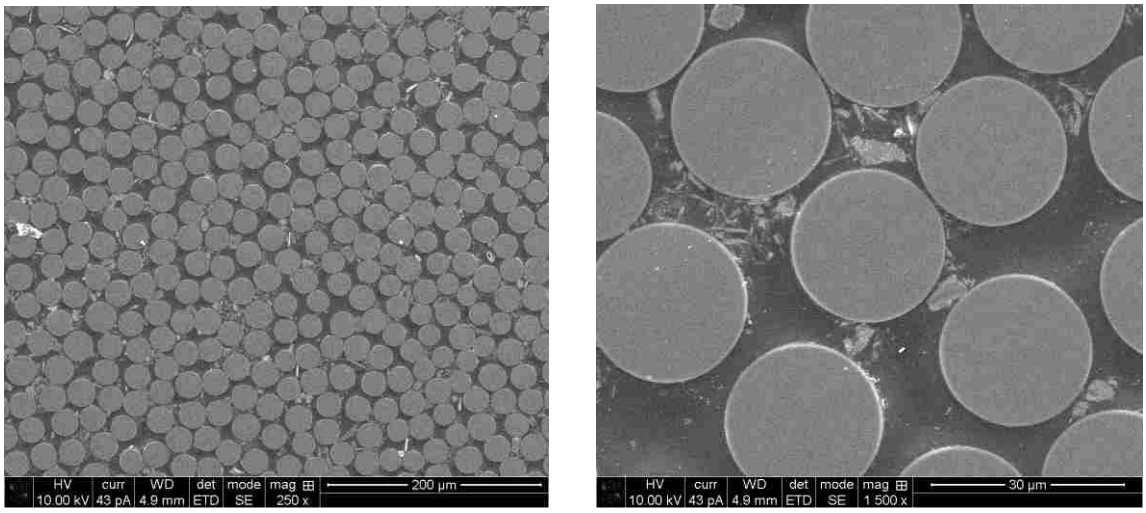

Figure 5.58. SEM images of the fibers at magnification levels of 250x (left) and 1500x (right) (Sierrita de la Cruz Bridge)

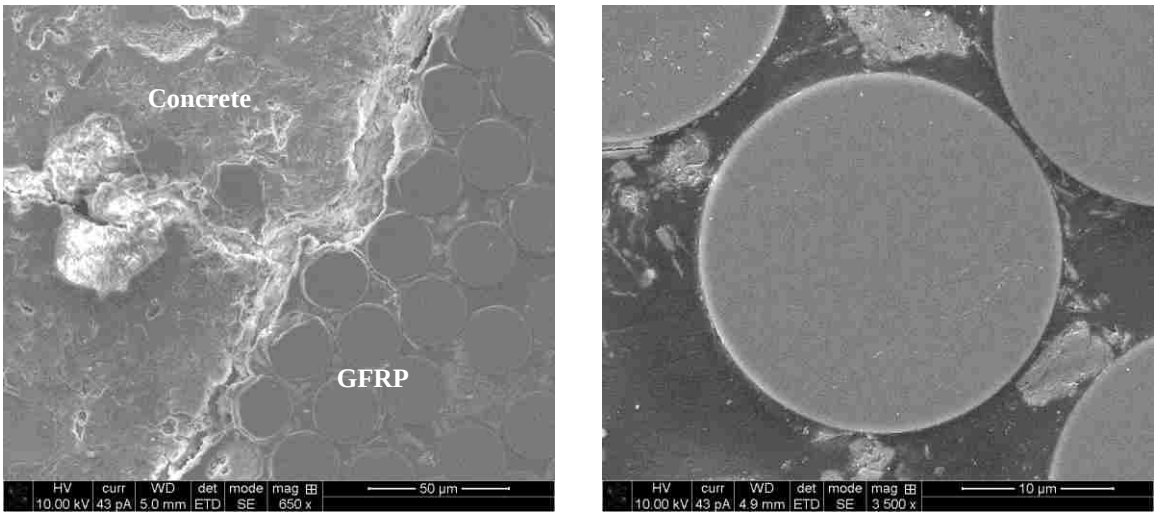

Figure 5.59. SEM images of the GFRP-concrete interface and single glass fiber at magnification levels of 650x (left) and 3500x (right) (Sierrita de la Cruz Bridge)

It should be noted that there were some cracks exhibited in Figures 5.54 and 5.56 on the surfaces of GFRP bars extracted from Walker Bridge. The concrete cylinders were extracted from the bottom of box culvert. Water often runs through the boxes of this bridge, causing the FRP bars to be influenced by water. On the other hand, no evidence of deterioration on the glass fibers was observed. Individual fiber still maintained integrity. Therefore, it should be concluded that the resin matrix may be aged after 18 years of field exposure because the bottom of the box culverts that were repeatedly submerged in river water deteriorated.

5.4.3.5 Energy Dispersive X-Ray Spectroscopy (EDS). This technique was used in association with SEM and its purpose was to categorize the existing chemical elements in the material. Helios NanoLab 600 was utilized to conduct this analysis, as illustrated in Figure 3.37. A 10 to 20 keV electron beam was directed at the surface of a GFRP bar. Two samples from Southview Bridge, three specimens from Walker Bridge (one was from the core with crack, two were from the core without crack), and two GFRP slices from Sierrita de la Cruz Bridge were prepared to perform this analysis. The representative results of these three bridges are illustrated in Figures 5.60 through 5.62. The Y-axis presents the counts (number of X-rays received and processed by the detector) and the X-axis shows the energy level of those counts. The other EDS results are available in Appendix C.

Principal chemical elements such as Si, Al, Ca (from the glass fibers), and C (from the resin matrix) were observed in the extracted GFRP samples. The results in this study are almost identical as the findings in the UM report [123, 125]. In addition, the presence of Na in these specimens should not be a sign of alkaline attack because it was also found in the control samples from the report of UM. The cause may be the contamination when preparing the specimens.

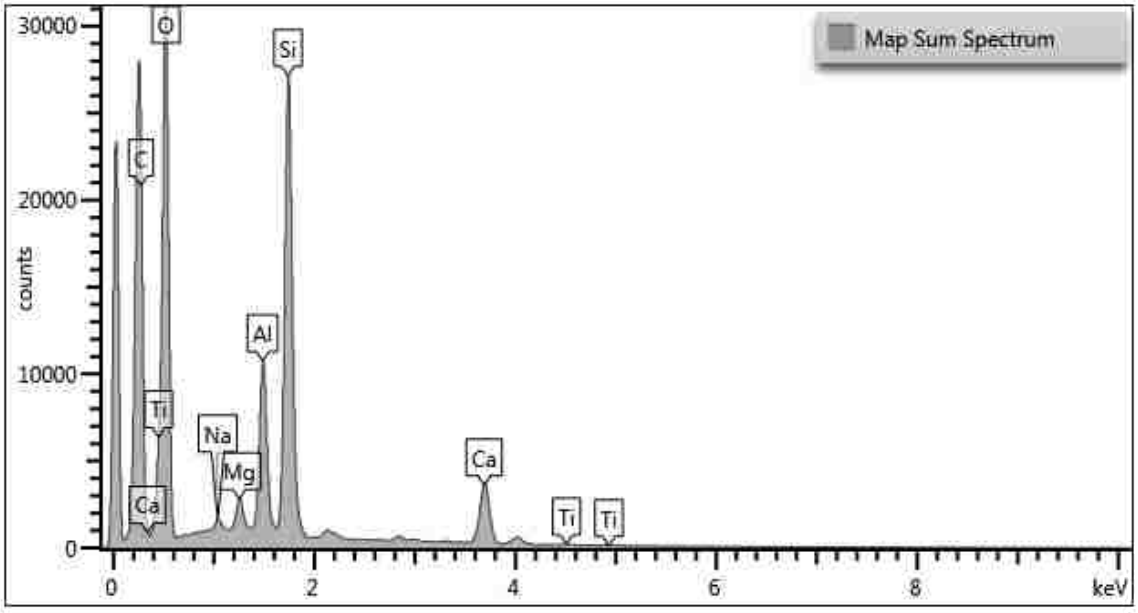

Figure 5.60. Results of the EDS analysis conducted on Sample 1 from Southview Bridge

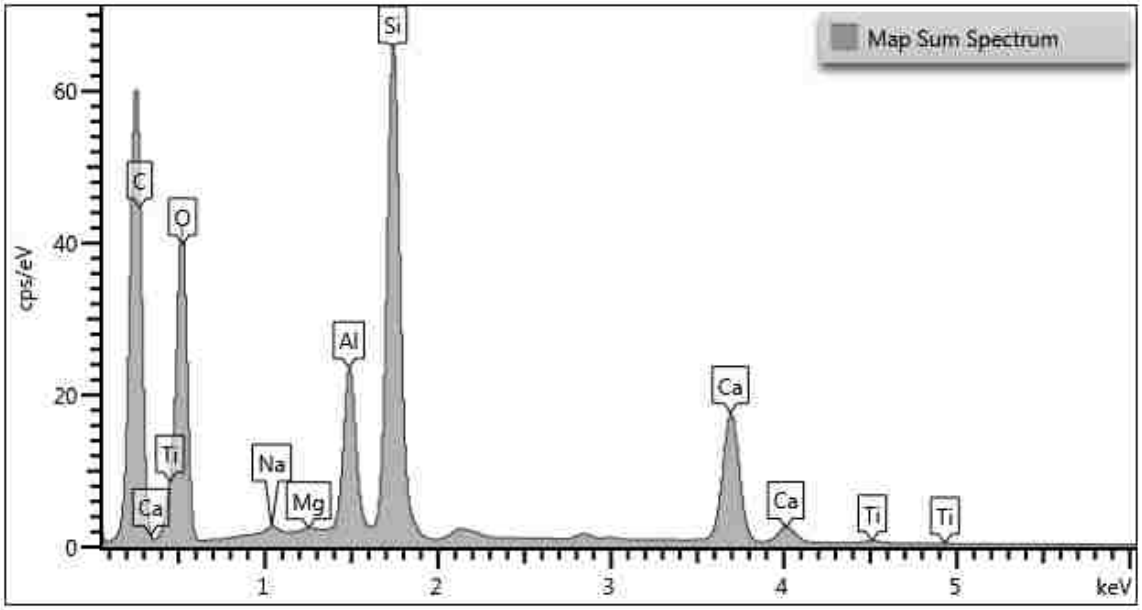

Figure 5.61. Results of the EDS analysis conducted on Sample 1 from Walker Bridge

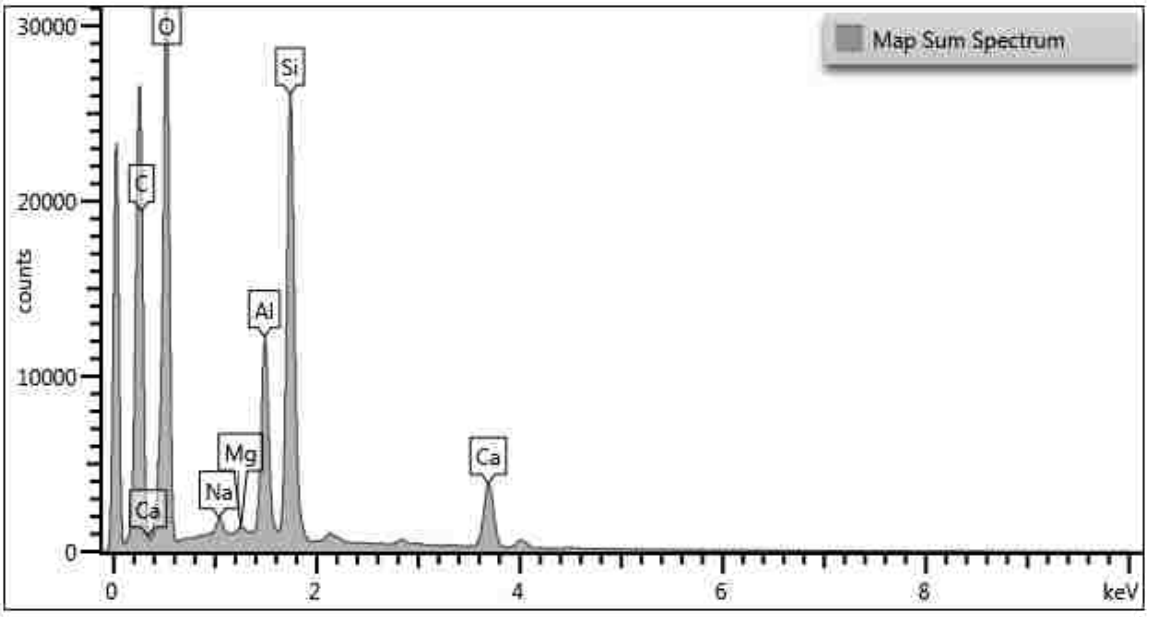

Figure 5.62. Results of the EDS analysis conducted on Sample 1 from Sierrita de la Cruz Bridge

Backscattered electron images of some GFRP specimens are provided at different magnification levels to show compositional contrast of existing elements and their distribution in fibers and resin matrix. The representative images of the GFRP samples that were extracted from these three bridges are exhibited in Figures 5.63, 5.64, and 5.65.

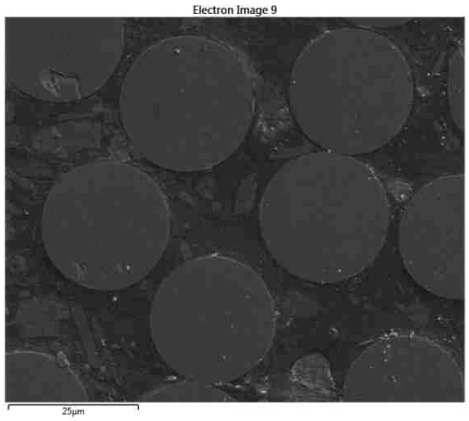

Conversion Units: 1 µm = 3.94 x 10^{-5} in.

Figure 5.63. Elemental scatter in sample 1 extracted from Southview Bridge

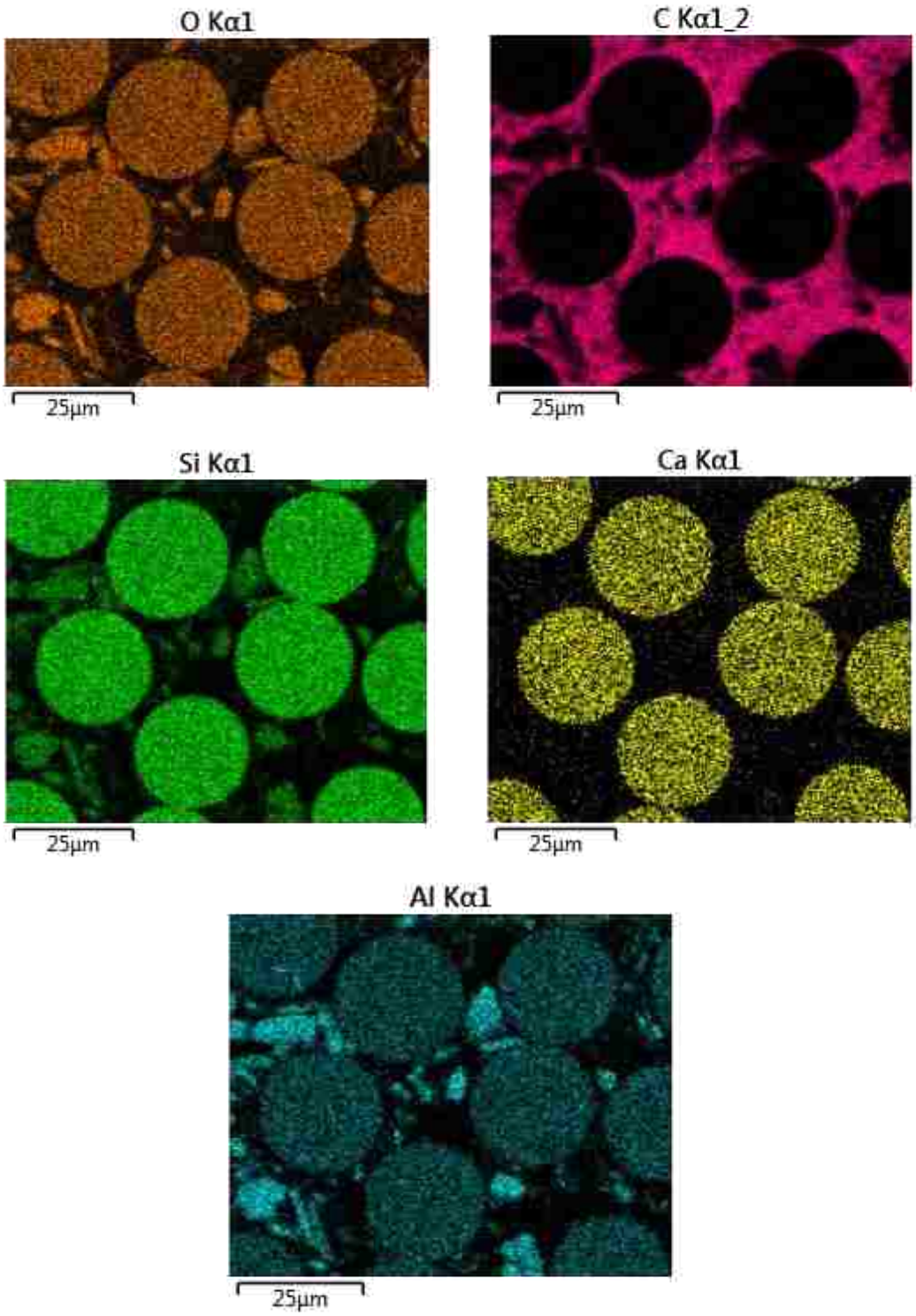

Conversion unit: 1 µm = 3.94 x 10^{-5} in.

Figure 5.63. Elemental scatter in sample 1 extracted from Southview Bridge (Cont.)

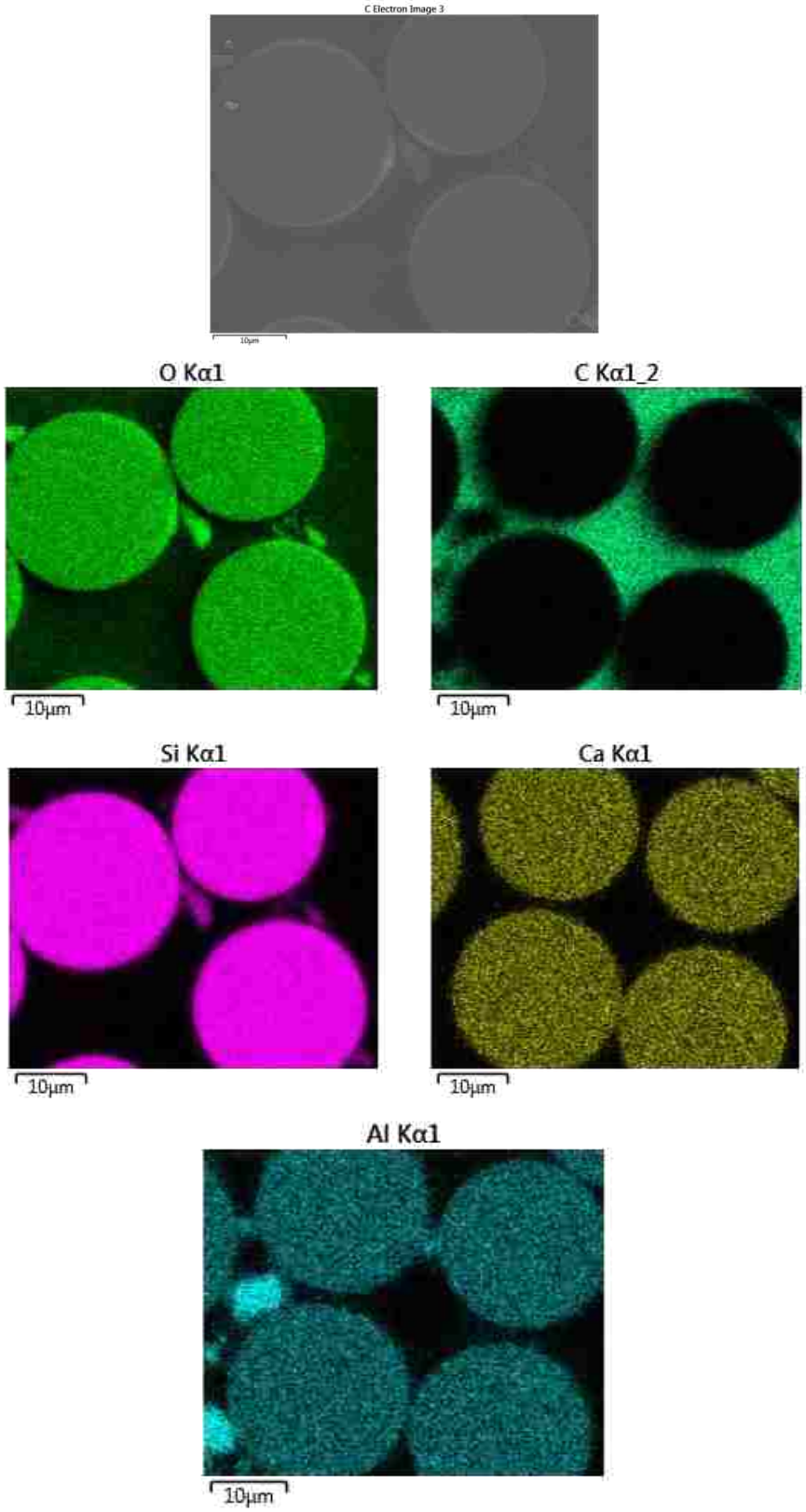

Conversion Units: 1 µm = 3.94 x 10^{-5} in.

Figure 5.64. Elemental scatter in sample 1 extracted from Walker Bridge

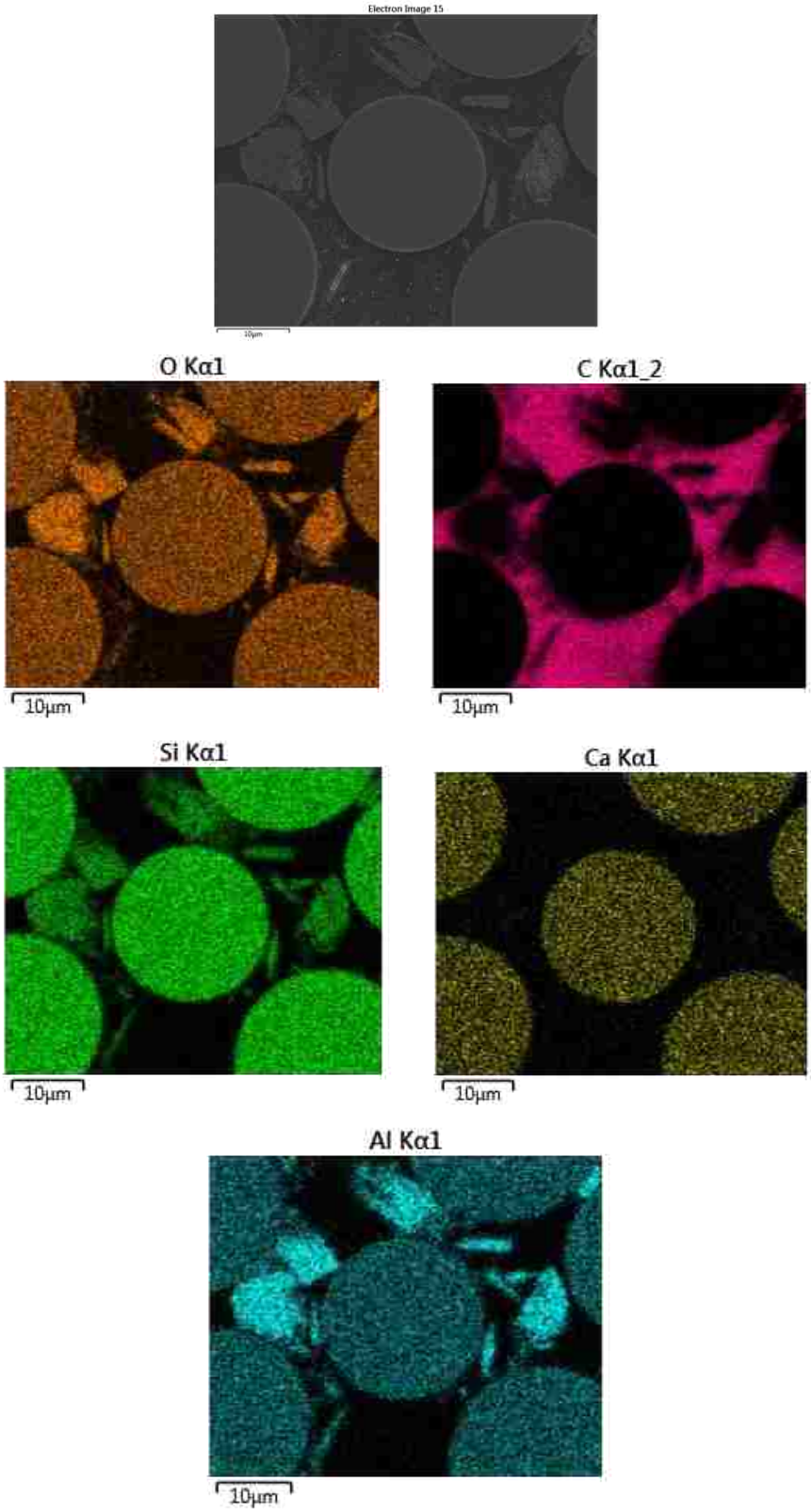

Conversion Units: 1 µm = 3.94 x 10^{-5} in.

Figure 5.65. Elemental scatter in sample 2 extracted from Sierrita de la Cruz Bridge

There was no change in chemical composition of fiber and resin matrix when comparing the results of the extracted samples in this study and the findings of the in-service and control specimens from the report of UM [123]. The silica from glass fibers was not dissolved in the alkaline environment of concrete after several years of service.

5.4.3.6 Fourier Transform Infrared (FTIR) spectroscopy. All resins contain ester bonds that are susceptive to various processes because they are the weakest link of the polymer. A deterioration mechanism of the resin may be the alkali hydrolysis of the ester linkages. It is well known that concrete is an alkaline environment. Therefore, this alkali hydrolysis is expected to some extent. When the hydrolysis reaction occurs, free hydroxyl ions (OH-) induce ester linkage attack and the resin chain is destroyed. Subsequently, the structure of the matrix is disrupted, resulting in the change of the material performance. Finally, if the resin deteriorates, it will not transfer stresses to the glass fibers or protect the fibers against alkaline attack. Changes in the amount of hydroxyl groups that were present in the GFRP bars provide insight into the hydrolysis reaction. Because the EDS cannot detect the elements in the GFRP samples lighter than sodium (Na), the OH- cannot be found. Consequently, FTIR analysis was performed to investigate the OH- in the samples.

The FTIR spectrometer uses an interferometer to modulate the wavelength from a broadband infrared source. A detector measures the intensity of transmitted or reflected light as a function of its wavelength. The signal obtained from the detector is an interferogram, which must be analyzed with a computer using Fourier transforms to obtain a single-beam infrared spectrum. The FTIR spectra are usually presented as plots of intensity versus wavenumber (in cm^{-1}). Wavenumber is the reciprocal of the wavelength.

In this study, NEXUS 670 (see Figure 5.66) was used to conduct this test. The samples that were used to perform the EDS analysis were also used to conduct this analysis. The wavenumber of hydroxyl groups in the GFRP samples was 3700 cm^{-1} in the FTIR spectra.

Figure 5.66. NEXUS 670 FT-1 R

Three various locations in each GFRP sample were measured. Representative results of the FTIR analysis for the in-service GFRP samples from Southview Bridge are illustrated in Figure 5.67. The other results of Walker Bridge and Sierrita de la Cruz Bridge are available in Appendix C.

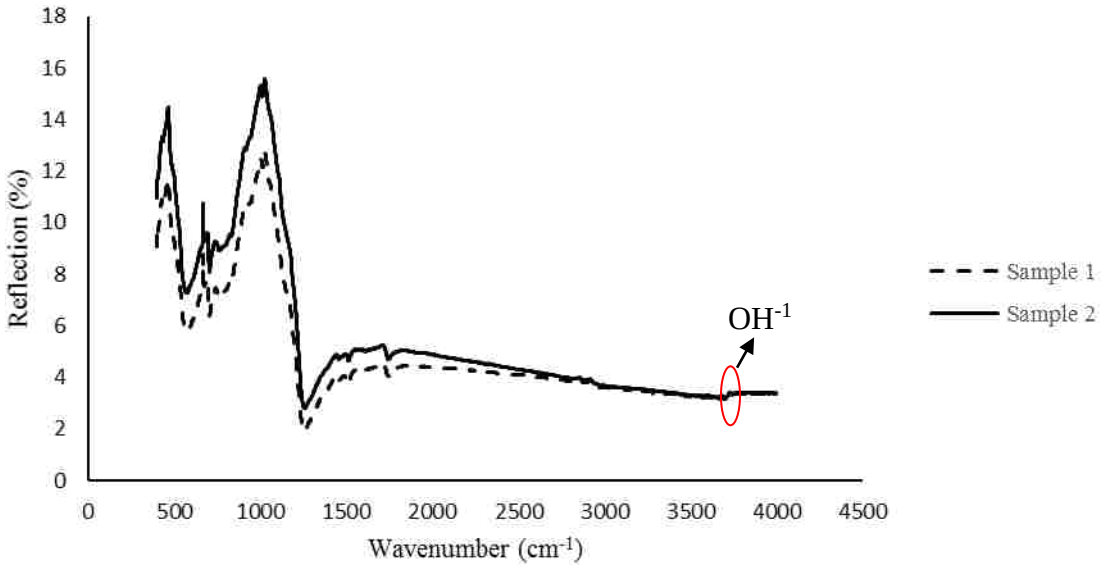

Conversion Units: 1 in. = 2.54 cm

Figure 5.67. FTIR spectra for GFRP samples in Southview Bridge

It can be seen in Figure 5.67 that there were hydroxyl groups in GFRP samples from Southview Bridge. It shows that there was no difference in the spectra of the two samples. Similar conclusions were drawn for the GFRP samples from other bridges. However, due to no control specimens tested in this time, it cannot be concluded that OH^{-1} was from the hydrolysis reaction. Therefore, FTIR analysis of control samples and comparison of the in-service and control specimens will be recommended as future work. Future cores can also be compared to results obtained herein.

5.4.4. The Test Results of Concrete and Discussions. This section includes pH measurements using two different approaches and chloride content.

5.4.4.1 pH measurements. The pH value of fresh concrete is roughly 13. The value at exposed surface will fall due to the reaction of carbon dioxide from the atmosphere and alkalis in the concrete. The process is known as carbonation. Depth of carbonated concrete will continue to develop over time. Because the carbonated concrete can allow corrosion of reinforcing bars, it may be important to determine the depth of carbonated concrete. The pH measurement was conducted primarily to provide a qualitative concrete pH value.

In this study, ASTM F710 (Section 5.2.1) [129] was used to perform this test. For this approach, concrete surface was ground by using sand paper, and concrete powder and particles were removed. Several distilled water drops were placed on the clean surface of concrete to form a puddle with roughly 1 in. (25.4 mm) diameter, and then the pH paper was dipped into the water. The results of this study were compared to the chart to determine the pH value.

The pH measurement method proposed by Grubb et al. [130] was also employed to conduct this test. For this method, some concrete powder samples were collected from the concrete surface. The powder was diluted in distilled water with 1:1 by weight. Then, this mixture was stirred uniformly, and pH paper was used to evaluate the pH value. These two approaches were compared to find a more precise method. In each of these three bridges, the pH measurements were evaluated in three different locations of concrete cylinder and consistent pH values were attained. Figures 5.68 through 5.72 illustrate some typical pH measurements of concrete for each bridge. The additional pH measurements are available in Appendix C.

Figure 5.68. pH measurement of sample 1 (Southview Bridge): ASTM F710 (left) and Grubb's method (right)

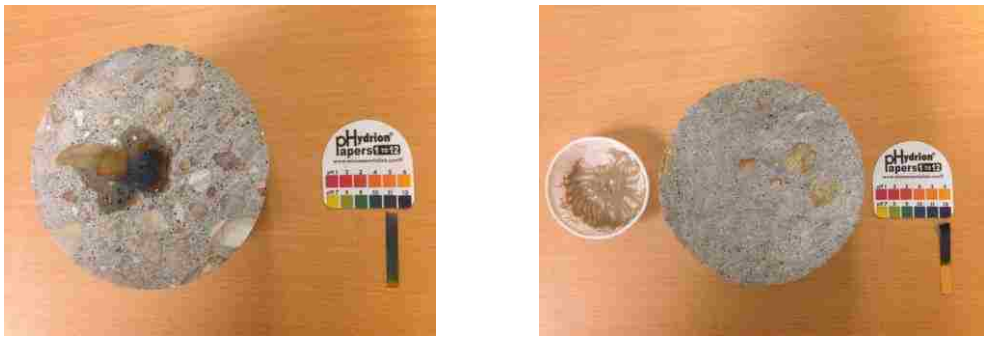

Figure 5.69. pH measurement of sample 2 (Southview Bridge): ASTM F710 (left) and Grubb's method (right)

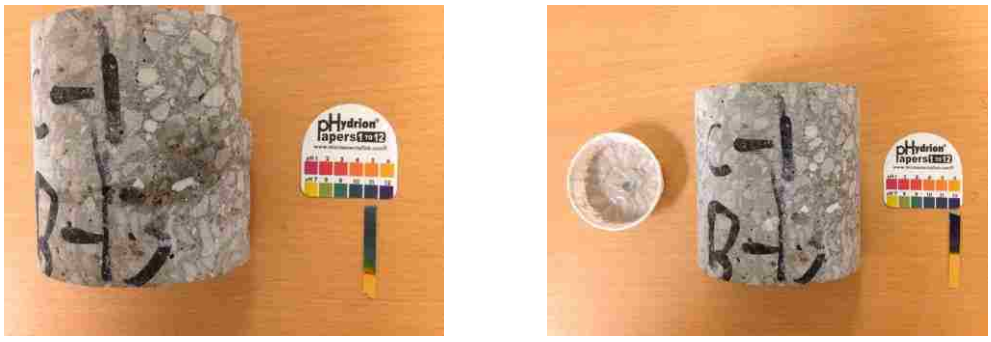

Figure 5.70. pH measurement of sample 1 (Walker Bridge): ASTM F710 (left) and Grubb's method (right)

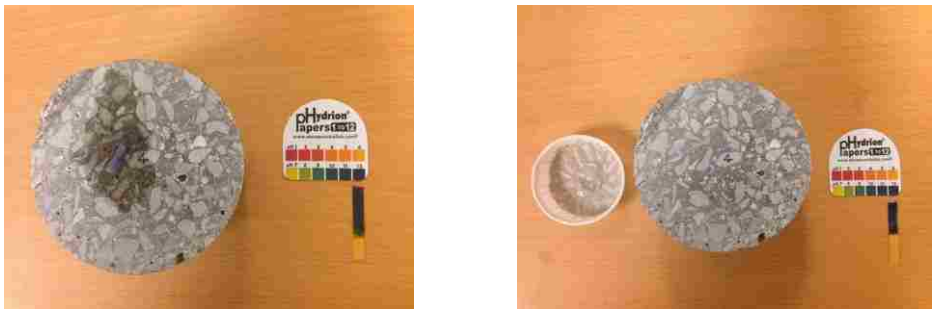

Figure 5.71. pH measurement of sample 2 (Walker Bridge): ASTM F710 (left) and Grubb's method (right)

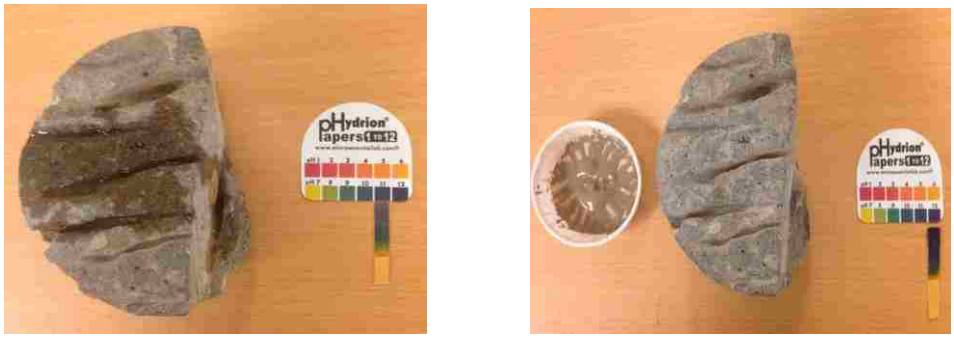

Figure 5.72. pH measurement (Sierrita de la Cruz Bridge): ASTM F710 (left) and Grubb's method (right)

It can be seen in Figures 5.68 through 5.72 that the pH values of concrete extracted from the three bridges were between 11 to 12 among all methods. The results of the concrete extracted from Walker Bridge and Sierrita de la Cruz Bridge were the same as those reported by UM. These results are also in agreement with expected values reported by Grubb [130]. It should be noted that using the approach recommended by Grubb and the coworkers should be more accurate than that of ASTM F710 (Section 5.2.1) since consistent results were attained by using this method in this study, as shown in Figures 5.68 through 5.71. Consequently, the approach suggested by Grubb et al. should be recommended, and it should be a more accurate method to determine the pH value of concrete. However, the procedure was simpler and faster to perform pH measurement when following ASTM F710 (Section 5.2.1).

5.4.4.2 Chloride content. There is a passive layer that forms on reinforcement in concrete environment due to the high pH value of concrete. Chloride ions that are commonly from deicing salts penetrate into concrete structure and ultimately destroy the passive layer of reinforcing bars, which influences the durability of the reinforcement in concrete. Therefore, chloride ions may be a significant factor affecting the durability of GFRP bars. There are two standards that can be followed to evaluate the content of chloride in concrete. This first standard is ASTM C1202 [131]. However, it does not subject the concrete to realistic conditions. It is only appropriate for research and development. Some studies have indicated that this standard overestimates chloride content of concrete in the field, especially the concrete made with supplementary cementitious materials such as fly ash, slag, and silica fume, etc. [132]. In order to correctly estimate a concrete's ability to resist chloride penetration in this study, ASTM C1543-10 [133] was adopted to perform this test.

There are two types of chloride analyses: acid-soluble and water-soluble. Acid-soluble analysis determines the total chloride content, including those chlorides trapped in the aggregate and paste. This should not be the actual chlorides that destroy the passive layer of the concrete. In contrast to this, water-soluble analysis only measures those chlorides free to deteriorate the passive layer of concrete [134]. Therefore, this technique was adopted to measure the chloride content in this study.

Some concrete powders from four cylinders extracted from these three bridges were collected. The samples had to weigh at least 0.053 oz. (1.5 g) to be considered appropriate. The powders were collected from four concrete cylinders that were extracted from these three bridges using a 3/8 in. (9.5 mm) drill bit. The test was conducted by using the Rapid Chloride Testing (RCT) equipment made by Germann Instruments, Inc. The 0.053 oz. (1.5 g) powder was poured into a vial that contains 0.304 fl oz. (9 mL) of the extraction liquid, and the vial was shaken for 5 minutes. The four powder slurries were maintained in room temperature environment for roughly 24 hours. The electrode was wetted by using the wet agent. In order to calibrate the electrode and develop a scale to determine the chloride content of the concrete powder, four calibration solutions that have known chloride content were used. The four calibration solutions contained 0.005%, 0.05%, 0.1%, and 0.3% chloride content. The electrode was inserted into every solution

and the voltage was measured. The voltages of the four solutions were approximately 100.5 mV, 49.7 mV, 31.6 mV, and 4.8 mV. These values were employed and then plotted on a chart in order to develop a curve for the rest of the testing. The electrode was ready to measure the voltages of these four slurries after the preparation and calibration. The electrode was inserted into the slurry and held steady until no change of the voltage reading. The voltages of these four slurries were recorded. The electrode should be cleaned by using distilled water after every use. This data recorded from different slurries was adopted to develop a chloride profile and determine chloride content of the concrete extracted from different bridges. The test results are illustrated in Table 5.10.

Table 5.10. The results of chloride contents for different bridges

Bridge		Voltage (mV)	Chloride content (%)
Walker Bridge	NC	69.8	0.0056
	C	97	0.0200
Southview Bridge		91.4	0.0076
Sierrita de la Cruz Bridge		66.1	0.0230

According to Broomfield's study [135], the risk of deterioration in concrete can be determined by the amount of chloride present in concrete. Table 5.11 exhibits the scale that Broomfield reported.

Table 5.11. Correlation between percent chloride by mass of concrete and deterioration risk [135]

% Chloride by mass of concrete	Deterioration risk
< 0.03	Negligible
0.03-0.06	Low
0.06-0.14	Moderate
> 0.14	High

It can be seen in Tables 5.10 and 5.11 that the chloride contents of concrete extracted from these three bridges is less than 0.03. Chloride ions in concrete may not destroy the passive layer on the GFRP bars. It can be concluded that chloride should not be a factor to deteriorate the durability of GFRP bars extracted from Southview Bridge, Walker Bridge, and Sierrita de la Cruz Bridge.

5.5. SUMMARY AND CONCLUSIONS

This is section focuses on the field inspections of Southview Bridge and Walker Bridge, and the physical, chemical, and microstructural properties of GFRP and concrete samples extracted the bridges.

5.5.1. Investigation for Southview Bridge. This bridge consists of three decks including the existing deck reinforced with steel, the deck reinforced with FRP bars, and the additional deck reinforced with steel. The majority of cracks were illustrated on the existing reinforced concrete deck. The maximum crack width was 0.1875 in. (4.76 mm). There is some mineral efflorescence on the surface of the bottom of decks.

5.5.2. Investigation for Walker Bridge. This bridge consists of 18 boxes reinforced with #2 GFRP bars. They were arranged in two rows of nine. Boxes 6, 8, 9, 17, and 18 did not illustrate any cracks. Cracks were observed only on the top for Box 1, 7, 10, and 11. The other boxes displayed only one crack on the top and another on the bottom. The maximum crack width was 0.0625 in. (1.60 mm).

5.5.3. Evaluation of Performance of GFRP Bars in Concrete. According to the results of the experimental tests performed on GFRP samples concrete and extracted from these three bridges, the following conclusions can be drawn:

1) For SBS test, the maximum load of #5 GFRP bar from Sierrita de la Cruz Bridge decreased by 4.2% and 8.3% when compared to the results of control samples and the specimen of UM, respectively. #6 GFRP specimen that was collected from Sierrita de la Cruz Bridge exhibited failure load decreases of 29.7% and 7.6% compared to the values of control samples and the specimen of UM, respectively. In addition, the failure load of #6 GFRP from Southview Bridge decreased by 18.0% compared to the result of the in-service specimen from Sierrita de la Cruz Bridge. For #2 GFRP bars from Walker Bridge, no difference of the failure loads

was observed between the bars that were extracted from the cores without crack and with crack.

2) Due to lack of the initial test results of fiber content prior to construction of Walker Bridge and Southview Bridge, there were not any identical manufactured lot bars for references to compare directly the results of #2 and #6 GFRP bars from Walker Bridge and Southview Bridge, respectively. The average fiber content of #6 GFRP bars from Southview decreased by 9.8% when compare to the result of control samples prior to the construction of Sierrita de la Cruz Bridge. However, these two types GFRP bars were from different production lots. This can result in different results for this test, as mentioned before. For the #5 and #6 GFRP bars from Sierrita de la Cruz Bridge, the measured fiber contents in this study were in close agreement with the control samples and in-service samples of UM.
3) Due to lack of T_g test results on GFRP samples prior to construction of these three bridges, there are no identical manufactured lot bars for references to compare to the results of Walker Bridge and Southview Bridge. However, T_g measurement of control specimens produced in 2015 that was reported by UM [123] may be considered as a reference. There is no significant difference between the results of this study and the value from the control GFRP bars.
4) For SEM analysis, in each of Southview Bridge and Sierrita de la Cruz Bridge, there was no sign of any deterioration in the GFRP bars extracted from these two bridges. None of the glass fibers lost any cross-sectional area in each of these two structures. There was no degradation of the fibers observed. And glass fibers were intact without any gap between the fibers and the surrounding resin matrix indicating no loss of bond between glass fibers and resin. It should be noted that there were some cracks on the surfaces of GFRP bars extracted from Walker Bridge. The concrete cylinders were extracted from the bottom of box culvert. Water often runs through the boxes of this bridge, causing the FRP bars to be influenced by water. On the other hand, no evidence of deterioration on the glass fibers was observed. Individual fiber still maintained integrity. Therefore, it should be concluded that the resin matrix may be aged after 18 years of field

exposure because the bottom of the box culverts that were repeatedly submerged in river water deteriorated.

5) For EDS analysis, the principal chemical elements including Si, Al, Ca (from the glass fibers), and C (from the resin matrix) were observed in the extracted GFRP samples. According to the report from UM, these results in this study are almost the same as their findings. In addition, the presence of Na in these specimens should not be a sign of alkaline attack because it was also found in the control samples from the report of UM. For FTIR analysis, there was no difference in the spectra between two GFRP samples that were extracted from the same bridge. However, due to no control specimens tested in this time, it cannot be concluded that OH^{-1} was from the hydrolysis reaction.
6) pH values of concretes that were extracted from the three bridges were between 11 to 12 whichever method was employed. The results of the concrete extracted from Sierrita de la Cruz Bridge were the same as those of the report from UM [123]. These results are also in agreement with expected values that Grubb reported [130]. It should be noted that using the approach recommended by Grubb and the coworkers should be more accurate than that of ASTM F710 (Section 5.2.1) since consistent results were attained by using this method in this study.
7) The chloride contents of concrete extracted from these three bridges less than 0.03 based on Broomfield's study. Chloride ions in concrete may not destroy the passive layer on the GFRP bars. It can be concluded that chloride should not be a factor to deteriorate the durability of GFRP bars extracted from Southview Bridge, Walker Bridge, and Sierrita de la Cruz Bridge.

6. CONCLUSIONS AND FUTURE RECOMMENDATION

6.1. CONCLUSIONS

In this research, three tasks were studied. The first task is long-term durability of concrete panels reinforced with steel and glass reinforced polymer (GFRP). The second one is a comprehensive durability study related to concrete elements reinforced with Steel Reinforced Polymer (SRP). The last one is assessment of existing FRP bridge structures exposed to field conditioning. According to this study, the following conclusions for each topic were obtained.

6.1.1. The First Topic. Axial restraining forced induced by the restrained shrinkage and temperature changes of these GFRP-reinforced panels caused the highest level of tensile stress at the fixed-fixed supports. This was the first multi-year true long-term GFRP RC study related to secondary reinforcement studies conducted in any available literature. The cracks occurred at or close to external supports or interior roller supports on the panels. The restrained shrinkage should be a major element that induced the cracking of panels.

According to Gilbert's analytical model, the numerical model of shrinkage cracking in fully restrained concrete members reinforced with FRP bars that were exposed to natural environment for seven years was established based on the modification of the coefficients of s_0 and s.

There was no sign to observe that glass fibers were damaged and resin matrix in GFRP rebars was deteriorated due to long-term exposure to alkaline concrete environment based on the observation of SEM images and DES analysis. There were some voids that were observed in GFRP samples, attributed to the deficiency due to the original process of manufacture other than the attack of alkaline in concrete environment.

It was concluded that current secondary reinforcement levels in the ACI 440.1R-06 standard may be appropriate for a timeframe of 1 or 2 years, but unconservative for much later ages such as 2400 days where high restraint levels exist. While physical damage to the bars did not occur, unsightly crack widths result and evidence of cracking in the transition zones between the GFRP bar and concrete.

6.1.2. The Second Topic. This study investigates environmental deterioration of SRP bonded to concrete. Ultimate flexural load capacity (three-point bending test) and direct tensile strength (pull-off test) reductions quantify the degradation due to accelerated aging exposure, and real-time weather and solar exposure.

6.1.2.1 Three-point bending test. Test results of the tests indicated that the externally bonded SRP strengthening systems illustrated durability performance that can be established by the experiments. The failure modes of all conditioned specimens were Failure Modes 2 and 3. When exposed to real-time weather and solar exposure, full immersion of tap water, hot water, and salt water for various periods, the concrete-covered substrate areas of the exposed specimens reduced significantly when compared to the counterparts of the control specimens.

For the deflections of RG and RNG specimens immersed in tap water and salted tap water, no apparent difference was observed, which means chloride ion should not be considered an issue to further deteriorate the bond performance SRP-to-concrete systems. Therefore, it can be concluded that water or moisture should be one of essential concerns to influence the bond durability between concrete and externally bonded SRP systems rather than deicing salt under the harsh environment. However, for RG and RNG specimens that were immersed in hot water at 122 ℉ (50 ℃), the losses of deflections were higher than those of the specimens that were submerged in tap water and salted tap water. Consequently, it should be determined that temperature is also a main issue to degrade the bond behavior of SRP-to-concrete systems.

Outdoor specimens exhibited higher loss of deflections and less concrete-covered substrate area, when compared to SRP beams exposed to EC even though they failed in Failure Mode 3. The possible description should be that more severe environmental conditions including UV radiation and more varying temperature and humidity further deteriorated the bond performance between SRP strengthening system and concrete substrate.

The significant strength loss of the outdoor specimens and the specimens exposed to full immersion was observed when compared to the control specimens. Therefore, the real-time weather exposure and water considerably influenced the bond durability of

SRP-to-concrete systems. There was no significant difference in ultimate strength between RG and RNG specimens.

A single environmental condition can not define the environmental reduction factor (C_E). For exterior exposure subjected to “wet environments”, while in “air environment” [25], an environmental reduction factor, C_E of 0.75 is suggested for the SRP strengthening system studied based on the results obtained. For an aggressive exposure environment, an environmental reduction factor, C_E, of 0.60 is suggested.

6.1.2.2 Direct pull-off test. The pull-off strength ratios of conditioned RG and RNG specimens exceeded 1.0. This was attributed to post-curing effect due to sufficient moisture or water. The conditioned specimens and control specimens showed a Failure Mode G. For the specimens exposed to outdoor, the failure modes of some samples were Mode G, the other samples were failed in Mode F. In addition, the results of this test exhibited a large degree of scatter and variation indicating the variability of this test method is less than ideal. Therefore, while a direct pull-off test might be considered a user friendly technology to evaluate the long-term bond performance of SRP-to-concrete systems in field, it may not be an effective avenue due to high testing variability and challenges to capture degradation at the physical interface between the repair system and concrete interface.

Different results were attained between the flexural bending and direct pull-off tensile tests. Through the results of this research and Deng’s conclusions on non-SPR repair systems, it can be suggested that flexural testing should be recommended because test results of the three-point loading tests can evaluate effectively the long-term bond performance of SRP-to-concrete systems under the real-time weather exposure and immersed environmental conditions. It also better represents the behavior of the actual flexural strengthening in the field. Moreover, a concrete strength of 6,000 psi (42 MPa) is suitable for ascertaining C_E under varying environmental conditions.

6.1.3. The Third Topic. This study includes two parts. Inspection of Southview and Walker bridges, and evaluation of performance of GFRP bars in concrete.

6.1.3.1 Investigation for Southview and Walker Bridges. For Southview Bridge, the majority of cracks were illustrated on the existing reinforced concrete deck. There was some mineral efflorescence on the surface of the bottom of decks. For Walker

Bridge, Boxes 6, 8, 9, 17, and 18 did not illustrate any cracks. Cracks were observed only on the top for Box 1, 7, 10, and 11. The other boxes displayed only one crack on the top and another on the bottom.

6.1.3.2 Evaluation of performance of GFRP bars in concrete. For GFRP specimens, SBS test, fiber content, T_g test, SEM analysis, DES analysis, and FTIR were performed. No indication of GFRP deterioration was observed. For concrete samples, pH values and chloride contents were measured. pH values of concretes that were extracted from the three bridges were between 11 to 12. The chloride contents of concrete extracted from these three bridges less than 0.03 based on Broomfield's study. Chloride ions in concrete may not destroy the passive layer on the GFRP bars. It can be concluded that these results did not show concrete degradation.

6.2. FUTURE RECOMMENDATIONS

This part focus on the future recommendations for the FRP bars extracted from concrete and the durability of concrete members reinforced with SRP.

6.2.1. The Durability Behavior of FRP Bar. The objective of this study was to investigate long-term performance of FRP bars in concrete structures exposed to aggressive environments. Since the conditions of this study were limited there are experimental testing that can be done to further build a larger data base of information. The following are recommendations for future research:

1. Perform more experimental testing of long-term restrained shrinkage cracking of FRP-reinforced concrete panels exposed to harsh environment.
2. Investigate the effects of shrinkage and creep on the crack patterns in the concrete panels reinforced with GFRP.
3. Develop theoretical formulas to estimate the cracking behavior of fully restrained concrete slabs.
4. Conduct more longitudinal tensile tests of control FRP specimens and FRP samples exposed to concrete environment.
5. Test more physical and chemical experiments of control and conditioned FRP specimens like SBS test, fiber contents, T_g measurement, FTIR analysis, etc. to increase the database and examine other bar manufacturers outside of the U.S.

6.2.2. The Durability Performance of Concrete Members Reinforced with SRP. The purpose of this study was to investigate the bond behavior ofconcrete members reinforced with SRP at different environmental conditionings to assemble database of current test results for ACI 440.9R-15. The following are recommendations for future research:

1. Perform more experimental tests of SRP concrete exposed to different environmental conditions with different time durations.
2. Develop a local bond-slip model and effective bond length of concrete members reinforced with SRP.
3. Analyze, with the help of a finite element software package, the bond behavior of concrete members reinforced with SRP at various environmental conditions.

APPENDIX A.

TOPIC 1

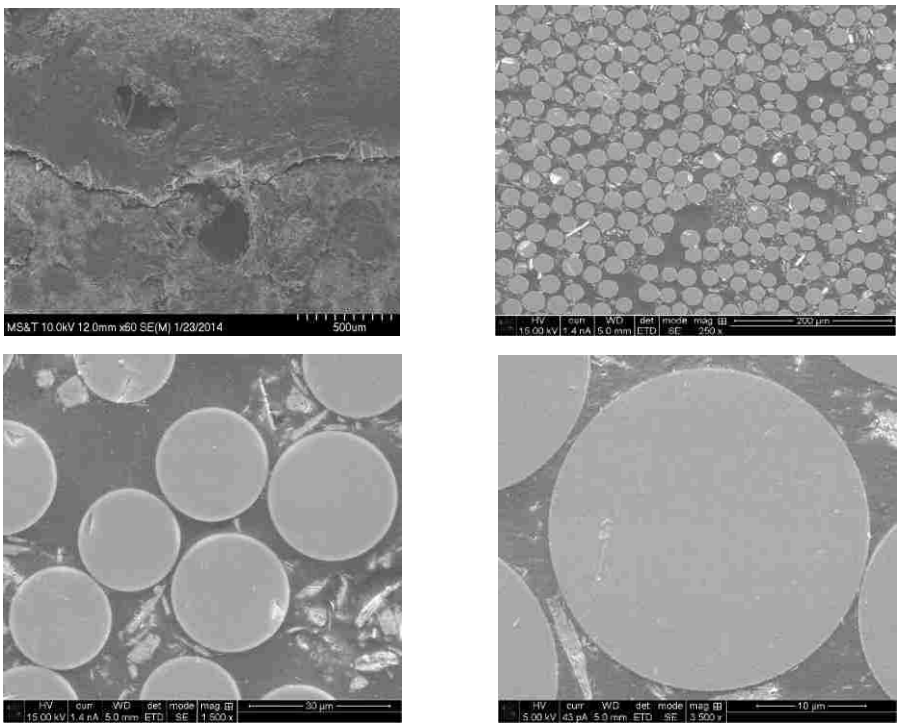

SEM images of panel P-3 at different solutions

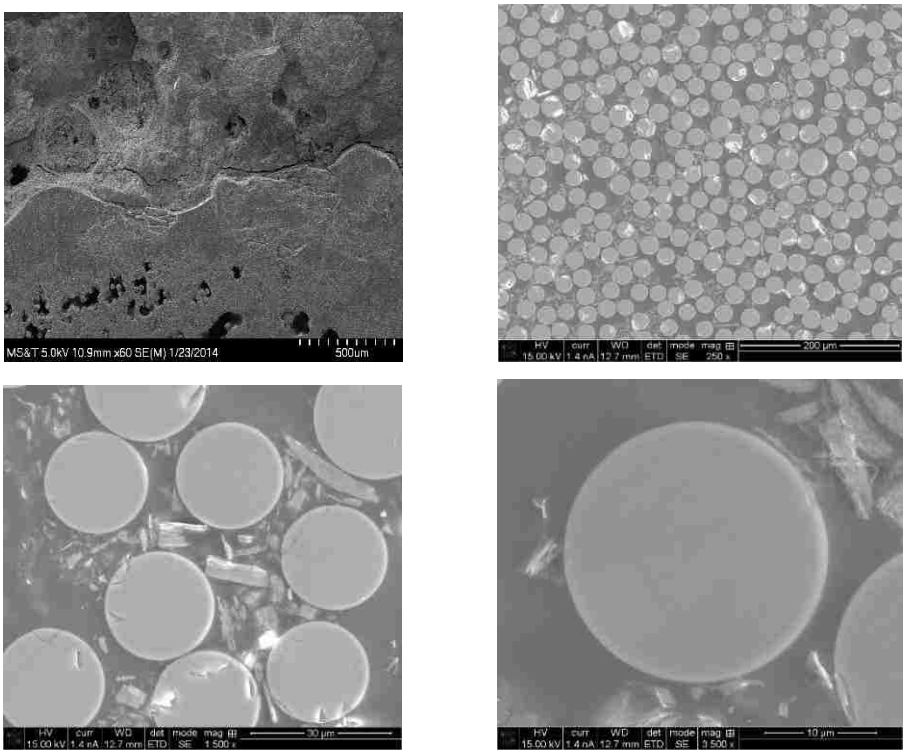

SEM images of panel P-4 at different solutions

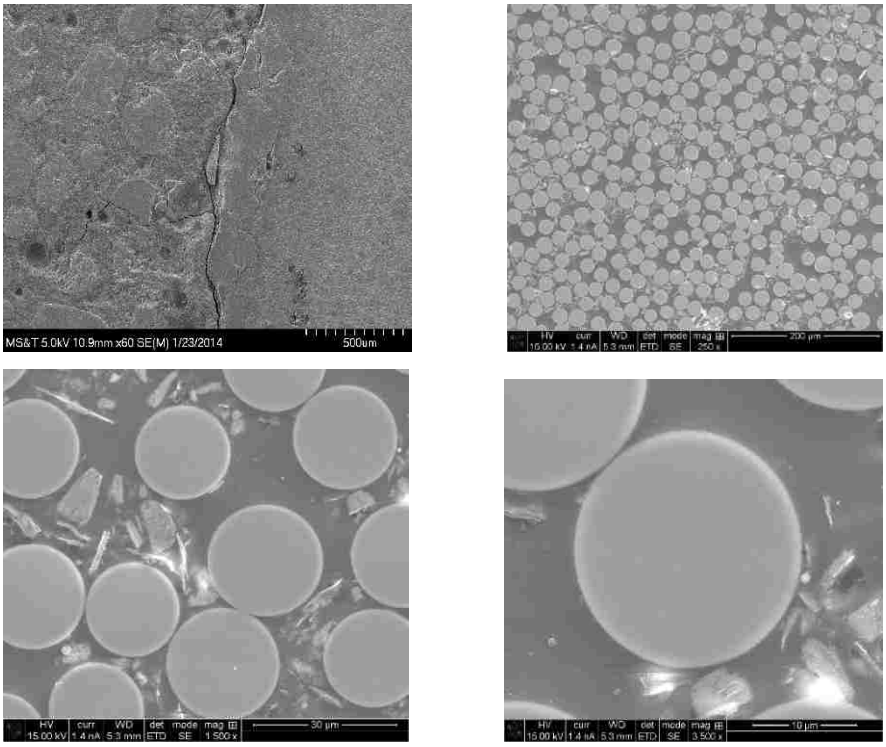

SEM images of panel P-5 at different solutions

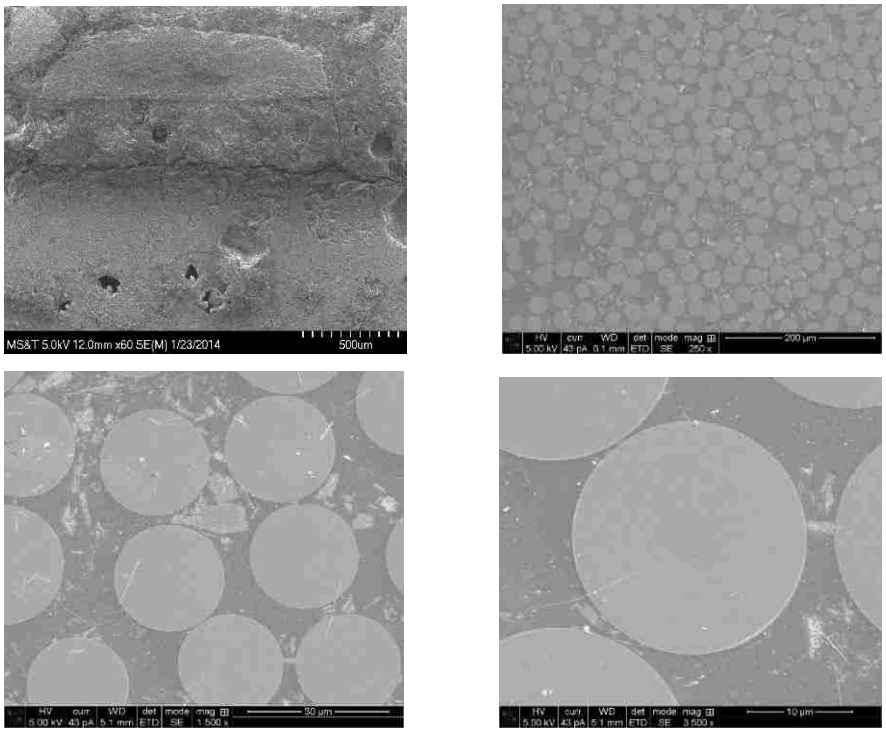

SEM images of panel P-6 at different solutions

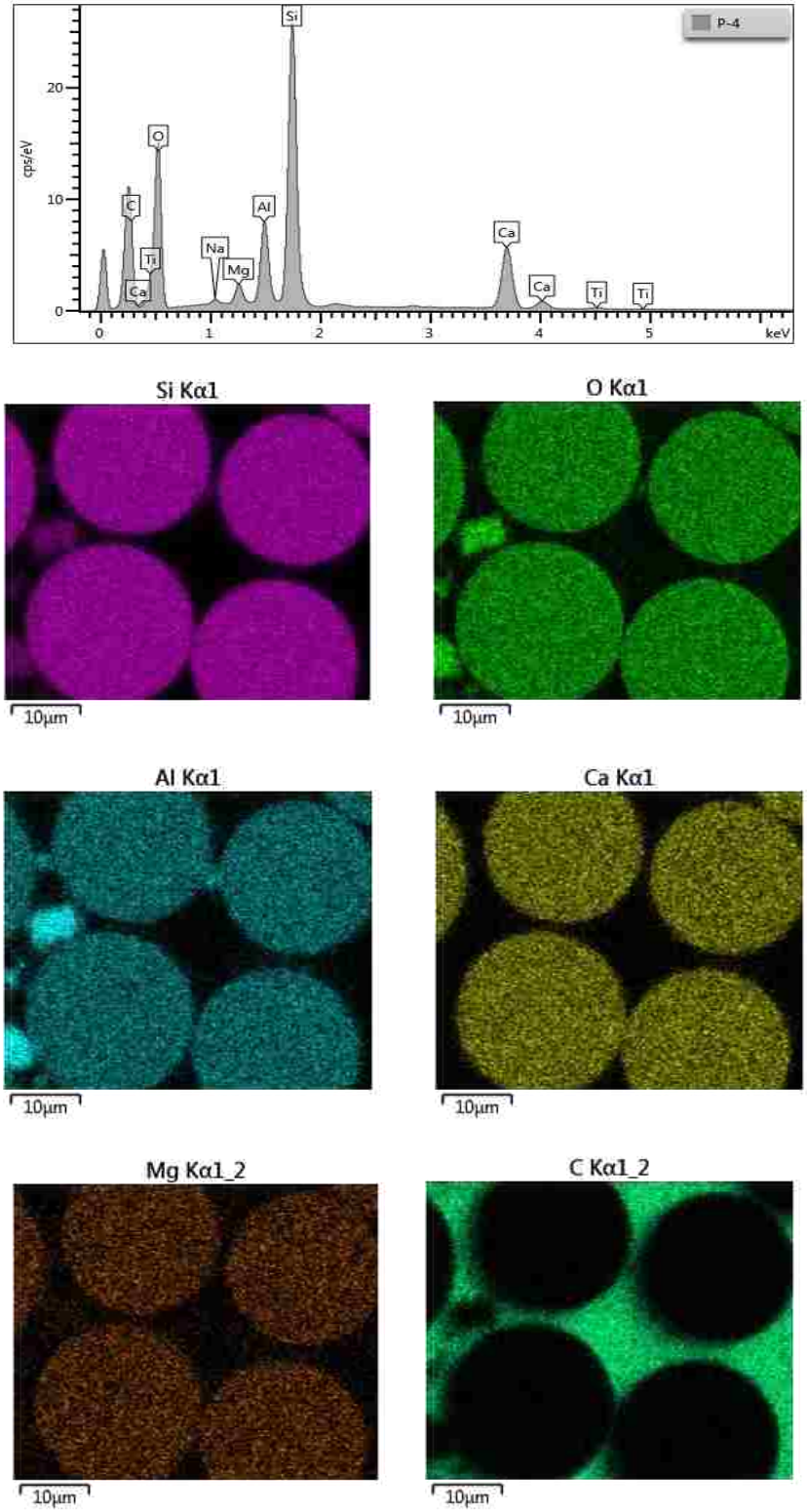

EDS analysis and Elemental scatter in GFRP rebar of panel P-4

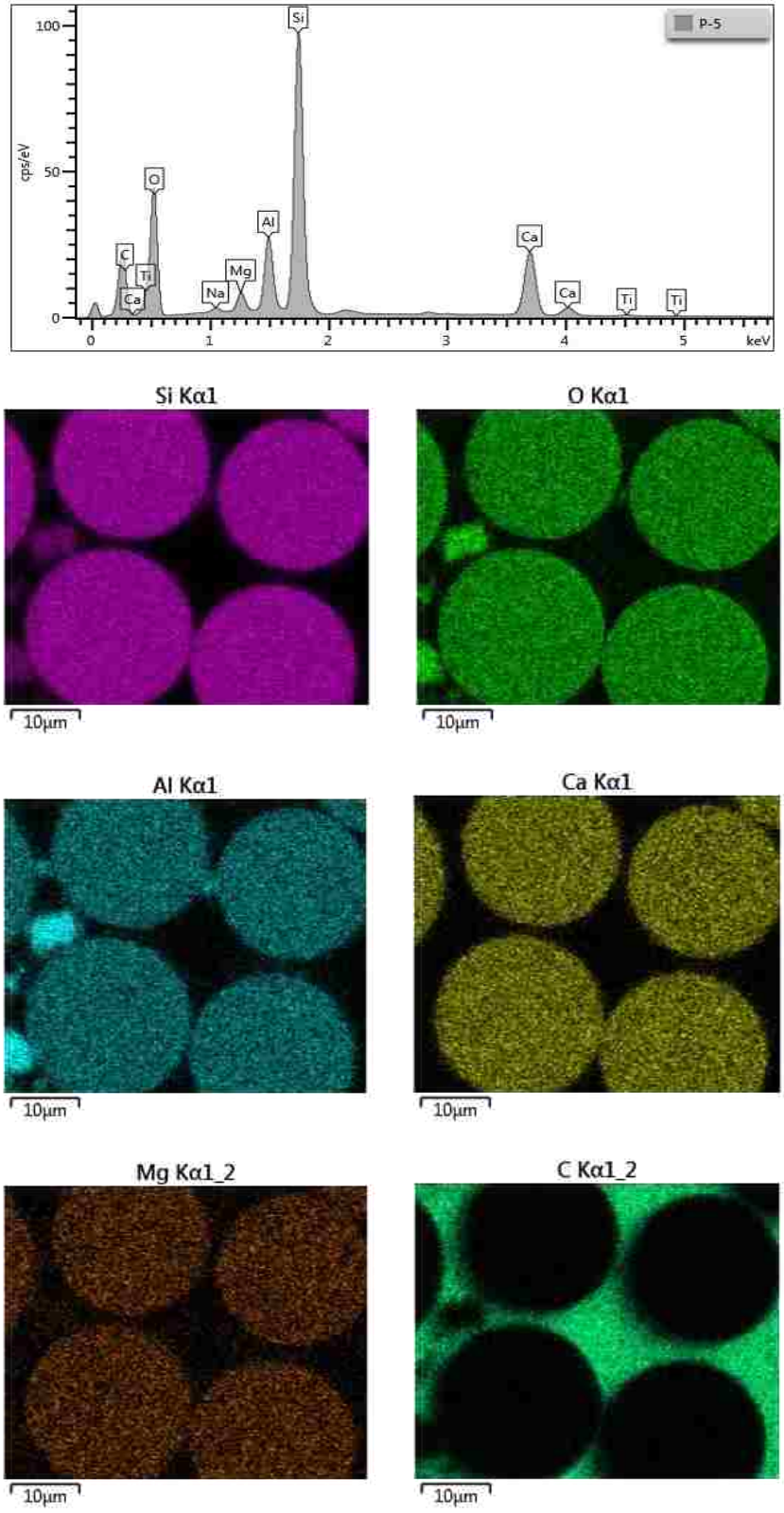

EDS analysis and Elemental scatter in GFRP rebar of panel P-5

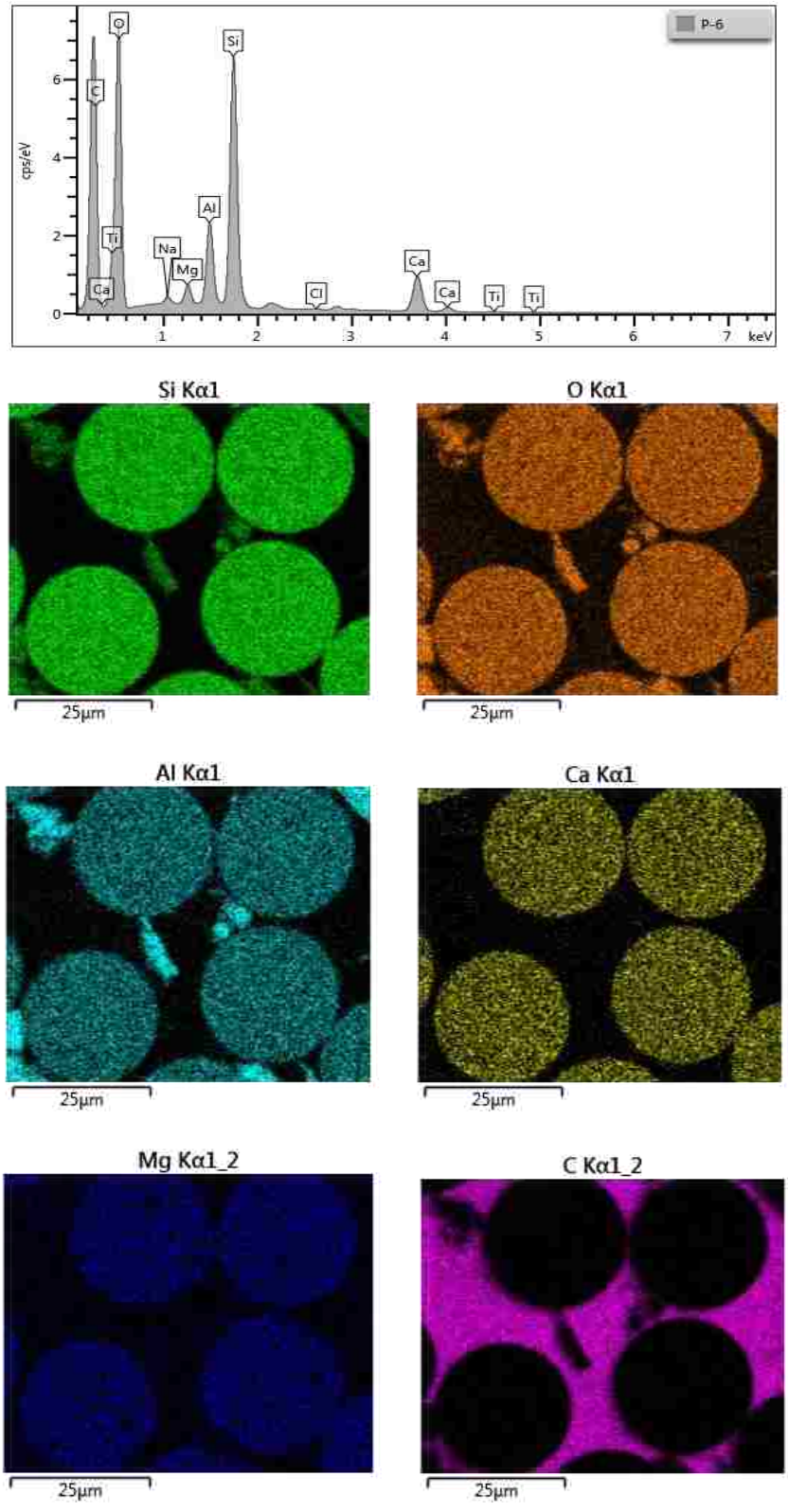

EDS analysis and Elemental scatter in GFRP rebar of panel P-6

APPENDIX B.

TOPIC 2

RG 2 (EC)

RG 4 (EC)

RNG 1 (EC)

RNG 4 (EC)

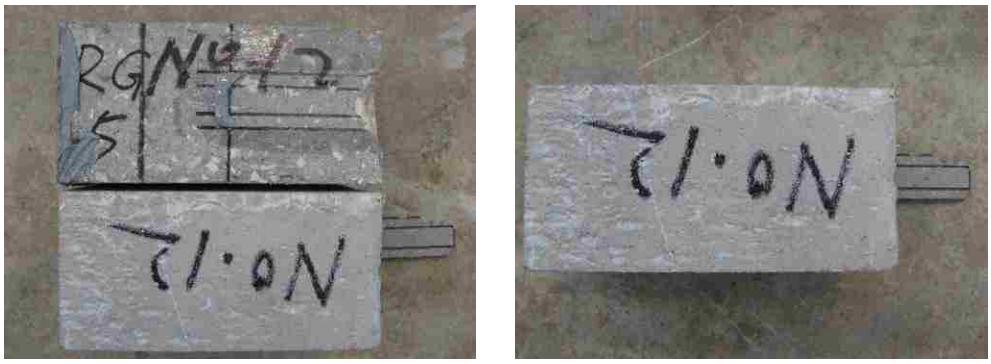

RG 5 (control, 1986 hrs)

RG 9 (control, 1986 hrs)

RNG 11 (control, 1986 hrs)

RNG 13 (control, 1986 hrs)

RG 2 (hot water)

RG 3 (hot water)

RNG 2 (hot water)

RNG 3 (hot water)

RG 4 (salt water 1500 hrs)

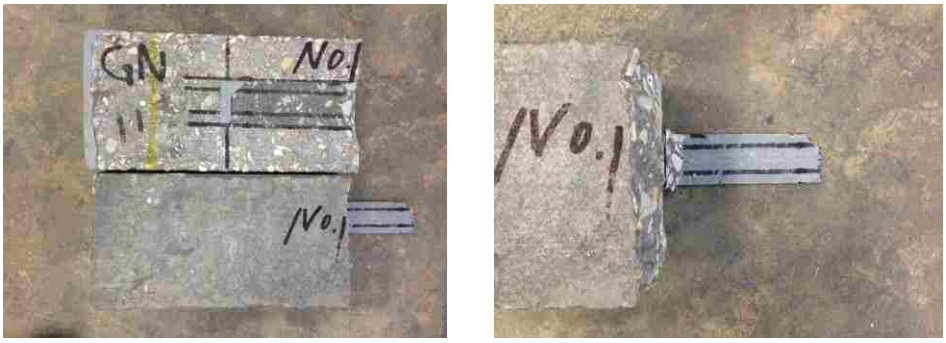

RG 11 (salt water 1500 hrs)

RG 2 (outside)

RG 8 (outside)

RNG 3 (outside)

RNG 6 (outside)

RG 6 (control 4000 hrs)

RG 7 (control 4000 hrs)

RNG 6 (control 4000 hrs)

RNG 8 (control 4000 hrs)

RG 12 (control 1 year)

RG 13 (control 1 year)

RNG 1 (control 1 year)

RNG 2 (control 1 year)

Pull-off RG and RNG specimens (EC)

Pull-off RG and RNG specimens (water)

Pull-off RG and RNG specimens (hot water)

Pull-off RG and RNG specimens (salt water 1500 hrs)

Pull-off RG and RNG specimens (salt water 4000 hrs)

Pull-off RG and RNG specimens (outside)

Pull-off RG and RNG specimens (control 1986 hrs)

Pull-off RG and RNG specimens (control 4000 hrs)

Pull-off RG and RNG specimens (control 1 year)

APPENDIX C.

TOPIC 3

Crack width of Southview Bridge

	Crack No.	Ave. crack width (in.)
Span 3	1	0.012
	2	0.012
	3	0.012
	4	0.01
	5	0.018
	6	0.032
	7	0.022
	8	0.0625
	9	0.0625
	10	0.0625
	11	0.032
	Conversion Unit: 1 in. = 25.4 mm	

Crack width of Southview Bridge

	Crack No.	Ave. crack width (in.)
Span 4	1	0.024
	2	0.014
	3	0.022
	4	0.032
	5	0.032
	6	0.0625
	7	0.032
	8	0.022
	9	0.026
	10	0.032
	11	0.018
	Conversion Unit: 1 in. = 25.4 mm	

Crack width of Southview Bridge

	Crack No.	Ave. crack width (in.)
Span 5	1	0.02
	2	0.016
	3	0.032
	4	0.01
	Conversion Unit: 1 in. = 25.4 mm	

Crack width of Southview Bridge

	Crack No.	Ave. crack width (in.)
Span 6	1	0.02
	2	0.012
	3	0.014
	Conversion Unit: 1 in. = 25.4 mm	

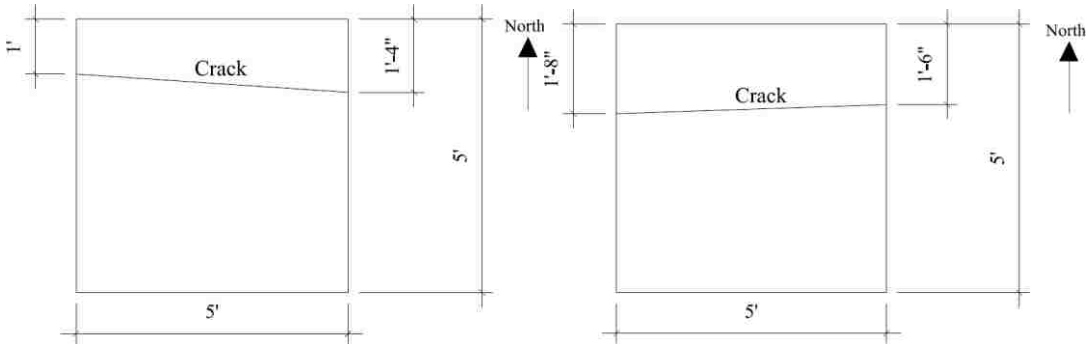

The locations of cracks on top (left) and bottom (right) of Box 4

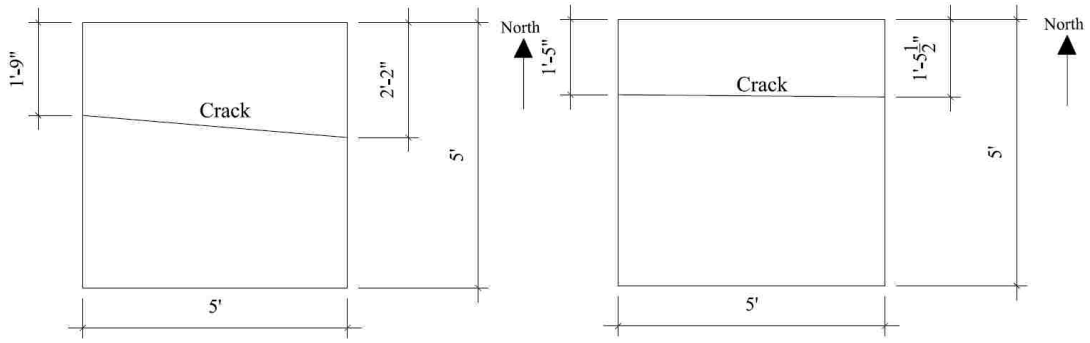

The locations of cracks on top (left) and bottom (right) of Box 5

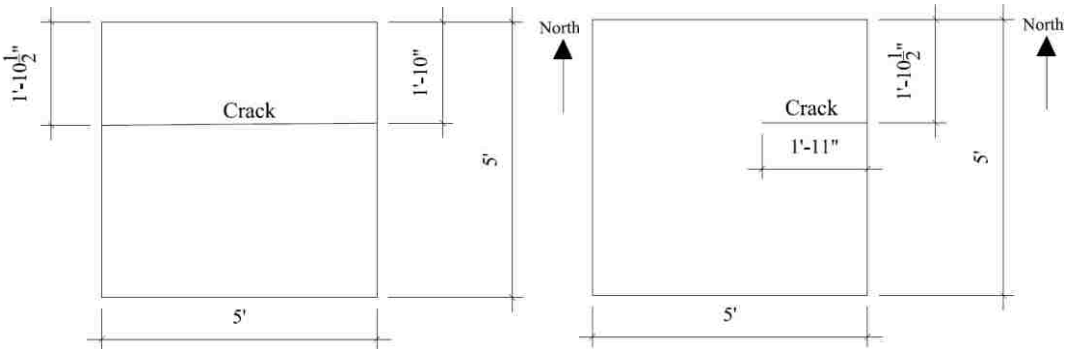

The locations of cracks on top of Box 7 (left) and bottom of Box 10 (right)

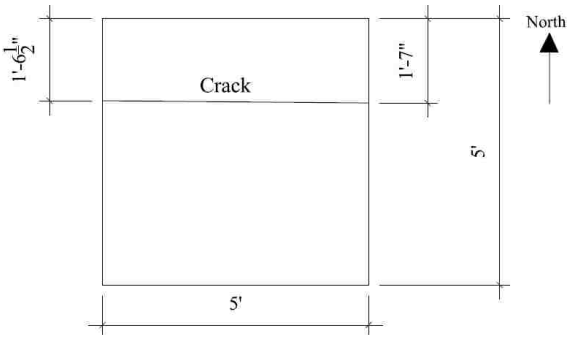

The locations of cracks on top of Box 11

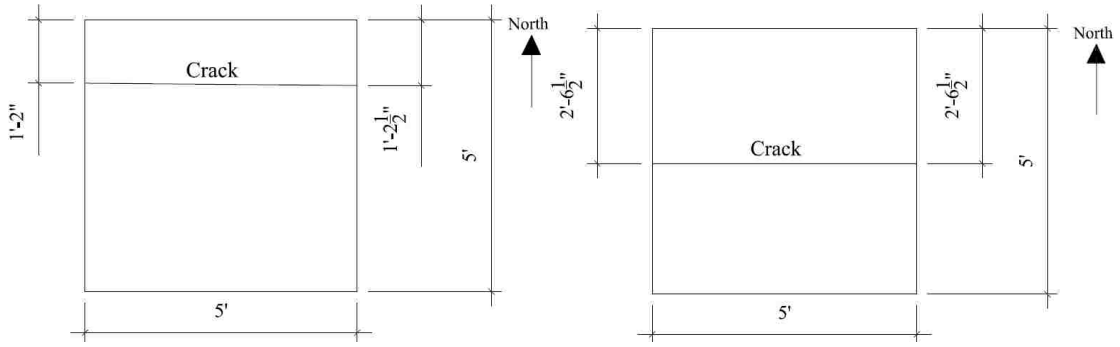

The locations of cracks on top (left) and bottom (right) of Box 12

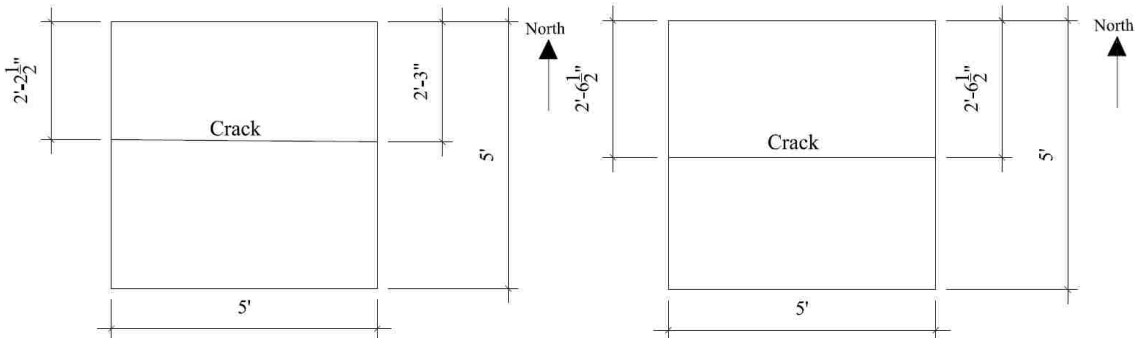

The locations of cracks on top (left) and bottom (right) of Box 13

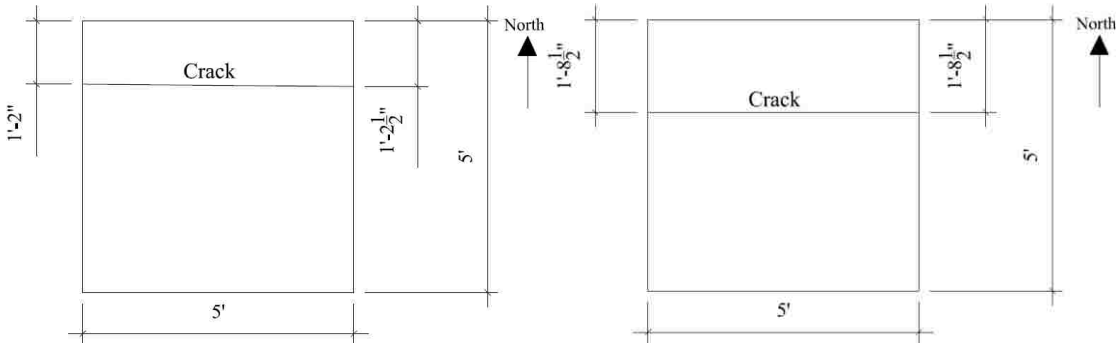

The locations of cracks on top (left) and bottom (right) of Box 14

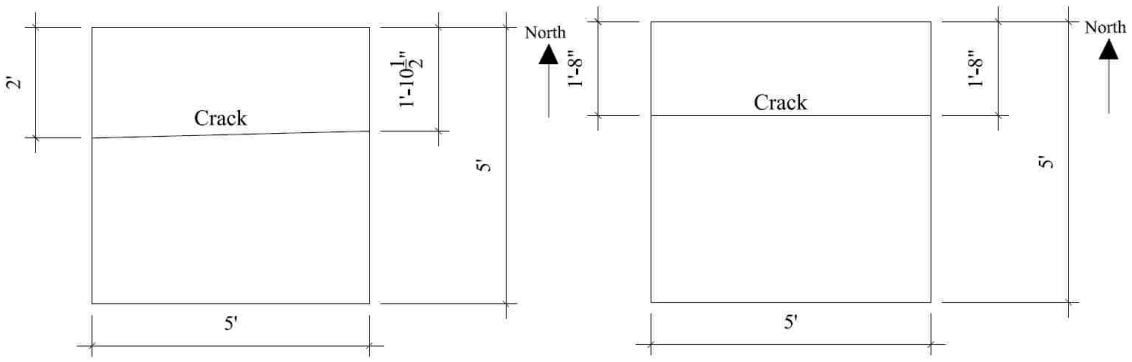

The locations of cracks on top (left) and bottom (right) of Box 15

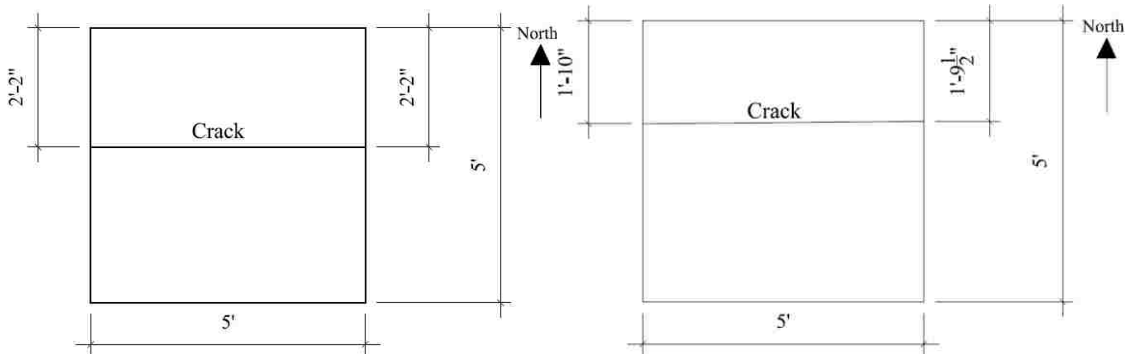

The locations of cracks on top (left) and bottom (right) of Box 16

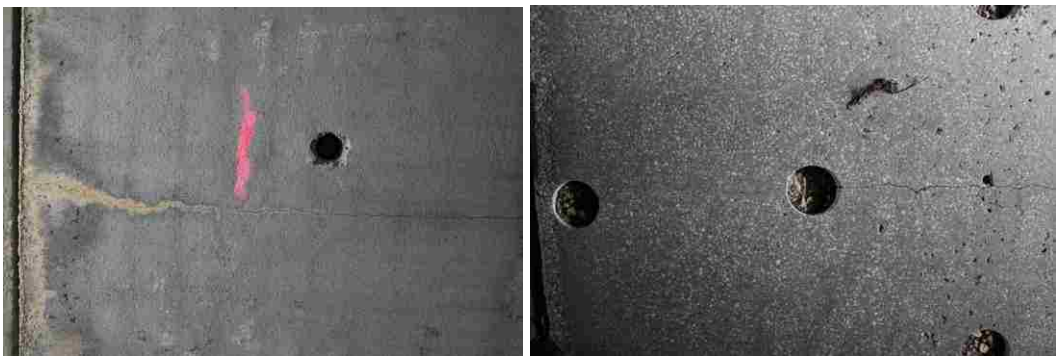

The cracks on the top (left) and bottom (right) of Box 3

The cracks on the top (left) and bottom (right) of Box 16

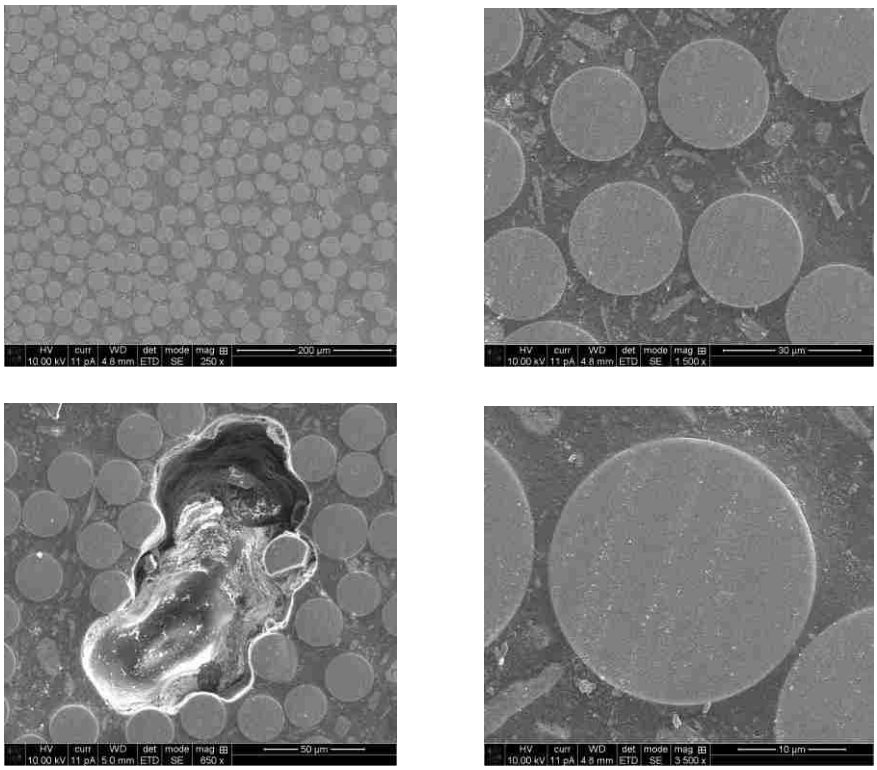

SEM images of sample 2 at different magnifications (Southview Bridge)

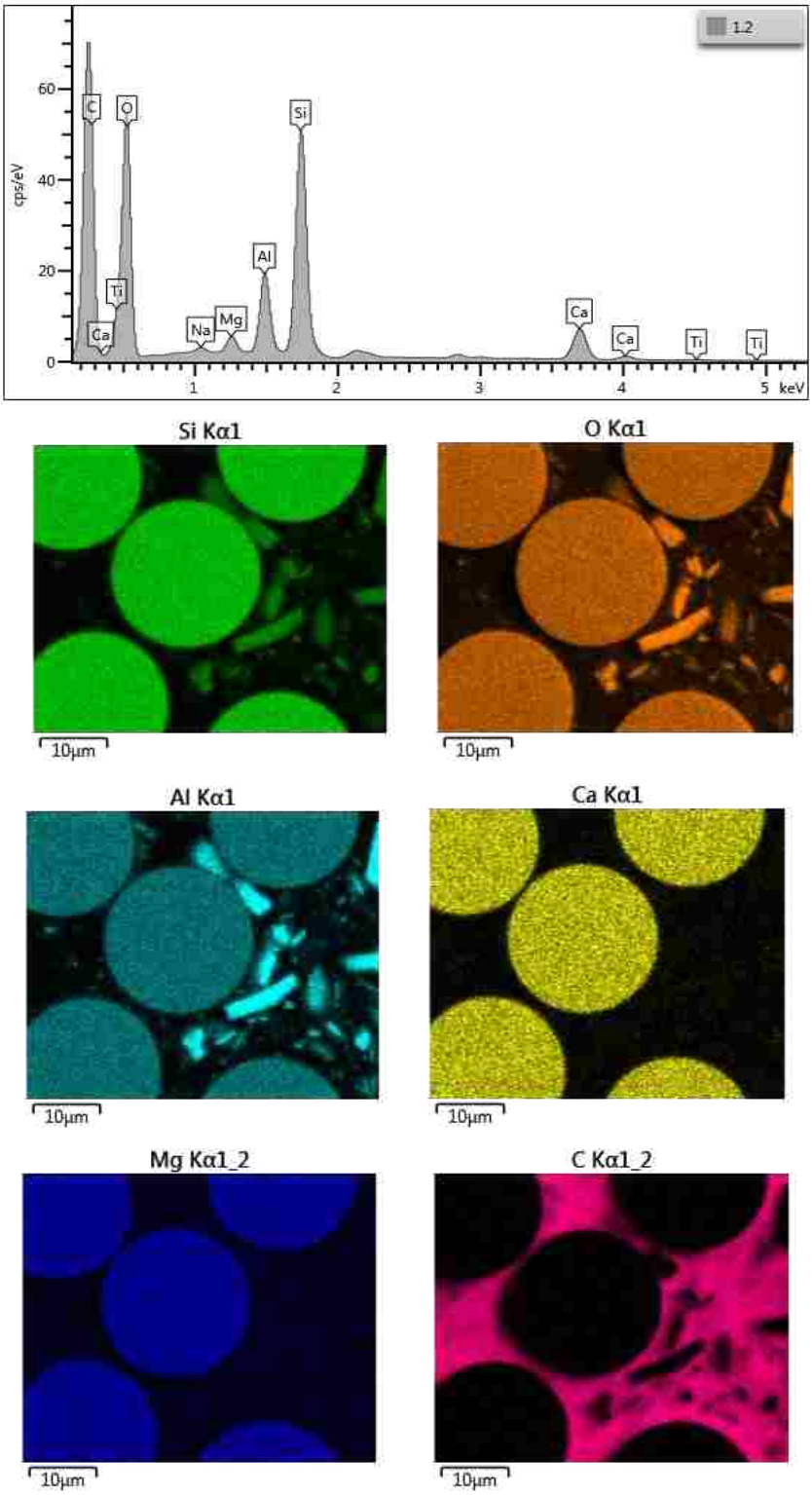

EDS analysis and elemental scatter of sample 2 (Southview Bridge)

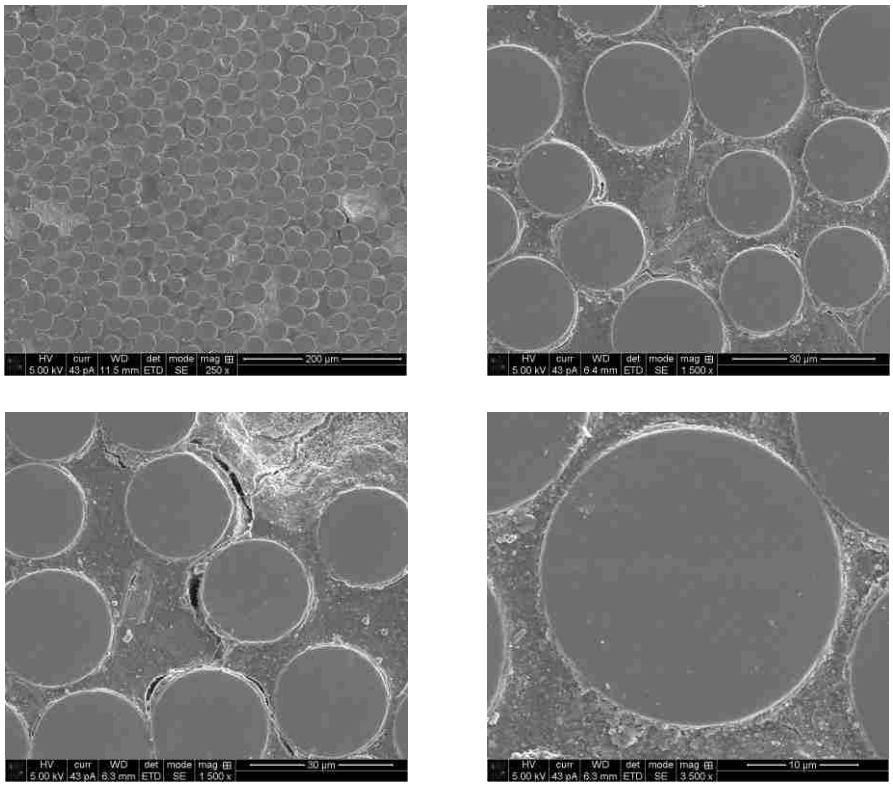

SEM images of sample 3 at different magnifications (Walker Bridge)

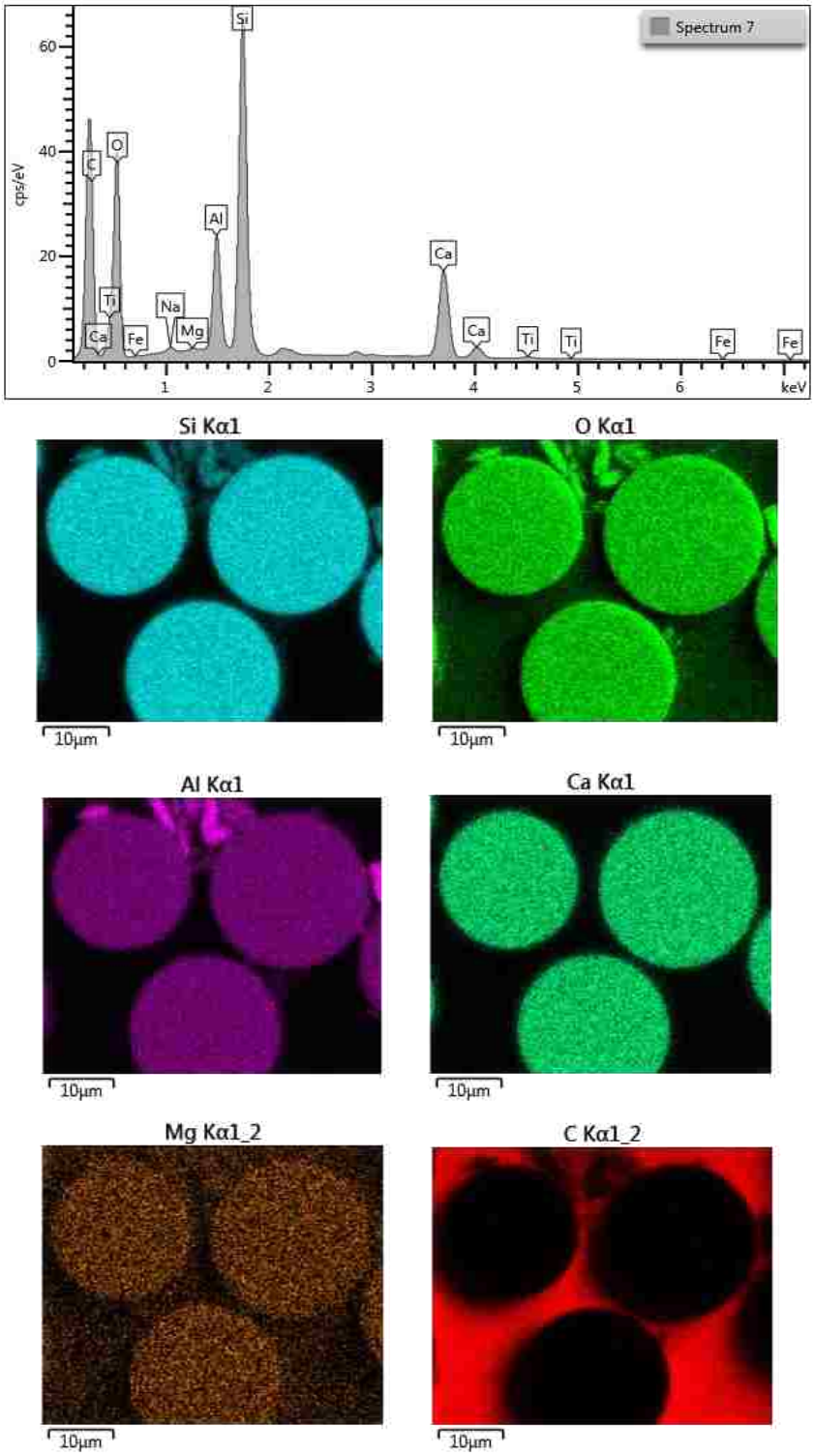

EDS analysis and elemental scatter of sample 2 (Walker Bridge)

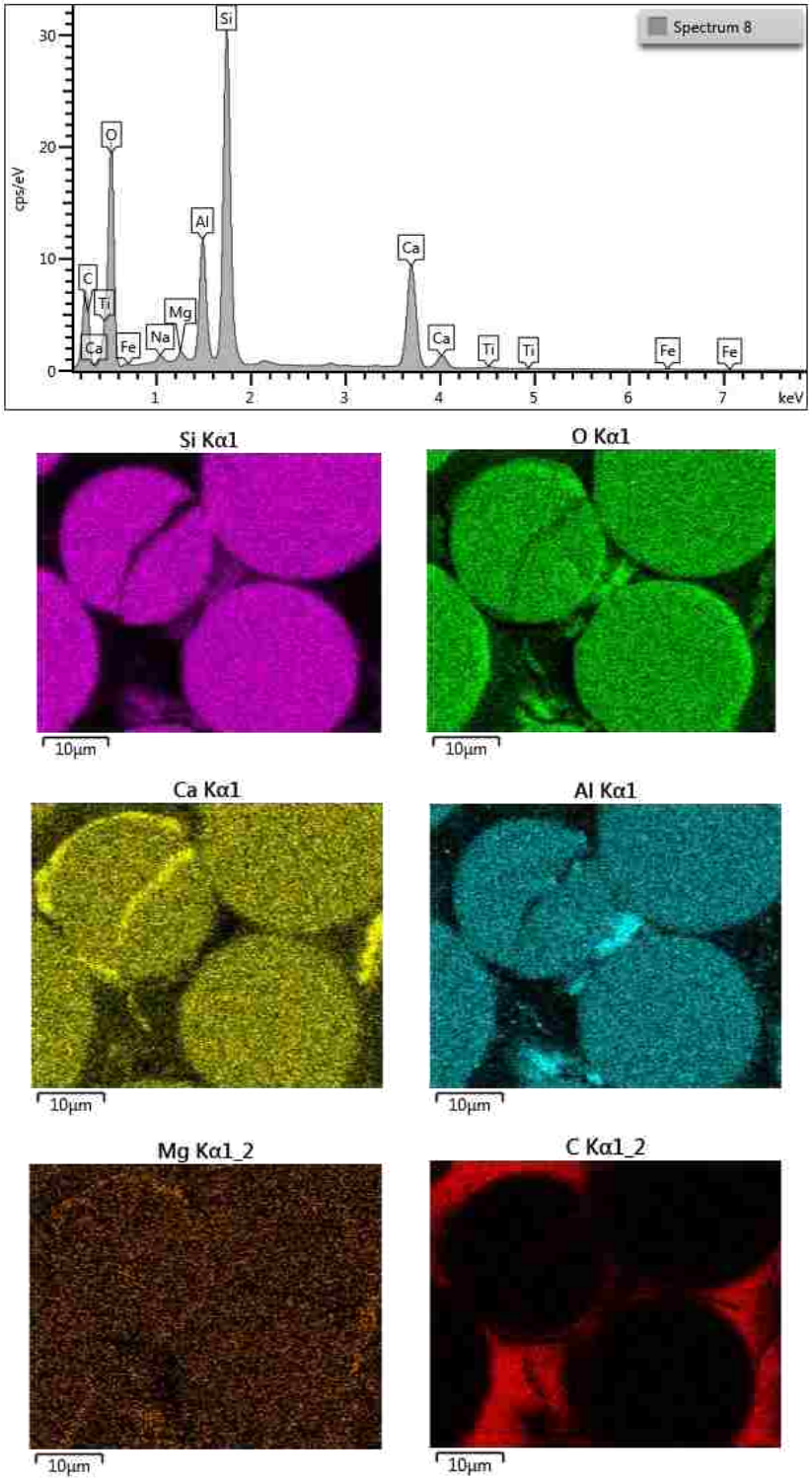

EDS analysis and elemental scatter of sample 3 (Walker Bridge)

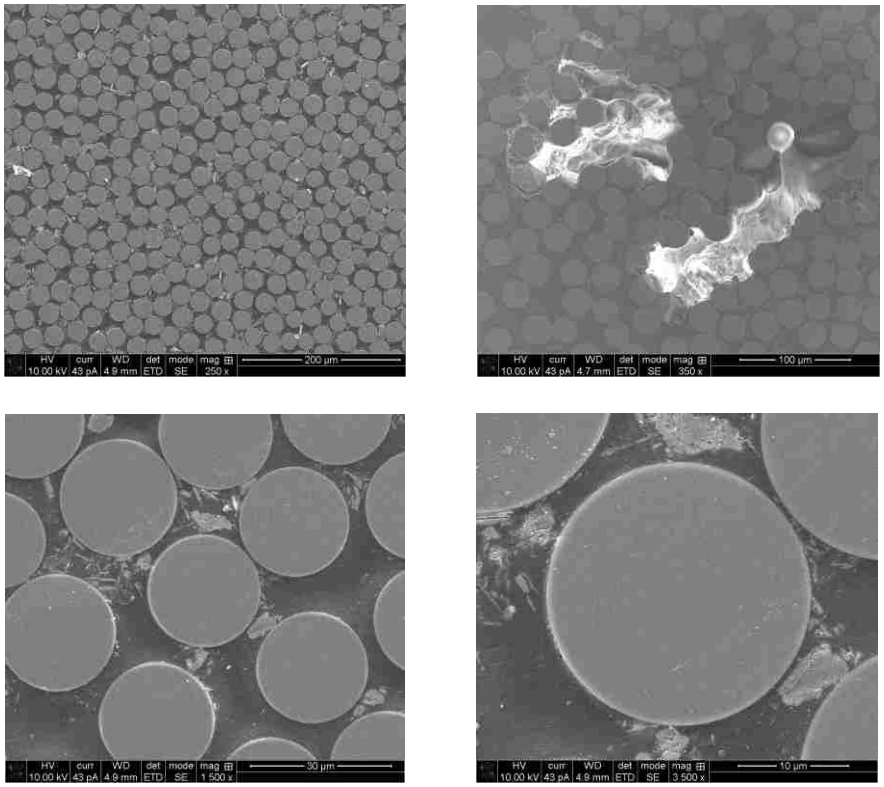

SEM images of sample 1 at different magnifications (Sierrita de la Cruz Bridge)

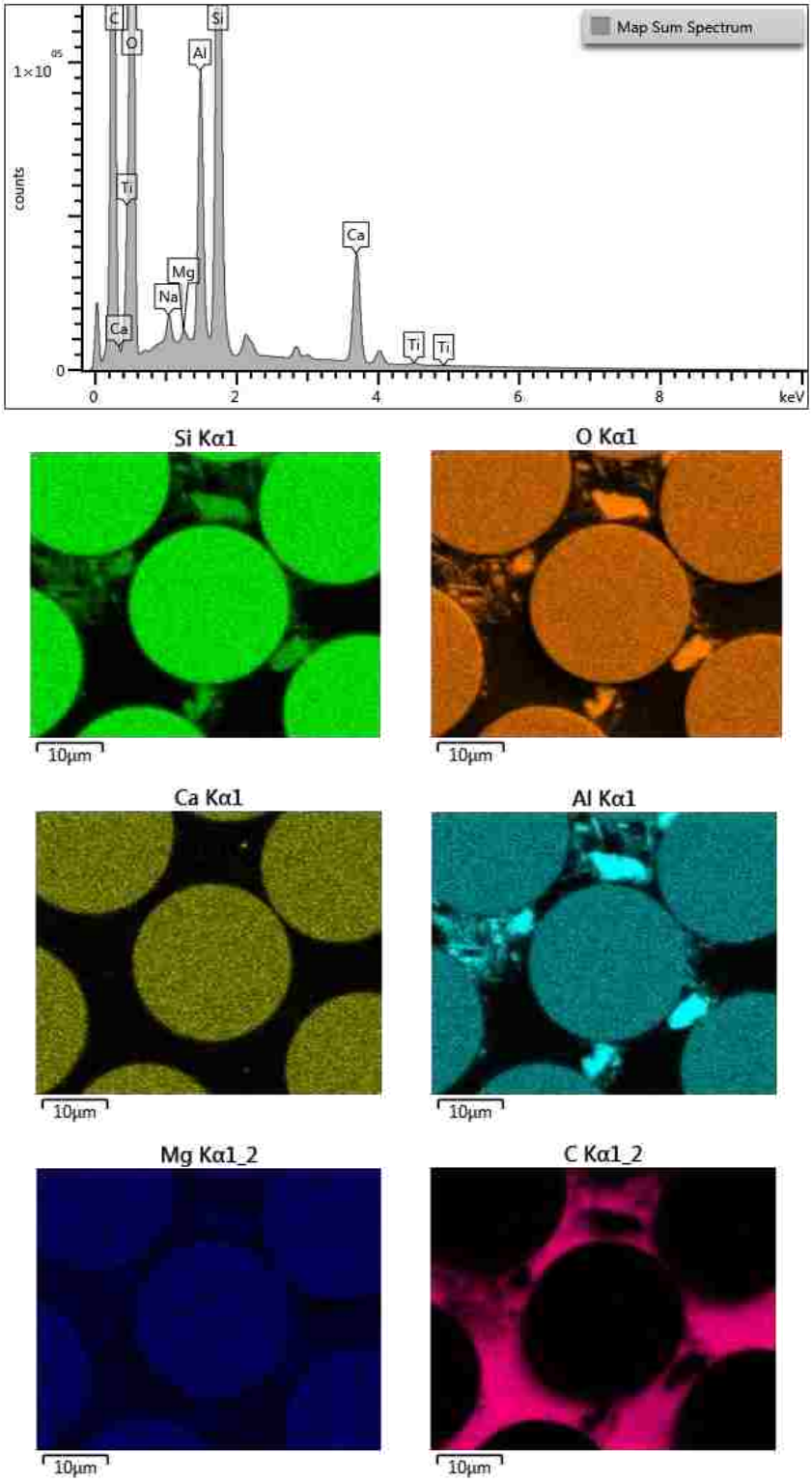

EDS analysis and elemental scatter of sample 1 (Sierrita de la Cruz Bridge)

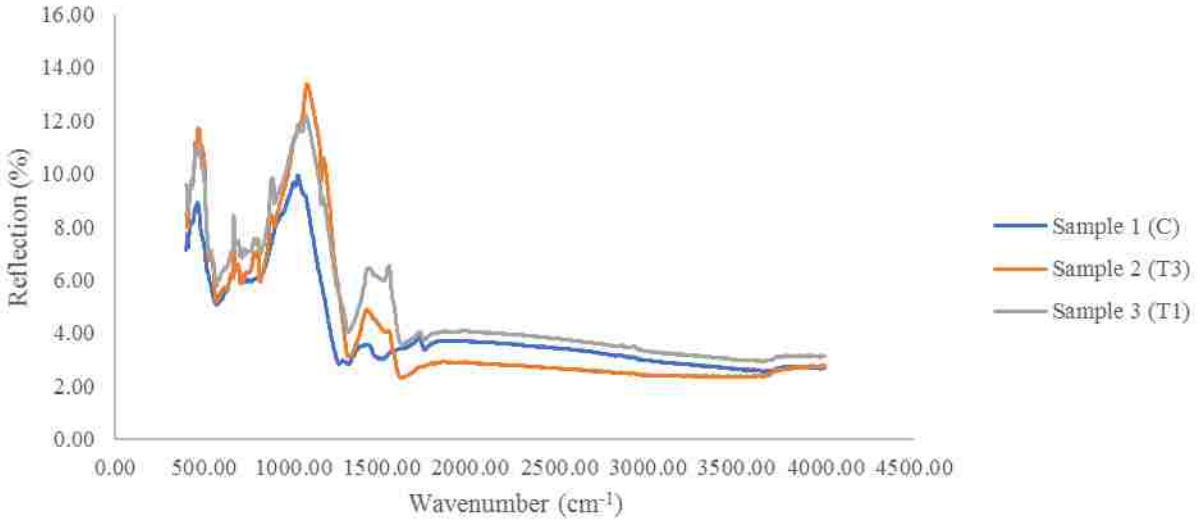

FTIR spectra for GFRP samples in Walker Bridge

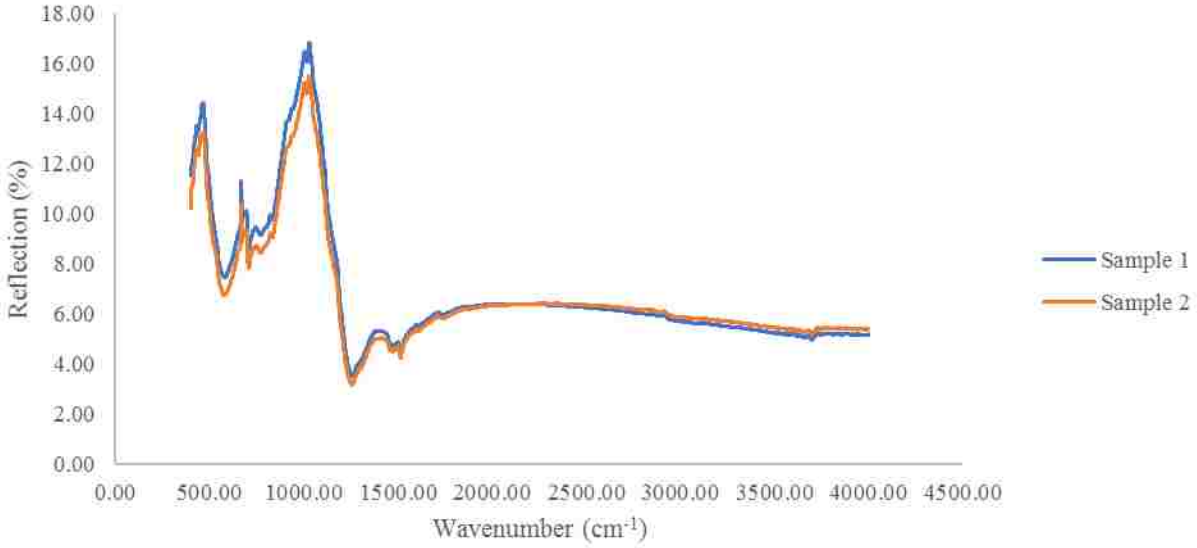

FTIR spectra for GFRP samples in Sierrita de la Cruz Bridge


pH measurements at various locations (Southview Bridge)


pH measurements using Grubb's method (left) and ASTM F710 (right) (Walker Bridge)


pH measurements using Grubb's method (left) and ASTM F710 (right) (Sierrita de la Cruz Bridge)

REFERENCES

[1] Hadid, R. and Saadeghvaziri, M. A., "Transverse cracking of concrete bridge decks: State-of-the-art," *Journal of Bridge Engineering,* 10(5), 503-510, (2005).

[2] Portland Cement Association PCA, "Durability of concrete bridge decks-A cooperative study." *Final Rep.*, Ill. (1970).

[3] Kosel, H. C. and Michols, K. A., "Evaluation of concrete deck cracking for selected bridge deck structures of Ohio Turnpike," *Rep., Ohio Turnpike Commission,* Construction Technology Laboratory, Ohio Department of Transportation, Columbus, Ohio, (1985).

[4] Iowa Department of Transportation Iowa DOT, "A study of transverse cracks in the Keokuk bridge deck," *Final Report,* Ames, Iowa, (1986).

[5] Cady, P. D., Carrier, R. E., Bkar, T., and Theisen, J. C., "Final report on durability of bridge deck concrete: Part 3: Condition of 249 four year old bridge decks," *PennDOT Contract No. 31057-H,* Dept. of Civil Engineering, Pennsylvania State University, University Park, Pa, (1971).

[6] Horn, M. W., Stewart, C. F., and Boulware, R. L., "Factors affecting the durability of concrete bridge decks: Normal versus thickened deck," *Interim Rep. No. 3, CA-HY-4101-3-72-11*, Bridge Department, California Division of Highways, Sacramento, California, (1972).

[7] Ramey, G. E., Wolff, A. R., and Wright, R. L., "Structural design actions to mitigate bridge deck cracking." *Practice Periodical on Structural Design Construction,* 2(3), 118–124, (1997).

[8] Krauss, P. D. and Rogalla, E. A., "Transverse cracking in newly constructed bridge decks," *NCHRP Rep. No. 380,* Transportation Research Board, National Research Council, Washington, D.C., (1996).

[9] McKeel, W. T., "Evaluation of deck durability on continuous beam highway bridges," *Rep. No. VHTRC 85-R32,* Virginia Highway and Transportation Research Council, Charlottesville, Va., (1985).

[10] La Fraugh, R. W. and Perenchio, W. F. "Phase I report of bridge deck cracking study West Seattle Bridge," *Rep. No. 890716,* Wiss, Janney, Elstner Associates, Northbrook, Ill., (1989).

[11] Cheng, T. T. and Johnson, D. W., "Incidence assessment of transverse cracking in bridge decks: Construction and material consideration," *Rep. No. FHWA/NC/85-002*, Vol. 1, Federal Highway Administration, Washington, D.C., (1985).

[12] Perfetti, G. R., Johnson, D. W., and Bingham, W. L., "Incidence assessment of transverse cracking in concrete bridge decks: Structural considerations," *Rep. No. FHWA/NC/85-002*, Vol. 2, Federal Highway Administration, Washington, D.C., (1985).

[13] Report Card for America's Infrastructure ASCE (2013).

[14] Report Card for Missouri's Infrastructure ASCE (2013).

[15] Koenigsfeld, D. and Myers, J. J., "Secondary Reinforcement for Fiber Reinforced Polymers Reinforced Concrete Panels," *Center for Infrastructure Engineering Studies Report* Number 03-45, (2003).

[16] Benmokrane, B., El-Salakawy, E. F., Desgagne, G. and Lackey, "Construction Testing and Monitoring of FRP Reinforced Concrete Bridge in North America," *Proceedings of the Fiber-Reinforced Polymer Reinforcement for Concrete Structures, FRPRCS-6*, 2, pp. 1311-1320, (2000).

[17] Toutanji, H. A. and Gomez, W., "Durability Characteristics of Concrete Beams Externally Bonded with FRP Composite Sheets," *Cement and Concrete Composites* 19, pp. 351-358, (1997).

[18] Wong, R. S. Y. and Vecchio, F. J., "Towards Modeling of Reinforced Concrete Members with Externally Bonded Fiber-Reinforced Polymer Composites," ACI Structural Journal, 100(1), pp. 47-55, (2003).

[19] Deng, J., Tanner, J. E., Mukai, D., Hamilton, H.R., and Dolan C.W, "Durability performance of carbon fiber-reinforced polymer in repair/strengthening of concrete beams," *ACI Material Journal*, 112 (2), pp. 247-257 (2015).

[20] Almusallam T. H., "Load-deflection behavior of RC beams strengthened with GFRP sheets subjected to different environmental conditions," Cement and Concrete Composites, 28, pp. 879-889, (2006).

[21] Wobbe, E., Silva, P., Barton, B. L., Dharani, L. R., Birman, V., Nanni, A., Alkhrdaji, T., Thomas, J., and Tunis, G. "Flexural capacity of RC beams externally bonded with SRP and SRG," In: *Proceeding of society for the advancement of material and process engineering*, symposium, Long Beach, CA., p. 20, (2004).

[22] ACI Committee 440, "Guide for the Design and Construction of Concrete Reinforced with FRP Bars," *American Concrete Institute*, Farmington Hills, (2006).

[23] Myers, J.J., Holdener, D., Merkle, W., and Hernandez, E., "Preservation of Missouri Transportation Infrastructures: Validation of FRP composite technology through field testing-in-situ load testing of bridges P-962, T-530, X-495, X-596 AND Y-298," University of Missouri-Rolla, (2008).

[24] ACI Committee 440.9R-15, "Guide to accelerated conditioning protocols for durability assessment of internal and external fiber reinforced polymer (FRP) reinforcement for concrete," *American Concrete Institute*, Farmington Hills, (2015).

[25] ACI committee 440, "Guide for the design and construction of externally bonded FRP systems for strengthening existing structures," *American Concrete Institute*, Farmington Hills, (2004).

[26] Wight, J. G. and MacGregor, J. K. "Reinforced concrete Mechanics and Design," *Fifth Edit*. Upper Saddle River: Prentice Hall, (2009).

[27] Nejadi, S., and Gilbert, I., "Shrinkage cracking and crack control in restrained reinforced concrete members," *ACI Struct. J.*, 101(6), pp. 840–845, (2004).

[28] ACI Committee 318-11, "Building code requirements for structural concrete and commentary," *American Concrete Institute*, Detroit, (2011).

[29] Branham, N., and Myers, J. J. "Secondary reinforcement requirements for concrete reinforced with GFRP," *Thesis of Master*, University of Missouri-Rolla, (2006).

[30] Myers, J. J. and Golden, C., "Investigation of Long-Term Crack Patterns in FRP and Steel Reinforced Concrete Panels," *Final Report*, University of Missouri-Rolla, (2007).

[31] Frosch, R. J. and Blackman, D. T., "Investigation of Bridge Deck Cracking in Various Bridge Superstructure Systems," *Final Report*, Purdue University, (2003).

[32] Japan Concrete Institute, "Autogenous Shrinkage of Concrete - Google Books," Eiichi Taz. London, (1999).

[33] Mindess, S., Young, J.F. and Darwin, D., "Concrete," *2nd edition*. Upper Saddle River, (2003).

[34] Byard, B., Schindler, A. Barnes, R., and Rao, A., "Cracking Tendency of Bridge Deck Concrete," *Transp. Res. Rec. J. Transp. Res. Board*, vol. 2164, pp. 122–131, (2010).

[35] Chen, R. and Choi, J., "Effects of GFRP reinforcing rebars on shrinkage and thermal stresses in concrete," *15th ASCE Eng. Mech.*, (2002).

[36] Gilbert, R., "Shrinkage, cracking and deflection-the serviceability of concrete structures," *Electron. J. Struct. Eng.*, (2001).

[37] Qiao. P., McLean, D., and Zhuang, J., "Mitigation strategies for early-age shrinkage cracking in bridge decks," *Final Report*, Washington State University, Olympia, (2010).

[38] Xi,Y., Shing, B., and Xie, Z., "Development of Optimal Concrete Mix Designs for Bridge Decks," *CDOT Rep. No. CDOT-DTD*, pp. 2001–2011, (2001).

[39] Folliard, K., Smith, C., Sellers, G., Brown, M., and Breen J., "Evaluation of Alternative Materials to Control Drying-Shrinkage Cracking in Concrete Bridge Decks," *Final Report*, The University of Texas at Austin, (2003).

[40] Delatte, N., Mack, E., and Cleary, J., "Evaluation of High Absorptive Materials to Improve Internal Curing of Low Permeability Concrete," *Final Report*, Cleveland State University, (2007).

[41] Gilbert, R. I., "Shrinkage cracking in fully restrained concrete members," *Struct. J.*, 89(2), 141-149, (1992).

[42] Nejadi, S., and Gilbert R. I., "Shrinkage cracking in fully-restrained reinforced concrete members," *Final Report*, University of New South Wales, Sydney, (2003).

[43] Ghatefar, A., "Effect of Reinforcement Ratio on Transverse Early-Age Cracking of GFRP-RC Bridge Deck Slabs," *J. Compos.*, 18(6), pp. 1–9, (2014).

[44] Ghatefar, A., El-Salakawy, E., and Bassuoni, M. T., "Early-age restrained shrinkage cracking of GFRP-RC bridge deck slabs: Effect of environmental conditions," *Cem. Concr. Compos.*, vol. 64, pp. 62–73, (2015).

[45] ACI-222R-01, "ACI 222R-01 Protection of Metals in Concrete Against Corrosion Reported by ACI Committee 222," *Design*, vol. 1, no. Reapproved, pp. 1–41, (2010).

[46] ISIS Canada, "Durability of fiber reinforced polymers in civil infrastructure," Winnipeg, (2006).

[47] MuFti, A., BaNthia, N., BeNMokraNe, B., Boulfiza, M., and Newhook, J., "Durability of GFRP composite rods," *Concr. Int.*, pp. 37–42, (2007).

[48] Phelan, R. S., Vann, W. P., and Bice, J., "FRP Reinforcing Bars In Bridge Decks Field Instrumentation And Short-Term Monitoring," *Final Report*, Texas Department of Transportation, Lubbock, (2003).

[49] Chen, Y., Davalos, J. F., Ray, I., and Kim, H. Y., "Accelerated aging tests for evaluations of durability performance of FRP reinforcing bars for concrete structures," *Compos. Struct.*, 78(1), pp. 101–111, (2007).

[50] Robert, M., Cousin, P., and Benmokrane, B., "Durability of GFRP Reinforcing Bars Embedded in Moist Concrete," *J. Compos. Constr.*,13(2), pp. 66–73, (2009).

[51] Davalos, J. F., Chen, Y., and Ray, I., "Long-term durability prediction models for GFRP bars in concrete environment," *J. Compos. Mater.*, 46(16), pp. 1899–1914, (2012).

[52] Dejke, V., "Durability of FRP Reinforcement in Concrete," *PhD Dissertation*, Chalmers University of Technology, (2001).

[53] Mukherjee, A. and Arwikar, S. J., "Performance of glass fiber-reinforced polymer reinforcing bars in tropical environments - Part II: Microstructural tests," *ACI Struct. J.*, 102(6), pp. 816–822, (2005).

[54] Trejo, D., Gardoni, P., Kim, J. J., and Zidek, J., "Long-Term Performance of GFRP Reinforcement: Technical Report," *Final Report*, The Texas A&M University, (2009).

[55] Dai J., Yokota H., Iwanami, M., and Kato, E., "Experimental investigation of the influence of moisture on the bond behavior of FRP to concrete interfaces," *J. Compos. Constr.*, 14(6), pp. 834–844, (2010).

[56] Tilly, G., "Durability of concrete repairs," CRC Press, (2011).

[57] Huang, X., Birman, V., Nanni, A., and Tunis, G., "Properties and potential for application of steel reinforced polymer and steel reinforced grout composites," *Compos. Part B Eng.*, 36(1), pp. 73–82, (2005).

[58] Lopez, A., Galati, N., Alkhrdaji, T., and Nanni, A., "Strengthening of a Reinforced Concrete bridge with externally bonded steel reinforced polymer (SRP)," *Compos. Part B Eng.*, 38(4), pp. 429–436, (2007).

[59] Phillis, S., Parretti, R., and Nanni, A., "Evaluation of FRP repair method for cracked bridge members," *Final Report*, Univerisity of Missouri-Rolla, (2005).

[60] Gartner, A., Douglas, E. P., Dolan, C. W., and Hamilton, H. R., "Small Beam Bond Test Method for CFRP Composites Applied to Concrete," *J. Compos. Constr.*, 15(1), pp. 52–61, (2011).

[61] Ekenel, M. and Myers, J. J., "Fatigue Performance of CFRP Strengthened RC Beams under Environmental Conditioning and Sustained Load," *J. Compos. Constr.*, 13(2), pp. 93–102, (2009).

[62] Gentry, T. R. and Husain, M., "Thermal compatibility of plastic composite reinforcement and concrete," vol. 3, pp. 82–86, (1999).

[63] Tepfers, R., "Cracking of concrete cover along anchored deformed reinforcing bars," *Mag. Concr. Res.*, (1979).

[64] Alves, J., El-Ragaby, A., and El-Salakawy, E., "Durability of GFRP Bars' Bond to Concrete under Different Loading and Environmental Conditions," *J. Compos. Constr.*, 15(3), pp. 249–262, (2011).

[65] Ayano, T. and Wittmann, F. H., "Drying, moisture distribution, and shrinkage of cement- based materials," vol. 35, pp. 134–140, (2002).

[66] Zhang, J., Gao, Y., Han, Y., and Sun, W., "Shrinkage and interior humidity of concrete under dry–wet cycles," *Dry. Technol.*, 30(6), pp. 583–596, (2012).

[67] ACI 440-08, “Guide for Modeling and Calculating Shrinkage and Creep in Hardened Concrete,” *American Concrete Institute*, Farmington Hills, MI, (2008).

[68] Favre, R., “Fissuration et Deformations,” Ecole Polytechnique Federale de Lausanne, Switzerland, (1983).

[69] Alsayed, S. H., “Flexural behaviour of concrete beams reinforced with GFRP bars,” *Cem. Concr. Compos.*, 20(1), pp. 1–11, (1998).

[70] Aiello, L., and Ombres, A.M, , “Load-Deflection Analysis of FRP Reinforced Concrete Flexural Members,” *J. Compos. Constr.*, vol. 4, pp. 164–171, (2000).

[71] Gravina, R. J. and Smith, S. T., “Flexural behaviour of indeterminate concrete beams reinforced with FRP bars,” *Eng. Struct.*, 30(9), pp. 2370–2380, (2008).

[72] ASTM D7205/D7205M-06 (Reapproved 11), “Standard test method for tensile properties of fiber reinforced polymer matrix composite bars,” American Society for Testing and Materials, (2011).

[73] ASTM C78/C78M-16, “Standard Test Method for Flexural Strength of Concrete (Using Simple Beam with Third-Point Loading),” American Society for Testing and Materials, (2016).

[74] Theriaule, M. and Benmokrane, B., “Effects of FRP Reinforcement Ratio and Concrete Strength on Flexural Behavior of Concrete Beams,” vol. 2, pp. 7–16, (1998).

[75] Al-Mahmoud, F., Mechling, J. M., and Shaban, M., “Bond strength of different strengthening systems - Concrete elements under freeze-thaw cycles and salt water immersion exposure,” *Constr. Build. Mater.*, vol. 70, pp. 399–409, (2014).

[76] Hardwire LLC, “What is Hardwire?” www.hardwirellc.com, Pocomoke City, Maryland, (2015).

[77] Sika Group, “Product Data Sheet: Sikadur 330, high-modulus, high-strength, impregnating resin,” (2014).

[78] Dolan, C. W., Tanner, J., and Mukai, D., Hamilton, H. R., and Douglas, E., “Research report for evaluating the durability of bonded CFRP repair/strengthening of concrete beams,” *Final Report*, University of Wyoming and University of Florida, (2009).

[79] Green, M. F., Bisby, L., Beaudoin, Y., and Labossière, P., "Effect of freeze-thaw cycles on the bond durability between fibre reinforced polymer plate reinforcement and concrete," *Can. J. Civ. Eng.*, 27(5), pp. 949–959, (2000).

[80] ASTM C39/C39M-16b, "Standard Test Method for Compressive Strength of Cylindrical Concrete Specimens," American Society for Testing and Materials, (2016).

[81] Myers. J. J., Shen. X., and Maerz, N. H., "Effect of Varied Surface Roughness, Putty Thickness and Concrete Strength on the Interfacial Bond Strength of FRP to Concrete," *Final Report*, The University of Missouri-Rolla, (2007).

[82] Chajes, M. J., Finch, W. W., Januszka, T. F., and Thomson, T. A., "Bond and Force Transfer of Composite-Material Plates Bonded to Concrete," *ACI Struct. J.*, 93(2), (1996).

[83] Pallempati, H., Beneberu, E., Yazdani, N., and Patel, S., "Condition Assessment of Fiber-Reinforced Polymer Strengthening of Concrete Bridge Components," *J. Perform. Constr. Facil.*, 30(6), pp. 1–9, (2016).

[84] ASTM D30, "Standard Test Method for Pull-Off Strength for FRP Bonded to Concrete Substrate," American Society for Testing and Materials, (2009).

[85] Mirmiran, A., Shahawy, M., Nanni, A., and Karbhari, V., "Bonded repair and retrofit of concrete structures using FRP composites : recommended construction specifications and process control manual," *NCHRP Report*, Transportation Research Board, (2004).

[86] ASTM D3039/D3039M, "Standard Test Method for Tensile Properties of Polymer Matrix Composite Materials," American Society for Testing and Materials, (2014).

[87] Wolff, E. G., "Moisture Effects on Polymer Matrix Composite," *SAMPE J.*, 29(3), pp. 13–20, (1993).

[88] Grace, N. F. and Singh, S. B., "Durability Evaluation of Carbon Fiber-Reinforced Polymer Strengthened Concrete Beams : Experimental Study and Design," *ACI Struct. J.*, 102(1), 40-53, (2005).

[89] National Weather Service Forecast, http://www.weather.gov, (2013) .

[90] NCDC (National Climatic Data Center), http://www.ncdc.noaa.gov, (2013).

[91] Au, C. and Büyüköztürk, O., "Peel and shear fracture characterization of debonding in FRP plated concrete affected by moisture," *J. Compos. Constr. ASCE*, 1091), pp. 35–47, (2006).

[92] Davalos, J. F., Kodkani, S. S., and Ray, I., "Fracture mechanics method for Mode-I interface evaluation of FRP bonded to concrete substrates," *J. Mater. Civ.*, 18(5), pp. 732–742, (2006).

[93] Nakaba, K., Kanakubo, T., Furuta, T., and Yoshizawa, H., "Bond behavior between fiber-reinforced polymer laminates and concrete," *ACI Struct. J.*, 98(3), pp. 359–367, (2001).

[94] Jia, J., Boothby, T., and Bakis, C., "Durability evaluation of glass fiber reinforced-polymer-concrete bonded interfaces," *J. Compos.*, 9(4), 348-359, (2005).

[95] Karbhari, V. and Engineer, M., "Effect of environmental exposure on the external strengthening of concrete with composites-short term bond durability," *J. Reinf. Plast.*, 15(12), 1194-1216, (1996).

[96] Pellegrino, C., Tinazzi, D. and Modena, C., "Experimental Study on Bond Behavior between Concrete and FRP Reinforcement Experimental Study on Bond Behavior between Concrete and FRP Reinforcement," 12(2), 180-189, (2008).

[97] Täljsten, B. and Blanksvärd, T., "Mineral-based bonding of carbon FRP to strengthen concrete structures," *J. Compos. Constr.*, 11(2), 120-128, (2007).

[98] Dai, J., Ueda, T., and Sato, Y., "Development of the Nonlinear Bond Stress–Slip Model of Fiber Reinforced Plastics Sheet–Concrete Interfaces with a Simple Method," *J. Compos. Constr.*, 9(1), pp. 52–62, (2005).

[99] Malvar, L. J., Joshi, N. R., Beran, J. A., and Novinson, T., "Environmental effects on the short-term bond of carbon fiber-reinforced polymer (CFRP) composites," *J. Compos. Constr.*, 7(1), pp. 58–63, (2003).

[100] Carrillo, O. R. M., "Evaluation The Bond Durability of FRP-Concrete Systems Subjected to Environmental Exposures," *Master Thesis*, Colorado State University, (2012).

[101] Benzarti, K., Chataigner, S., Quiertant, M., and Marty, C., "Accelerated ageing behaviour of the adhesive bond between concrete specimens and CFRP overlays," *Build. Mater.*, 25(2), 523-538, (2011).

[102] ASTM D7522/D7522M-15, "Standard Test Method for Pull-Off Strength for FRP Bonded to Concrete Substrate," American Society for Testing and Materials, (2009).

[103] Shen, X., "Effect of surface roughness and putty thickness on the bond performance of FRP laminates," *Master Thesis*, University of Missouri--Rolla, (2002).

[104] Ouyang, Z., and Wan, B., "Numerical simulation of bond deterioration between cfrp plate and concrete in moisture environment," *Third International Conference on FRP Composites in Civil Engineering*, pp. 395-398, (2006).

[105] Ouyang, Z., "Durability of bond between FRP and concrete in moist environments: Experimental, numerical and analytical study," *PhD. Dissertation*, Marquette University, (2007).

[106] Maria, A., Mariaenrica, F., and Domenico, A., "Effects of Environmental Conditions on Performance of Polymeric Adhesives for Restoration of Concrete Structures," *J. Mater. Civ. Eng.*, 14(2), pp. 185-189, (2002).

[107] Tu, L. and Kruger, D., "Engineering properties of epoxy resins used as concrete adhesives," *Mater. J.*, 93(1), 26-35, (1996).

[108] Wan, B., Petrou, M., and Harries, K., "The effect of the presence of water on the durability of bond between CFRP and concrete," *J. Reinf. Plast.*, 25(8), 875-890 (2006).

[109] El-Hawary, M., Al- Khaiat, H., and Fereig, S., "Performance of epoxy-repaired concrete in a marine environment," *Cem. Concr. Res.*, 30(2), pp. 259-266, (2000).

[110] Liau, W. B. and Tseng, F. P., "The effect of long-term ultraviolet light irradiation on polymer matrix composites," *Polym. Compos.*, 19(4), pp. 440-445, (1998).

[111] Green, M. F., Bisby, L. A., Beaudoin, Y., and Labossière, P., "Effect of freeze-thaw cycles on the bond durability between fibre reinforced polymer plate reinforcement and concrete," *Can. J. Civ. Eng.*, 27(5), pp. 949-959, (2000).

[112] Dutta, P. K. and Hui, D., "Low-temperature and freeze-thaw durability of thick composites," *Compos. Part B*, vol 27B, pp. 371-379, (1996).

[113] Fabio, N., Ludovico, M. D., De Caso Basalo, F. J., Prota, A., and Nanni, A., "Tensile behavior of epoxy based FRP composites under extreme service conditions," *Compos. Part B: Eng.*, 43(3), pp. 1468-1474, (2012).

[114] Ludovico, M. D., Piscitelli, F., Prota, A., Lavorgna, M., Mensitieri, G., and Manfredi, G., "Improved mechanical properties of CFRP laminates at elevated temperatures and freeze-thaw cycling," *Constr. Build. Mater.*, vol. 31, pp. 273-283, (2012).

[115] Hawileh, R. A., Abdalla, J. A., Hasan, S. S., Ziyada, M. B., and Abu-Obeidah, A., "Models for predicting elastic modulus and tensile strength of carbon, basalt and hybrid carbon-basalt FRP laminates at elevated temperatures," *Constr. Build. Mater.*, vol. 114, pp. 364-373, (2016).

[116] Mufti, A., "Durability of GFRP reinforced concrete in field structures," *Proc. 7th Int. Symp. Fiber Reinf. Polym. Reinf. Concr. Struct. - FRPRCS-7*, pp. 889-895, (2005).

[117] Uomoto, T., "Durability of FRP as reinforcement for concrete structures," *Compos. Mater. Build. Struct. 3rd Int. Conf.*, pp. 423-437, (1996).

[118] Holdener, D., Myers, J. J., and Nanni, A., "AN OVERVIEW OF COMPOSITES USAGE IN BRIDGE FACILITIES IN THE STATE OF MISSOURI, *Proceedings of the International Conference and Exhibition on Reinforced Plastics*, Mumbai, India, (2008).

[119] Federal Highway Administration, "National Bridge Inspections Standards Regulation (NBIS)," (2004).

[120] Fico, R., Galati, N., Prota, A., and Nanni, A., "Southview Bridge Rehabilitation in Rolla, Missouri," *Final Report*, Univeristy of Missouri-Rolla, (2006).

[121] Alkhrdaji, T. and Nanni, A., "Development and Technology Construction and Long-Term Monitoring of a Concrete Box Culvert Bridge Reinforced with GFRP Bars," *Final Report*, University of Missouri-Rolla, (2001).

[122] ASTM D4475-02, "Standard Test Method for Apparent Horizontal Shear Strength of Pultruded Reinforced Plastic Rods By the Short-Beam Method," American Society for Testing and Materials, (2002).

[123] Gooranorimi, O., Dauer, E., Myers, J. J., and Nanni, A., "Long-term Durability of GFRP Reinforcement in Concrete : A Case Study after 15 Years of Service," Interim report, University of Miami, (2016).

[124] ASTM D2584, "Standard Test Method for Ignition Loss of Cured Reinforced Resins," American Society for Testing and Materials, (2011).

[125] Gooranorimi, O., Myers, J. J., and Nanni, A., "GFRP Reinforcements in Box Culvert Bridge: A Case Study after Two Decades of Service," *ASTM Symp.*, (2017).

[126] AC 454, "Acceptance Criteria for Fiber-Reinforced Polymers (FRP) Bars for Internal Reinforcement of Concrete Members," *Int. Code Counc. Serv.*, (2015).

[127] Miyazaki, C. L., Medeiros, I. S., Santana, I. L., Matos, J. D. R., and Rodrigues Filho, L. E., "Heat treatment of a direct composite resin: influence on flexural strength," *Braz. Oral Res.*, 23(3), pp. 241-247, (2009).

[128] ASTM E1640-13, "Standard Test Method for Assignment of the Glass Transition Temperature By Dynamic Mechanical Analysis," American Society for Testing and Materials, (2013).

[129] ASTM F710-11, "Standard Practice for Preparing Concrete Floors to Receive Resilient Flooring," American Society for Testing and Materials, (2011).

[130] Grubb, J. A., Limaye, H. S., and Kakade, A. M., "Testing pH of Concrete," *Concr. Int.*, 29(4), pp. 78-83, (2007).

[131] ASTM C-1202-12, "Standard Test Method for Electrical Indication of Concrete's Ability to Resist Chloride Ion Penetration," American Society for Testing and Materials, (2012).

[132] Vivas, E., Boyd, A. J., Hamilton III, H. R., and Bergin, M., "PERMEABILITY OF CONCRETE- COMPARISON OF CONDUCTIVITY AND DIFFUSION METHODS," *Final Report*, University of Florida, Gainesville, (2007).

[133] ASTM C1543-10a, "Standard Test Method for Determining the Penetration of Chloride Ion into Concrete by Ponding," American Society for Testing and Materials, (2010).

[134] Missouri Department of Transportation, “Self-Consolidating Concrete (SCC) for Infrastructure Elements Report E – Hardened Mechanical Properties and Durability Performance,” *Final Report*, Missouri University of Science and Technology, Rolla, (2012).

[135] Broomfield, J. P., “Corrosion of Steel in Concrete: Understanding, Investigation and Repair,” *Second Edition*. Taylor & Francis, (2007).

[136] Karbhari, V.M. “Durability of Composites for Civil Structural Applications,” *First Edition*, Woodhead Publishing, London, UK, pp 384, (2007).

[137] Nkurunziza, G. Benmokrane, B. Debaiky, A. S. and Masmoudi, R., “Effect of Sustained Load and Environment on Long-Term Tensile Properties of Glass Fiber-Reinforced Polymer Reinforcing Bars,” ACI Structures Journal, Vol 102, No. 4, pp 615-621, (2005).

VITA

Wei Wang was born in Shenyang City, Liaoning Province, China. He was admitted to the Shenyang University in Shenyang in 1996. He got his Bachelor's degree in Civil Engineering with grade excellent with honor in 2000. He received his Master's degree from Lanzhou University of Technology in 2004 in Structural Engineering. Wei became a PhD candidate in civil engineering since January 2012 at Missouri University of Science and Technology.

Wei became an active member in student chapter and social organizations including Chi Epsilon (Civil Engineering Honor Society), American Concrete Institute (ACI), American Society of Civil Engineers (ASCE), and the Center for Infrastructure Engineering Studies. He was awarded ICRI Great Plains Chapter Scholarship in 2012. In July 2017, he received his PhD degree in Civil Engineering from Missouri University of Science and Technology.